SPRAYED GLASS FIBER REINFORCED POLYMERS IN SHEAR STRENGTHENING AND ENHANCEMENT OF IMPACT RESISTANCE OF REINFORCED CONCRETE BEAMS

by

SAYED MOHAMAD SOLEIMANI

B.Sc., Sharif University of Technology, Tehran, Iran, 1991
M.A.Sc., The University of British Columbia, 2002

A THESIS SUBMITTED IN PARTIAL FULFILLMENT OF
THE REQUIREMENTS FOR THE DEGREE OF

DOCTOR OF PHILOSOPHY

in

THE FACULTY OF GRADUATE STUDIES

(Civil Engineering)

THE UNIVERSITY OF BRITISH COLUMBIA

November 2006

ABSTRACT

Shear failure of reinforced concrete (RC) beams is often sudden and catastrophic. A timely shear strengthening of deficient RC beams is therefore critical in view of maintaining public safety.

In this dissertation, the effectiveness of externally bonded sprayed glass fiber reinforced polymer (Sprayed GFRP) in shear strengthening of RC beams under both quasi-static and impact loading was investigated. Direct comparisons were drawn with hand-applied, site-impregnated FRP fabric. To study RC beams under impact loads, a unique test setup was developed. In this setup, both the striking hammer and the specimen supports are instrumented and accelerometers are mounted on the specimen to accurately measure specimen inertial loads and to provide a proper dynamic analysis of the system. A total of 77 RC specimens were tested with and without FRP strengthening.

Given that bond between FRP and concrete is the critical link, in the shear strengthening program, different techniques were used to enhance the bond between concrete and Sprayed GFRP. It was found that roughening the concrete surface using a pneumatic chisel and using mechanical fasteners were the most effective techniques. Also, Sprayed GFRP applied on 3 sides (U-shaped) was more effective than 2-sided Sprayed GFRP in shear strengthening under both static and impact loading. GFRP, both sprayed and fabric, increased the shear load carrying capacity of RC beams and their energy absorption capacities, but Sprayed GFRP, especially U-shaped, was more effective than fabric GFRP. An increase of up to 105% in load carrying capacity of strengthened RC beams was observed under impact loading with respect to un-strengthened RC beams.

Simple equations were proposed to calculate the contribution of Sprayed GFRP in shear capacity of RC beams under quasi-static and impact loadings. Analysis of data indicated that the load carrying capacity of strengthened RC beams both under quasi-static and impact conditions was governed by the effective strain capacity of the Sprayed GFRP, which was, in turn, governed by the GFRP configuration and its bond with concrete. Future research should therefore focus on enhancing the strain capacity of the FRP when used as externally bonded reinforcement for structural strengthening.

TABLE OF CONTENTS

LIST OF TABLES

LIST OF FIGURES

ACKNOWLEDGEMENTS

First of all I would like to thank Allah for lightening up my path towards him, especially when I needed it the most. During my life I have always felt his presence and thank him for teaching me the best ways of knowing him better and deeper, one of them being through the study of engineering sciences.

This research could not have been performed without the contribution from a number of valued individuals. First and for most, I would like to give my special thanks to my research supervisor, Professor Nemkumar Banthia, for his continued support, advice and encouragement throughout my doctoral program. I found him an interesting person to work with. Also his intelligence and abilities amaze me all the time. He is an understandable and open-minded person and I found him not only to be the best supervisor, but also a trustful friend and a good listener.

I would also like to thank Professor Sidney Mindess and Professor Aftab Mufti for their constructive and patient review of my thesis. I am also grateful to Mr. John Chandra and Mr. Gary Pinder of John's Custom Fiberglass for spraying the GFRP on concrete specimens for this research. The efforts of Mr. Doug Hudniuk, Mr. Doug Smith, Mr. John Wong and Mr. Scott Jackson in setting up the equipment and instruments are also greatly appreciated. I would also like to thank my colleagues, Rishi Gupta, Amir Mirsayah, Yashar Khalighi, Alireza Biparva, Reza Mortazavi, Hanfeng Xu, John Zhang, Ankit Bhargava and Manote Sappattipakorn whom I found them pleasurable persons to interact with. My special thanks go to Mr. Fariborz Majdzadeh for his valuable and continued help during my research.

Last but not least; I am extremely grateful to my family for being there during the hardest moments and for sharing with me the bright moments. My wife, Nahid, and my son, Ahmad, encouraged me all the time and without their help I could never be able to complete this job.

For Nahid and Ahmad;

Without whose help, support, care and patience this would never become a reality.

Thank you from the bottom of my heart.

1

INTRODUCTION

1.1. Overview

The research project described within this dissertation deals with shear strengthening of reinforced concrete (RC) beams using sprayed glass fiber reinforced polymer (GFRP) composites. It is now believed that by applying a thin coating of fiber reinforced polymer onto the surface of a reinforced/under-reinforced/un-reinforced concrete beam, its load-carrying capacity, energy absorption potential and stiffness can be increased.

Hitherto, the effectiveness of externally bonded GFRP for shear strengthening in increasing the load-carrying capacity of RC beams under impact loading has not been investigated. Here, a setup for testing RC beams under impact loading was designed and developed. Behavior of RC beams under different rates of loading was studied, and finally, RC beams strengthened in shear with Sprayed GFRP were tested under impact.

1.2. Strengthening Techniques for Concrete Structures

A significant number of facilities including transportation infrastructures in the United States and Canada were constructed during the first half of the 20^{th} century using reinforced concrete. Many of these structures, particularly those that form part of the civil infrastructure, have reached the end of their planned service life. Deterioration in the form of steel corrosion, concrete cracking and spalling is prevalent and in addition,

many of these structures are experiencing loads that are significantly higher than the design loads. One example is the revisions to building codes such as the need to carry heavier loads or higher traffic volumes. Seismic performance requirements also add to the need for strengthening and rehabilitation of existing and/or older structures. Because of these factors, many structural and materials engineers are faced with the challenge of evaluating and implementing successful and economical repair, rehabilitation and strengthening techniques.

In particular, shear strengthening of RC beams is one of the most-needed techniques in repair and rehabilitation of concrete structures. Deficiency in shear strength of existing RC beams can occur for several reasons such as increased service loads on the structure, deficiencies in the shear design procedures in older codes and corrosion of stirrups which are protected by a thinner concrete cover compared to the longitudinal reinforcing bars.

There are different solutions to this problem. The following gives a brief description of the different methods that can be employed for shear strengthening and rehabilitation of existing RC beams.

Span Shortening: In this method additional supports are installed underneath existing members. Appropriate materials to be used in this method include cast-in-place concrete and structural steel members. Connections to the existing structure can be facilitated using bolts and adhesive anchors.

Fiber Reinforced Polymer (FRP) and Steel Reinforced Polymer (SRP) Composites: FRP composites are high strength, non-corrosive materials. They are lightweight reinforcement in the form of paper-thin fabric sheets and laminates [1 – 25], thin sprayed layers [26 – 29], or bars [30] that are bonded to the outer surface of concrete members to increase their load-carrying capacity. These composites have been used extensively in aerospace, automotive, and sport-equipment industries and are now becoming a mainstream technology for strengthening and repair of concrete, timber, and

more recently, masonry structures. Important properties of FRPs for structural strengthening and repair include their speed and ease of installation, non-corrosive properties, lower cost, and aesthetic appeal. FRP composites will be discussed in more details in the following chapters.

In addition to FRPs, steel reinforced polymer (SRP) composites have recently been used as externally bonded reinforcement [31]. The steel fabric used in the SRP is composed of unidirectional high strength steel cords. Steel fabric is cut into sheets to be applied to the surface of reinforced concrete beams using epoxy resin.

Bonded Steel Plates: Effectiveness of externally bonded steel plates has been studied for flexural [32 – 43] and shear [44 – 46] strengthening of RC beams. This method was developed in the 1960s in Switzerland and Germany [37]. In this method of strengthening, steel elements (e.g. steel plates, channels, angles, or built-up members) are glued to the concrete surface by a two-component epoxy adhesive to create a composite system and improve flexural and shear strength.

In addition to epoxy adhesive, mechanical anchors are usually used to ensure that the steel element will share external loads in case of adhesive failure. In this method, since steel is exposed, a suitable system must be used to protect the steel element from corrosion, especially in harsh environments.

External Post Tensioning: composite steel-concrete beams were used for the first time in the Rock Rapids Bridge in Iowa in 1894 [47]. Research in development of shear connection between slabs and steel beams for a better composite action goes back to 1950s [48]. The earliest research on external prestressing of composite beams was carried out in 1959 [49].

The use of external post-tensioning tendons is an innovative method for repair and strengthening of RC beams. If using straight tendons, the external post-tensioning can be achieved by welding end anchorages and use of post-tensioning cables. The prestress is applied by having a dead- and a live-end as in conventional post-tensioning techniques.

In this type of strengthening, active external force is applied to the structural member to resist higher loads. This effective method has been used successfully in parking structures and cantilevered members. Prior to external prestressing, all existing cracks must be epoxy-injected to ensure that the prestressing force will be distributed uniformly in the member.

Section Enlargement: In this method a bonded reinforced concrete is added to an existing structural member in the form of an overlay or a jacket. This method can be applied to beams, columns, slabs and walls to increase their load-carrying capacity. A typical enlargement is approximately 2 to 6 inches (5 to 15 mm) thick, and therefore, self-compacting concrete can be used for an easier placement, especially in the presence of reinforcing bars. Since this method needs forming, it may not be a cost-effective solution for structural strengthening of RC beams. It may also result in loss of space and reduced headroom.

1.3. Objectives and Scope

The scope of this project was to investigate the use of sprayed glass fiber reinforced polymers as a shear strengthening method for existing reinforced concrete beams under different loading rates with three objectives as follow:

1. To determine the effectiveness of this technique under quasi-static loading condition with an emphasis on increasing the bond between Sprayed GFRP and concrete surface;
2. To study shear- and flexural failure of unstrengthened reinforced concrete beams under impact loading; and
3. To determine the efficiency of Sprayed GFRP as a means of shear strengthening of RC beams under impact loading.

The following are the original contributions of this research study:

1. Building an impact test setup to study the behaviour of RC beams under different stress/strain rate of loading;
2. Developing an innovative and simple technique of deriving useful information from impact tests;
3. Developing a practical method to effectively apply a thin layer of Sprayed GFRP for shear strengthening of RC beams;
4. Investigating and improving the strength of bond between FRP and concrete; and
5. Deriving design equations to predict the capacity of RC beams strengthened with Sprayed GFRP in shear under both static and impact loading, with and without mechanical fasteners.

2

LITERATURE SURVEY

2.1. Introduction

The research performed throughout this project deals with shear strengthening of RC beams using Sprayed GFRP composites. This technique as compared to externally bonded FRP fabrics and laminates is quite new for strengthening of RC structures. Hence, a limited number of publications are available with respect to this technique. On the other hand, externally bonded FRP including glass, carbon, and aramid (e.g. Kevlar) fibers have been studied for flexural and shear strengthening of RC beams and strengthening of RC columns extensively. As a result, new guidelines are available to design concrete structural elements strengthened with externally applied FRP such as the American ACI 440.2R-02 [50], Canadian CSA-S802-02 [51], ISIS design manual [52], and European *fib*-TG9.3-01 [53].

Fundamentally, all of these techniques (i.e. fabric, laminate, and spray) are alike in that all involve the attachment of extra reinforcement (i.e. FRP composite) to the surface of an existing RC member. This chapter will discuss the results obtained by researchers around the world on shear strengthening of RC beams using externally bonded FRP composites.

Since the behavior of RC beams with and without GFRP strengthening has been investigated in this study, previous research projects related to this topic will also be addressed. To the best of the author's knowledge, the effectiveness of externally bonded

FRP as a means of shear strengthening of RC beams under impact loading has not been investigated and this research project is the first of its kind.

As mentioned in Chapter 1, steel plates can also be epoxy bonded to the face of the concrete structure for strengthening purposes. Although this is an effective rehabilitation technique, there are some disadvantages with the use of steel such as difficulties in handling the heavy steel plates with a density of 7850 kg/m^3, corrosion of steel, especially at the steel/epoxy interface, and costs associated with the labour and time involved in this technique.

FRP composites, on the other hand, possess superior advantages such as high strength to weight ratio (i.e. high specific strength), high stiffness to weight ratio (i.e. high specific stiffness), tailorable mechanical and physical properties, weathering and corrosion resistant, formability to large complex shapes, mature technology, and low cost in many cases.

Glass, carbon and aramid fibers are different fibers that are used in production of FRP composites. Each one of these fibers has its own advantages and disadvantages. Glass fibers are inexpensive and have good physical and mechanical properties including strength, modulus and impact resistance, high strength to weight ratio, high resistance to chemical attack (C-glass) and moisture (E-glass), and good insulation characteristics. In addition, they can be fabricated by a wide range of production techniques. Disadvantages of glass fibers include brittleness, reduction of tensile strength in presence of water (especially in A-glass fibers), and static fatigue (tensile strength is reduced under sustained loads as the growth of surface flaws is accelerated owing to stress corrosion by atmospheric moisture). Surface defects can also change the properties considerably.

Carbon fibers have very high strength and modulus (sometimes as high as two times that of steel), retain their properties at high temperatures and possess high fatigue strengths. They also have negative coefficient of thermal expansions

(-0.4 to -1.6 × 10^{-6}/°C in fiber direction) which makes them useful in applications where high stiffness and dimensional stability are required, such as space structures. Disadvantages of carbon fibers include low impact resistance, high electrical conductivity, rapid reaction with many metals, they are also expensive (cheapest low-quality carbon fiber is more expensive than glass fiber) and require strict quality control.

Aramid fibers have excellent specific strength, high impact resistance (i.e. high strain to failure), good resistance to temperature, and good fatigue performance. They are also good insulators of both electricity and heat. Disadvantages of aramid fibers include poor compression strength, susceptibility to moisture, ultra-violet and visible light. FRP composites made with aramid fiber demonstrate higher creep rate than glass or carbon composites.

A comparison of the important characteristics of FRP products from these fiber types is shown in Table 2.1 [54].

Table 2.1 – *Comparison of characteristics of FRP sheet products from different fibers*

Characteristics	Carbon	Aramid	E-glass
Tensile strength	Very good	Very good	Very good
Compressive strength	Very good	Inadequate	Good
Stiffness	Very good	Good	Adequate
Long term behavior	Very good	Good	Adequate
Fatigue behavior	Excellent	Good	Adequate
Bulk density	Good	Excellent	Adequate
Alkaline resistance	Very good	Good	Inadequate*
Cost	Adequate	Adequate	Very good

** From accelerated tests; newly obtained field data indicates that this may not be that adverse an issue.*

2.2. FRP Materials for Shear Strengthening of RC Beams

Many concrete structures such as bridges that are in use today have exceeded their design life. In the USA alone, over 30% of their 500,000 bridges are deficient in terms of stiffness and strength [55]. On the other hand, code requirements have been changed, the shear requirements have become more stringent for concrete girders and especially for bridges, and allowable traffic loads have been increased. Some elements of these structures have also been weakened due to corrosion of steel rebars containing longitudinal (tension and compression) and vertical (shear) reinforcements. Therefore, rehabilitation and strengthening of these concrete structures is one of the priorities for engineers today. In fact, this new challenge necessitates a close collaboration between structural and materials experts. Advantages of FRP composites, as mentioned earlier, have encouraged researchers around the world to focus on the externally bonded FRP composites for strengthening of concrete slabs, columns and beams.

Flexural strengthening of reinforced concrete (RC) beams and slabs, and confinement of circular and rounded-edge rectangular concrete columns using FRP have been studied extensively and are well documented. Shear strengthening of RC beams with FRP, on the other hand, needs further investigations. There are a very limited number of papers available in which the behavior of RC beams strengthened for flexure with FRP has been investigated under dynamic/impact loading [56 - 60] and to the best of author's knowledge there is no single report available on behavior of RC beams strengthened in shear with FRP under impact loading.

Due to the brittle behaviour of plain concrete in tension, shear failure in RC beams is generally catastrophic. It is also one of the primary reasons for building collapses during earthquakes. Therefore, shear strengthening of RC beams with FRP needs to be investigated extensively.

Two major failure modes for RC beams strengthened in shear using externally bonded FRP have been reported: 1) FRP has peeled off at the concrete-FRP interface (FRP debonding), and 2) FRP has fractured in tension. Due to stress concentrations at

debonded areas or at the corners, FRP fracture in tension may occur at a stress lower than the FRP tensile strength. Clearly, shear capacity of RC members strengthened in shear with externally bonded FRP depends on the mode of failure.

The very first study on shear strengthening of RC beams using externally bonded FRP composites dates back to 1992 [61]. In this study, RC beams with and without externally bonded GFRP laminates to the vertical sides in the shear-critical zones were tested and a simple model was developed to predict the contribution of GFRP composites to the shear capacity of RC beams. Models used often to calculate the contribution of steel stirrups in shear capacity of RC beams were used in analysis. The maximum allowable strain was determined by experiments.

The second study reported in the literature was carrier out by a Japanese researcher, Uji [62]. Reinforced concrete beams were strengthened in shear using CFRP laminates bonded to the vertical sides or wrapped-around carbon fabrics.

The first attempt to use aramid fibers for shear strengthening of RC beams is reported by Dolan et al. [63]. They concluded that AFRP composites as shear retrofit reinforcement are promising.

Al-Sulaimani et al. [64] modeled the contribution of GFRP composite laminates, in the form of plates or strips, based on the shear stress capacity of the FRP-concrete interface. They reported average shear stresses during peeling-off equal to 0.8 MPa and 1.2 MPa for plates and strips, respectively.

Reinforced concrete beams strengthened in shear with wrapped-around CFRP were tested by Ohuchi et al. [65]. In their model, they assumed a limiting strain for the external reinforcement equal to the tensile failure strain of CFRP or ⅔ of it, depending on FRP thickness.

RC beams strengthened with glass, aramid, and carbon FRP composites have been studied by Chajes et al. [66]. The contribution of FRP to shear capacity of RC beams was modeled by assuming a limiting FRP strain, approximately 0.005, determined by experiments. In another study by Marval et al. [67], CFRP composites were used as means of shear strengthening. They stated that by limiting the FRP strain to that at tensile fracture of the composite, analogous to commonly adopted procedure for steel stirrups, the contribution of CFRP composite to shear capacity can be calculated.

Shear strengthening of large scale RC beams with CFRP composites was also reported by Vielhaber and Limberger [67], in which the presence of FRP prevented brittle shear failure. Test results on concrete beams strengthened in shear using CFRP composites have also been reported by Sato et al. [69]. Debonding of external reinforcement (i.e. CFRP composites) was observed and a simple model which counts for partial shear transfer by the debonded CFRP was developed.

The first systematic attempt to review the literature on RC flexural members strengthened in shear with FRP up to 1997 has been made by Triantafillou [70]. He derived the following equation to calculate the FRP contribution to shear capacity of RC beams:

$$V_{frp,d} = \frac{0.9}{\gamma_{frp}} E_{frp} \rho_{frp} \varepsilon_{frp,e} b_w d(\sin\beta + \cos\beta) \tag{2.1}$$

where, γ_{frp} is partial safety factor for FRP in uniaxial tension (approximately equal to 1.15, 1.20 and 1.25 for CFRP, AFRP and GFRP, respectively [71]), b_w is the minimum width of the concrete cross section over the effective depth, d is the effective depth of cross section, and β is the angle of fiber direction in FRP material to longitudinal axis of the member. The axial rigidity of bonded FRP was expressed by $E_{frp}\rho_{frp}$, where

E_{frp} is elastic modulus of FRP in the principal fiber orientation and ρ_{frp} is FRP reinforcement ratio:

$$\rho_{frp} = \frac{2t_{frp}}{b_w} \tag{2.2}$$

for continuously bonded shear reinforcement of thickness t_{frp}, and

$$\rho_{frp} = (\frac{2t_{frp}}{b_w})(\frac{w_{frp}}{s_{frp}}) \tag{2.3}$$

for FRP reinforcement in the form of strips, where w_{frp} is the width of the FRP strips and s_{frp} is their spacing. The relationship between $\varepsilon_{frp,e}$ and $E_{frp}\rho_{frp}$ was obtained from the best-fit second order equation up to $E_{frp}\rho_{frp}$ = 1 GPa and by the equation of a straight line for $E_{frp}\rho_{frp}$ > 1 GPa. Thus the polynomial functions that relate the FRP strain at shear failure of the member (i.e. effective strain, $\varepsilon_{frp,e}$) to the axial rigidity of externally bonded strips or sheets are as follows:

$$\varepsilon_{frp,e} = \begin{cases} 0.0119 - 0.0205(E_f\rho_f) + 0.0104(E_f\rho_f)^2 & if \;\; 0 \le E_{frp}\rho_{frp} \le 1 \\ -0.00065(E_f\rho_f) + 0.00245 & if \;\; E_{frp}\rho_{frp} > 1 \end{cases} \tag{2.4}$$

Equation (2.4) has been derived using curve fitting on about 40 different sets of test data published by different researchers and show $\varepsilon_{frp,e}$ would be reduced by reducing $E_{frp}\rho_{frp}$ product. Triantafillou [70] also suggested that the value of $E_{frp}\rho_{frp} = 0.4GPa$ can be used to determine the limiting area fraction of FRP, ρ_{frp}, beyond which the effectiveness of strengthening ceases to be positive.

Triantafillou and Antonopoulos [25] stated that the above mentioned modeling (equation (2.4)) had three shortcomings as follows:

1. FRP fracture was assumed to occur simultaneously with shear failure (concrete diagonal tension), whereas in reality it may occasionally appear after the peak load (shear capacity) is reached;
2. One equation was used to describe both FRP fracture and debonding, regardless of the type of FRP material (CFRP versus AFRP or GFRP);
3. The concrete strength, which is expected to affect debonding, was not introduced as a design variable.

To overcome these shortcomings, they proposed the following equation to predict design shear capacity provided by FRP, $V_{frp,d}$:

$$V_{frp,d} = \frac{0.9}{\gamma_{frp}} E_{frp} \rho_{frp} \varepsilon_{frpk,e} b_w d(\sin\beta + \cos\beta) \tag{2.5}$$

where,

$$\varepsilon_{frpk,e} = \alpha \varepsilon_{frp,e} \leq \varepsilon_{\max} \tag{2.6}$$

$\varepsilon_{frpk,e}$ is the characteristic effective FRP strain in principal fiber direction, α is the reduction factor = 0.8, $\varepsilon_{\max}$ is the limiting value of characteristic effective FRP strain = 0.005. γ_{frp}, the partial safety factor can be obtained from Table 2.2. $\varepsilon_{frp,e}$ is the effective FRP strain in principal fiber direction (mean value) which can be calculated as follows:

for fully wrapped CFRP: $$\varepsilon_{frp,e} = 0.17 \left(\frac{f_c'^{2/3}}{E_{frp} \rho_{frp}} \right)^{0.30} \varepsilon_{frp,u} \tag{2.7}$$

for side or U-shaped CFRP jackets:

$$\varepsilon_{frp,e} = \min[0.65\left(\frac{f_c'^{2/3}}{E_{frp}\rho_{frp}}\right)^{0.56} \times 10^{-3}, 0.17\left(\frac{f_c'^{2/3}}{E_{frp}\rho_{frp}}\right)^{0.30} \varepsilon_{frp,u}] \quad (2.8)$$

for fully wrapped AFRP: $$\varepsilon_{frp,e} = 0.048\left(\frac{f_c'^{2/3}}{E_{frp}\rho_{frp}}\right)^{0.47} \varepsilon_{frp,u} \quad (2.9)$$

where f_c' is the compressive strength of concrete (MPa), E_{frp} is the modulus of elasticity of the FRP (GPa), and $\varepsilon_{frp,u}$ is the ultimate FRP tensile strain.

Table 2.2 – *Values of partial safety factor,* γ_{frp}

Condition	FRP Composite		
	CFRP	AFRP	GFRP
If failure is combined with or followed by FRP fracture	1.2	1.25	1.3
If FRP debonding dominates	1.3	1.3	1.3
If $\varepsilon_{frpk,e} = \varepsilon_{\max}$	1.3	1.3	1.3

When the proposed value for $\varepsilon_{\max}$ (i.e. 0.005) is divided by the material safety factor (γ_{frp} from Table 2.2), it yields a value approximately equal to 0.004. This value has been suggested by Priestley and Seible [72] and Khalifa et. al. [73] as a maximum strain to maintain the integrity of concrete and secure activation of the aggregate interlock mechanism.

It is worth mentioning that equations (2.7) to (2.9) have been developed using 76 sets of experimental data of RC beams strengthened in shear from different researchers. A summary of failure modes of theses investigated RC beams is provided in Table 2-3.

It is clearly seen that when FRP had not been wrapped around the RC beam the failure mode was debonding of FRP most of the time. This was even more obvious when the FRP was provided on the sides of RC beam only.

Table 2.3 – *Failure mode of 76 RC beams strengthened in shear by carbon, aramid or glass FRP analyzed by Triantafillou and Antonopoulos [25]*

	FRP configuration		
	Wrapped around	Bonded to sides	U-shaped
Number of specimens in which FRP fractured at shear failure	49	1	4
Number of specimens in which FRP debonding occurred	0	15	7

It is apparent that in practice, wrapping FRP around the RC beam is not possible since usually no such beam in reinforced concrete structures exists, and if it does, it will unlikely need any strengthening, especially for shear. That is why they have recommended when full wrapping is not feasible (for instance, when there is no access to the top side of T-beams), FRP strips should be attached to the compressive zone of the RC member through the use of simple mechanical anchors.

Triantafillou and Antonopoulos [25] have also proposed the following expression as the limiting value of $E_{frp}\rho_{frp}$ for debonding to be suppressed:

$$(E_{frp}\rho_{frp})_{\lim} = \left(\frac{0.65\times10^{-3}\alpha}{\varepsilon_{\max}}\right)^{1/0.56} f_c'^{2/3} = 0.018 f_c'^{2/3} \qquad (2.10)$$

For values of $E_{frp}\rho_{frp}$ below $(E_{frp}\rho_{frp})_{\lim}$, the design is governed by the limiting FRP strain (i.e. $\varepsilon_{\max}$), no FRP failure mechanism will occur and therefore, the contribution of FRP to shear capacity is proportional to $E_{frp}\rho_{frp}$. For values of $E_{frp}\rho_{frp}$ exceeding $(E_{frp}\rho_{frp})_{\lim}$, failure is governed by:

1. Debonding combined with shear failure, if FRP is not properly anchored; or
2. Shear fracture combined with or followed by CFRP fracture, if the composite material is anchored properly (fully-wrapped here).

Concrete strength plays an important role in the first case, whereas in the second case, $E_{frp}\rho_{frp}$ becomes more important.

As an additional recommendation, they also proposed a limitation for the spacing s_f of strips, if they are used vertically as follows:

$$s_f \leq 0.8d \tag{2.11}$$

The JCI code [74] format is identical to equation (2.5) except that 0.9 is replaced by 1/1.15 (= 0.87).

Khalifa et al. [73] proposed the following equation to calculate the shear capacity provided by FRP, V_{frp}:

$$V_{frp} = E_{frp}\rho_{frp}R\varepsilon_{frp,u}b_w d(\sin\beta + \cos\beta) \tag{2.12}$$

where R, the ratio of effective strain to ultimate strain ($R = \frac{\varepsilon_{frp,e}}{\varepsilon_{frp,u}}$), is given by:

$$R = \begin{cases} 0.5622(E_{frp}\rho_{frp})^2 - 1.2188(E_{frp}\rho_{frp}) + 0.778 \le 0.5 \quad \text{for rupture} \\ \text{mode of failure for } E_{frp}\rho_{frp} < 1.1 \text{ GPa} \\ \dfrac{0.0042(f_c')^{2/3} w_{frp,e}}{(E_{frp}t_{frp})^{0.58}\varepsilon_{frp,u}d} \quad \text{for debonding mode of failure} \end{cases} \tag{2.13}$$

where $w_{frp,e}$ = efficient width of an FRP sheet, which is given by the following equation for different wrapping schemes:

$$w_{frp,e} = \begin{cases} d - L_e & \text{if the sheet is in the form of a U - jacket} \\ d - 2L_e & \text{if the sheet is bonded to the sides only} \end{cases} \tag{2.14}$$

in which the effective bond length, L_e, is given by:

$$L_e = e^{6.134 - 0.58\ln(t_{frp}E_{frp})} \tag{2.15}$$

Adhikary and Mutsuyoshi [12] tested 7 RC beams strengthened with CFRP sheets in shear. They concluded that the model proposed by Khalifa et al. [73] (i.e. equation (2.12)) estimated the shear contribution of CFRP sheets for beams having full-side bonding and U-wrap layout with satisfactory accuracy and the model proposed by Triantafillou and Antonopoulos [25] (i.e. equation (2.5)) was reasonable for beams with U-wrap layout only. They also concluded that the beams should be reinforced by FRP sheets up to the maximum possible section depth to achieve the best strengthening effects.

Bousselham and Chaallal [75] have mentioned three factors that would increase the complexity of the shear problem in shear-strengthened RC beams as new characteristics include:

1. Since FRP composites are externally bonded to the concrete surface, bond mechanism and adherence are more important than those in internal shear steel reinforcement;
2. There are a wide range of FRP products available for structural strengthening, and by taking into account the variety of fiber orientation and the strengthening scheme, the number of parameters that influence the resistance mechanism will increase;
3. FRP composites behave linearly in tension up to the failure, but steel and concrete do not behave this way.

Bousselham and Chaallal [75] analyzed test results of 100 RC beams strengthened in shear using externally bonded carbon, glass, and aramid FRP composites from papers published in a decade (1992 to 2002). They analyzed this database in terms of a) the properties of FRP composites; b) the shear span (*a/d*) ratio; c) the shear steel reinforcement ratio; d) the longitudinal steel reinforcement ratio; and e) the scale effect. It is worth noting that about 76% of beams strengthened in shear with FRP composites, either on sides or U-shaped, have shown debonding at failure. Among those beams which experienced FRP fracture at failure, 71% were wrapped around, 27% were U-shaped, and only 2% were strengthened on their sides. Clearly, all beams with FRP wrapped around them have shown FRP fracture at failure.

Although they mentioned that the configuration of FRP composites played an important role in influencing the rupture scenario (i.e. while all beams strengthened by FRP wrap failed when FRP fractured, those strengthened with glued FRP on their sides failed mainly by FRP debonding), they did not exclude wrapped FRP beams from their discussion when relating, for example, mode of failure with *a/d*, shear span ratio. As a result they concluded that when *a/d* was greater than 3.2, failure occurred by debonding of FRP composites, although there was no beam with wrapped FRP with $a/d > 3.2$.

They further concluded that the contribution of the FRP composites in gaining shear strength is more significant in shallow beams than in deep beams (i.e. $a/d < 2.5$).

Considering their discussion, it seems that the parameter *a/d* should be studied further to find out its importance in calculating shear strength of RC beams with externally bonded FRP composites. The same has been mentioned by Matthys and Triantafillou [76].

Chaallal et al. [6], Bousselham and Chaallal [75], and Pellegrino and Modena [13] have shown that the gain in shear strength generally decreases as the ratio $E_s\rho_s / E_{frp}\rho_{frp}$ decreases, where E_s is elastic modulus of transverse steel reinforcement and ρ_s is the transverse steel reinforcement ratio. This shows that FRP shear strengthening is more effective when there is a lack of transverse steel reinforcement.

Longitudinal steel reinforcement will also affect the shear strength of RC beams, the greater the longitudinal steel reinforcement ratio (ρ_w), the greater the shear strength will be [77]. As a result, Bousselham and Chaallal [75] concluded that for RC beams strengthened in shear by externally bonded FRP composites, the greater the ratio $E_s\rho_w / E_{frp}\rho_{frp}$, the smaller the gain in shear capacity.

Triantafillou [70] demonstrated that the FRP bond transfer length for small size beams strengthened in shear (excluding RC beams wrapped around with FRP), in general, is smaller than that for large beams. Although this statement makes sense, it is contrary to what was reported by Bousselham and Chaallal [75]. Keeping in mind that FRP thickness is an important factor while considering size effect, clearly, more experimental work is required to evaluate the size effect influence on shear strengthening of RC beams using externally bonded FRP composites.

Deniaud and Cheng [16] published a review paper on shear design methods for RC beams strengthened with FRP sheets and compared the adequacy of each method by using their test results on 16 full-scale T-beams. They used models proposed by Chaallal et al. [78], Khalifa et al. [73], CSA-S806-00 [79], Malek and Saadatmanesh [80] and compared the results with modified shear friction method and strut-and-tie model. They

concluded that the modified shear friction method was the most promising one in evaluating the shear contribution of the FRP sheets among the available methods. The general formulation of the shear capacity of any RC beam with externally bonded FRP can be written as follows:

$$V_r = V_c + V_s + V_{FRP} \tag{2.16}$$

where V_r is total resisting shear load, V_c is shear load resistance attributed to concrete, V_s is shear load resistance provided by the stirrups, and V_{FRP} is shear load resistance provided by the FRP sheets.

In the modified shear friction method V_c (for T-girders), V_s, and V_{FRP} are defined as:

$$V_c = 0.25k^2 f_c^{'}(A_{cf} \tan\theta_{cf} + A_{cw} \tan\theta_{cw}) \text{ (for T-girders)} \tag{2.17}$$

where, $f_c^{'}$ is the compressive strength of concrete, A_{cf} is the effective flange concrete area, A_{cw} is web concrete area, θ_{cf} is the crack angle with respect to the longitudinal axis of the beam in the flange and θ_{cw} is the crack angle with respect to the longitudinal axis of the beam in the web and k is an experimentally determined factor as follows:

$$k = 2.1(f_c^{'})^{-0.4} \tag{2.18}$$

$$V_s = A_v f_{vy} n_s \tag{2.19}$$

where, A_v is the vertical steel area, f_{vy} is the yield strength of the stirrups, and n_s is the total number of stirrups crossing the concrete shear plane.

$$V_{FRP} = A_{frp} f_{frp} \frac{d_{frp} \sin\alpha}{s_{frp} \tan\theta_c} (\sin\alpha + \cos\alpha \tan\theta_c) \quad (2.20)$$

where, A_{frp} is the FRP sheet area, d_{frp} is the FRP height along the side of the beam web, s_{frp} is the FRP sheet bands spacing, α is the angle between the principal direction of the FRP sheets and the longitudinal axis of the beam, θ_c is the crack angle with respect to the longitudinal axis of the beam, and f_{frp}, the effective FRP stress, is expressed by the following equation:

$$f_{frp} = E_{frp} \varepsilon_{\max} R_L \quad (2.21)$$

where E_{frp} is the elastic tensile modulus of the FRP sheets in the principal direction of the fibers, $\varepsilon_{\max}$ is the maximum FRP strain over the remaining bonded length, and R_L is the ratio of the remaining bonded width over total width crossing the concrete web crack.

Chen and Teng [22] also proposed a new design equation to calculate the shear load resistance provided by the FRP strips while reviewing some other existing design proposals. They expressed the contribution of FRP to the shear capacity by the following formula (FRP rupture is the dominant mode of failure):

$$V_{FRP} = 2 \frac{f_{frp,ed}}{\gamma_{frp}} t_{frp} w_{frp} \frac{h_{frp,e} (\sin\beta + \cos\beta)}{s_{frp}} \quad (2.22)$$

where, t_{frp} is the thickness of FRP, w_{frp} is the width of FRP strips perpendicular to the fiber orientation, $h_{frp,e}$ is effective height of FRP bonded on beam sides (= $0.9d$ when U jackets are bonded over the full height of a beam where d is the distance from

the beam compression face to centroid of outermost layer of steel tensile reinforcement for flexure), β is the angle of first fiber orientation measured clockwise from horizontal direction for left side of shear strengthened beam, s_{frp} is the center-to-center spacing of FRP strips measured along longitudinal axis, γ_{frp} is the partial safety factor in a limit state design approach (they suggested a value of 1.25), and $f_{frp,ed}$ is defined as:

If FRP rupture is the dominant mode of failure: $f_{frp,ed} = D_{frp-1}\sigma_{frp,\max}$ (2.23)

If FRP debonding is the dominant mode of failure: $f_{frp,ed} = D_{frp-2}\sigma_{frp,\max,d}$ (2.24)

For shear strengthening using side strips/plates, $f_{frp,ed}$ will be calculated using equation (2.24), whereas, for U-jacketing it will be the smaller value obtained by equations (2.23) and (2.24).

Finally, they proposed equations to calculate the maximum design stress in FRP when FRP rupture is the dominant mode of failure ($\sigma_{frp,\max}$), the maximum design stress in FRP, when FRP debonding is the dominant mode of failure ($\sigma_{frp,\max,d}$), and the stress distribution factors (D_{frp-1} and D_{frp-2}).

They have also rightly mentioned that for unidirectional continuous FRP plates/sheets:

$$s_{frp} = \frac{w_{frp}}{\sin\beta} \tag{2.25}$$

Therefore, $s_{frp} = w_{frp}$ only if $\beta = 90^o$ (fibers are oriented vertically). It is worth noting that $s_{frp} = w_{frp}$ has been used even in design guidelines such as concrete society technical report no. 55 [81] for continuous sheets without giving suitable consideration

to the fiber direction. Cao et al. [82], following the same procedure, proposed an empirical model to predict the FRP contribution to the shear strength of RC beams strengthened with complete FRP wraps at FRP debonding.

Adhikary et al. [7] reported that the FRP sheets with bonded anchorage that extends to the top face of the beam are much more effective for shear strengthening of RC beams than the U-shaped wrap. Strengthened RC specimens using a U-shaped scheme for strengthening failed due to the debonding of the FRP sheets. They proposed different equations for CFRP and AFRP sheets to calculate their effective strain values with and without bonded anchorage to the top face of the beam.

Kachlakev and McCurry [18] studied the behavior of full-scale RC beams retrofitted for shear and flexural with FRP laminates. This study, like some other studies that have not been included in this chapter, had an important shortcoming. They extended the FRP laminates underneath the supports (i.e. applied FRP laminates to a length that was greater than the beam span) for flexural strengthening and also for shear strengthening. This configuration which is not practical will also prevent debonding failure and will result in totally misleading results. They stressed an important point that; "designers should realize that the added flexural capacity of FRP to most RC beams is not an amazing structural accomplishment". Since adding flexural FRP increases the amount of flexural reinforcement, an RC beam may become an over-reinforced member which, in turn, reduces its ductility. Over-reinforced RC beams are not able to undergo visible deflections before ultimately losing their load carrying capacity. This should be understood that these beams are very likely to fail in shear or by concrete crushing which are catastrophic failures and are undesirable. This point has also been mentioned by Sheikh et al. [5].

Shear rehabilitation of G-girder bridges in Alberta using fiber reinforced polymer sheets has been reported by Deniaud and Cheng [15]. They used CFRP and GFRP sheets and found that the woven fabric glass materials performed better than the unidirectional carbon FRP sheets. They also concluded that the inclined sheets were found to be more

effective than the vertical sheets. Pellegrino and Modena [13] reported the results of 9 large-size RC beams strengthened in shear by CFRP composites. They concluded that the increase in load carrying capacity depended on the quantity of the FRP strengthening, and was correlated to the stiffness of steel stirrups and FRP sheets. They found that the potential use of anchors might reduce the probability of FRP debonding since this type of failure was observed in all the beams strengthened by FRP sheets on their sides. Finally, they concluded that the contribution of CFRP sheets in shear strength of RC beams was less than the values calculated with the model proposed by Khalifa et al. (i.e. equation (2.12)). As a result, they proposed a new reduction factor that should be replaced with R in the model proposed by Khalifa et al.

Wong and Vecchio [83] reported that the externally bonded FRP composites could enhance the strength and stiffness of RC members and as a result could change the failure mode of shear-critical beams. They also concluded that the premature debonding of the FRP laminates must be prevented to avoid any reduction in RC beam ductility and to use the full capacity of the expensive composite materials.

Wang and Chen [17] proposed a discrete segment analysis and model to analyze the RC beams externally bonded with FRP laminates. The outcomes obtained by using this model were in good agreement with the experimental results.

Täljsten [20] has suggested that approximately 55% of the maximum measured strain value in FRP should be used for engineering design.

Reed and Peterman [23] used CFRP sheets for strengthening of prestressed concrete bridge girders and found CFRP stirrups could increase the shear capacity of the girders by nearly 30% compare to those with no shear strengthening. Zhang et al. [10] used CFRP laminates for shear strengthening of deep RC beams. They found that for deep beams with CFRP strips, when shear span to depth ratio (a/d) decreased, the shear contribution of vertical CFRP decreased, while on the other hand, the contribution of horizontal and 45° CFRP increased. They also concluded that the use of anchorage by

means of U-shaped CFRP wrapping scheme would greatly increase the shear capacity, but as a/d decreased, the anchorage in vertical direction did not seem to help the shear strength. They also introduced a reduction factor R that had to be applied to reduce the ultimate tensile stress of the CFRP laminates while calculating the shear strength of the deep RC beam. Zhang and Hsu [11] also proposed equations to calculate the shear contribution of CFRP laminates for continuous fiber sheets and strips.

Another design method has been recently proposed by Aprile and Benedetti [19] which can predict several failure modes including premature failure due to flexural or shear failure in external composite reinforcement. They have used an experimental database including 123 beams strengthened in flexure or shear to verify their proposed equation and found that the average error was in the order of 20%.

Deniaud and Cheng [2 and 9] studied the shear behavior of RC T-beams with externally bonded FRP sheets. They concluded that the amount of internal reinforcement would affect the contribution of the FRP sheets to the shear capacity of the T-beam. They also reported that the plane sections did not remain plane in the shear span when a certain load level was reached. All their 5 T-beams failed in shear by debonding and peeling-off the FRP sheets. They pointed out that triaxial glass fiber reinforcement was more effective than the unidirectional one to provide a ductile mode of failure.

T-girders strengthened in shear with CFRP fabric were tested by Chaallal et al. [6]. They found that as the number of CFRP layers was increased, the rate of increase and decrease of the strains diminished, resulting in a quasi-constant strain of approximately 0.004. This value has also been mentioned by ISIS Canada Design Manual No.4 [52] as the limiting value for $\varepsilon_{frp,e}$, while the Japan Building Disaster Prevention Association [84] has recommended a value of 0.007 for shear strengthening of RC beams with CFRP. They also proposed an equation to predict the contribution of CFRP to the ultimate shear capacity which was a function of shear span *a/d* ratio. They also concluded that CFRP fabric increased the ductility of the T-girders.

In-service evaluation of a reinforced concrete T-beam bridge FRP strengthening system has been reported by Hag-Elsafi et al. [85]. They concluded that the quality of the bond between the FRP laminates and concrete, and the effectiveness of the retrofit system have not been changed after two years in service.

Vougioukas et al. [86] used compressive-force path (CFP) and truss analogy (TA) methods to design RC beam-column joints repair or strengthening using FRP sheets. They have concluded that with the use of FRP sheets, designed in compliance with the CFP method, achieved the strength and ductility levels inherent in the levels of performance of current seismic provisions, whereas TA method could not always ensure that the design aims were fulfilled with the same level of reliability as the CFP method.

Islam et al. [21] showed that using an externally bonded FRP system in the beam web can increase the shear strength of deep RC beams effectively.

2.3. Design Codes for Shear Strengthening of RC Beams Using FRP Materials

There are different design codes available to calculate the contribution of FRP composites in shear strength of RC beams strengthened in shear. Here, a summary of these available equations are provided.

2.3.1 European *fib*-TG9.3: The *fib* (International Federation for Structural Concrete) Task Group on FRP composites has published a technical report in July 2001 [53] in which, the following equations are provided for shear strengthening of RC beams using externally bonded FRP:

$$V_{frp,d}[kN] = \frac{0.9}{\gamma_{frp}} E_{frp} \rho_{frp} \varepsilon_{frpk,e} b_w d(\cot\theta + \cot\alpha)\sin\alpha \qquad (2.26)$$

$$\varepsilon_{frpk,e} = k\varepsilon_{frp,e} \qquad (2.27)$$

$$\rho_{frp} = \frac{2t_{frp}\sin\alpha}{b_w} \tag{2.28}$$

$$\rho_{frp} = \left(\frac{2t_{frp}}{b_w}\right)\left(\frac{w_{frp}}{s_{frp}}\right) \tag{2.3}$$

where,

E_{frp} = elastic modulus of FRP in the principal fiber orientation, GPa

ρ_{frp} = FRP reinforcement ratio

w_{frp} = the width of the FRP strips, mm

s_{frp} = the spacing between FRP strips, mm

b_w = minimum width of cross section over the effective depth, mm

d = effective depth of cross section, mm

θ = angle of diagonal crack with respect to the member axis, assumed equal to 45°

α = angle between principal fiber orientation and longitudinal axis of member

k = reduction factor = 0.8

γ_{frp} = the partial safety factor is taken from Table 2.4 if failure involves FRP fracture (combined with or following diagonal tension), or = 1.3 if bond failure leading to peeling-off dominates.

$\varepsilon_{frp,e}$ = the mean value of the effective FRP strain and can be calculated using equations (2.7) to (2.9).

The equations provided by *fib*-TG9.3 [53] are derived from the work done by Triantafillou and Antonopoulos [25] with some minor modifications.

Table 2.4 – *FRP Material safety factor,* γ_{frp}

FRP type	Application type A [1]	Application type B [2]
CFRP	1.20	1.35
AFRP	1.25	1.45
GFRP	1.30	1.50

[1] Application Type A: Application of prefab FRP externally bonded reinforcement systems under normal quality control conditions. Application of wet lay-up systems if all necessary provisions are taken to obtain a high degree of quality control on both the application conditions and the application process.

[2] Application Type B: Application of wet lay-up systems under normal quality control conditions. Application of any system under difficult on-site working conditions.

2.3.2 Canadian ISIS Design Manual No.4: ISIS Canada (Intelligent Sensing for Innovative Structures) has published a design manual for strengthening RC structures with externally-bonded FRP composites [52]. The following equations are provided for shear strengthening of RC beams using externally bonded FRP:

$$V_{frp}[N] = \frac{\phi_{frp} E_{frp} \varepsilon_{frp,e} A_{frp} d_{frp} (\sin\beta + \cos\beta)}{s_{frp}} \tag{2.29}$$

$$A_{frp} = 2t_{frp} w_{frp} \tag{2.30}$$

$$\varepsilon_{frp,e} = \min(R.\varepsilon_{frp,u}, \frac{\alpha\phi_{frp} k_1 k_2 L_e}{9525}, 0.004) \tag{2.31}$$

$$R = \alpha\lambda_1 \left[\frac{f_c'^{2/3}}{E_{frp}\rho_{frp}} \right]^{\lambda_2} \tag{2.32}$$

$$\rho_{frp} = \frac{2t_{frp} w_{frp}}{b_w s_{frp}} \tag{2.33}$$

$$k_1 = \left[\frac{f_c'}{27.65}\right]^{2/3} \tag{2.34}$$

$$k_2 = \frac{d_{frp} - n_e L_e}{d_{frp}} \tag{2.35}$$

$$L_e = \frac{25350}{(t_{frp} E_{frp})^{0.58}} \tag{2.36}$$

$$s_{frp} \leq w_{frp} + \frac{d}{4} \tag{2.37}$$

where,

t_{frp} = total thickness of FRP reinforcement, mm

w_{frp} = the width of FRP shear reinforcement measured perpendicular to fibers, mm

ϕ_{frp} = resistance factor for FRP

E_{frp} = modulus of elasticity of FRP, MPa

$\varepsilon_{frp,e}$ = effective strain of FRP reinforcement

d_{frp} = effective depth of FRP strips, is measured from the free end underneath the slab to the bottom of the internal steel stirrups, or is equal to h when the section is totally wrapped, mm

β = angle between inclined FRP strips and the longitudinal axis of the member

s_{frp} = spacing of FRP shear reinforcement along the longitudinal axis of the member, mm

$\varepsilon_{frp,u}$ = ultimate strain of FRP reinforcement

α = reduction coefficient = 0.8

f_c' = specified compressive strength of concrete, MPa

b_w = minimum width of cross section over the effective depth, mm

n_e = number of free ends of an FRP stirrups on one side of the beam (=2 for FRPs on lateral faces, =1 for U-shaped FRPs)

d = distance from extreme compression face to the centroid of compression steel reinforcement, mm

$$CFRP \text{ rupture } \begin{cases} \lambda_1 = 1.35 \\ \lambda_2 = 0.30 \end{cases}$$

$$AFRP \text{ and } GFRP \text{ rupture } \begin{cases} \lambda_1 = 1.23 \\ \lambda_2 = 0.47 \end{cases}$$

2.3.3 CSA-S806-02: The Canadian Standard Association has published a manual for Design and Construction of Building Components involving Fibre-Reinforced Polymers [51]. The following equations are provided for shear strengthening of RC beams using externally bonded FRP:

$$V_F(N) = \frac{\phi_F A_F E_F \varepsilon_F d_f}{s_F} \tag{2.38}$$

where,

ϕ_F = resistance factor of FRP composites (= 0.75, CSA-S806-02: Clause 7.2.7.2)

A_F = cross-sectional area of FRP composite reinforcement or of unit width of continuous FRP wrap, mm^2

E_F = modulus of elasticity of FRP composite, MPa

ε_F = tensile strain at the level of FRP composites under factored loads; it is either 0.004 or 0.002:

$$\varepsilon_F = \begin{cases} 0.004 & \text{for U - shaped wrap continuous around the bottom of the web} \\ 0.002 & \text{for side bonding to the web (and only in cases where} \\ & \text{sufficient development length cannot be provided)} \end{cases}$$

d_f = distance from extreme compression fibre to centroid of tension reinforcement, mm

s_F = spacing of FRP shear reinforcement of a beam or unit width (i.e. 1.0) of a continuous FRP shear reinforcement, mm

2.3.4 ACI 440.2R-02: American Concrete Institute has also published a guide for the design and construction of externally bonded FRP systems for strengthening concrete structures [50]. An additional reduction factor ψ_f must be applied to the contribution of the FRP system. For bond-critical shear reinforcement (three-sided U-wraps or bonded face plies), a value of 0.85 is recommended for ψ_f, while 0.95 is recommended for contact-critical shear reinforcement (completely wrapped members). The following equations are provided for shear strengthening of RC beams using externally bonded FRP:

$$V_f(N) = \frac{A_{fv} f_{fe} (\sin\alpha + \cos\alpha) d_f}{s_f} \tag{2.39}$$

$$A_{fv} = 2nt_f w_f \tag{2.40}$$

$$f_{fe} = \varepsilon_{fe} E_f \tag{2.41}$$

for completely wrapped around members:

$$\varepsilon_{fe} = 0.004 \le 0.75\varepsilon_{fu} \tag{2.42}$$

for U-wraps and bonding on two sides:

$$\varepsilon_{fe} = \kappa_v \varepsilon_{fu} \le 0.004 \tag{2.43}$$

$$\kappa_v = \frac{k_1 k_2 L_e}{11900\varepsilon_{fe}} \le 0.75 \tag{2.44}$$

$$L_e = \frac{23300}{(nt_f E_f)^{0.58}} \tag{2.45}$$

$$k_1 = \left(\frac{f_c'}{27}\right)^{2/3} \tag{2.46}$$

$$k_2 = \begin{cases} \dfrac{d_f - L_e}{d_f} & \text{for U - wraps} \\ \dfrac{d_f - 2L_e}{d_f} & \text{for two sided wraps} \end{cases} \tag{2.47}$$

where,

n = number of plies of FRP reinforcement

t_f = nominal thickness of one ply of the FRP reinforcement, mm

w_f = width of the FRP reinforcement plies, mm

ε_{fe} = effective strain level in FRP reinforcement; strain level attained at section failure, mm/mm

E_f = tensile modulus of elasticity of FRP, MPa

ε_{fu} = design rupture strain of FRP reinforcement, mm/mm

f_c' = specified compressive strength of concrete, MPa

d_f = depth of FRP shear reinforcement as shown in Figure 2.1, mm

α = angle of inclination of stirrups, degrees

s_f = spacing FRP shear reinforcement as described in Figure 2.1, mm

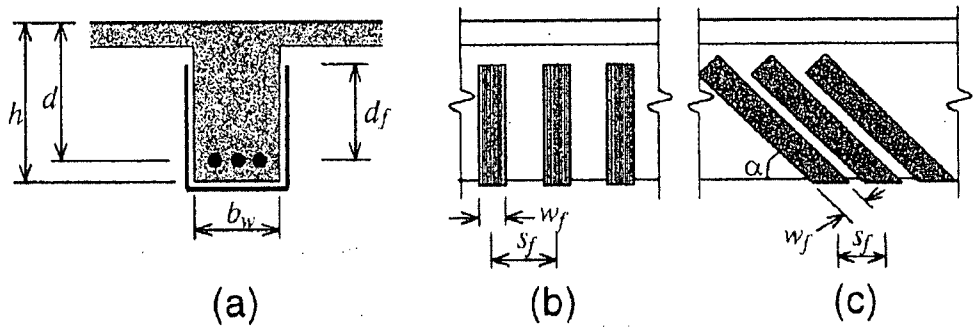

Figure 2.1 – *Dimensional Variables used in Shear-Strengthening using FRP Laminates [50]*

2.4. Behavior of RC beams under Impact Loading

Impact and impulsive loadings can be important for some structures. Examples of these loadings include: vehicle, aircraft or ship accident; falling and swinging objects; flying objects generated by explosion; extreme water-wave action; internal or external gaseous explosion; extreme wind loading; and detonation of highly explosive materials.

Material properties will change under high strain rates of loading. As a result, RC beams made of reinforcing bars and concrete will response differently at different loading rates. The earliest dynamic tests on concrete in compression date back to 1917 [87]. After many years of inactivity, more dynamic tests on concrete have been carried out in the past 50 years. Many researchers such as Atchley and Furr [88], Scott et al. [89], Dilger et al. [90], Malkar et al. [91], and Soroushian et al. [92] found an increase of about 25% in both stress and strain at failure by increasing the rate of loading, while other researchers such as Watstein [93] and Malvar and Ross [94] reported 85% and sometimes more than 100% increase in compressive strength of concrete under dynamic loads. Concrete static compressive strength [88], aggregate type [95] and concrete condition (i.e. wet versus dry) [96] also affect the strain-rate sensitivity of concrete compressive strength. In general, the lower the static concrete strength, the higher the strength gain due to strain rate. Also the faster the material is strained, a higher dynamic strength gain is expected. For the dynamic strength of the concrete, f'_{cd}, US Department of the Army Technical Manual [97] suggests a 25% increase over the static concrete strength, f'_c.

The tensile strength of concrete, as reported by Malvar and Ross [94], is more sensitive to strain rates compare to its compressive strength. They reported a 600% increase in concrete tensile strength when the strain rate was increased from 10^{-6} s^{-1} to 200 s^{-1}. They proposed the following equations for the effect of high strain rates on tensile strength of concrete:

$$DIF = \frac{f_{td}}{f_{ts}} = \left(\frac{\dot{\varepsilon}}{\dot{\varepsilon}_s}\right)^{\delta} \qquad if \ \dot{\varepsilon} \le 1s^{-1} \qquad (2.48)$$

$$DIF = \frac{f_{td}}{f_{ts}} = \beta\left(\frac{\dot{\varepsilon}}{\dot{\varepsilon}_s}\right)^{1/3} \qquad if \ \dot{\varepsilon} > 1s^{-1} \qquad (2.49)$$

where,

$\log \beta = (6\delta) - 2$

$$\delta = \frac{1}{1 + 8\left(\frac{f_c^{'}}{f_{co}^{'}}\right)}$$

$DIF = \frac{f_{td}}{f_{ts}}$ = Dynamic Increase Factor

f_{td} = dynamic tensile strength of concrete, MPa

f_{ts} = static tensile strength of concrete, MPa

$\dot{\varepsilon}$ = high strain rate up to 10^4 s^{-1}

$\dot{\varepsilon}_s$ = static strain rate between 10^{-6} to 10^{-5} s^{-1}

$f_c^{'}$ = compressive strength of concrete, MPa

$f_{co}^{'}$ = fraction of the compressive strength of concrete, can be assumed 10MPa

Strain-rate sensitivity of steel has also been studied and reported by researchers [98 - 99]. A review of loading rate effects on concrete and reinforcing steel [100] indicates that the modulus of elasticity and ultimate strain of reinforcing bars both remain nearly constant, but yield stress and strain increase with rate. Malvar [101] proposed the following equations for the effect of high strain rates on yield and ultimate strengths of reinforcing bars:

$$DIF_{yeild\ stress} = \frac{f_{yd}}{f_{ys}} = \left(\frac{\dot{\varepsilon}}{10^{-4}}\right)^{[0.074-0.04\left(\frac{f_{ys}}{414}\right)]} \quad (2.50)$$

$$DIF_{ultimate\ stress} = \frac{f_{ud}}{f_{us}} = \left(\frac{\dot{\varepsilon}}{10^{-4}}\right)^{[0.019-0.009\left(\frac{f_{ys}}{414}\right)]} \quad (2.51)$$

where,

$DIF_{yeild\ stress}$ = Dynamic Increase Factor to calculate dynamic yield stress of steel

$DIF_{ultimate\ stress}$ = Dynamic Increase Factor to calculate dynamic ultimate stress of steel

f_{yd} = dynamic yield stress of steel, MPa

f_{ys} = static yield stress of steel, MPa

f_{ud} = dynamic ultimate stress of steel, MPa

f_{us} = static ultimate stress of steel, MPa

$\dot{\varepsilon}$ = strain rate, s^{-1}

Since compressive (and tensile) strength of concrete and yield strength of steel will increase when loaded at a high strain-rate, it is apparent that increasing the strain-rate will increase the flexural capacity of reinforced concrete beams. Bertero et al. [102] tested simply supported beams at high strain-rates of 0.004 s^{-1} and 0.04 s^{-1}. They found that both stiffness and moment capacity of RC beams would increase at high strain-rates. They cautioned that this increase might change the failure mode from ductile flexural failure to a brittle shear failure mode when sufficient shear reinforcement was not provided. Similar findings were also reported by Takeda et al. [103].

Wakabayashi et al. [99] also performed dynamic tests on RC beams under a high strain-rate of 0.01 s^{-1}. They found that load carrying capacity of RC beams increased by about 30% when a high strain-rate loading was applied. They also found that the

compressive strength of concrete and the tensile strength of steel increased linearly with the logarithm of strain-rate.

Banthia [104] used a drop weight impact machine to carry out impact tests on RC beams. He found that the peak bending loads obtained under impact loading were higher than those obtained under static loading. He pointed out that after a certain hammer drop height, increase in the peak bending loads was not significant. He also concluded that shear reinforcement enhanced the impact resistance of RC beams by confining the concrete and increasing the beam's ductility. For RC beams made of high strength concrete, he found that an increase in the stress-rate decreased their rigidity and hence, their ductility, and contrary to the behavior of normal strength RC beams, an increase in the drop hammer height actually reduced the fracture energy.

Bentur et al. [105] rightly mentioned that the inertial loading (i.e. the load required to accelerate the specimen) effect must be separated from the total load measured by the instrumented tup. They concluded that in many instances, only a small portion of the total load was involved in beam bending itself.

Kishi et al. [106] studied the ultimate strength of flexural-failure-type RC beams under impact loading. They tested 8 simply supported RC beams with a clear-span of 2 m. Impact tests were performed using a free-falling 200 kg steel weight onto the mid-span. They recorded impact force experienced by the falling steel weight, reaction forces at the supports, and the mid-span deflection, while impact velocity (1 m/s to 6 m/s), rebar ratio (0.42% to 2.98%) and cross-sectional area of the beams (160 × 240, 200 × 220 and 160 × 160) were taken as variables. The $\frac{V_{usc}}{P_{usc}}$ was in the range of 1.90 to 6.04, where V_{usc} is static shear capacity (kN) and P_{usc} is the static bending capacity (kN). They assumed that when the cumulative residual displacement of RC beam approached 2% of its clear-span, the ultimate failure occurred. They also noticed that the impact force increased very rapidly up to a maximum value at the very beginning of the test and decreased to almost zero, irrespective of the beam type. In contrast, they observed that

the reaction force (evaluated as summing up the values recorded by the supports) increased linearly to a maximum value and then stayed at almost the same value until the displacement reached its maximum value, and then decreased to zero. They assumed a parallelogram for reaction-displacement relationship. From these observations they concluded that the maximum reaction force, instead of the maximum impact force, should be used to estimate the RC beam flexural strength under impact loading. They found that the maximum reaction force for all RC beams exceeded 2 times their static bending capacity. They also calculated that the input kinetic energy to RC beams was 1.1 to 2.0 times higher than the absorbed energy by beams during the failure (area under the reaction force vs. mid-span displacement).

Ando et al. [107] performed impact tests on RC beams without stirrups using a falling weight. The RC beams tested in their program were simply supported and the impact load was applied at the mid-span of the beams using a 300 kg steel weight. They used instrumented supports to record reaction forces of the RC beams during the impact loading. The velocity of this weight at the point of impact was 1, 2, 3, 5 and 6 m/s. At 1m/s, the beam reacted elastically, but for higher velocities loads entered the elasto-plastic region and/or ultimate state. Reinforcing bar ratios of 0.0182 and 0.008 were used for a cross-section of 150 mm × 250 mm with different spans of 1 m, 1.5 m, and 2 m. They concluded that when shear/bending capacity ratio was less than 1.0, RC beams collapsed from severe diagonal cracks developed from the loading point (i.e. mid-span) to the supports. Reaction force was linearly increased to a maximum and after that it was gradually decreased. The hysteresis loop of reaction force versus mid-span displacement could be assumed as a triangle. Finally, they observed that for RC beams without stirrups, when shear type failure occurred, the ratio of R_{ud} / P_{us} (R_{ud}= maximum reaction force in dynamic loading, P_{us}= static shear capacity obtained from static loading test) was in the range of 1.0 to 1.5. They then concluded that essentially the impact shear capacity of RC beams was equal to their static shear capacity.

In another study Kishi et al. [108] tested 19 simply supported RC beams all of them 200 mm × 400 mm × 2400 mm in dimensions. An impact load was applied at mid-span

by dropping a 400 kg steel weight. They also used instrumented supports to record reaction forces of the RC beams during the impact loading. Tensile reinforcing bar ratio for all beams was 0.027 but different shear reinforcing bar ratios were used (i.e. 0.0, 0.002, and 0.004). For all beams, the static bending capacity was higher than static shear capacity, meaning that they should fail in shear. They observed that the reaction force, irrespective of beam type, increased almost linearly to an absolute maximum value with an increment of the impact velocity. After this point, the reaction force did not increase by increasing the impact velocity. Contradictory to Ando et al. [107], they found that the ratio of R_{ud} / P_{us} for all RC beams were in the range of 2.7 to 3.1 (this ratio was reported in the range of 1.0 to 1.5 by Ando et al. [107]).They concluded that when static bending capacity was higher than static shear capacity, the impact-resistant design for shear-failure-type RC beams could be performed by using the static shear capacity.

Kishi et al. [109] also studied impact behavior of shear-failure-type RC beams without shear rebar. All RC beams were of 150 mm width and 250 mm depth in cross section, with rebar and shear-span ratios taken as variables. An impact load was applied at the mid-span of the RC beam by dropping a free-falling 300 kg steel weight. They assumed that an RC beam reached its ultimate state when it was split into two or three parts due to diagonal cracks developed from the loading point at the mid-span to the supports. They used load cells at the supports and at the impact point (steel weight) and observed:

1. A high-frequency component in the impact force at the very beginning of the impact force.
2. When impact force reached its maximum value, no deflection was yet recorded at the mid-span.
3. Primary stiffness estimated using the reaction force was similar to that of static loading.
4. The reaction force wave behaved similar to the displacement wave.

From these observations, they suggested that the impact-resistant capacity may be more rationally estimated by the maximum reaction force rather than using the maximum impact force. Banthia [104] and Bentur et al. [105], as mentioned earlier, also pointed out that the maximum impact force was not the real beam bending force. As a result, they used the maximum reaction force of RC beams in their analysis. They found that the values of R_{ud} / P_{us} for all beams were in the range of 1.0 to 1.5, whereas the values of R_{ud} / V_{us} were distributed from 1.5 to 2.5. (R_{ud}= maximum reaction force in dynamic loading, P_{us}= static shear capacity obtained from static loading test, and V_{us}= calculated shear capacity using a conventional prediction equation). They concluded that the impact shear capacity of an RC beam could be considered 50% higher than its calculated static shear capacity. The suggested that shear-failure-type RC beams without shear reinforcement and under impact loading could be designed with a certain safety margin by assuming a dynamic response ratio ($\frac{\text{maximum dynamic reaction force}}{\text{required static shear capacity}}$) of 1.5 and absorbed input energy ratio ($\frac{E_a}{E_k}$) of 0.6, where E_a is the absorbed energy estimated using the loop-area of the reaction force vs. displacement curve, and E_k is the input kinetic energy ($=\frac{1}{2}mV^2$, m : mass of the steel weight, V : impact velocity).

Abbas et al. [110] proposed a three-dimensional nonlinear finite element analysis of reinforced concrete targets under impact loading. They showed that their model was capable of carrying out impact analysis and predict cracking.

2.4. Behavior of RC Beams Strengthened with Externally Bonded FRP Composites under Impact Loading

As mentioned earlier, there are only a limited number of studies available where RC beams strengthened with externally bonded FRP were investigated. Jerome and Ross [111] tested laboratory-scale plain-concrete beams (76 mm × 76 mm × 760 mm with

no reinforcing bars) which were impulsively loaded to failure in a drop-weight impact machine. The beams were externally reinforced on their tension (bottom) side or on their three sides excluding the top surface by CFRP laminates. They observed that the average peak amplitude of the tup load increased with an increase in drop height, along with associated increases in the peak inertial load and peak bending load. They calculated the bending load as the difference between the tup load and the inertial load and concluded that for beams externally reinforced with CFRP, the average dynamic peak bending load was always greater than the static peak bending load, even at low drop heights. They mentioned that for a given drop height, a beam had a fixed capacity to absorb energy. They also reported that the failure mechanism did not change when the tests were performed quasi-statically or dynamically.

Erki and Meier [58] tested four 8 m beams externally strengthened for flexure, two with CFRP laminates and two with steel plates. They presented impulse loading experiments on strengthened beams by raising up one end of the beam and dropping it on the support. They found that although RC beams externally strengthened for flexure with CFRP laminates performed well under impact loading, they could not provide the same energy absorption as beams externally strengthened with steel plates. They recommended that additional anchoring of the CFRP laminates should be used to improve the impact resistance of the beam. In their tests, CFRP laminates failed by debonding.

Eight 3 m RC beams strengthened with CFRP laminates in flexure were tested by White et al. [59] under impact loading. The beams were tested in four-point bending. They concluded that:

1. CFRP laminates increased the flexural capacity and stiffness of strengthened RC beams but reduced their energy absorption capacity and ductility.

2. The amount of CFRP reinforcement, steel reinforcement, and failure mode affected the contribution of CFRP laminates in flexural strengthening of RC beams under impact loading.

3. A 5% increase in flexural capacity, stiffness, and energy absorption was observed for CFRP strengthened beams rapidly strained (dynamic loading) over similar beams loaded slowly (quasi-static loading).

Tang and Saadatmanesh [57] studied the impact effects on concrete beams strengthened with FRP laminates. Carbon or Kevlar FRP laminates were bonded to the top and bottom faces of concrete beams with epoxy. 5 beams were tested in total: 2 strengthened with Kevlar, 2 with carbon and one control unretrofitted beam. They observed that the capacity of concrete beams to resist impact loading and reduce the maximum deflection was increased when FRP laminates were applied. They also noticed that the stiffer carbon FRP laminates reduced the deflection.

Tang and Saadatmanesh [56] also tested 27 beams; 5 beams containing steel reinforcement (reported in [57]) and 22 beams with no steel reinforcement. Carbon or Kevlar FRP laminates were bonded to the top and bottom faces of concrete beams using epoxy. The impact force was delivered with a steel drop weight. They concluded that while the ultimate load in static loading was much less than that cylindrical in shape under impact loading (i.e. the sum of the reaction forces), the ultimate deflection of the beam under static loading was larger that of the beam under impact loading. They suggested that the use of bidirectional composite laminates can control the longitudinal cracking in concrete beams.

Hamed and Rabinovitch [60] modelled the dynamic behavior of RC beams strengthened in bending with externally bonded FRP composites. Simulations were performed under three types of dynamic loads including impulse load, harmonic load, and seismic base excitation.

As mentioned earlier, there is no report available yet on the behavior of shear-strengthened RC beams under impact loading. The work reported in this dissertation is therefore the first of its kind.

3

MATERIALS

3.1. Concrete

In this study, all concrete mixes had the same amounts of sand, aggregate, water and cement. Mixture proportions are given in Table 3.1. For each mixture, four 100×200 mm cylinders were cast in a standard way. Compaction of concretes was achieved by using a vibrating table. Specimens were de-molded after 24 hours and stored for an additional 28 days at 23±3°C and 100% relative humidity. Concrete cylinders were tested under compression while concrete beams were prepared for strengthening using externally bonded FRP. No admixture was used in making the concrete specimens.

Table 3.1 – *Concrete mix proportions*

Component	kg/m^3 of Concrete
Water	186
Portland Cement	310
Fine Aggregate	950
Coarse Aggregate	950

3.1.1 Water

All mixing water was taken directly from the City of Vancouver drinking water supply.

3.1.2 Portland Cement

CSA Type 10 (ASTM Type I) Normal Portland cement manufactured by Lafarge Canada Inc. was used throughout the research. Proper care was taken to ensure that only cement not exceeding a certain age was used in order to keep consistency in the property of hardened concrete.

3.1.3 Fine Aggregate (Sand)

Saturated Surface-Dry (SSD) clean river sand with a fineness modulus of about 2.5 was used in all mixtures. The concrete sand was purchased from Lafarge Canada Inc. and had a relative density of 2.70 and an SSD absorption value of 1.0%.

3.1.4 Coarse Aggregates (Gravel)

Crushed gravel with a maximum size of 14 mm was used in all mixtures. This aggregate was also purchased from Lafarge Canada Inc. It had a relative density of 2.71, an SSD absorption value of 1.24% and a dry rodded density of 1550 kg/m^3 (ASTM C 127 [112]).

3.2 GFRP Spray System

In this section the general description and characteristics of the GFRP spray components are discussed. The GFRP spray system includes resin, catalyst, coupling agent, and glass fiber.

3.2.1 Resin

The resin used throughout the research was the AROPOL 7241T-15 polyester resin manufactured by Ashland Specialty Chemicals. Physical and mechanical properties of this resin are listed in Table 3.2

Table 3.2 – *Physical and mechanical properties of polyester resin*

Property	Value	Unit
Density of liquid	1.07	gr/cm^3
Density of solid	1.17	gr/cm^3
Tensile strength	62	MPa
Tensile modulus	3.65	GPa
Elongation at break	2.5	%
Flexural strength	105	MPa
Flexural modulus	40.7	GPa

3.2.2 Catalyst

The catalyst which was used to initiate curing of the resin was Methyl Ethyl Ketone Peroxide (MEKP) also manufactured by Ashland Specialty Chemicals. MEKP was added as 3% by volume of polyester resin (average value). This provided a gel time of approximately 15 minutes at 20°C. At higher temperatures a lesser amount and at lower temperature a higher amount of MEKP was used. In general, 2 to 4% catalyst content was used, depending on the conditions. In general, a 15 minutes gel time was the target.

3.2.3 Coupling Agent

ATPRIME® 2, manufactured by Reichhold Company, was used as the coupling agent to improve the GFRP to concrete bond. ATPRIME® 2 is a two-component urethane-based primer system which can be applied with a brush or roller to prepared surfaces to form chemical bonding. The two components of ATPRIME® 2 must be mixed before using. One part of ATPRIME® 2A by weight should be mixed with four parts of ATPRIME® 2B by weight. The mixture can be used after 30 minutes. The pot life of blended ATPRIME® 2 is approximately 12 hours at 27°C and 50% relative humidity. Specific gravity of ATPRIME® 2A is 1.23 and ATPRIME® 2B is 1.01. One kilogram of blended ATPRIME® 2 covers approximately 10 to 20 m^2 of surface area. A minimum of 2 hours at ambient temperature is needed to allow the primer to be cured. Polyester resin can be applied over the cured, primed surface, but if the primed surface is

left for more than 24 hours, re-application will be necessary to obtain full interlaminar bond strength.

3.2.4 Glass Fiber Rovings

The glass fiber used in the GFRP spraying system was Advantex® 360RR chopper roving manufactured by Owens Corning. It is an improved form of E-glass. The roving format refers to a number of continuous glass filaments which are gathered together into a single bundle or yarn, without the introduction of a mechanical twist. These rovings are then wound and packaged in a tubeless configuration specifically designed for use with the chopper gun application technique used here. Physical and mechanical properties of this glass fiber roving are listed in Table 3.3.

Table 3.3 – *Physical and mechanical properties of Advantex® glass fiber*

Property	Value	Unit
Density	2624	kg/m^3
Diameter	9-30	μm
Tensile strength	3200-3750	MPa
Elastic modulus	80	GPa
Elongation at break	4.5	%

3.3 GFRP Fabric (Wabo®MBrace) System

In this section the general description and characteristics of the GFRP Wabo®MBrace are discussed. The GFRP Wabo®MBrace system includes primer, putty, saturant, and glass fiber all manufactured by Degussa Construction Chemicals [113].

3.3.1 Primer

Wabo®MBrace primer is a low viscosity, 100% solids, polyamine cured epoxy. As the first applied component of the Wabo®MBrace system, this primer is used to penetrate the pore structure of cementitious substrate and to provide a high bond base coat for the Wabo®MBrace system. As per manufacturer's recommendations, the

substrate must be thoroughly cured dry, and free of oils, curing solutions, mold release agents, and dust at the time of application. Wabo®MBrace primer consists of two components,; part A and part B. Mix ratio by volume is 3 to 1 and by weight is 100 to 30 (Part A to Part B). Part A and part B should be blended using a mechanical mixer until a homogeneous mixture is achieved which requires approximately 3 minutes mixing time. Wabo®MBrace primer can be applied when the temperature is between 10°C and 50°C. Physical and mechanical properties of Wabo®MBrace primer are listed in Table 3.4.

Table 3.4 – *Physical and mechanical properties of Wabo®MBrace primer [113]*

Property	Value	Unit
Density	1102	kg/m^3
Installed thickness (approx)	0.075	mm
Tensile yield strength	14.5	MPa
Tensile strain at yield	2.0	%
Tensile elastic modulus	717	MPa
Tensile ultimate strength	17.2	MPa
Tensile rupture strain	40	%
Poisson's ratio	0.48	----
Compressive yield strength	26.2	MPa
Compressive strain at yield	4.0	%
Compressive elastic modulus	670	MPa
Compressive ultimate strength	28.3	MPa
Compressive rupture strain	10	%
Flexural yield strength	24.1	MPa
Flexural strain at yield	4.0	%
Flexural elastic modulus	595	MPa
Flexural ultimate strength	24.1	MPa
Flexural rupture strain	Large deformation with no rupture	%

3.3.2 Putty

Wabo®MBrace putty is a 100% solids non-sag epoxy paste for use with the Wabo®MBrace composite strengthening system. It is used to level the surface and to provide a smooth surface to which the Wabo®MBrace saturant will be applied. Wabo®MBrace putty consists of two components,; part A and part B. Mix ratio by volume is 3 to 1 and by weight is 100 to 30 (Part A to Part B). Wabo®MBrace putty can be applied before or after the primer coat has achieved full cure, but should be applied within 48 hours of applying the Wabo®MBrace primer to the substrate to ensure proper adhesion. Surface with a tack-free primer coat must be cleaned of any dust, oils, or other surface contaminates. Part A and part B must be mechanically premixed separately for 3 minutes. After premixing, Part A and part B should be blended using a mechanical mixer until a homogeneous mixture is achieved which requires approximately 3 minutes additional mixing time. As per manufacturer's recommendations, Wabo®MBrace putty should be applied to the primed substrate using a spring-steel trowel, and should be used only to fill small voids and smooth small offsets in the substrate. Thick applications of the Wabo®MBrace putty are not recommended. Wabo®MBrace putty can be applied when the temperature is between 10°C and 50°C. Physical and mechanical properties of Wabo®MBrace putty are listed in Table 3.5 [113].

Table 3.5 – *Physical and mechanical properties of Wabo®MBrace putty [113]*

Property	Value	Unit
Density	1258	kg/m^3
Tensile yield strength	12	MPa
Tensile strain at yield	1.5	%
Tensile elastic modulus	1800	MPa
Tensile ultimate strength	15.2	MPa
Tensile rupture strain	7	%
Poisson's ratio	0.48	----
Compressive yield strength	22.8	MPa
Compressive strain at yield	4	%
Compressive elastic modulus	1076	MPa
Compressive ultimate strength	22.8	MPa
Compressive rupture strain	10	%
Flexural yield strength	26.2	MPa
Flexural strain at yield	4	%
Flexural elastic modulus	895	MPa
Flexural ultimate strength	27.6	MPa
Flexural rupture strain	7	%

3.3.3 Saturant

Wabo®MBrace saturant is a 100% solids, low viscosity epoxy material that is used to encapsulate Wabo®MBrace carbon, glass, or aramid fiber fabrics. Wabo®MBrace saturant provides a high performance FRP laminate when reinforced with the fibers. Wabo®MBrace saturant consists of two components,; part A and part B. Mix ratio by volume is 3 to 1 and by weight is 100 to 34 (Part A to Part B). Wabo®MBrace saturant should be applied to substrates prepared with Wabo®MBrace primer and Wabo®MBrace putty. Wabo®MBrace saturant can be applied before or after the primer and putty coats have achieved full cure, but should be applied within 48 hours of applying the Wabo®MBrace putty to the substrate to ensure proper adhesion. Surface with a tack-free primer/putty coat must be cleaned of any dust, oils, or other surface contaminates. Part A

and part B must be mechanically premixed separately for 3 minutes. After premixing, Part A and part B should be blended using a mechanical mixer until a homogeneous mixture is achieved which requires approximately 3 minutes additional mixing time. As per manufacturer's recommendations, Wabo®MBrace saturant can be applied using a ⅜" nap roller. Wabo®MBrace saturant can be applied when the temperature is between 10°C and 50°C. Physical and mechanical properties of Wabo®MBrace saturant are listed in Table 3.6.

Table 3.6 – *Physical and mechanical properties of Wabo®MBrace saturant [113]*

Property	Value	Unit
Density	983	kg/m^3
Tensile yield strength	54	MPa
Tensile strain at yield	2.5	%
Tensile elastic modulus	3034	MPa
Tensile ultimate strength	55.2	MPa
Tensile rupture strain	3.5	%
Poisson's ratio	0.40	----
Compressive yield strength	86.2	MPa
Compressive strain at yield	5	%
Compressive elastic modulus	2620	MPa
Compressive ultimate strength	86.2	MPa
Compressive rupture strain	5	%
Flexural yield strength	138	MPa
Flexural strain at yield	3.8	%
Flexural elastic modulus	3724	MPa
Flexural ultimate strength	138	MPa
Flexural rupture strain	5	%

3.3.4 Glass Fiber Fabrics

Wabo®MBrace E-glass fiber fabrics are dry fabrics constructed of high quality E-glass fibers. Physical and mechanical properties of Wabo®MBrace E-glass fiber fabric (EG 900) are listed in Table 3.7 [113].

Table 3.7 – *Physical and mechanical properties of Wabo®MBrace E-glass fiber fabric (EG 900) [113]*

Property	Value	Unit
Density	2600	kg/m^3
Nominal thickness	0.353	mm/ply
Ultimate tensile strength	3600	MPa
Tensile elastic modulus	80	GPa
Ultimate rupture strain	4.5	%

4

GFRP APPLICATION PROCESS

4.1 Introduction

There are different techniques available to apply externally bonded FRP composites on the surface of concrete structural members. Since in this study both spray and fabric systems were used, the application process for these two systems is discussed next.

4.2 GFRP Spray System

A Venus-Gusmer H.I.S. Chopper Unit equipped with a 'Pro Gun' spray gun was used in this research (Figure 4.1). It is portable equipment and can be used easily on-site. This system contains three major parts; a resin pump which pumps the polyester resin from the drum, a catalyst pump which pumps the Methyl Ethyl Ketone Peroxide (MEKP) to the nozzle, and a spray/chopper unit (Figure 4.2). To run this equipment, a compressed air source with a minimum capacity of 0.5 m^3/minute is required. There is no need for electrical power supply unless used in cold weather conditions (<16°C) when an electrical resin heater is required.

The resin and the catalyst are separately transported into the spray gun. They do not come into contact until they reach the mixing nozzle at the front of the gun. The catalyst content can be changed, but it is usually between 1 to 3% of the final mixture. This proportion will affect the time for curing the composite and is related to the temperature of the environment.

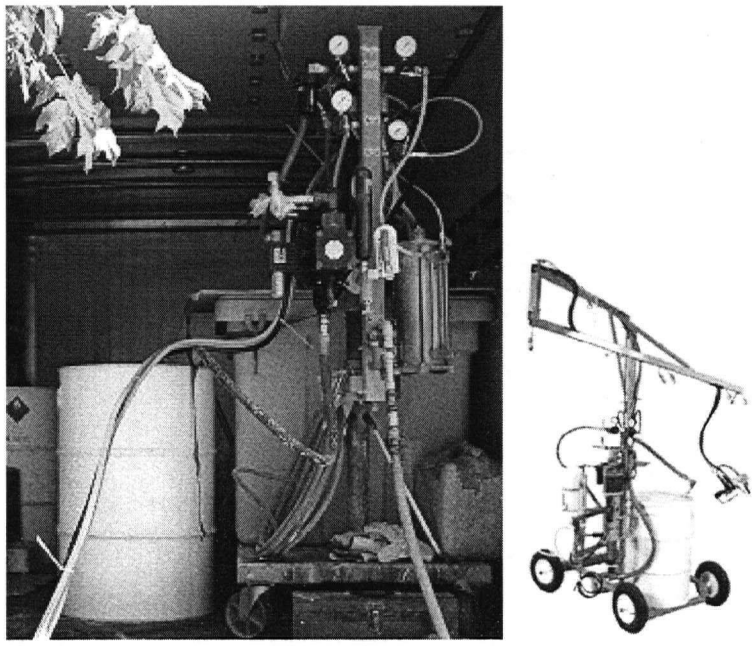

Figure 4.1 – *GFRP Spray Equipment*

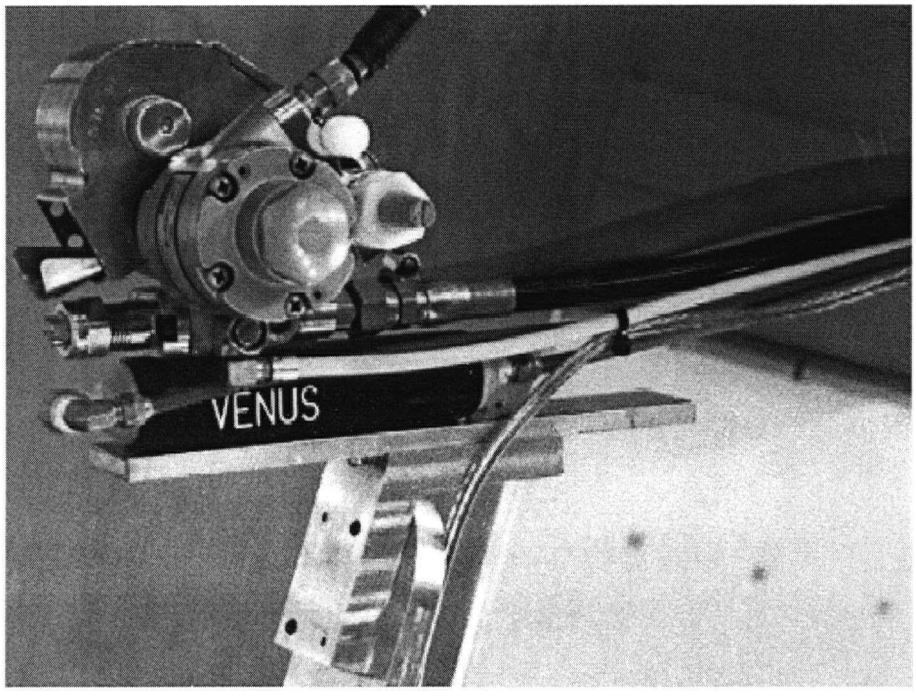

Figure 4.2 – *GFRP Spray/Chopper Unit*

At the nozzle, there are inlets for air and the solvent. Air powers the chopper unit and the solvent is used to flush the resin and catalyst at the end of each period of operation. The glass fibers in the form of roving (i.e. a large number of fibers bundled together) are brought to the chopper unit (Figure 4.3). One of the rollers inside the chopper unit has evenly spaced blades which cut the glass fibers into a prespecified length. By changing this roller (i.e. the number of blades on the roller) the length of the chopped fibers can be changed. The chopper unit used in this research project was able to produce chopped fibers from 8 to 48 mm in length. These chopped fibers are forced out by air flow. The rotation of the rollers inside the chopper unit also helps a smooth flow of fibers (Figure 4.4).

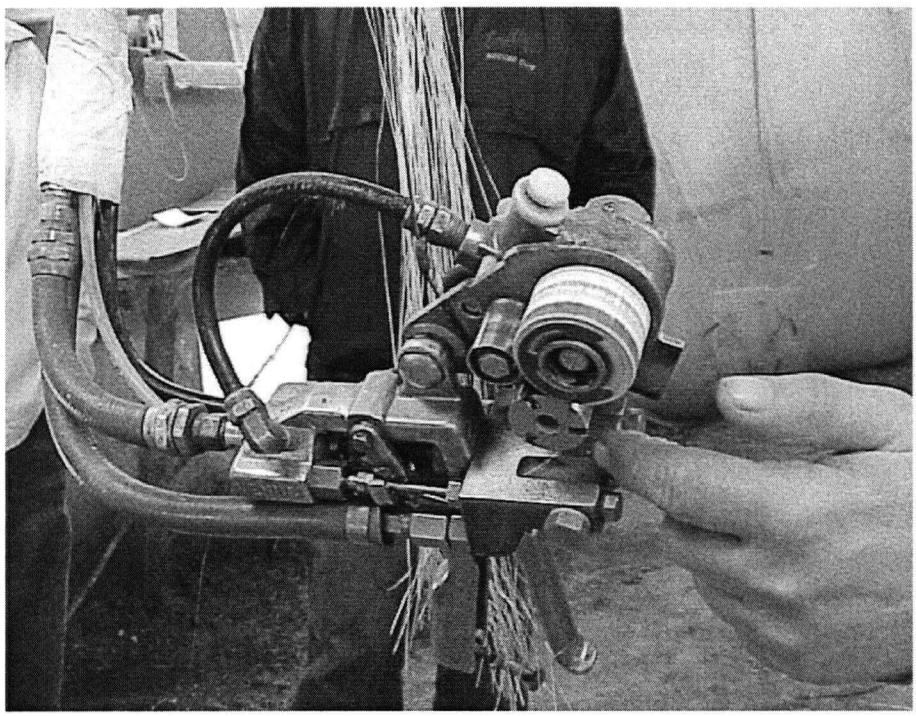

Figure 4.3 – *Chopper Unit*

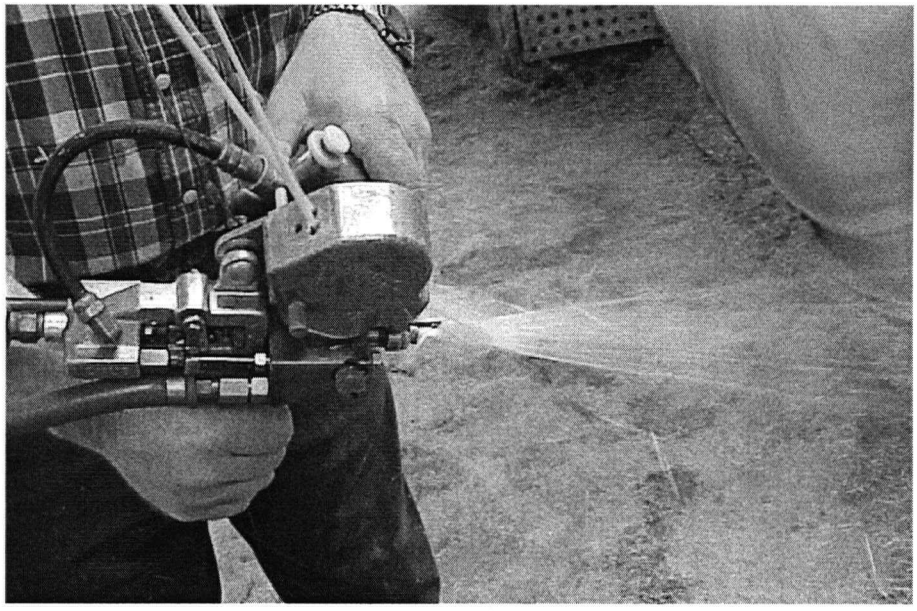

Figure 4.4 – *Spraying Chopped fibers*

The gun sprays the mixture of resin and catalyst with the chopped fibers onto the spraying surface (Figure 4.5). A spring steel roller is used to force out the entrapped air voids and to produce a consistent thickness (Figure 4.6). The final product is a 2-D randomly distributed fibers encapsulated by a catalyzed resin.

Figure 4.5 – *GFRP Spray*

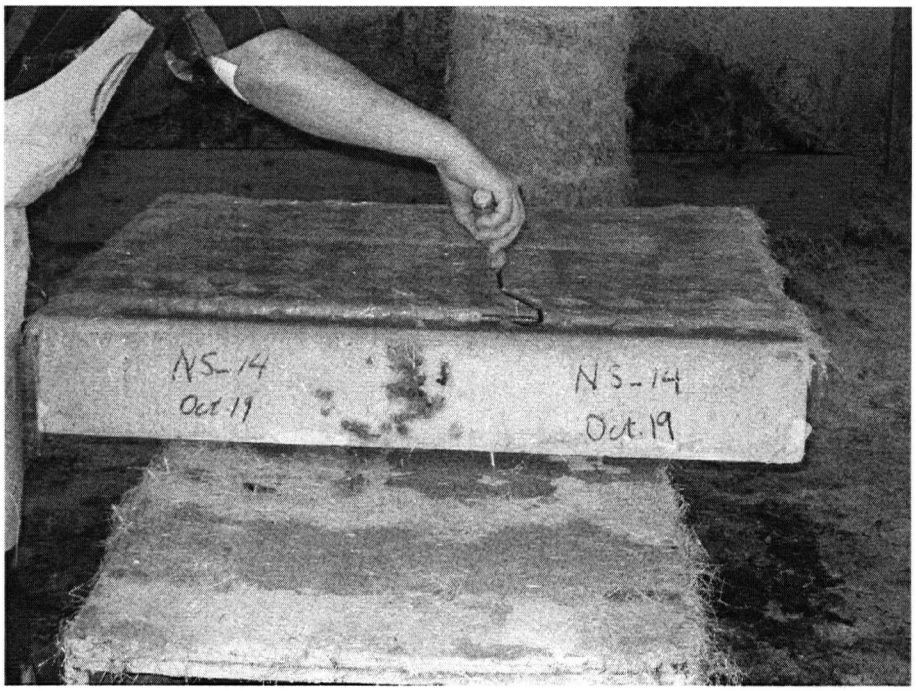

Figure 4.6 – *A Spring Steel Roller is used to force out entrapped air voids and to make a consistent thickness*

Although the operation of the GFRP spraying equipment is quite simple and straight forward, being able to produce an exact thickness of placement needs practice. It is also important to note that it is hard to apply Sprayed GFRP around sharp corners which is, comparatively speaking, even worse in the case of fabric GFRP. Depending on the fiber length, in general, all sharp corners should be rounded off to a minimum radius of 35 mm.

4.3 GFRP Fabric (Wabo®MBrace) System

In this study the Wabo®MBrace composite strengthening system, as an externally bonded GFRP system, was also used. The Wabo®MBrace fabric based system is installed by a technique known as wet lay-up. This technique involves applying the lightweight, flexible fiber fabrics onto a prepared surface of a structural member using uncured polymer resins. Once the resins cure, the result is a high strength bonded FRP

laminate. The following steps must be followed onto a properly prepared concrete surface to make a complete Wabo®MBrace system:

1. Wabo®MBrace Primer, a low viscosity, high solids epoxy is applied onto the concrete surface using a roller (see Figure 4.7).

2. Wabo®MBrace putty, a high solids, non-sag paste epoxy material is applied using a squeegee or trowel to level uneven surfaces (see Figure 4.8).

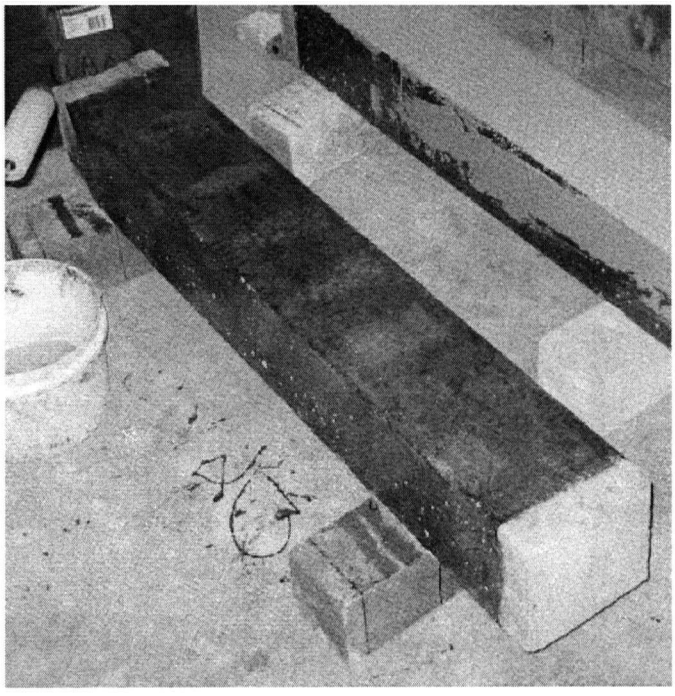

Figure 4.7 – *Wabo®MBrace Primer is applied on the beam's surface*

3. Wabo®MBrace saturant, a high solids resin is applied using a roller to begin saturation of the fiber reinforcement sheets.

4. Wabo®MBrace fiber reinforcement (see Figure 4.9), the backbone of the Wabo®MBrace composite strengthening system is placed into the first layer of wet saturant.

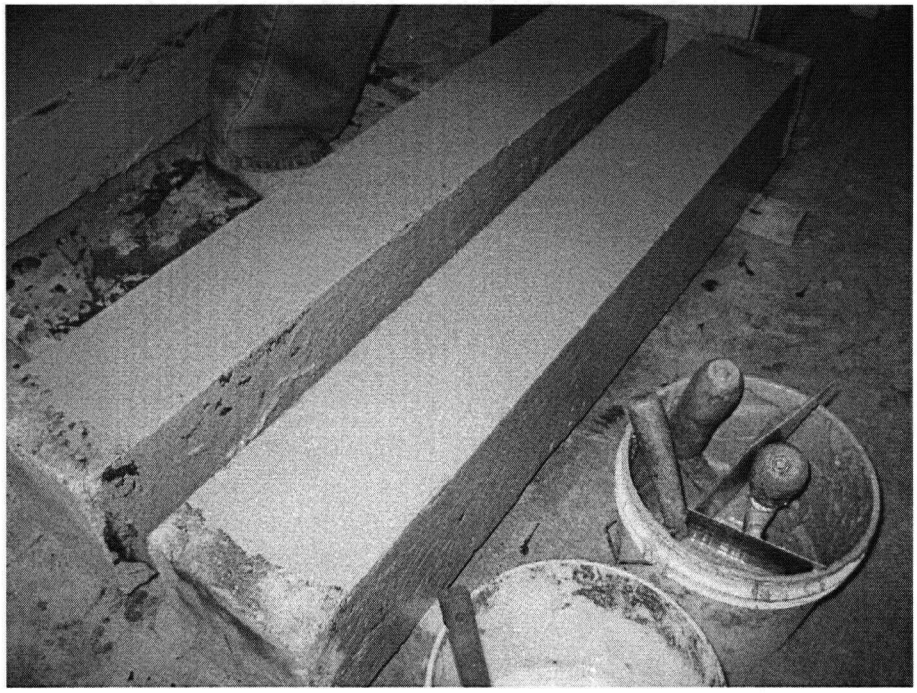

Figure 4.8 – *Wabo®MBrace Putty is applied on the beam's primed surface*

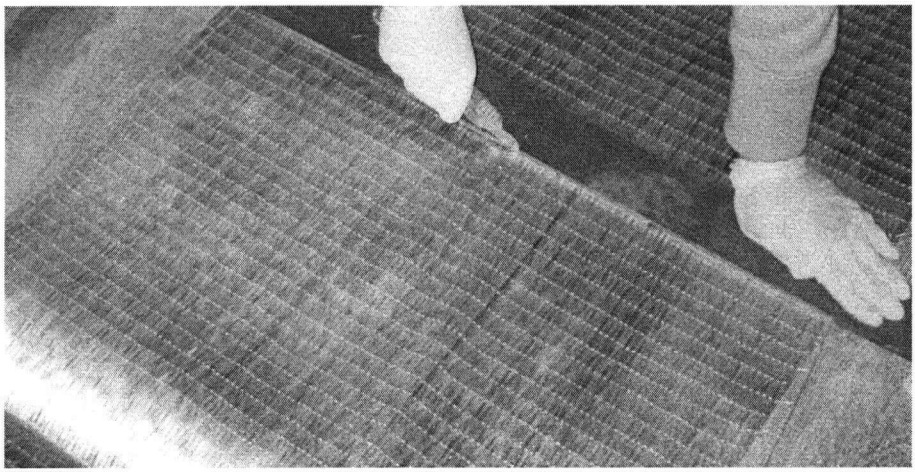

Figure 4.9 – *Wabo®MBrace E-glass fiber is getting cut in proper length*

5. The second coat of Wabo®MBrace saturant is applied using a roller. For multiple plies, steps 3, 4, and 5 should be repeated (see Figure 4.10).

6. Optional Wabo®MBrace topcoat, high solids, high gloss, corrosion-resistant topcoat is applied to provide a protective/aesthetic outer layer, where required. This step

was skipped in this research given that all the beams were tested shortly after strengthening.

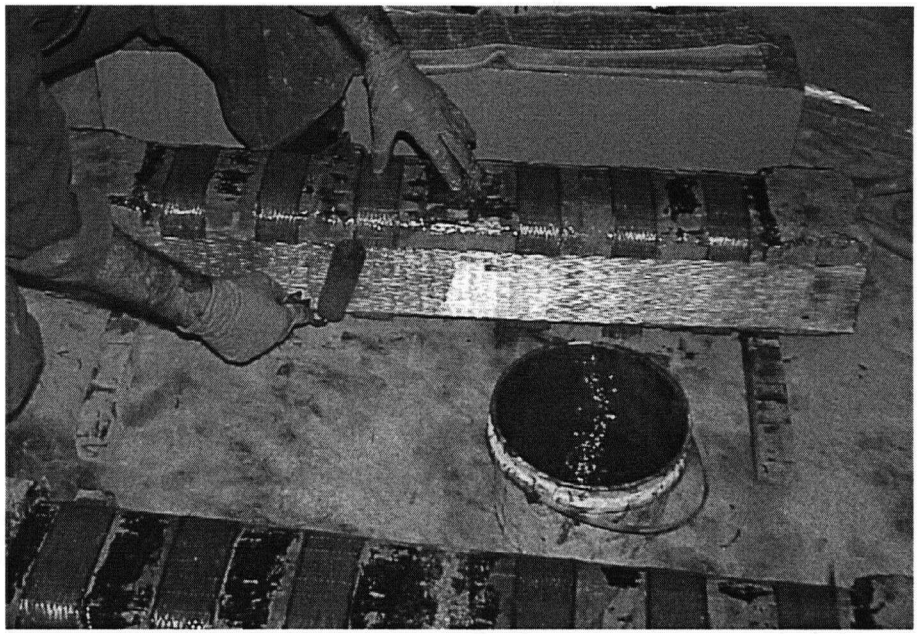

Figure 4.10 – *Wabo®MBrace Saturant and E-glass fiber fabric are applied on the beam's surface which was coated with primer and putty*

5

MATERIAL PROPERTIES

5.1 Fabric GFRP Properties

The properties of Wabo®MBrace EG 900 (unidirectional E-glass fiber fabric referred as fabric GFRP throughout this thesis), as per manufacturer's report are given in Table 5.1. From experience, the actual cured thickness of a single ply laminate (fiber plus saturating resin) is 1.0 to 1.5 mm. The tensile properties given here which can be used in design equations were derived by testing cured laminates as per ASTM D3039 [114]. The stress-strain relationship for this product is shown if Figure 5.1 [113].

Table 5.1 – *Wabo®MBrace EG 900 properties*

Tensile Properties	Value	Unit
Ultimate Tensile Strength	1517	MPa
Tensile Modulus	72.4	GPa
Ultimate Tensile Strength per Unit Width	0.536	kN/mm/ply
Tensile Modulus per Unit Width	25.6	kN/mm/ply
Ultimate Rupture Strain	2.1	%

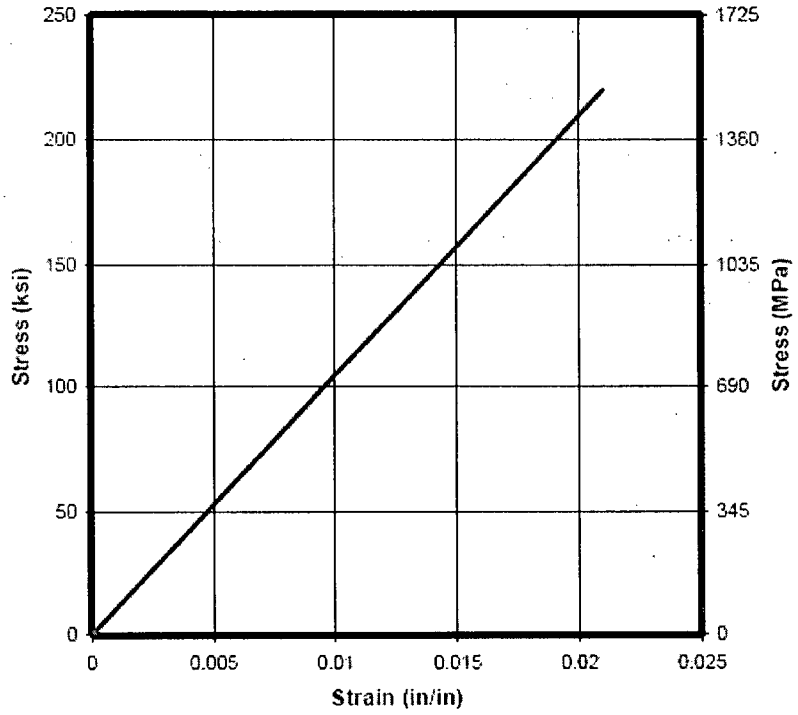

Figure 5.1 – *Stress-strain relationship for Wabo®MBrace E-glass fiber fabric (EG 900) [113]*

5.2 Sprayed GFRP Properties

In this research study Sprayed GFRP composite was used as the main material for strengthening RC beams. GFRP was sprayed by skilled nozzlemen throughout the research and as a result the quality and properties of sprayed materials were consistent. The properties of Sprayed GFRP containing different fiber length were studied by Boyd [115]. Based on his results and discussion, a fiber length of 32 mm was chosen to be used in this study which gave a higher strain at rupture compared to other fiber lengths. The properties of this material are discussed below.

5.2.1 Density

As mention earlier, a constant length of 32 mm was used for chopped fibers in Sprayed GFRP composites in this research study. Using ASTM D2584 [116], the average density of final cured Sprayed GFRP composite was found to be 1473 kg/m^3 with a Coefficient of Variation of 0.9%.

5.2.2 Fiber Volume Fraction

In this research, ASTM D2584 [116] was used to determine the fiber volume fraction of Sprayed GFRP composites. Fiber volume fraction for final cured Sprayed GFRP composite was found to be 24.7% with a Coefficient of Variation of 1.5%.

5.2.3 Tensile Properties

To evaluate the tensile properties of Sprayed GFRP, as discussed in detail by Boyd [115], a few coupons were made (Figure 5.2). Fabrication of these coupons involved spraying a flat sheet of GFRP onto a pane of glass which was first covered with a thin sheet of plastic serving as a bond breaker. The coupons were later cut from the cured laminate plate. Dimensions of these coupons are given in Figure 5.2. Two notches were also made at the middle of the specimens to predefine the failure location as shown in Figure 5.2.

Sprayed GFRP coupons were tested using a Baldwin 400 kip Universal Testing Machine. The two ends of the specimens were gripped using friction wedge grips and the elongations to break, over a gauge length of 50 mm at the middle of the specimens' length (Figure 5.2), were measured using an LVDT based extensometer attached to the specimen. Test setup is shown in Figure 5.3. Average thickness and width of the specimens at the middle of their length (i.e. at the location of notches) were measured accurately using a caliper. These values were used to calculate the cross-sectional area of the specimen on which the load was applied. A specimen after failure is shown in Figure 5.4.

Applied load and elongation were recorded constantly using a data acquisition system. Stress-strain data were calculated and plotted to obtain the ultimate tensile strength, modulus of elasticity and elongation to break. These values are reported in Table 5.2 and stress-strain response is shown in Figure 5.5.

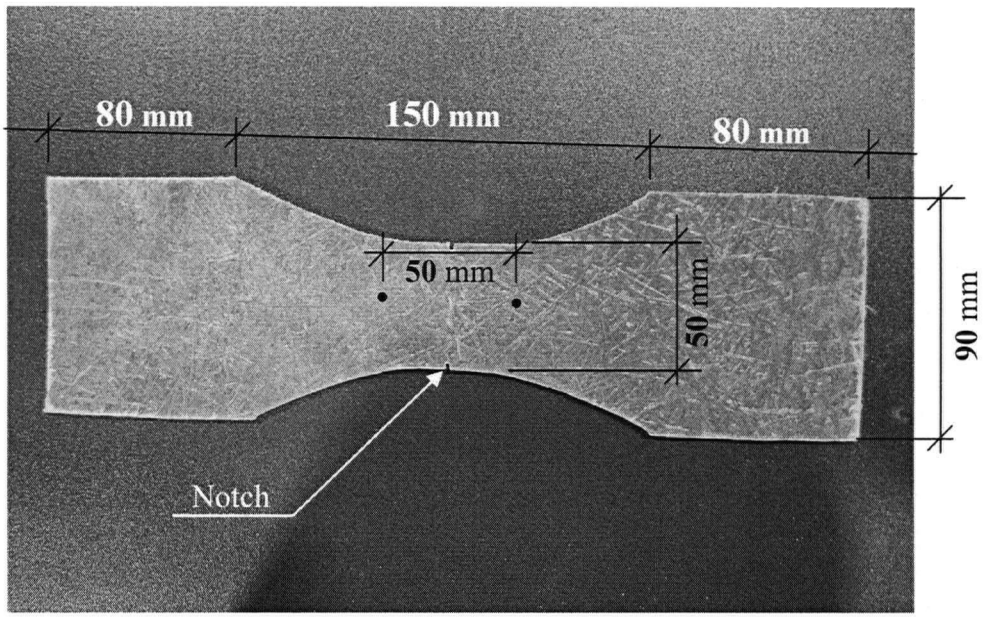

Figure 5.2 – *Sprayed GFRP Specimen Dimensions.*

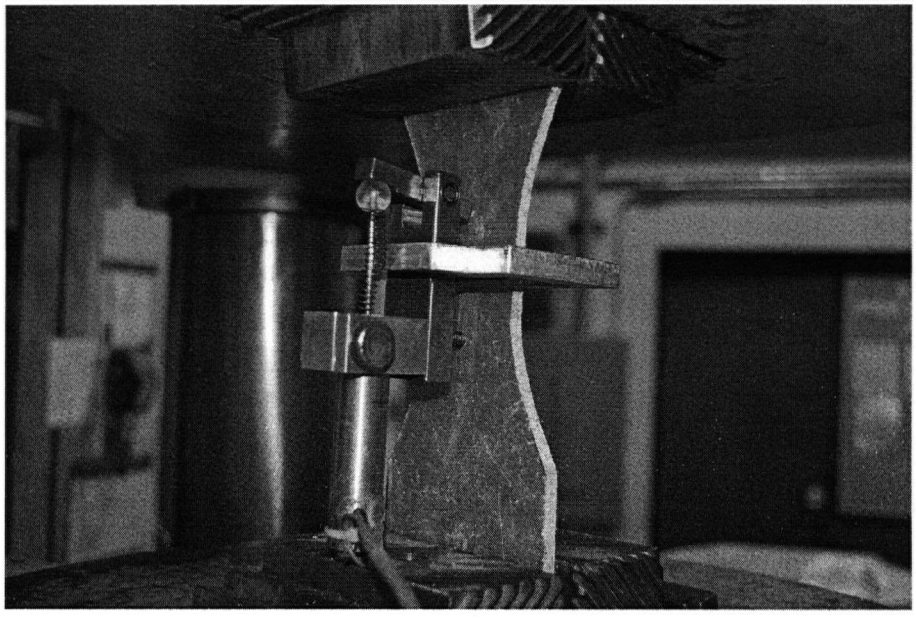

Figure 5.3 – *Apparatus to Measure Tensile Properties of Sprayed GFRP.*

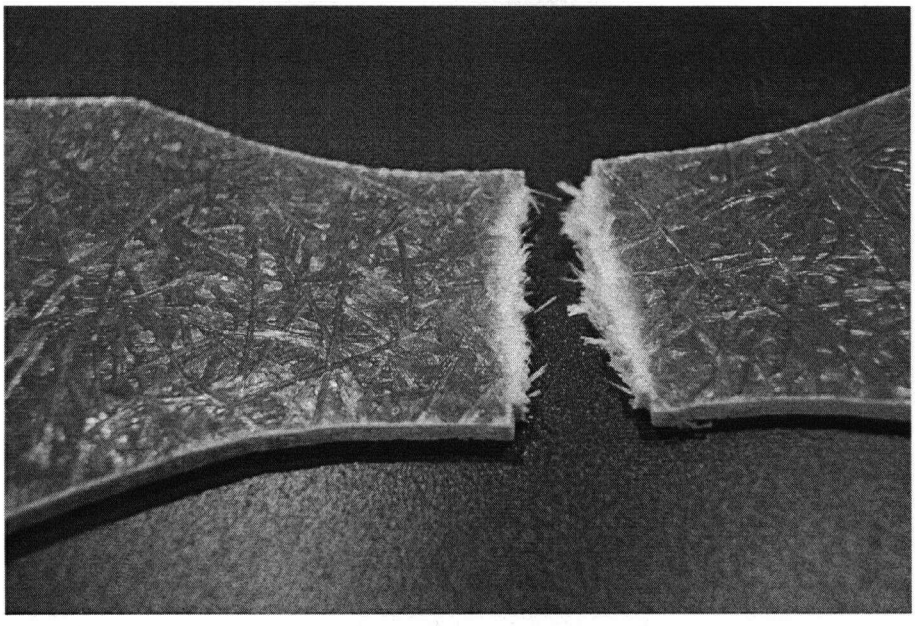

Figure 5.4 – *Sprayed GFRP Specimen after Test. Notice Presence of Both Fiber Fracture and fiber Pull-out.*

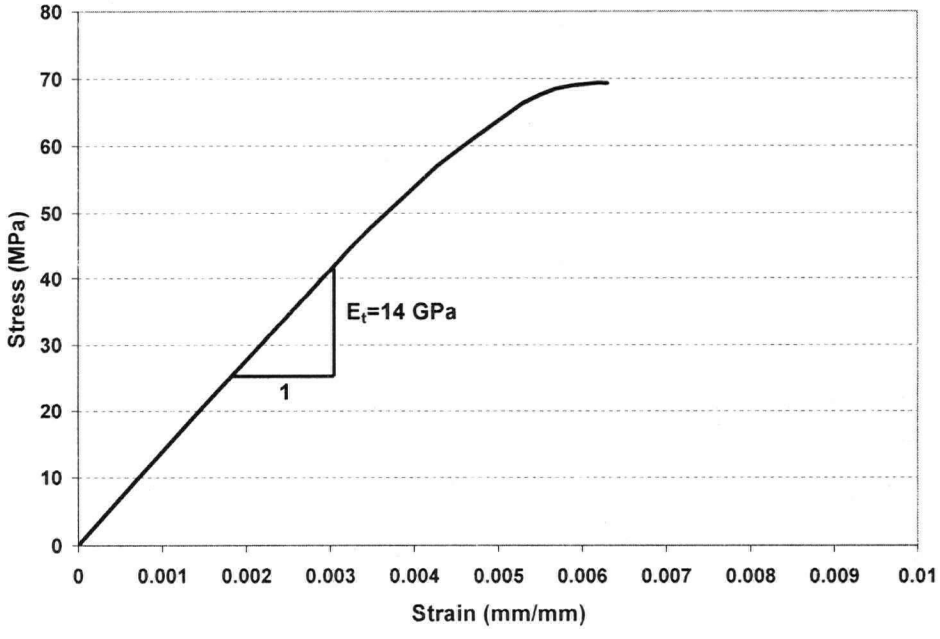

Figure 5.5 – *Stress-Strain Response of Sprayed GFRP.*

Table 5.2 – *Sprayed GFRP properties*

Tensile Properties	Value	Unit
Ultimate Tensile Strength	69	MPa
Tensile Modulus	14	GPa
Ultimate Rupture Strain	0.63	%

5.3 Reinforcing Bar Properties

In this research 3 different sizes of reinforcing bars (rebars) were used: Φ 4.8, M-10 and M-20. These rebars specimens were tested in tension as per ASTM A370 using a Baldwin 400 kip Universal Testing Machine (Figure 5.6). Properties of these rebars are tabulated in Table 5.3.

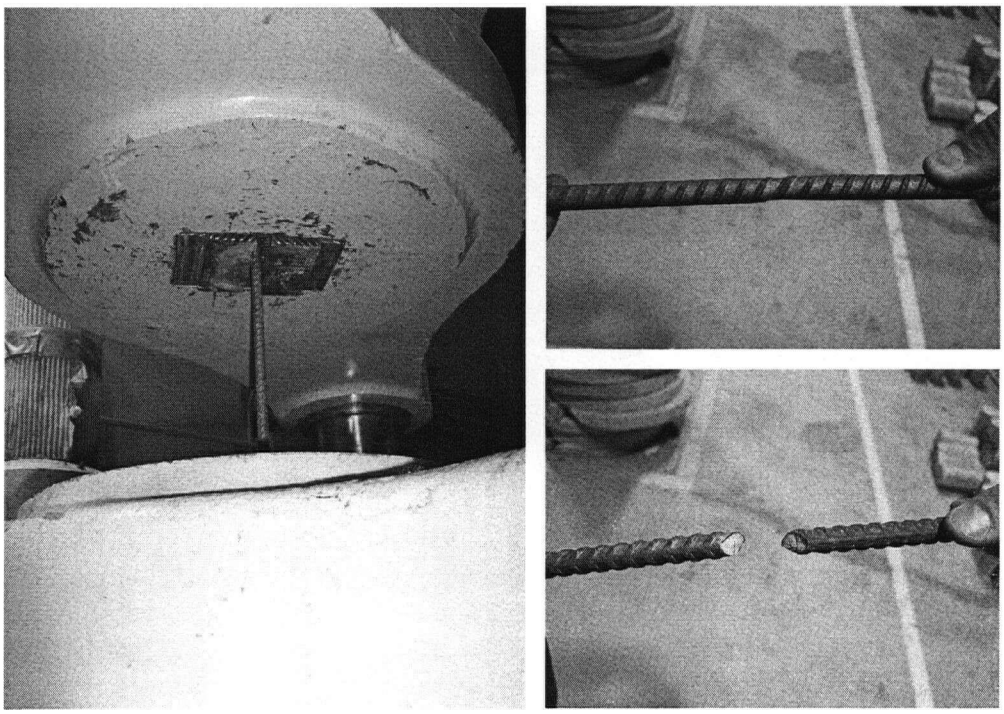

Figure 5.6 – *Tension Test on Reinforcing Bars.*

Table 5.3 – *Reinforcing bar properties*

Reinforcing Bar	Area (mm^2)	Yield Strength, F_y (MPa)	Ultimate Strength, F_u (MPa)
Φ 4.8	18.1	600	622
M-10	100	474	720
M-20	300	440	695

6

DEVELOPMENT OF IMPACT SETUP FOR TESTING RC BEAMS

6.1 Introduction

The behavior of reinforced concrete (RC) beams under impact loading has been investigated by several researchers as discussed previously in Chapter 2. However, a number of questions remain unanswered. One of the main objectives of this research was to design and build an impact testing setup to answer some of these questions. The total load as recorded by the instrumented tup was one of the main measurements carried out by previous researchers. The bending load applied on RC beams was then calculated by subtracting the inertia load (i.e. the load required to accelerate the specimen) from the recorded tup load. It was noted that for brittle materials like concrete, the values of the inertia load could be much larger than the load consumed in stressing the beam.

In this study, to overcome the problem associated with the inertia effects, instrumented support anvils as well as an instrumented tup were used. The drop weight impact machine used in this research and a unique setup for evaluating the behavior of RC beams under impact loads are discussed in this chapter.

6.2 Drop Weight Impact Machine

A drop weight impact machine with a capacity of 14.5 kJ was used in this research study. A mass of 591 kg (including the striking tup) can be dropped from as high as 2.5 m ($2.5\ \text{m} \times 591\ \text{kg} \times 9.81\ \text{m/s}^2 \div 1000 = 14.5\ \text{kJ}$). During a test, the hammer is raised to a certain height above the specimen using a hoist and chain system. At this position, air brakes are applied on the steel guide rails to release the chain from the hammer. By releasing the breaks, the hammer falls and strikes the specimen. Figure 6.1 shows the impact machine.

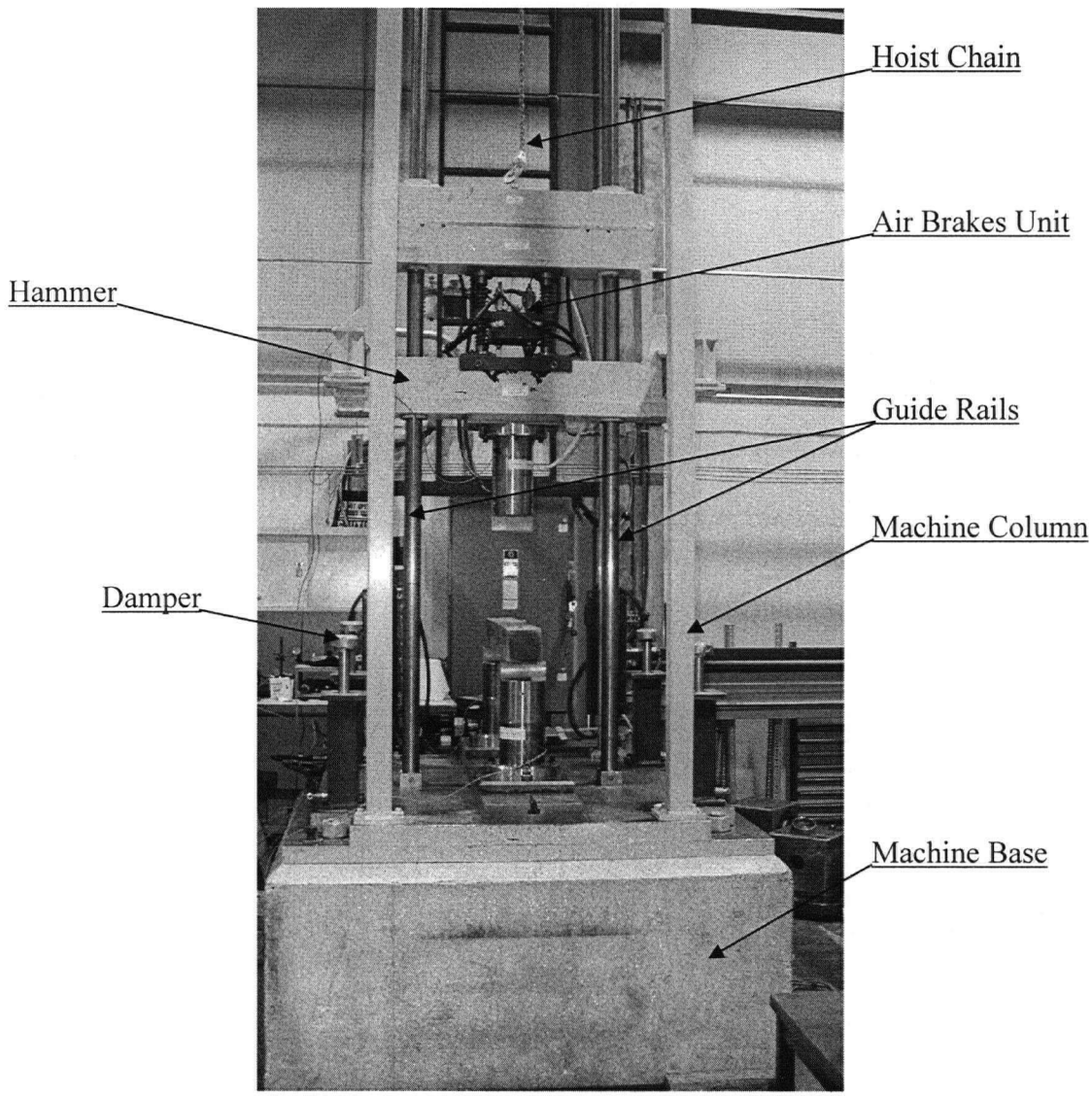

Figure 6.1 – *The 14.5 kJ Drop Weight Impact Machine*

6.3 Test Setup

Developing a reliable and accurate test setup for impact test of RC beams was one of the primary objectives of this research. This setup was made using accurate load cells which were then designed, built and calibrated.

6.3.1 Load Cells Design

Three load cells were designed and built at the University of British Columbia for this research project. Different loading caps such as flat surface, blade (line load), or point-load can be mounted on the top of each load cell using the threads provided on the top portion of the load cell and inside the cap (Figure 6.2). A 0.2 mm gap is provided around the cap when an appropriate cap is screwed tightly over a load cell. The load is transferred from the cap to the load cell through the contact surface as shown in Figure 6.3. This gap provides protection to the important part of the load cell where strain gauges are attached. When load increases, the gap gets smaller and it will be closed before the yielding of load cell occurs. At this point, load is transferred to the bottom portion of the load cell with a larger cross-sectional area and, this in turn, decreases the stress experienced by the load cell and prevents its yielding.

Load cell assemblies and their details are shown in Figures 6.3 to 6.5. Two load cells sitting on a 1.524 m steel anvil (rail) will be referred as load cells A and C throughout this thesis, while the third one which is bolted to the impact machine's hammer (striking tup) will be referred as load cell B. Beam span can be adjusted by moving the two support load cells and is in the range of 370 mm to 1150 mm for this setup.

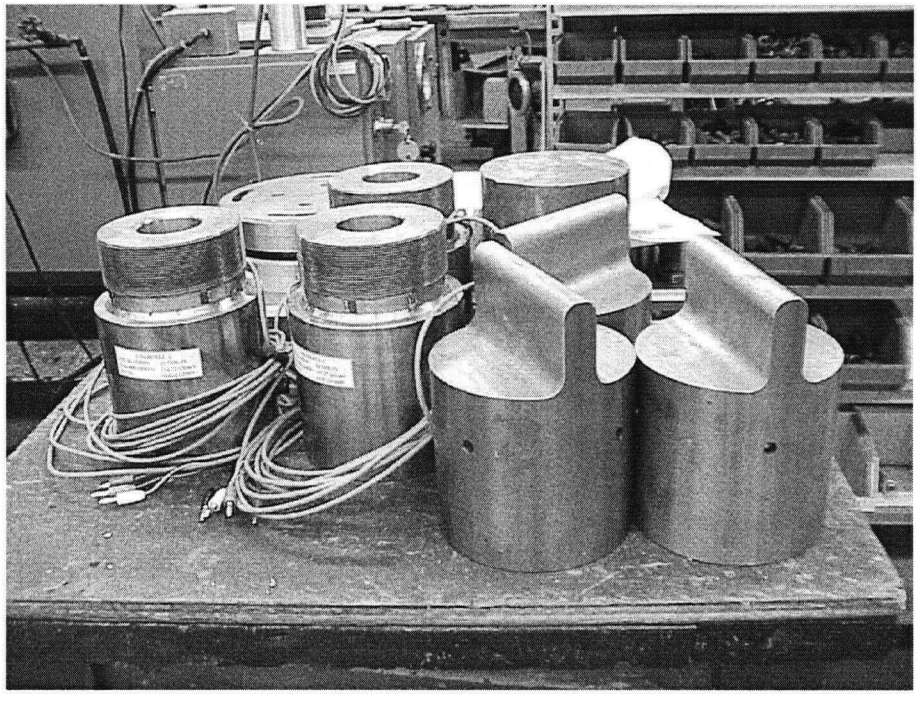

Figure 6.2 – *Load Cells and Blade Caps*

6.3.2 Load Cells Calibration

The output from the strain gauges used in all three load cells (i.e. load cells A, B and C) was in the form of voltage signals. To convert these signals into loads, the load cells need to be calibrated. As mentioned in Chapter 2, the modulus of elasticity and ultimate strain of reinforcing bars (and steel, in general) remain nearly constant, but yield stress and yield strain increase with increase in loading rate [100]. As a result, a static calibration can be used, although these load cells were loaded by impact (e.g. dynamic loading). A similar approach has been adopted by others [104].

The calibration curves for all three load cells are shown in Figure 6.6. Note a perfect linear relationship between the output voltage signal and load reading and the absence of hysteretic losses.

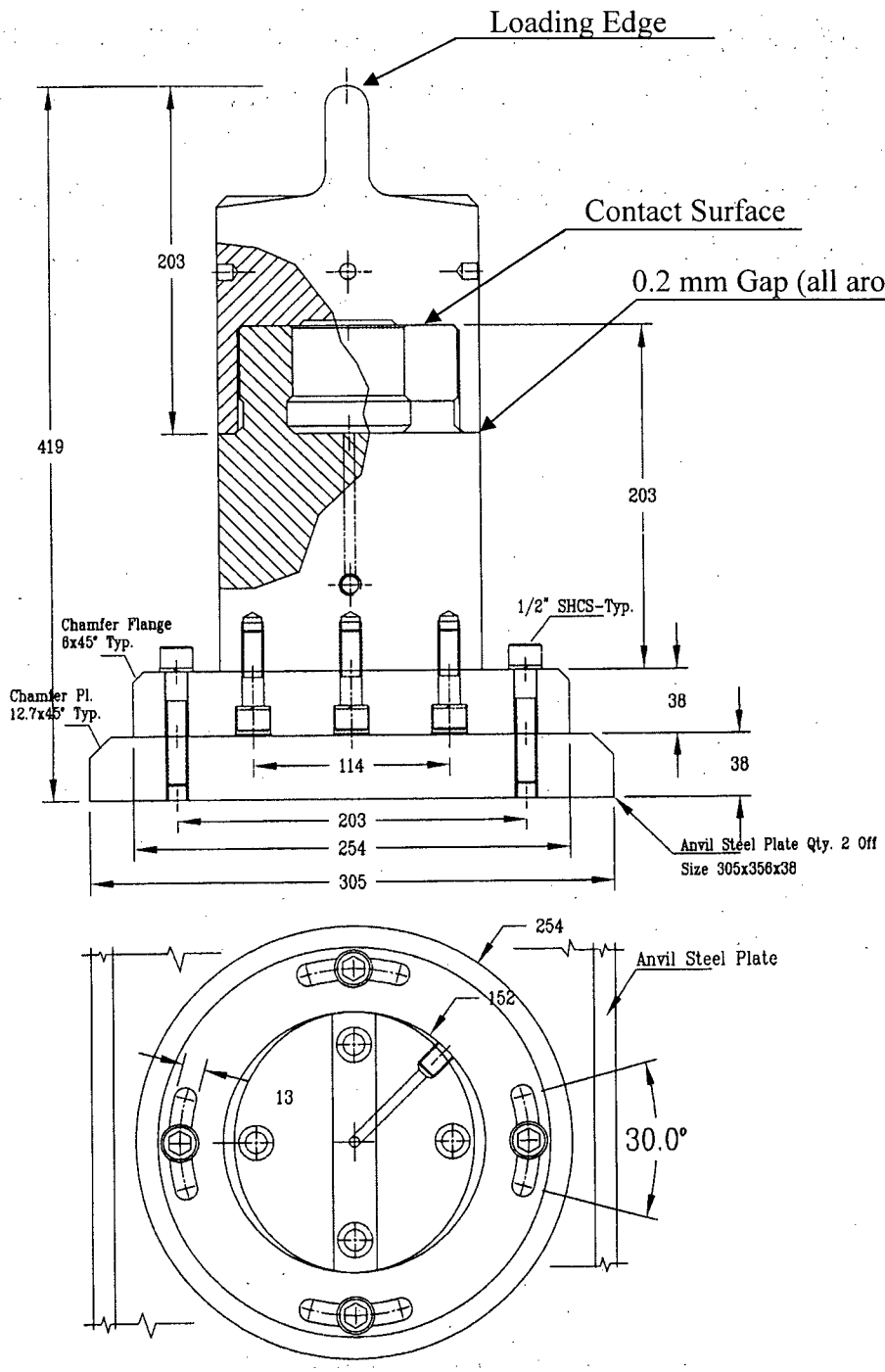

Figure 6.3 – *Anvil Support Load Cell Assembly – Plan and Elevation View*

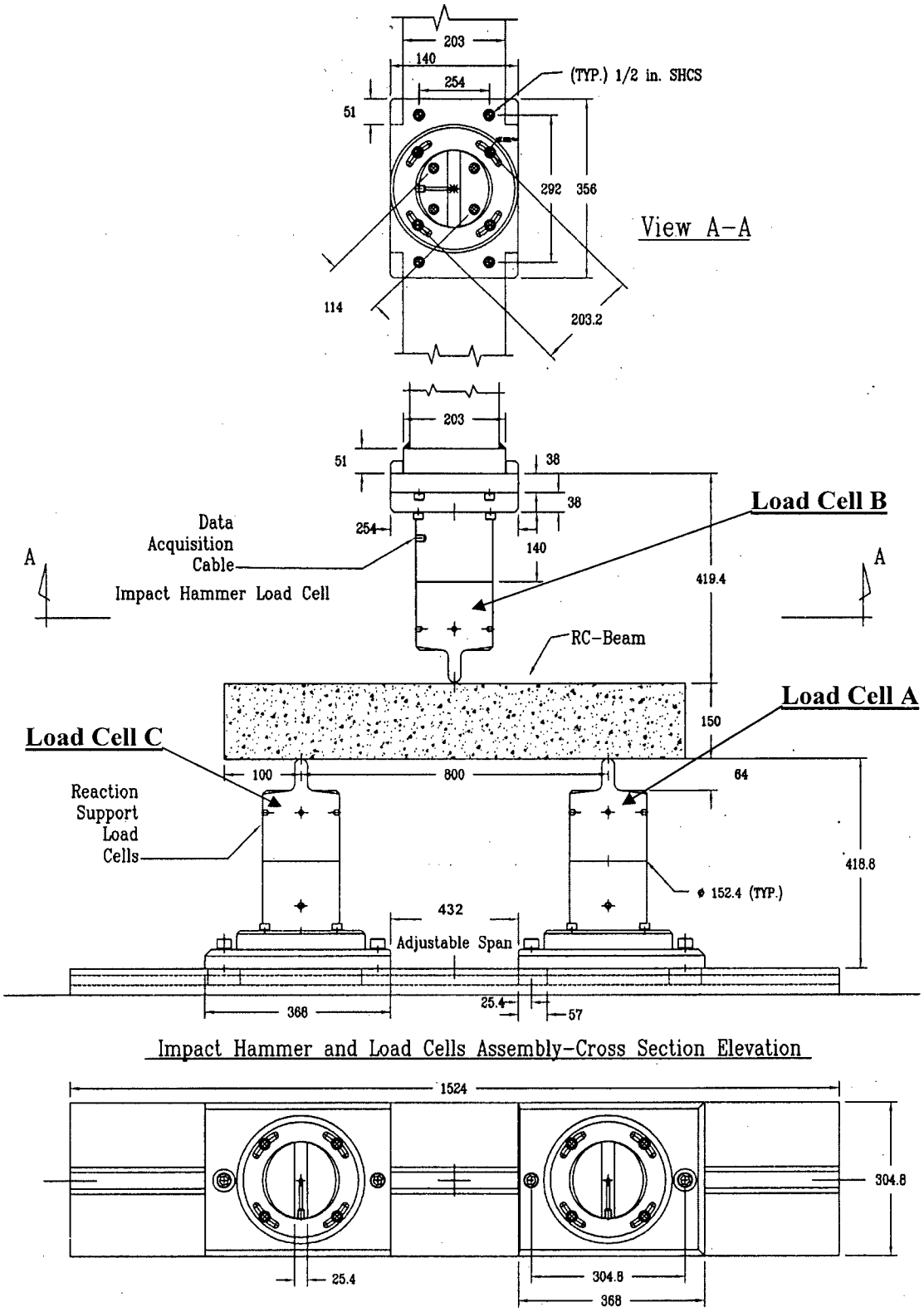

Impact Hammer and Load Cells Assembly–Cross Section Elevation

Anvil Support Load Cells Assembly – Plan and Elevation View

Figure 6.4 – *Load Cells Assembly*

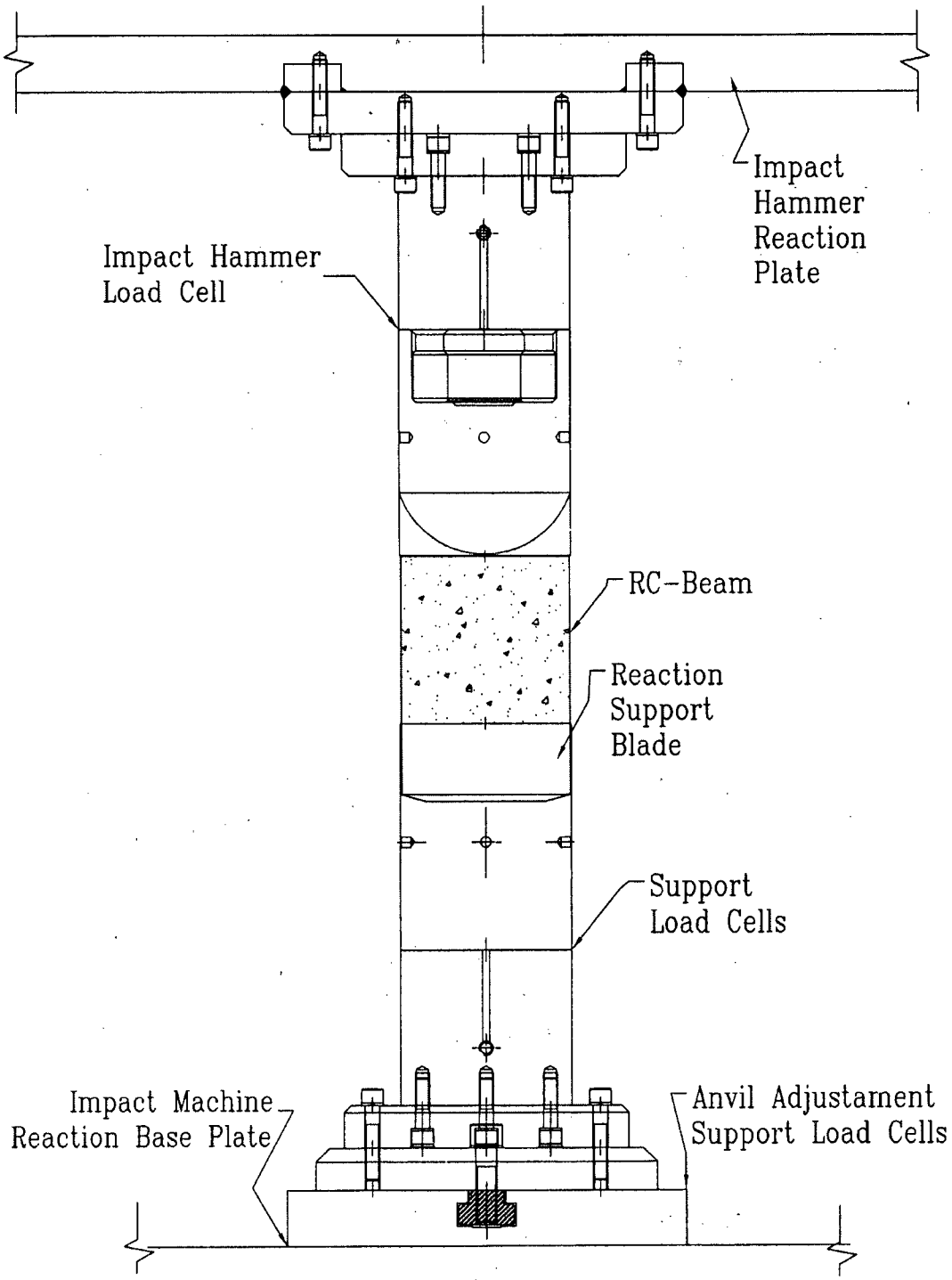

Figure 6.5 – *Impact Hammer and Load Cells – Side Elevation*

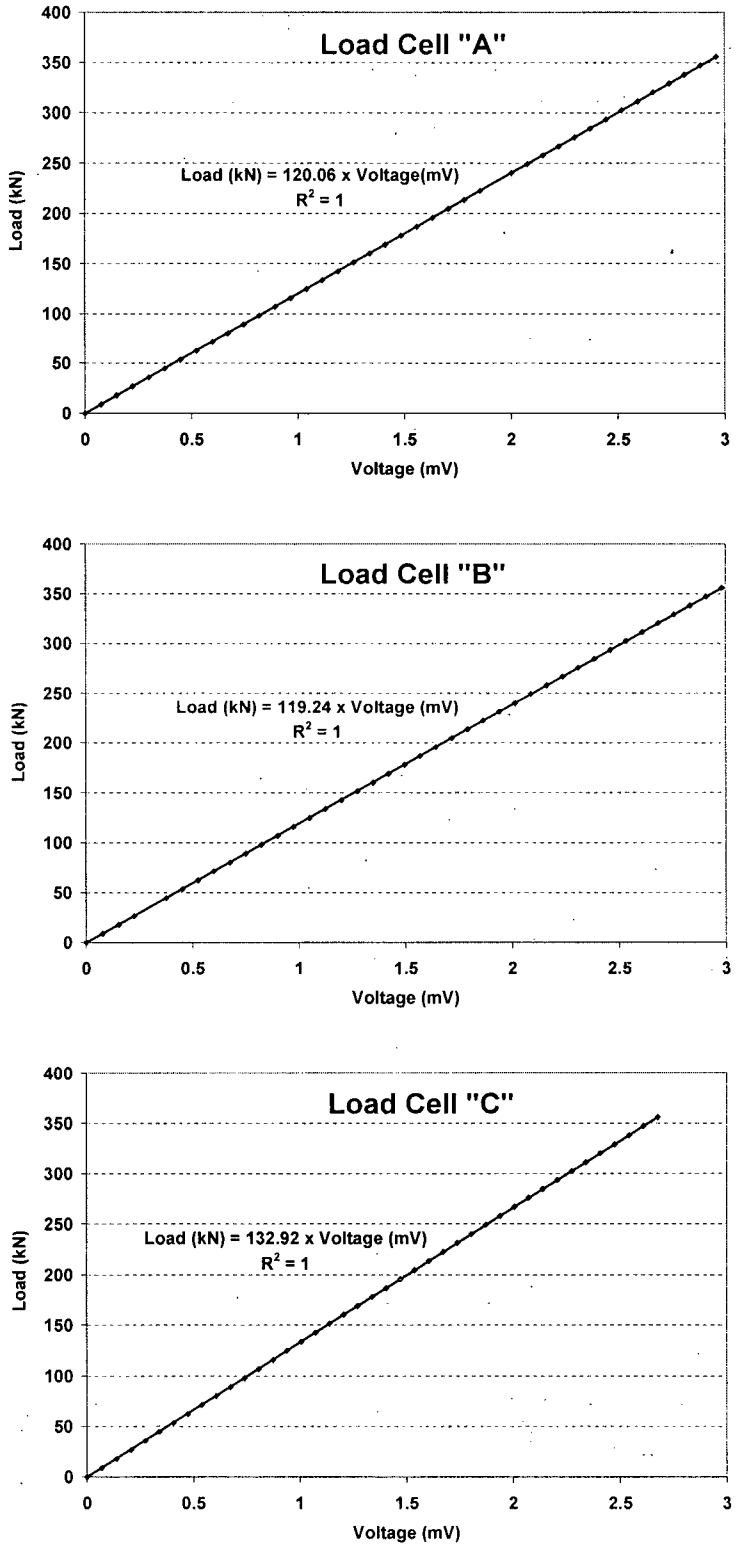

Figure 6.6 – *Calibration of Load Cells A (Support Load Cell), B (Striking Load Cell) and C (Support Load Cell)*

6.3.3 Steel-Yoke at the Supports

In this research study simply supported RC beams were tested under quasi-static and impact loading conditions. During the first few tests, it was discovered that if the specimen was not prevented from vertical movements at the supports, within a very short period of first contact of hammer with the specimen, contact with the support was lost and as a result, loads read by the support load cells were not correct. This phenomenon was further verified by using a high speed camera (1700 frames per second). As a result loads recorded by the support load cells for two identical tests were totally different. Figure 6.7 shows the impact test setup for the first few tests when the above mentioned problem was noticed.

To overcome this problem, the vertical movement of RC beams at the supports was restrained using two steel yokes (Figure 6.8). In order to assure that the beams are still simply supported, these yokes are pinned at the bottom, to allow rotation during beam loading (Figure 6.9). To allow an easier rotation, a round steel bar was welded underneath the top steel plate where the yoke touched the beam (Figure 6.8).

Figure 6.7 – *Impact Test Setup without Steel Yokes*

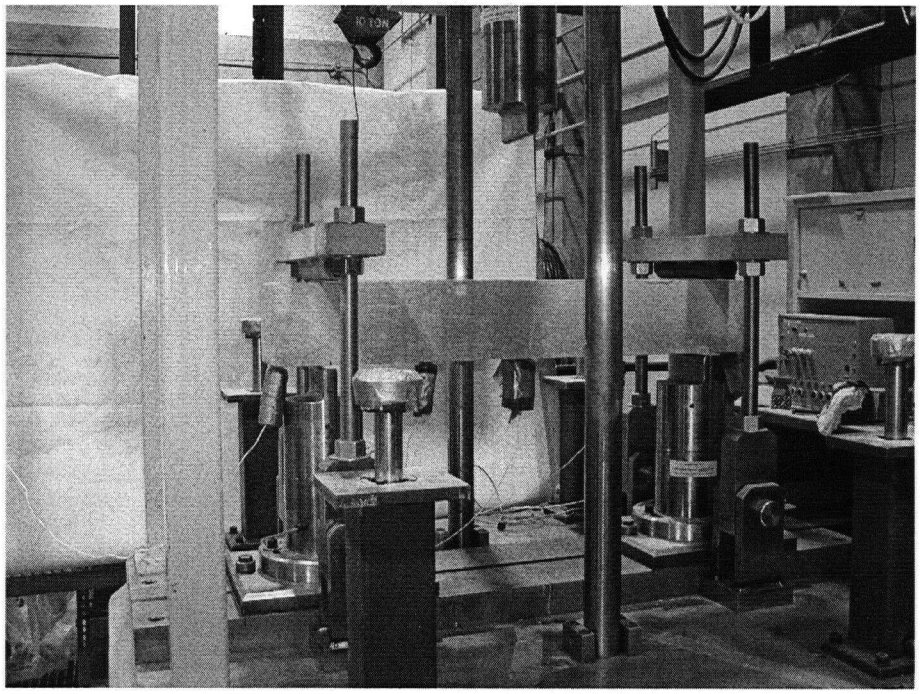

Figure 6.8 – *Impact Test Setup with Steel Yokes*

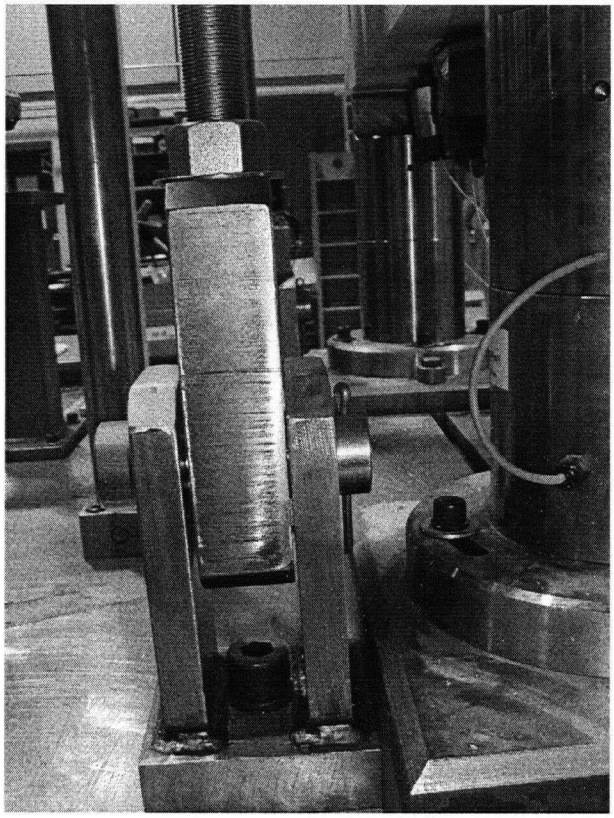

Figure 6.9 – *Steel Yokes are Pinned at the Bottom End (i.e. Rotation is Free)*

6.4 Data Acquisition System

National Instruments™ VI Logger, a flexible tool specifically designed for data logging applications was used in all impact tests. VI Logger is a stand-alone, configuration-based data logging software. Using this software, data from up to 8 channels were recorded with a frequency of 100 kHz (i.e. up to 800,000 data points per second). A sample of this software user interface is shown in Figure 6.10.

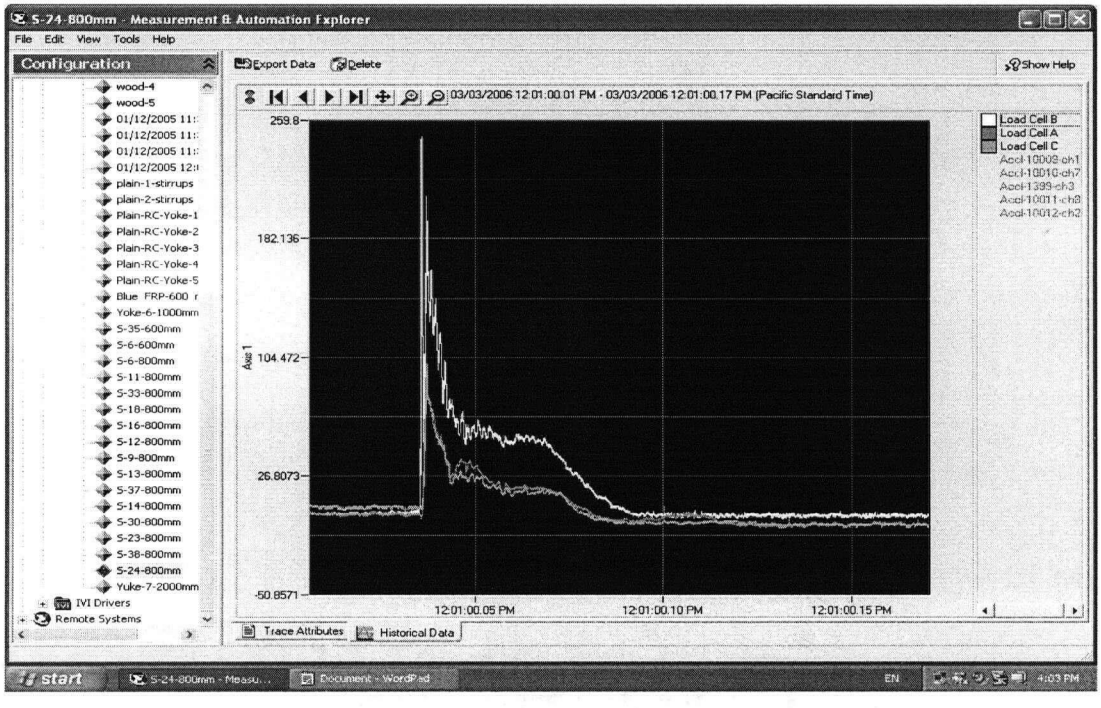

Figure 6.10 – *User Interface of VI Logger Software*

7

BEHAVIOR OF RC BEAMS UNDER IMPACT LOADING

7.1 Introduction

Researchers have used the data recorded by the striking tup to study impact behavior of simply supported plain, fiber-reinforced or conventionally reinforced concrete beams. As mentioned in Chapter 6, it has been noted by many that this load could not be considered as the bending load experienced by the concrete beam. A portion of this load is used to accelerate the beam, and therefore, finding the exact bending load versus time has been one of the most challenging tasks for impact researchers. To capture a true bending load versus time response a new test setup was designed and built for this study and was described in Chapter 6.

This setup was used to study the behavior of RC beams under impact loading. In this Chapter test results of RC beams under quasi-static and impact loads with various impact velocities are provided and discussed.

7.2 Beam Design and Testing Procedure

A total of 14 identical RC beams were cast to investigate the behavior of RC beams under impact loading. These beams contained flexural as well as shear reinforcement. These beams were 1 m in total length and were tested over an 800 mm span. Load configuration and cross-sectional details are shown in Figure 7.1.

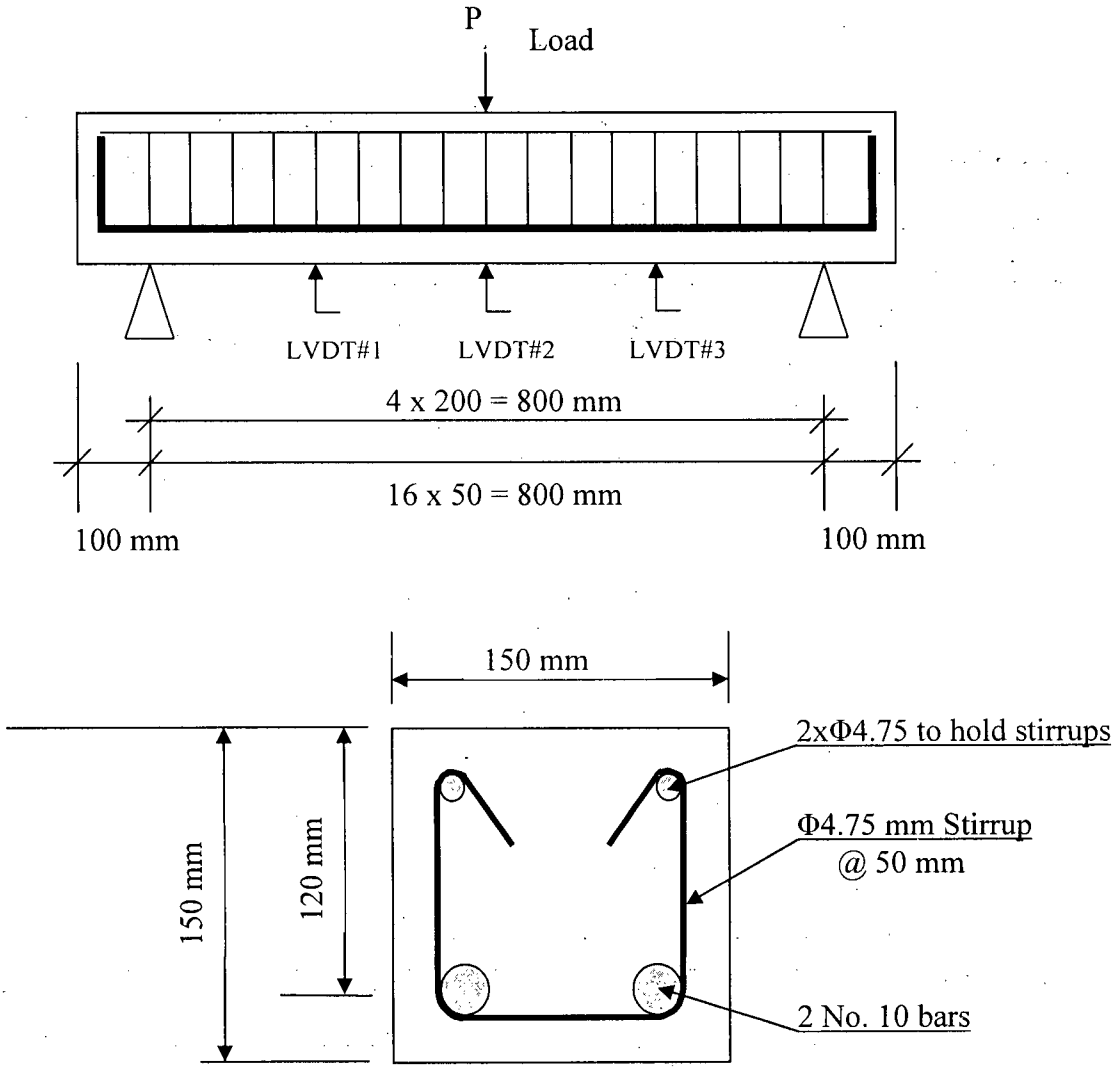

Figure 7.1 – *Load Configuration and Cross-Sectional Details of RC Beams*

Nine beams were tested under impact with different impact velocities ranging from 2.8 m/s to 6.26 m/s, three beams were tested under quasi-static, 3-point loading, and the remaining two beams were strengthened by fabric GFRP and one was tested under quasi-static and the other one under impact loading (impact velocity = 3.43 m/s). Table 7.1 shows the beam designations and configuration.

Table 7.1 *–RC Beams Designations*

Beam No.	Quasi-Static Loading	Impact Loading Drop Height, h (mm)					Steel Yokes at the Supports	GFRP Fabric
		400	500	600	1000	2000		
BS-1	✓	—	—	—	—	—	NA	—
BS-2	✓	—	—	—	—	—	NA	—
BS-3	✓	—	—	—	—	—	NA	—
BS-FRP	✓	—	—	—	—	—	NA	✓
BI-400	—	✓	—	—	—	—	✓	—
BI-500-NY-1	—	—	✓	—	—	—	—	—
BI-500-NY-2	—	—	✓	—	—	—	—	—
BI-500-1	—	—	✓	—	—	—	✓	—
BI-500-2	—	—	✓	—	—	—	✓	—
BI-500-3	—	—	✓	—	—	—	✓	—
BI-600	—	—	—	✓	—	—	✓	—
BI-1000	—	—	—	—	✓	—	✓	—
BI-2000	—	—	—	—	—	✓	✓	—
BI-600-FRP	—	—	—	✓	—	—	✓	✓

Notes: **BS**-X: **B**eam under **S**tatic loading, **BI**-XXXX-X: **B**eam under **I**mpact loading and XXXX shows the drop height in mm, **NY**: **N**o **Y**okes were used, FRP: FRP fabric on three sides.

Parameters needed for calculating load carrying capacity of this RC beam are tabulated in Table 7.2.

Table 7.2 – *Properties of RC Beams*

Parameter	Definition	Value	Unit
b	Width of compression face of member	150	mm
h	Overall depth of beam	150	mm
d	Distance from extreme compression fiber to centroid of tension reinforcement	120	mm
f_c'	Specified compressive strength of concrete	44	MPa
f_y	Specified yield strength of tension reinforcement	474	MPa
f_{ys}	Specified yield strength of shear reinforcement	600	MPa
A_s	Area of tension reinforcement	200	mm^2

Calculations (see Appendix A) show that if resistance factors are not considered, the capacity of this beam under quasi-static loading is 51 kN at which tension reinforcement starts yielding. It is also worth noting that the beam was designed in accordance with CSA Standard A23.3-94 to produce a typical flexural failure mode since enough stirrups were provided to prevent shear failure.

In quasi-static loading conditions, all of the beams (i.e. BS-1, BS-2 and BS-3) were tested in 3-point loading using a Baldwin 400 kip Universal Testing Machine. ASTM C78 *Flexural Strength of Concrete* specifies a rate of increase in the flexural stress of 0.86 – 1.21 MPa/min for flexural testing. In a simply supported 3-point loading beam the flexural stress in the concrete is determined as:

$$R = \frac{3Pl}{2bh^2} \tag{7.1}$$

where,

R = flexural stress in concrete (MPa)

P = applied load (N)

l = span length (mm)

b = specimen width (mm)

h = specimen height (mm)

Rearranging this equation for the applied load P gives:

$$P = \frac{2Rbh^2}{3l} \tag{7.2}$$

Substituting the above mentioned flexural stress range for R (0.86 to 1.21 MPa), along with values for b (150 mm), h (150 mm) and l (800 mm) a loading range of 2419 – 3403 N/min was determined. In this research project the load was monitored visually throughout the testing to ensure a consistent loading rate within this range with a target of 2900 N/min. Three LVDTs were used to capture the deflection at the mid-span as well as two additional points along the beam span as shown in Figure 7.1. The test setup for quasi-static loading is shown in Figure 7.2. Applied loads and deflections were constantly monitored and recorded using a data acquisition unit and PC.

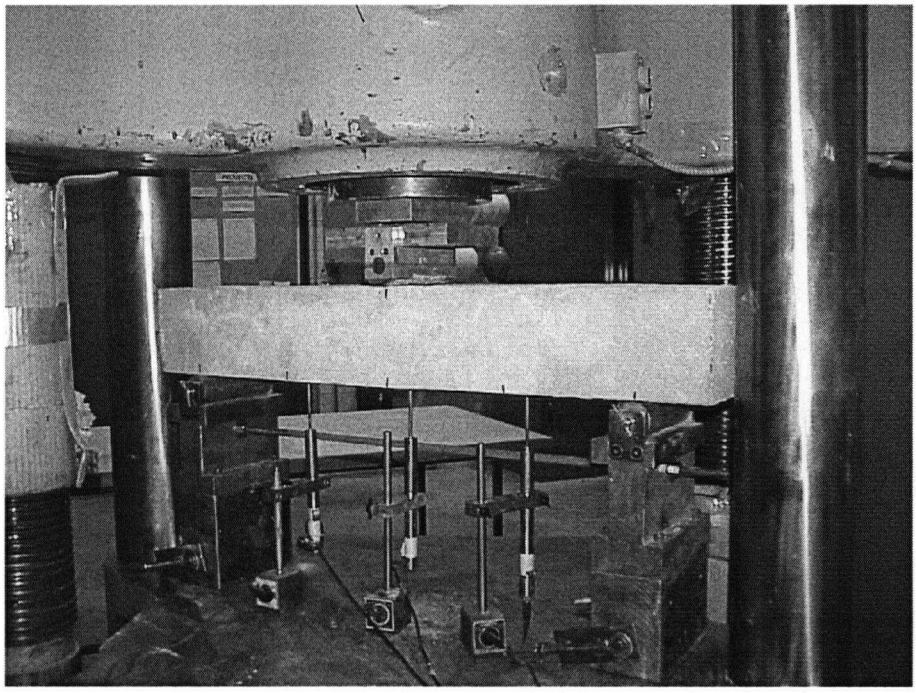

Figure 7.2 – *Beam Test Setup under Quasi-Static Loading*

7.3 Results and Discussion

7.3.1 Quasi-Static Loading

Three beams, BS-1 to BS-3, were tested under 3-point quasi-static loading. The load vs. mid-span deflection is shown in Figure 7.3.

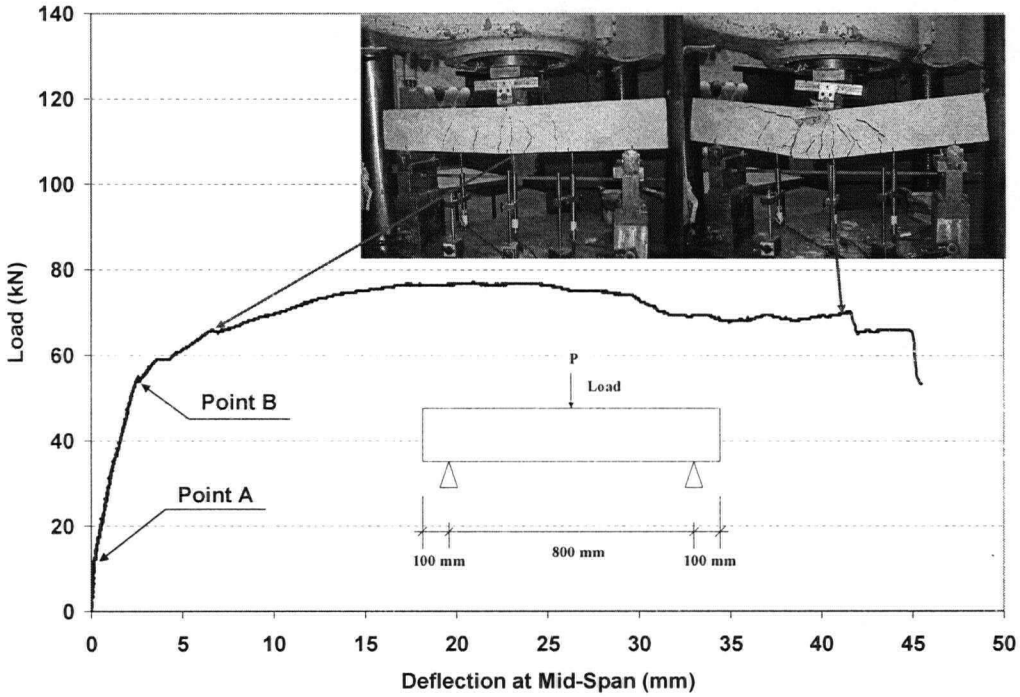

Figure 7.3 – *Load vs. Deflection Curve for RC Beam with a Flexural Failure Mode*

The results among the three beams were quite consistent. The load vs. deflection curve for beam BS-1, shown in Figure 7.3, represents a typical flexural failure mode in RC beams. Load vs. deflection response for other two beams (i.e. BS-2 and BS-3) was very similar to that of beam BS-1. Initially, the beam was uncracked (i.e. from the beginning of the curve till Point A). The cross-sectional strains at this stage were very small and the stress distribution was essentially linear. When the stresses at the bottom side of the beam reached concrete tensile strength, cracking occurred. This is shown as Point A in Figure 7.3. After cracking, the tensile force in the concrete was transferred to the steel reinforcing bars (rebars). As a result, less of the concrete cross section was effective in resisting moments and the stiffness of the beam (i.e. the slope of the curve) decreased. Eventually, when applied load was increased, the tensile reinforcement

reached the yield point shown by Point B in Figure 7.3. Once yielding had occurred, the mid-span deflection increased rapidly with little increase in load carrying capacity as shown in Figure 7.3. The beam failed due to crushing of the concrete at the top of the beam.

As mentioned in Section 7.2, the calculated capacity of this beam under quasi-static loading is 51 kN. Experimental test result showed 54 kN capacity for this beam, corresponding to Point B in Figure 7.3. Thus there is a good agreement between theoretical and experimental values for load carrying capacity of this RC beam, with an error less than 6%.

7.3.2 Impact Loading

An instrumented drop-weight impact machine as explained in Section 6.2 was utilized in the course of this research program. Potential energy stored in the hammer at height h is transferred to the RC beam by dropping it freely. The guide rails (shown in Figure 6.1) were cleaned to make sure that the hammer would drop freely. At the instance of impact, the hammer develops a velocity V_h by:

$$V_h = \sqrt{2gh} \tag{7.3}$$

where,

V_h = the velocity of the falling hammer at the instance of impact (m/s)

g = the acceleration due to gravity (m/s^2) = 9.81 m/s^2

h = the drop height (m)

Equation (7.3) can be rewritten as:

$$V_h = 4.43\sqrt{h} \tag{7.4}$$

For all impact tests using the drop-weight machine, PCB Piezotronics™ accelerometers were employed (see Figure 7.4). These accelerometers were screwed into

mounts which were glued to the specimens prior to testing. Piezoelectric accelerometers rely on the piezoelectric effect of quartz or ceramic crystals to generate an electrical signal that is proportional to applied acceleration. The piezoelectric effect produces an opposed accumulation of charged particles on the crystal. This charge is proportional to applied force or stress. In an accelerometer, the stress on the crystals occurs as a result of the seismic mass (shown as (m) in Figure 7.5) imposing a force on the crystal. The structure shown in Figure 7.5 obeys Newton's second law of motion:

$$F = m.a \tag{7.5}$$

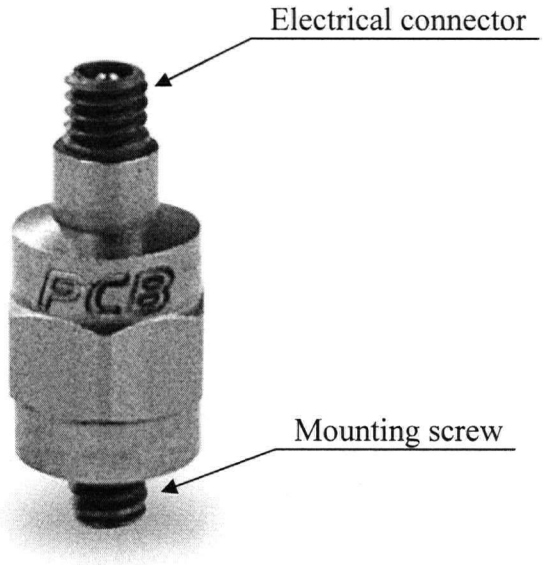

Figure 7.4 – *PCB Piezotronics™ accelerometer*

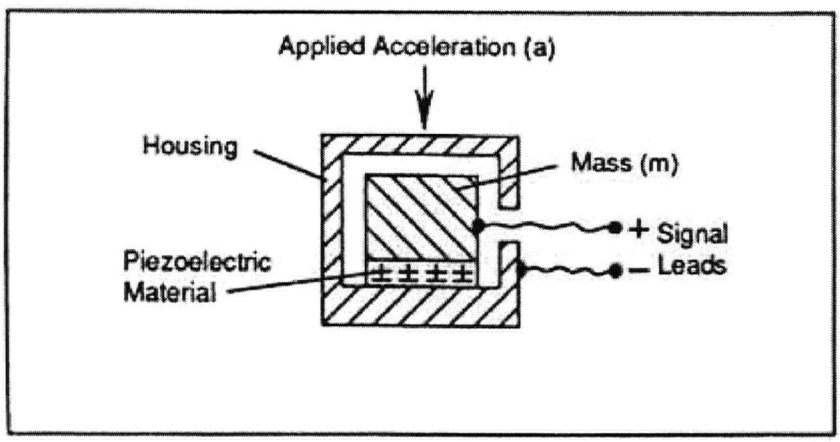

Figure 7.5 – *Structure of a Piezoelectric Accelerometer*

where,

F = applied force (N)

m = mass (kg)

a = acceleration (m/s^2)

Therefore, the total amount of accumulated charge is proportional to the applied force, and the applied force is proportional to acceleration. Electrodes collect and wires transmit the charge to a signal conditioner that may be remote or built into the accelerometer. Once the charge is conditioned by signal conditioning electronics, the signal is available for display, recording, analysis, or control. Properties of the accelerometer used in this research project are tabulated in Table 7.3.

Table 7.3 – *Properties of PCB Piezotronics™ accelerometer*

Property	Value	Unit
Measurement Range	±4900	m/s^2
Sensitivity (±10%)	1.02	$mV/(m/s^2)$
Frequency Range (±5%)	2.0 to 10000	Hz
Resonant Frequency	≥60	kHz
Non-Linearity	≤1	%
Overload Limit	±98100	m/s^2
Sensing Element	Quartz	____
Housing Material	Titanium	____
Weight	1.7	gr
Electrical Connector	5-44 Coaxial	____
Mounting Thread	5-40 Male	____
Mounting Torque	90 to 135	N.cm

The velocity and displacement histories at the location of accelerometers were obtained by integrating the acceleration history with respect to time using the following equations:

$$\dot{u}_0(t) = \int \ddot{u}_0(t).dt \tag{7.6}$$

$$u_0(t) = \int \dot{u}_0(t).dt \tag{7.7}$$

where,

$\ddot{u}_0(t)$ = acceleration at the location of the accelerometer

$\dot{u}_0(t)$ = velocity at the location of the accelerometer

$u_0(t)$ = displacement at the location of the accelerometer

Accelerations at different locations along the beam were recorded with a frequency of 100 kHz using National Instruments™ VI Logger software. Locations of the accelerometers are shown in Figure 7.6.

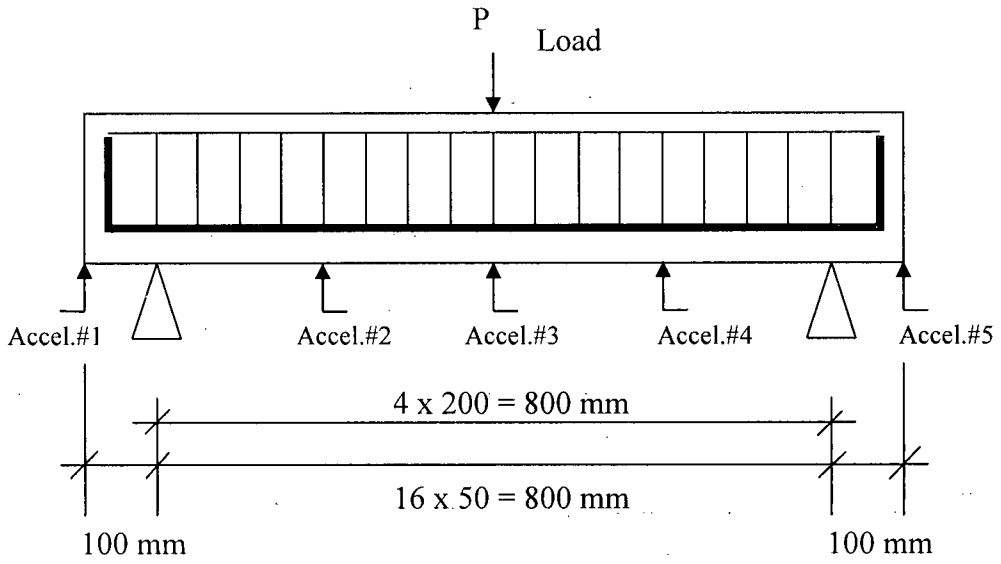

Figure 7.6 – *Location of the Accelerometers in Impact Loading*

During the impact, striking load at the tup load cell as well as reaction forces at the support load cells were recorded with the same frequency of 100 kHz using National Instruments™ VI Logger software.

As mentioned earlier, the contact load between the specimen and the hammer is not the true bending load on the beam, because of the inertia reaction of the beam. A part of the tup load is used to accelerate the beam from its rest position. Since structural engineers have been trained to think in terms of equilibrium of forces, they use D'Alembert's principle of dynamic equilibrium to write equilibrium equations in dynamic load conditions. This principle is based on the notion of a fictitious inertia force. This force is equal to the product of mass times its acceleration and acting in a direction opposite to the acceleration. D'Alembert's principle of dynamic equilibrium states that with inertia forces included, a system is in equilibrium at each time instant. As a result, a free-body diagram of a moving mass can be drawn and principles of statics can be used to develop the equation of motion. Thus, one can conclude that in order to obtain the actual bending load on the specimen the inertia load must be subtracted from the observed tup load. It is also important to note that the tup load throughout this study was taken as a point load acting at the mid-span of the beam, whereas the inertia load of the beam is a body force distributed throughout the body of the beam. This distributed body force can be replaced by an equivalent inertia load, $P_i(t)$, which can then be subtracted from the tup load , $P_t(t)$, to obtain a true bending load, $P_b(t)$, which acts at the mid-span. Therefore, at any time t, the following equation can be used to obtain the true bending load that the beam is experiencing [105]:

$$P_b(t) = P_t(t) - P_i(t) \tag{7.8}$$

where,

$P_b(t)$ = true bending load at the mid-span of the beam at time t

$P_t(t)$ = tup load at time t

$P_i(t)$ = a point load representing inertia load at the mid-span of the beam at time t equivalent to the distributed inertia load

According to Banthia [104], the inertia load (and as a result the true bending load) can be calculated using the following equations:

- when the displacements between the supports are assumed to be linear:

$$P_i(t) = \rho A \ddot{u}_0(t)\left[\frac{l}{3} + \frac{8l_{oh}^3}{3l^2}\right] \tag{7.9}$$

- when the displacements between the supports are assumed to be sinusoidal, while the displacements on the overhanging portion of the beam are assumed to be linear:

$$P_i(t) = \rho A \ddot{u}_0(t)\left[\frac{l}{2} + \frac{2\pi^2 l_{oh}^3}{3l^2}\right] \tag{7.10}$$

where,

ρ = mass density of the beam material (kg/m^3)

A = cross-sectional area of the beam (m^2)

$\ddot{u}_0(t)$ = acceleration at the centre of the beam at time t (m/s^2)

l = span of the beam between two supports (m)

l_{oh} = length of the over-hanging portion of the beam (m)

In this research program, support anvils in addition to the tup were instrumented in order to obtain valid and true bending load at any time t directly from the experiment. Therefore, true bending load at time t, $P_b(t)$, which acts at the mid-span can also be obtained by adding the reaction forces at the support anvils at time t:

$$P_b(t) = R_A(t) + R_C(t) \tag{7.11}$$

where,

$P_b(t)$ = true bending load at the mid-span of the beam at time t

$R_A(t)$ = reaction load at support A at time t

$R_C(t)$ = reaction load at support C at time t

as shown in Figure 7.7.

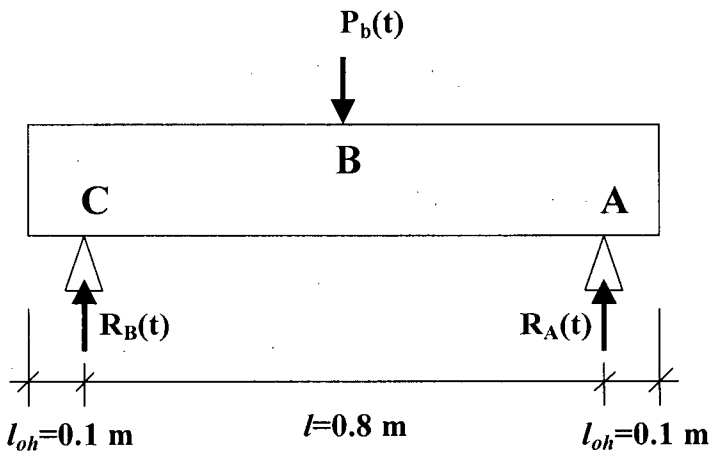

Figure 7.7 – *True Bending load and Reaction Forces at Time t*

Nine identical beams were tested under impact loading. For the first two tests, the steel yokes as described in Section 6.3.3 were not used. In the following Section, results obtained from these two beams are discussed to explain why the upward movement at the support locations should be prevented by using steel yokes. Following that, results from other beams are discussed where steel yokes were used.

7.3.2.1 No Steel Yokes at the Supports

Two identical beams (i.e. BI-500-NY-1 and BI-500-NY-2, see Table 7.1) were tested under 500 mm drop height while no steel yokes were used to prevent upward movement of these beams at the support locations at the instance of impact. Figure 7.8 shows one of these beams before dropping the hammer and Figure 7.9 shows the same beam after failure.

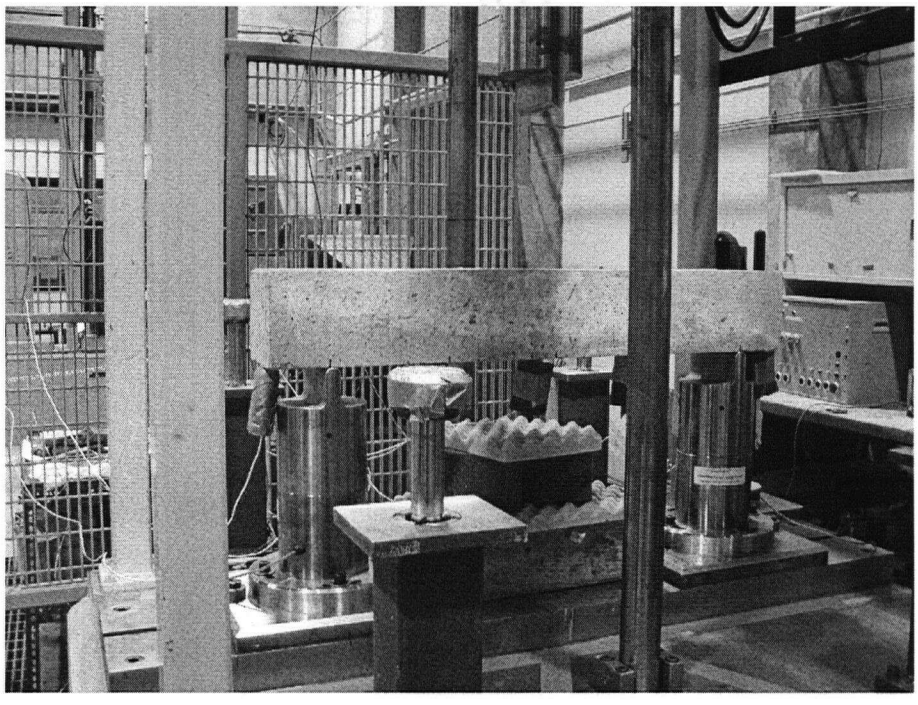

Figure 7.8 – *RC Beam before Impact Test, No Steel Yoke Was Used*

Figure 7.9 – *RC Beam after Impact Test, No Steel Yoke Was Used*

Load vs. time histories of these beams are shown in Figures 7.10 and 7.11. It is clear that while these beams were exactly the same, maximum loads experienced by

them (i.e. the summation of loads recorded by the supports, $P_b(t)$) were totally different.

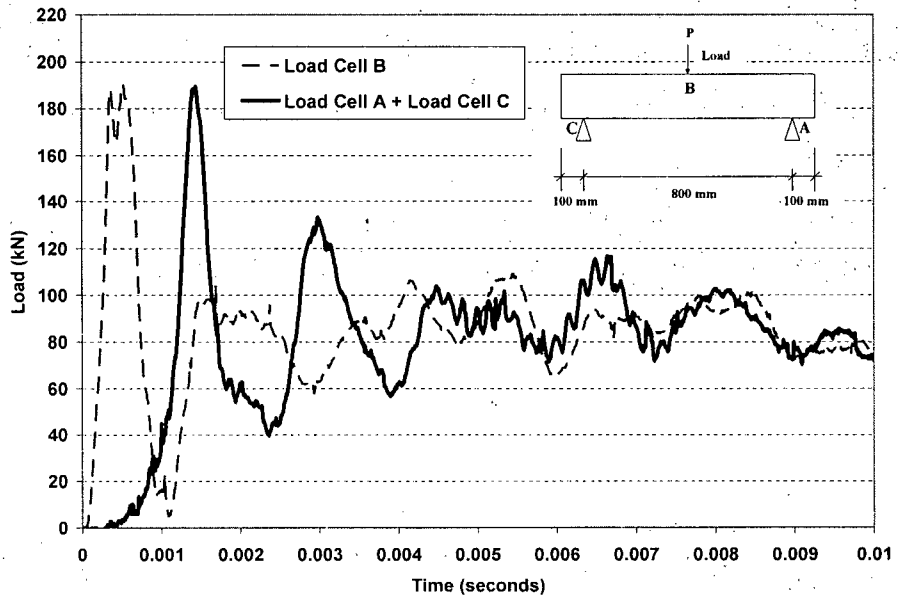

Figure 7.10 – *Load vs. Time for Beam BI-500-NY-1, No Steel Yoke Was Used*

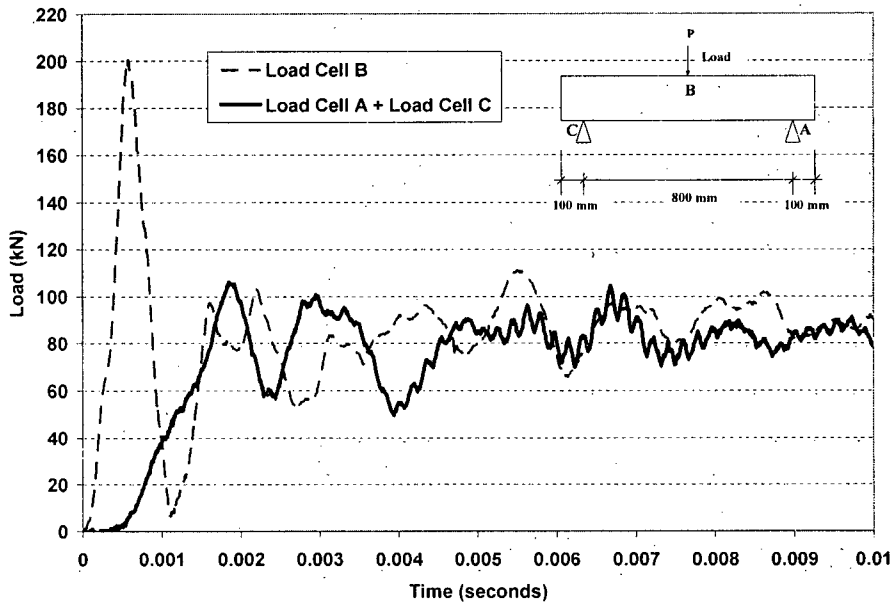

Figure 7.11 – *Load vs. Time for Beam BI-500-NY-2, No Steel Yoke Was Used*

It is worth noting that the maximum loads recorded by the tup (i.e. $P_t(t)$ from striking load cell: load cell B) and also the shape of the load vs. time curves are very similar for the two beams. There is also a time lag between the tup load and the support reaction as shown in Figures 7.10 and 7.11. This lag which was approximately equal to 0.001 seconds was needed for the stress waves to travel from the striking load cell at the beam mid-span to the supports as explained by Banthia et al. [117].

Since true bending loads, $P_b(t)$, obtained from support load cells were quite different for beams with the same configuration and under the same impact loading, it was decided to build two steel yokes at the location of the supports to make sure that the conditions at the support for a simply supported beam would be met.

7.3.2.2 Steel Yokes at the Supports

Steel yokes as explained in Section 6.3.3 were built and used to verify that inconsistent support condition was the main reason for not getting a stable and reliable load history for true bending load, $P_b(t)$. To support this statement, three identical beams (i.e BI500—1, BI-500-2 and BI-500-3), the same as the other two beams reported in the previous Section (i.e. BI-500-NY-1 and BI-500-NY-2), were tested under a 500 mm drop height and steel yokes were used to prevent upward movement of beams at the support locations at the instant of impact. Figures 7.12 and 7.13 show one of these beams before and after dropping the hammer.

Load vs. time histories of these beams are shown in Figures 7.14 to 7.16. There are three important points to mention here:

1. True bending load, $P_b(t)$, obtained from support load cells (load cell A + load cell C) are pretty much the same for all three beams.
2. Maximum tup load (denoted as load cell B) recorded by the striking hammer is not consistent and is in the range of 158 kN to 255 kN.

3. True bending loads recorded by the supports are more stable compared to those obtained in the first two tests with no steel yokes.

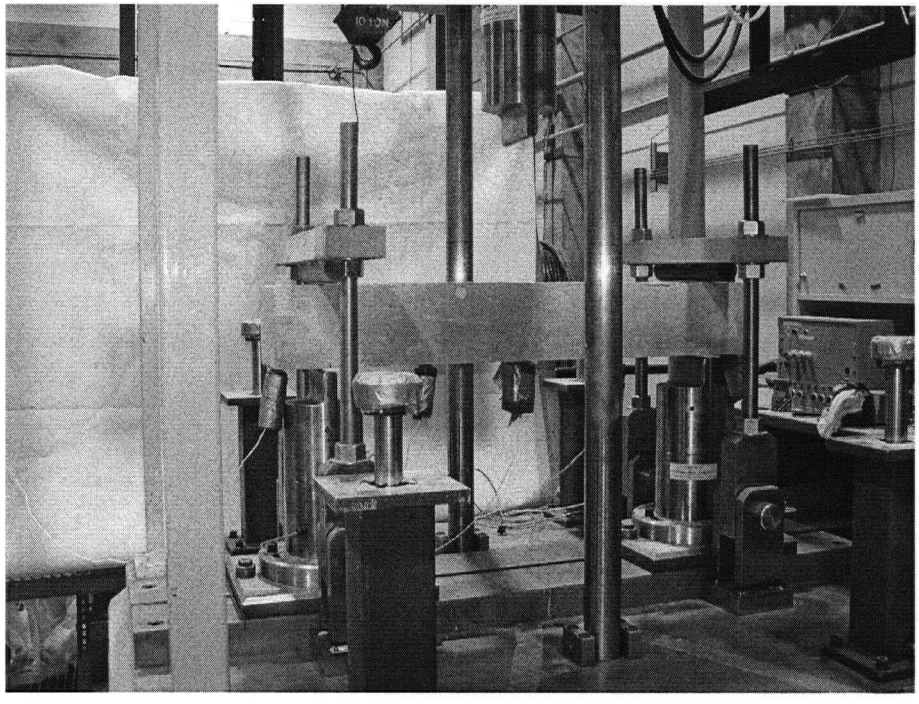

Figure 7.12 – *RC Beam before Impact Test, Steel Yokes Were Used*

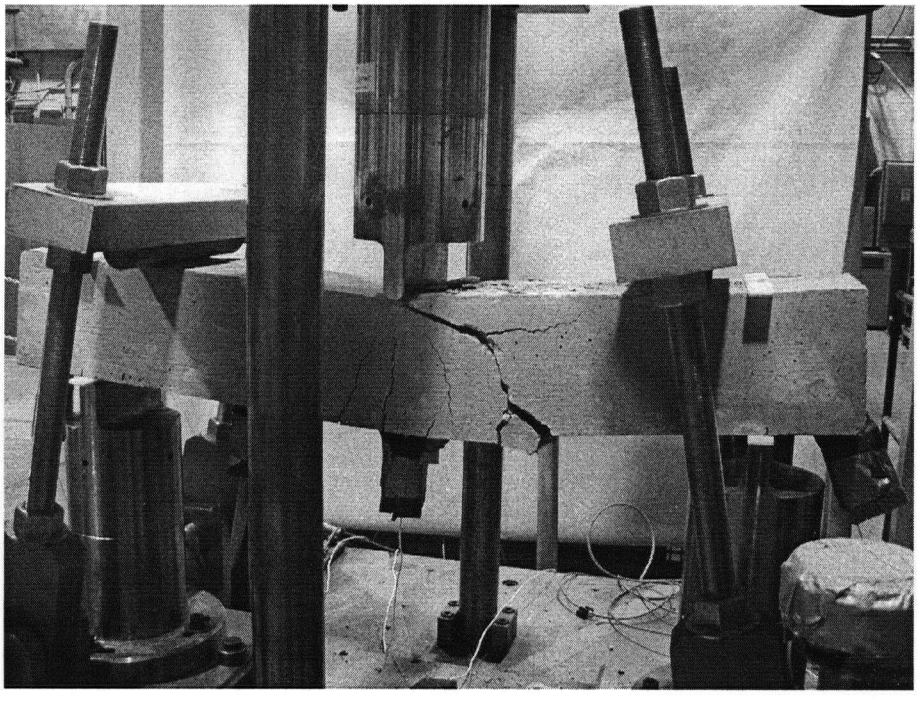

Figure 7.13 – *RC Beam after Impact Test, Steel Yokes Were Used*

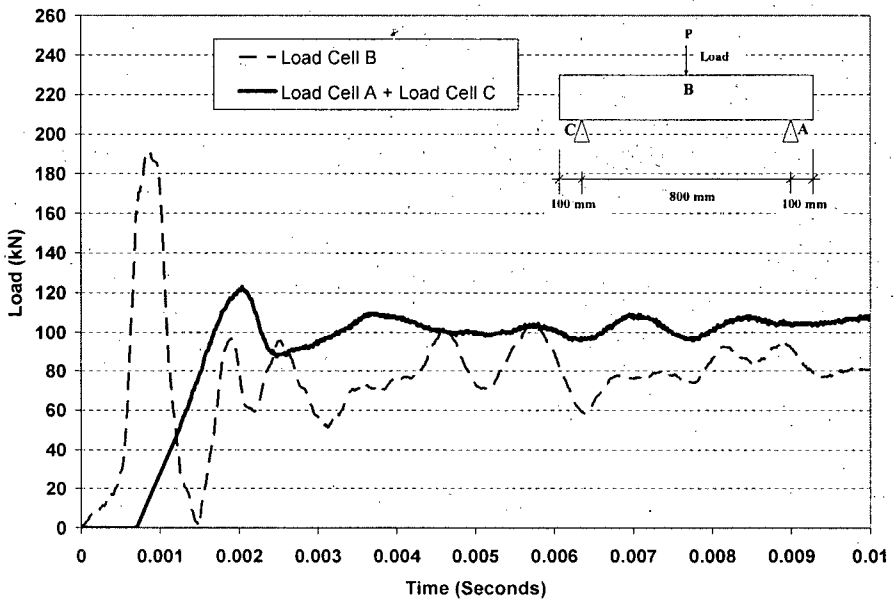

Figure 7.14 – *Load vs. Time for Beam BI-500-1, Steel Yokes Were Used*

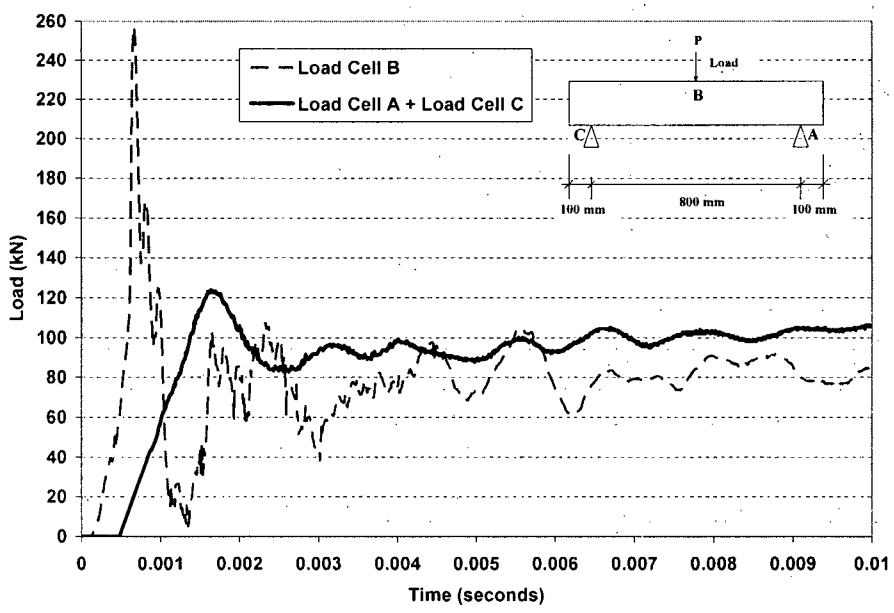

Figure 7.15 – *Load vs. Time for Beam BI-500-2, Steel Yokes Were Used*

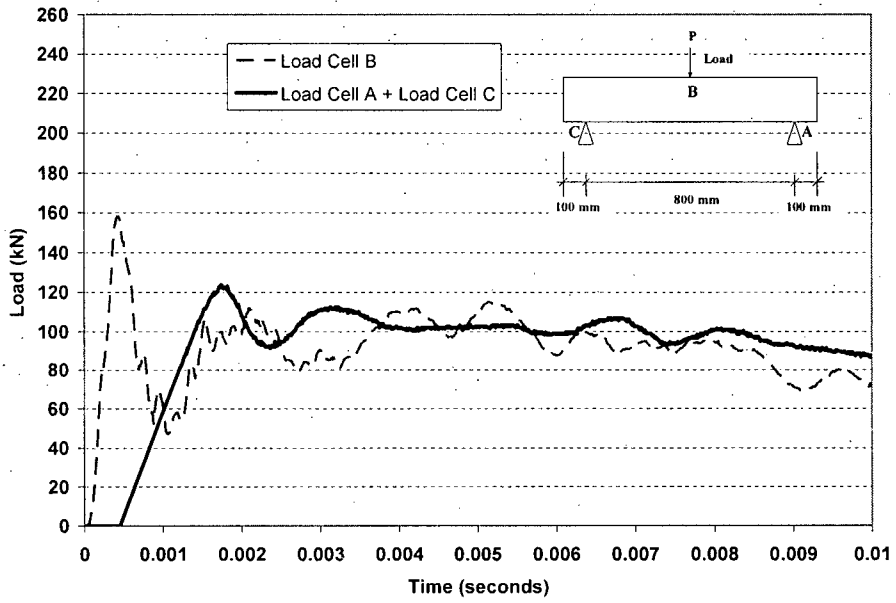

Figure 7.16 – *Load vs. Time for Beam BI-500-3, Steel Yokes Were Used*

In the light of the above, it was decided to use steel yokes throughout this research project to get a more stable and reliable results. It is also worth mentioning that the results obtained from the two support load cells are quite similar to each other and the peak load in both load cells occurred at the same time as expected. This phenomenon can be seen in Figure 7.17 for the case of beam B1-500-2.

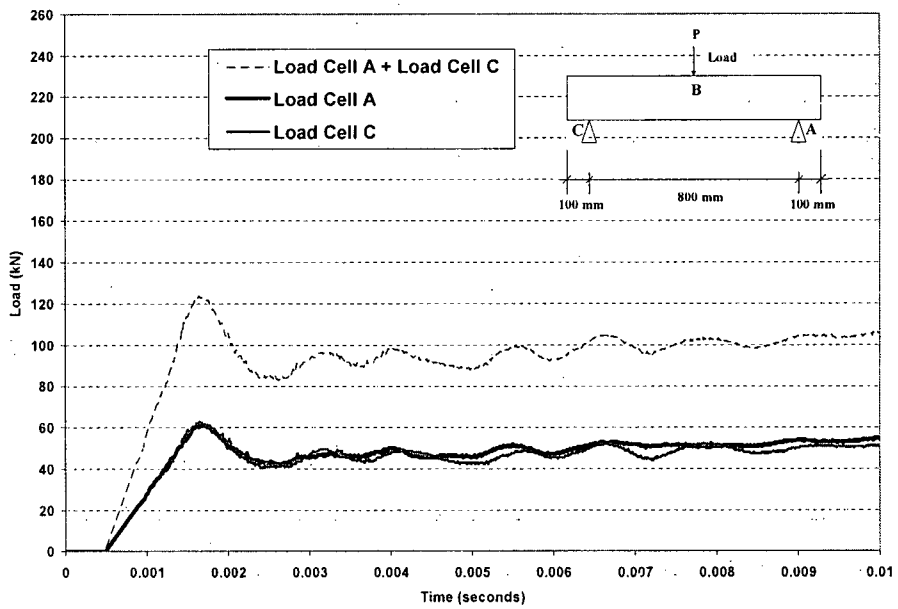

Figure 7.17 – *Load vs. Time for Support Load Cells in Beam BI-500-2*

Equations (7.6) and (7.7) were used to calculate the displacement of RC beam at the locations of the accelerometers. For beam BI-500-1, the displacement curves along half of the beam's length are shown in Figures 7.18 to 7.23. Since the beam failed in flexure, the displacement on the other half of the beam was symmetrical to the displacement shown in these Figures. The diamond-shaped points in these Figures show the actual displacement of the beam. The best fit lines are drawn and their equations along with their R^2 values are given. The displacements shown in Figures 7.18 to 7.23 were recorded at 0.001, 0.002, 0.003, 0.005, 0.014 and 0.023 seconds after the impact, respectively.

Therefore, one can conclude that the deflected shape for a simply supported RC beam at any time instant t under impact loading produces a linear deflection profile and can be approximated by a V-shape consisting of two perfectly symmetrical lines.

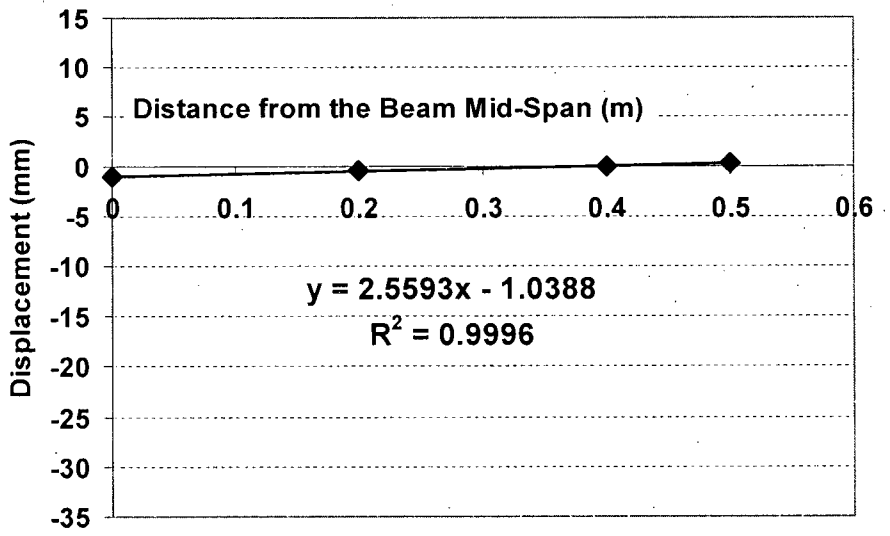

Figure 7.18 – *Displacement of Beam BI-500-1, t=0.001 s*

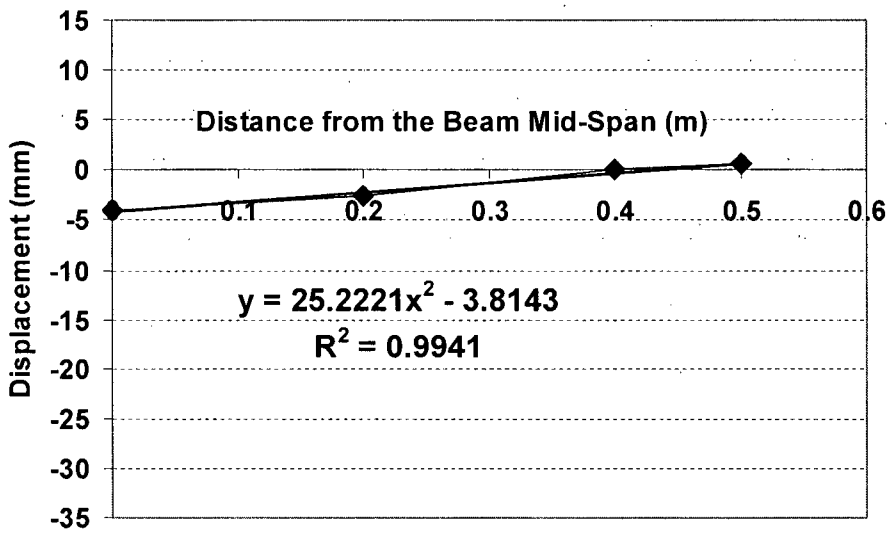

Figure 7.19 – *Displacement of Beam BI-500-1, t=0.002 s*

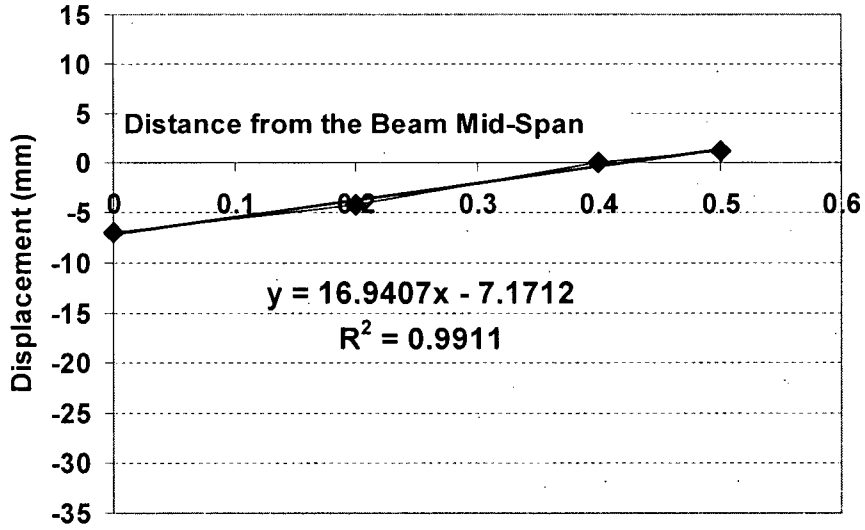

Figure 7.20 – *Displacement of Beam BI-500-1, t=0.003 s*

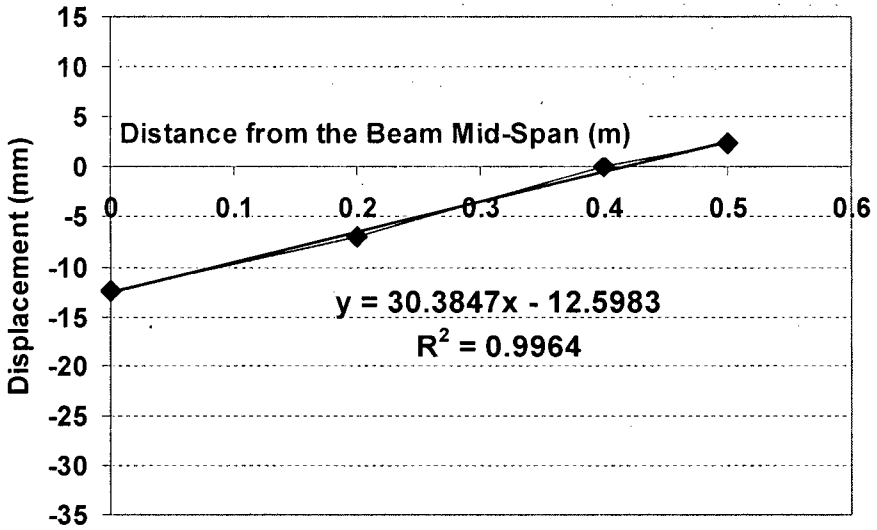

Figure 7.21 – *Displacement of Beam BI-500-1, t=0.005 s*

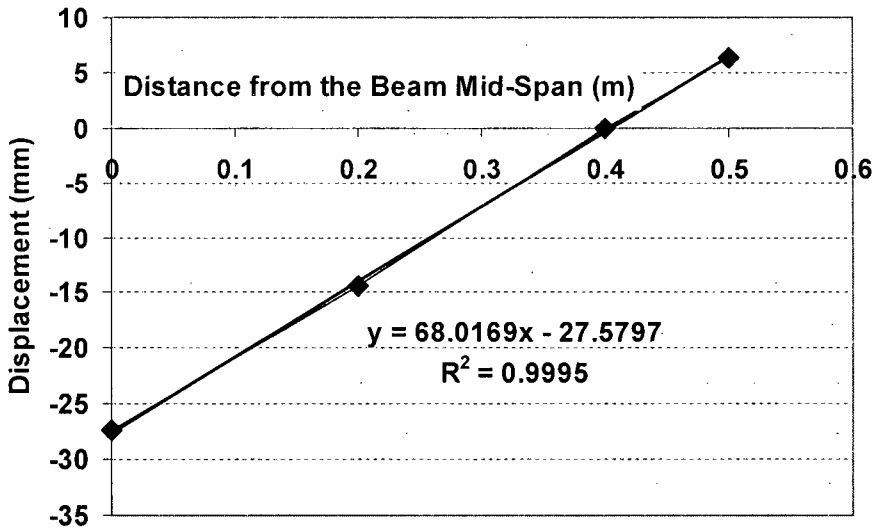

Figure 7.22 – *Displacement of Beam BI-500-1, t=0.014 s*

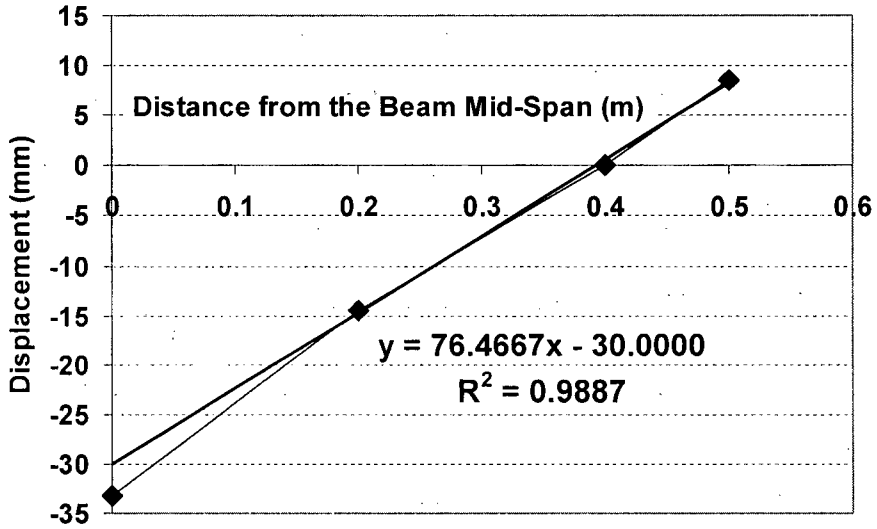

Figure 7.23 – *Displacement of Beam BI-500-1, t=0.023 s*

The impact velocities at the instant of impact for the hammer with a mass of 591 kg for different drop heights are calculated using equation (7.4) and given in Table 7.4.

Table 7.4 – *Impact Velocity for Different Drop Height*

Drop Height (mm)	Velocity (m/s)
400	2.8
500	3.13
600	3.43
1000	4.43
2000	6.26

As an example the velocity vs. time calculated by equation (7.6) for beam BI-500-2 is shown in Figure 7.24. Interestingly, the velocity of the hammer at the instant of

impact (3.13 m/s from Table 7.4) and the maximum velocity of the beam (which occurred 0.001 s after the impact as show in Figure 7.24) are very similar to each other. This, at least to some extent, can explain why the tup load at the very beginning of impact decreased almost to zero, after a very rapid increase to a maximum value (see Figure 7.15). In other words, the beam was accelerated by the hammer and reached its maximum velocity while at the same time (i.e. t = 0.001 s) the tup load (load cell B) decreased to zero as the beam sped away from the hammer and lost contact. The hammer was back to contact with the beam after some time (in the case of BI-500-2, after about 0.0005 s) and the load rose again. Some time after impact started (in the case of BI-500-2, after 0.035 s) the velocity of both (i.e. hammer and beam) decreased to zero.

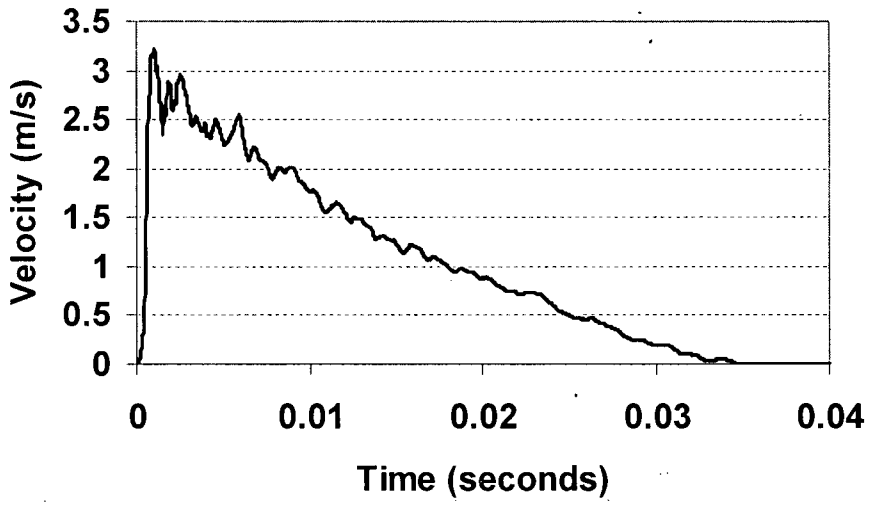

Figure 7.24 – *Velocity vs. Time at the Mid-Span, Beam BI-500-2*

Stressing load vs. mid-span deflection curves for beams BI-400, BI-500-1, BI-500-2, BI-500-3, BI-600, BI-1000 and BI-2000 are shown in Figures 7.25 to 7.31, respectively. The numbers 400, 500, 6000, 1000 and 2000 as explained in Table 7.1 refer to the drop height in mm. Equation (7.11) was used to find the true bending load and equations (7.6) and (7.7) were used to find the deflection at mid-span from acceleration histories of mid-span accelerometers (accelerometer #3 in Figure 7.6) in

each case. To provide a meaningful comparison, loads are drawn up to 140 kN and mid-span deflection up to 50 mm in all cases.

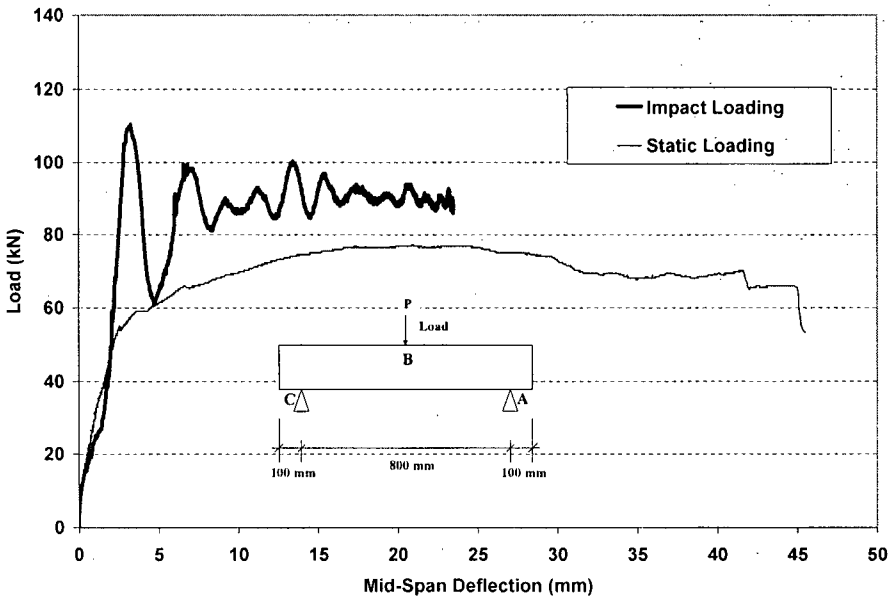

Figure 7.25 – *Load vs. Mid-Span Deflection, Beam BI-400*

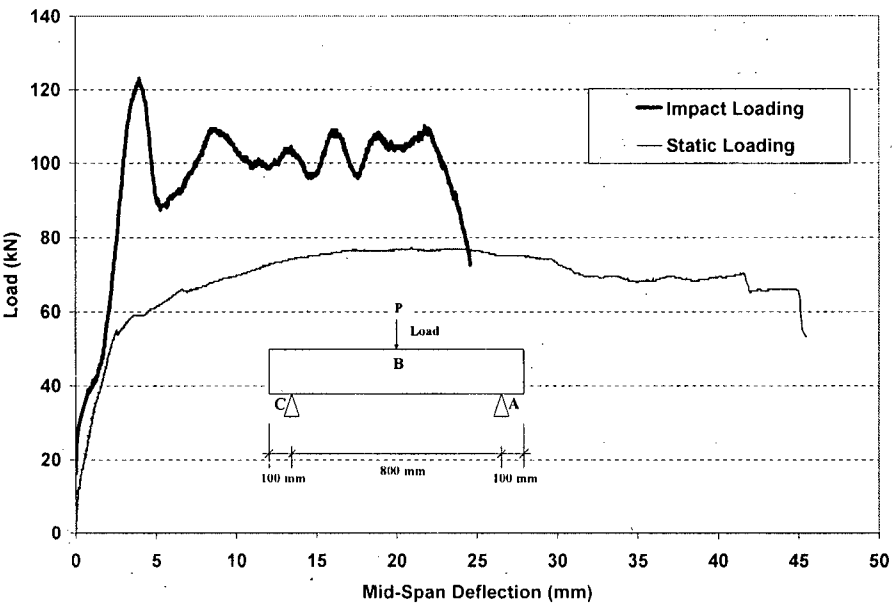

Figure 7.26 – *Load vs. Mid-Span Deflection, Beam BI-500-1*

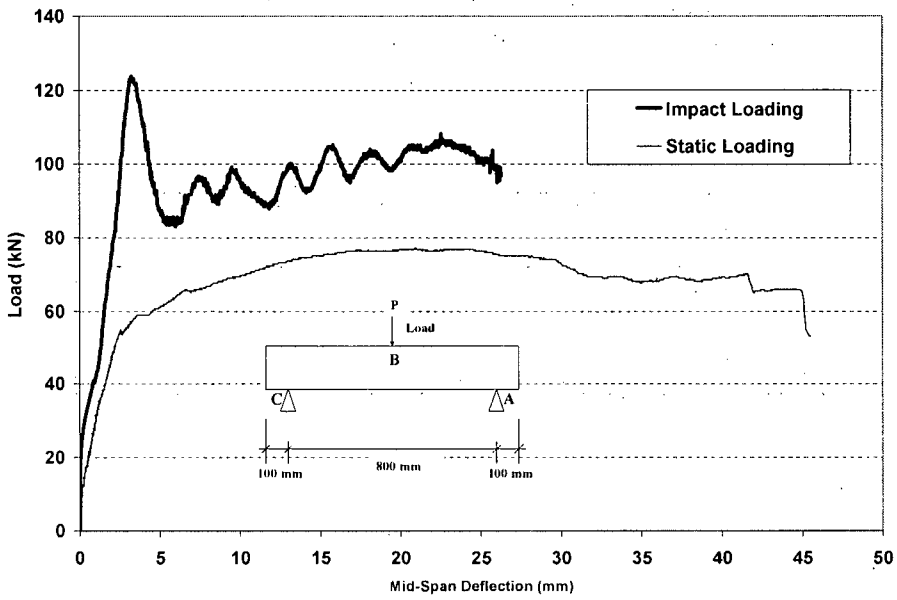

Figure 7.27 – *Load vs. Mid-Span Deflection, Beam BI-500-2*

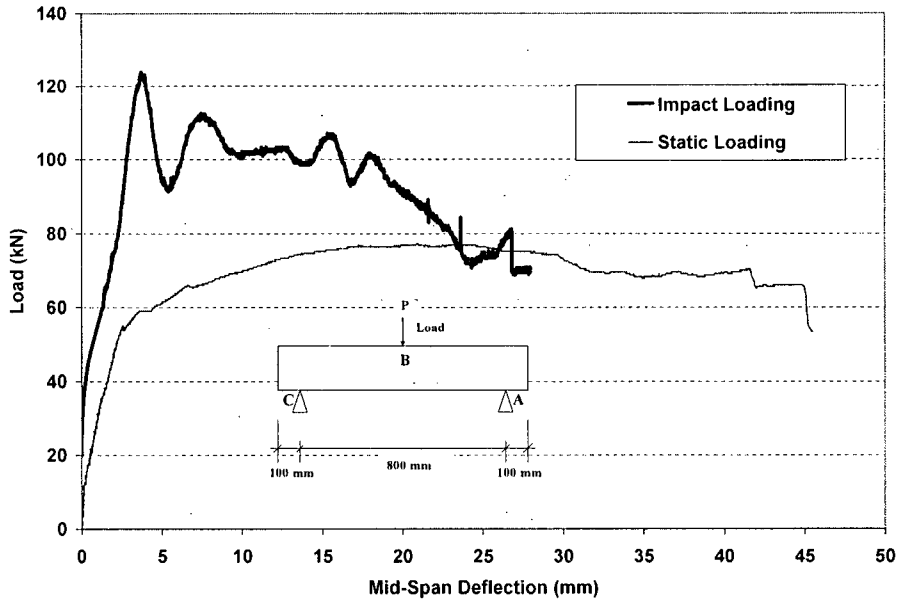

Figure 7.28 – *Load vs. Mid-Span Deflection, Beam BI-500-3*

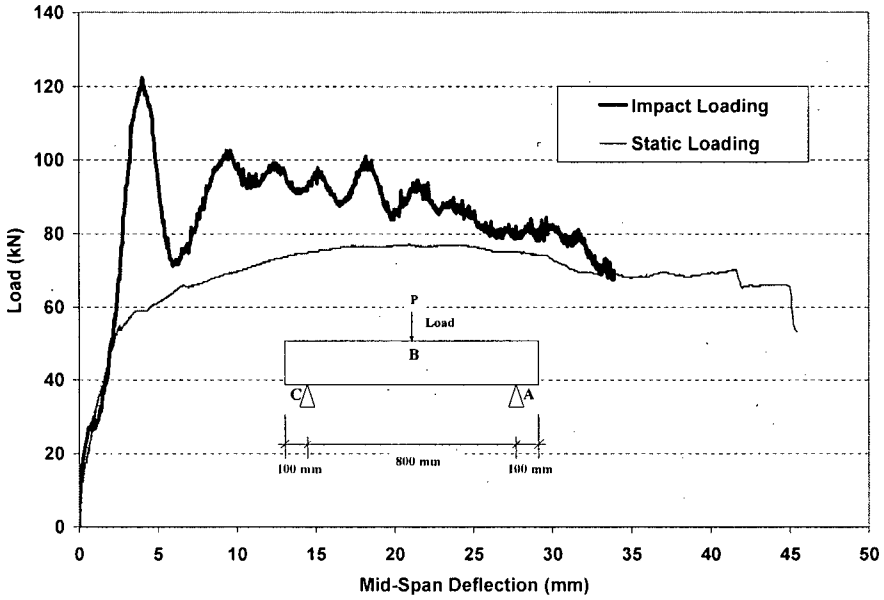

Figure 7.29 – *Load vs. Mid-Span Deflection, Beam BI-600*

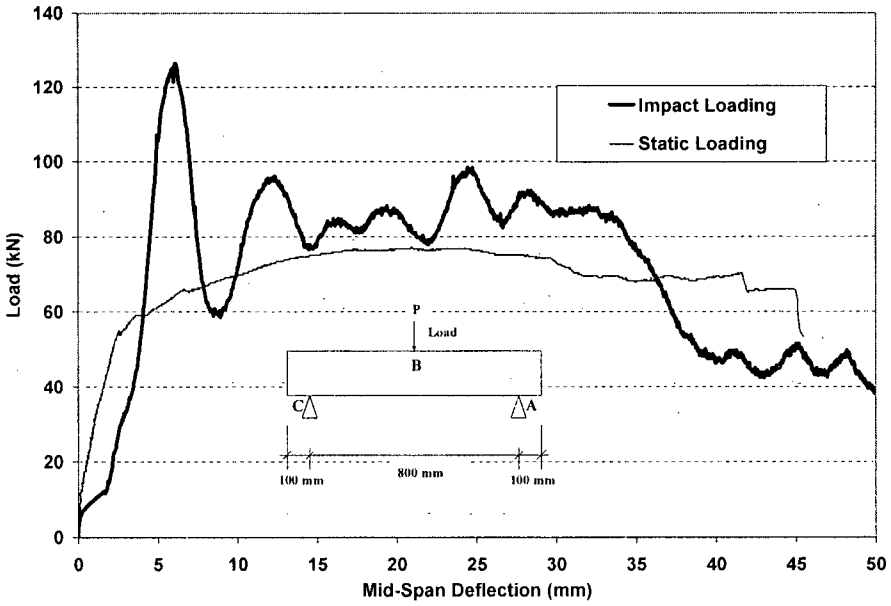

Figure 7.30 – *Load vs. Mid-Span Deflection, Beam BI-1000*

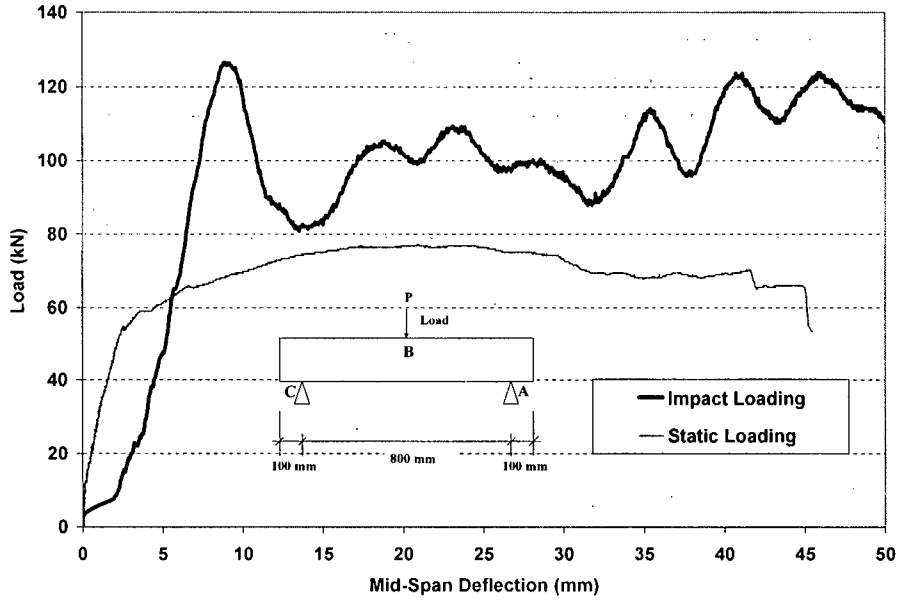

Figure 7.31 – *Load vs. Mid-Span Deflection, Beam BI-2000*

Load vs. mid-span deflection of the same beam tested under static loading is also included in each graph to show the differences between beam responses to different loading rates.

As mentioned earlier, one of the most important endeavors of this research project was to prove that at any time t, the true bending load should be calculated by equation (7.11) (i.e. the summation of two support load cells). To support this claim, tup load, as well as the true bending load (the summation of two support load cells), vs. mid-span deflection for beams BI-400, BI-500-1, BI-500-2, BI-500-3, BI-600, BI-1000 and BI-2000 are shown in Figures 7.32 to 7.38, respectively. A picture of the beam after failure is also included in each Figure.

It is clear that while the recorded tup load in these beams, in general, increased with increasing drop height, at a constant drop height, the maximum value for tup load was not steady. On the other hand, beyond a certain drop height, the maximum true bending load (i.e. load ell A + load cell C) did not change with increasing drop height.

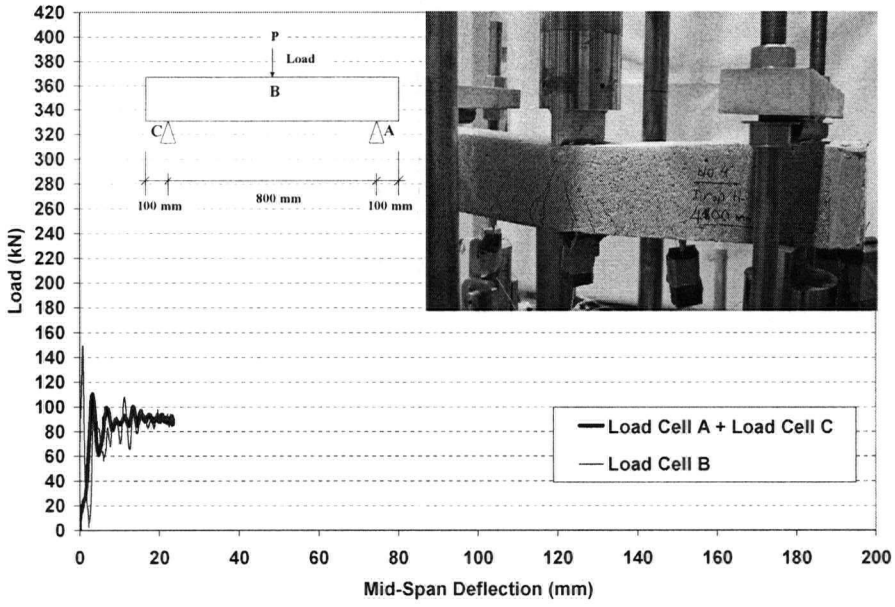

Figure 7.32 – *Tup Load vs. Mid-Span Deflection, Beam BI-400*

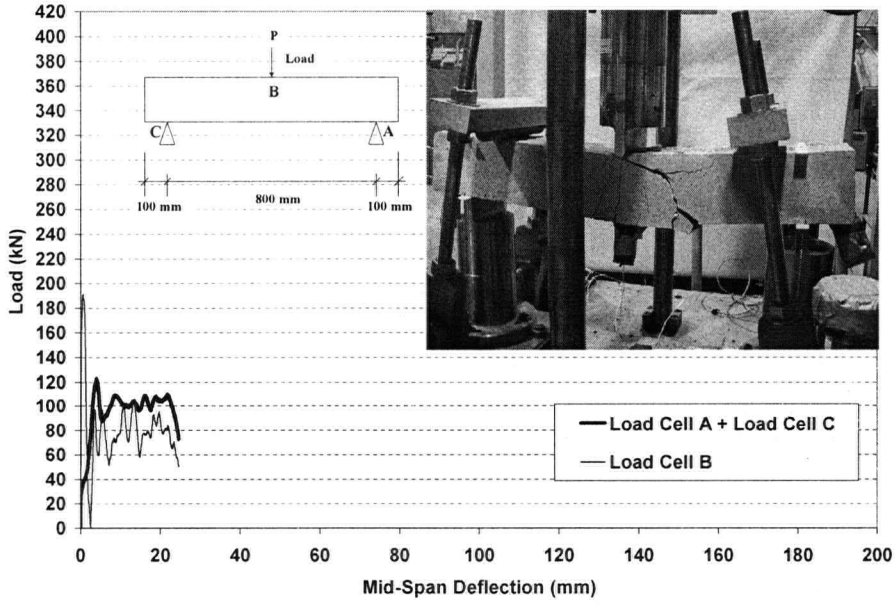

Figure 7.33 – *Tup Load vs. Mid-Span Deflection, Beam BI-500-1*

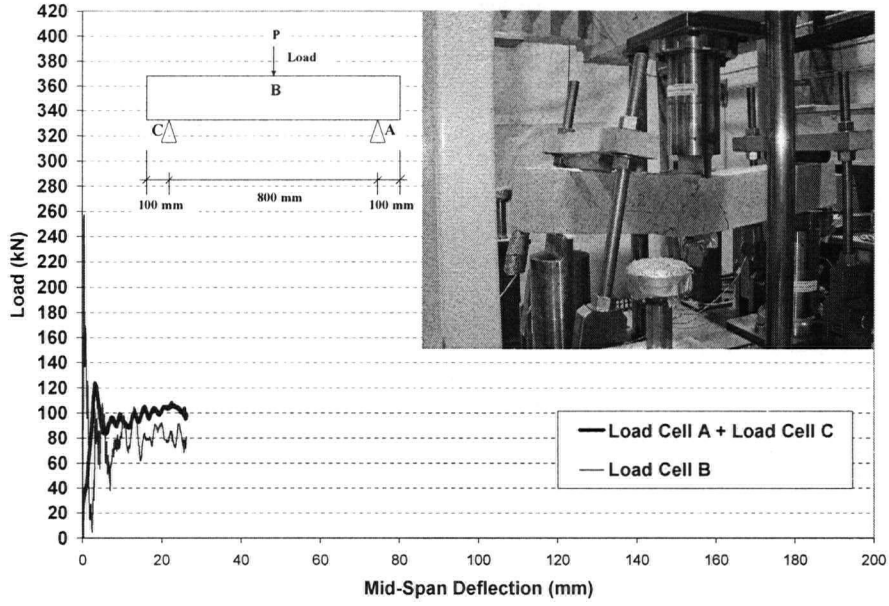

Figure 7.34 – *Tup Load vs. Mid-Span Deflection, Beam BI-500-2*

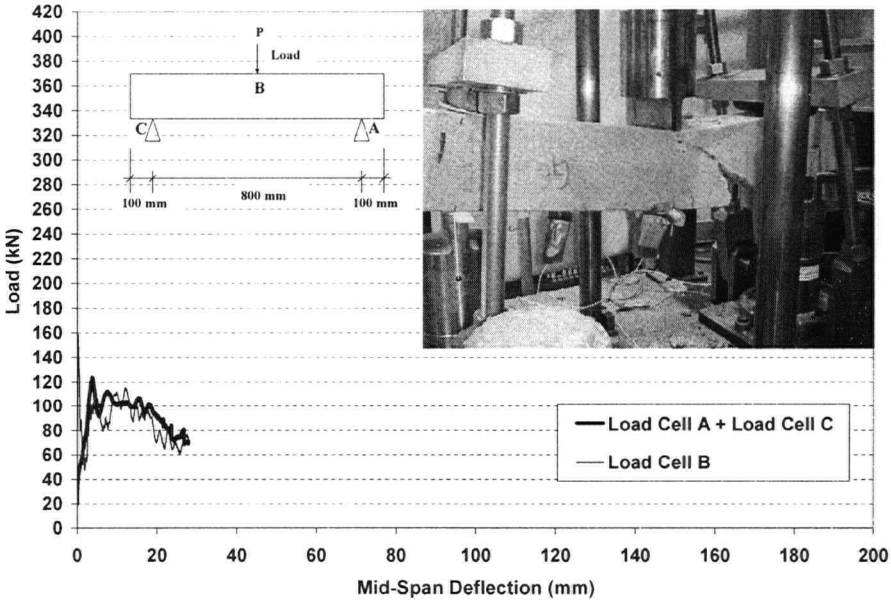

Figure 7.35 – *Tup Load vs. Mid-Span Deflection, Beam BI-500-3*

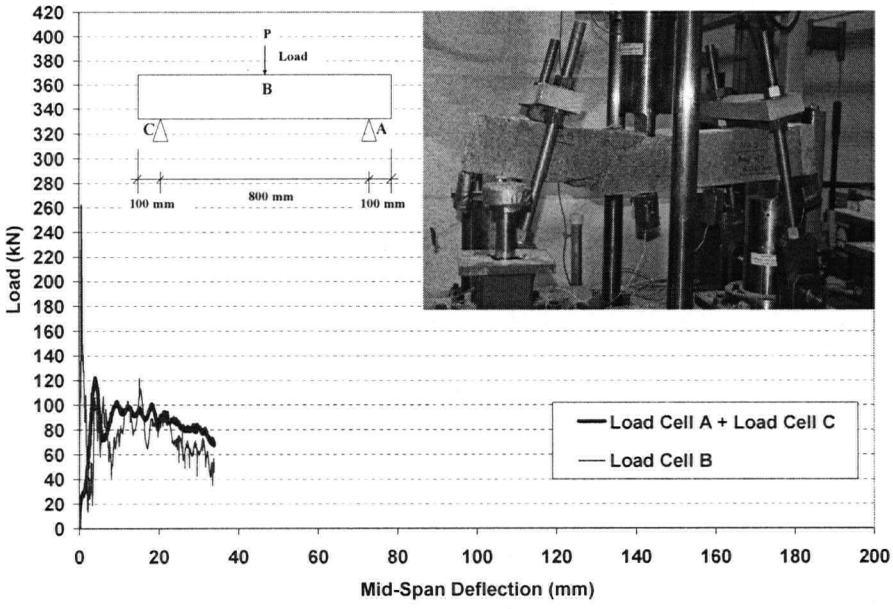

Figure 7.36 – *Tup Load vs. Mid-Span Deflection, Beam BI-600*

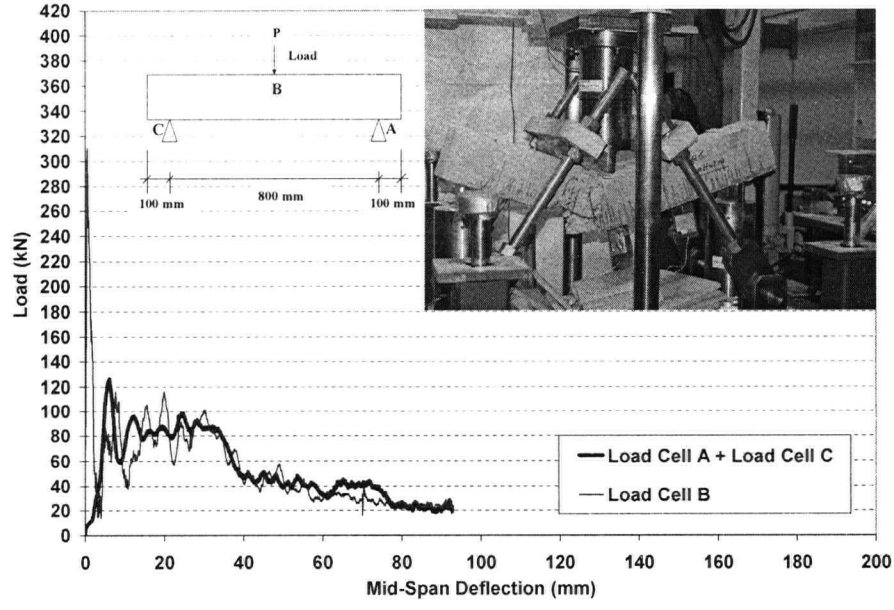

Figure 7.37 – *Tup Load vs. Mid-Span Deflection, Beam BI-1000*

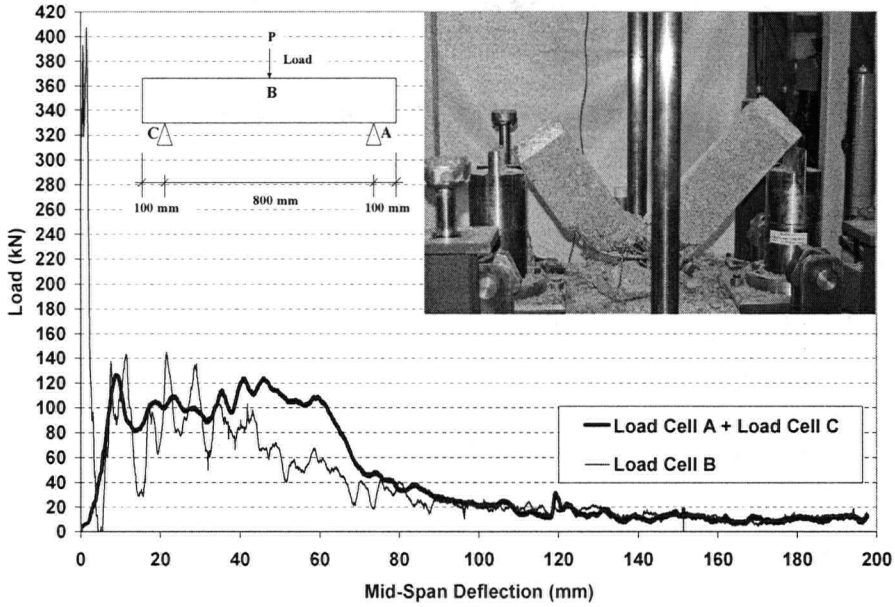

Figure 7.38 – *Tup Load vs. Mid-Span Deflection, Beam BI-2000*

Maximum recorded tup loads for beams tested under different drop heights are compared in Figure 7.39. Maximum recorded true bending loads (summation of support load cells) are shown in Figure 7.40.

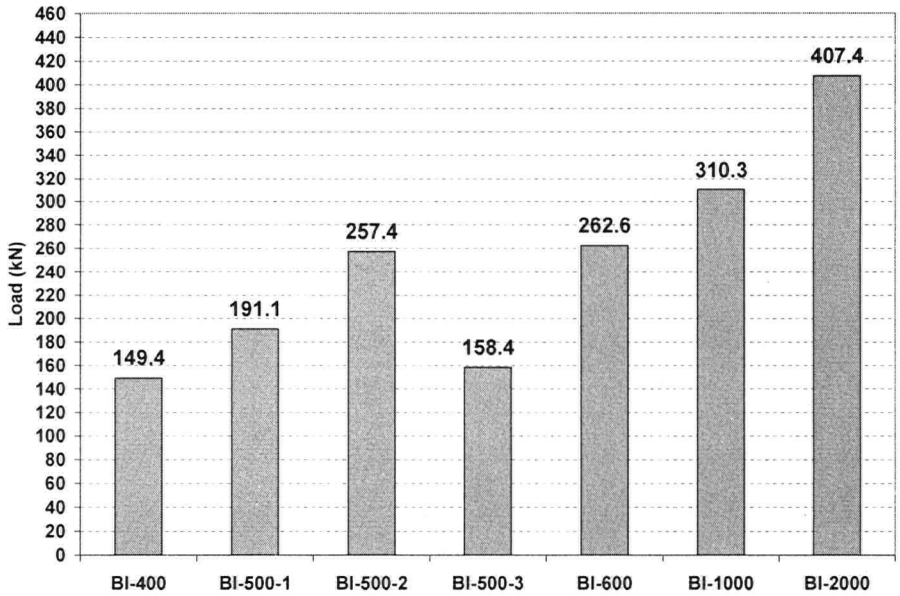

Figure 7.39 – *Maximum Recorded Tup Load for Different Beams/Drop Height*

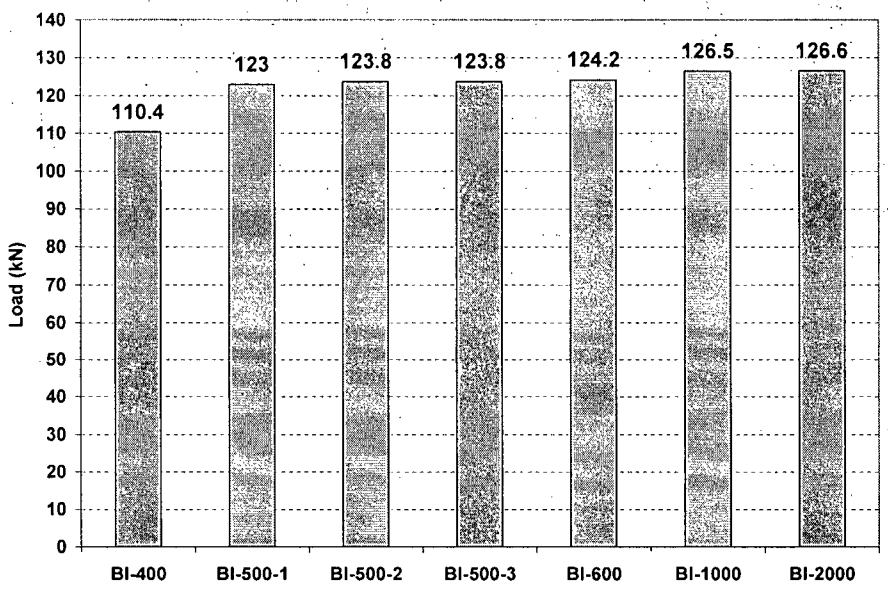

Figure 7.40 – *Maximum Recorded True Bending Load for Different Beams/Drop Height*

Bending load at failure vs. impact velocity is shown in Figure 7.41. Bending load at failure is defined as the maximum recorded true bending load for impact loading. This is also the load at which, presumably, the steel rebars in tension start yielding for static loading.

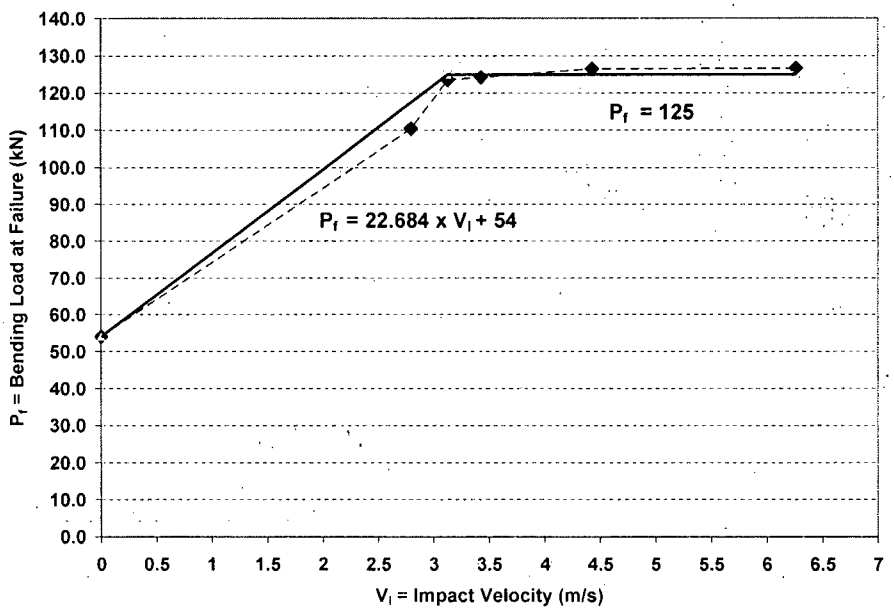

Figure 7.41 – *Bending Load at Failure vs. Impact Velocity*

It may be seen that bending load at failure increased by increasing the velocity of the impact hammer until it reached a velocity of about 3 m/s. After this point, the bending load at failure was independent of impact velocity and stayed constant. It is very important to note that for this hammer with a mass of 591 kg, a minimum drop height is needed to make the RC beam fail. For example a drop height of only 100 mm of this hammer most probably would not break the beam, but failure may occur if a heavier hammer is employed. Since the impact velocity is directly related to hammer drop height, one can conclude that for a given hammer mass, there exists a certain threshold velocity (or drop height) after which the bending load at failure will not increase by increasing the velocity. This threshold velocity for the hammer used in this research was found to be 3 m/s. Figure 7.41 also shows that the impact bending capacity of this RC beam is about 2.3 times its static bending capacity. Therefore, an impact coefficient of 2.3 can be used to estimate the impact bending capacity of this RC beam from its static bending capacity.

Equation (7.8) can be rewritten as:

$$P_i(t) = P_t(t) - P_b(t) \tag{7.12}$$

where,

$P_i(t)$ = a point load representing inertia load at the mid-span of the beam at time t equivalent to the distributed inertia load

$P_t(t)$ = tup load at time t

$P_b(t)$ = true bending load at the mid-span of the beam at time t

Therefore, inertia load at any time t is the difference between tup load and true bending load. Equation (7.11) is the most accurate way to obtain true bending load at any time instant t, and as explained earlier, can be done using instrumented support anvils. As an example, inertia load for beam BI-400 calculated by equation (7.12) is shown in Figure 7.42. The values obtained by equation (7.12) are the most accurate values coming from a fully instrumented test setup. Inertia load predicted by equations

(7.9) and (7.10) are also shown in Figure 7.42. Real values of bending load for the same beam as well as bending load predicted by equations (7.8), (7.9) and (7.10) are shown in Figure 7.43.

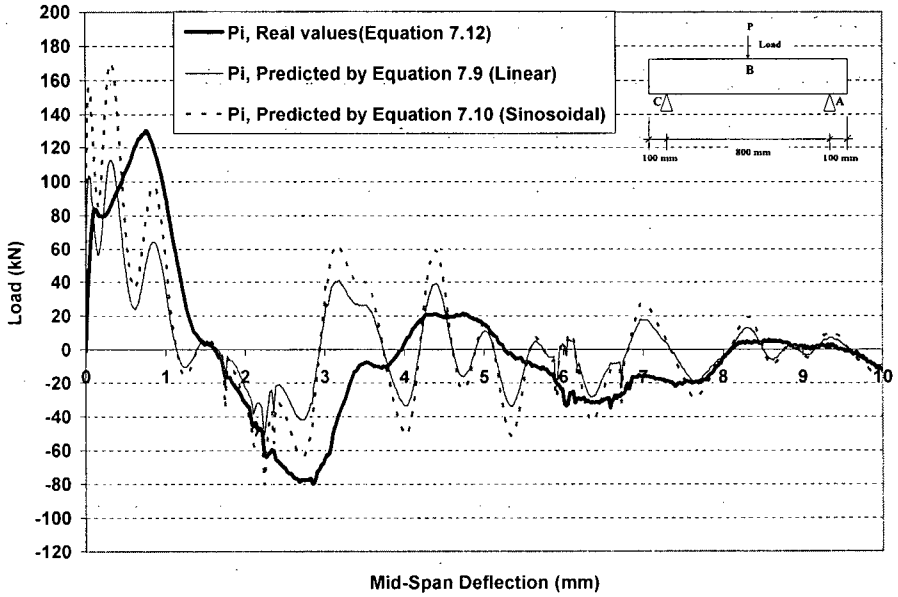

Figure 7.42 – *Inertia Load for Beam BI-400*

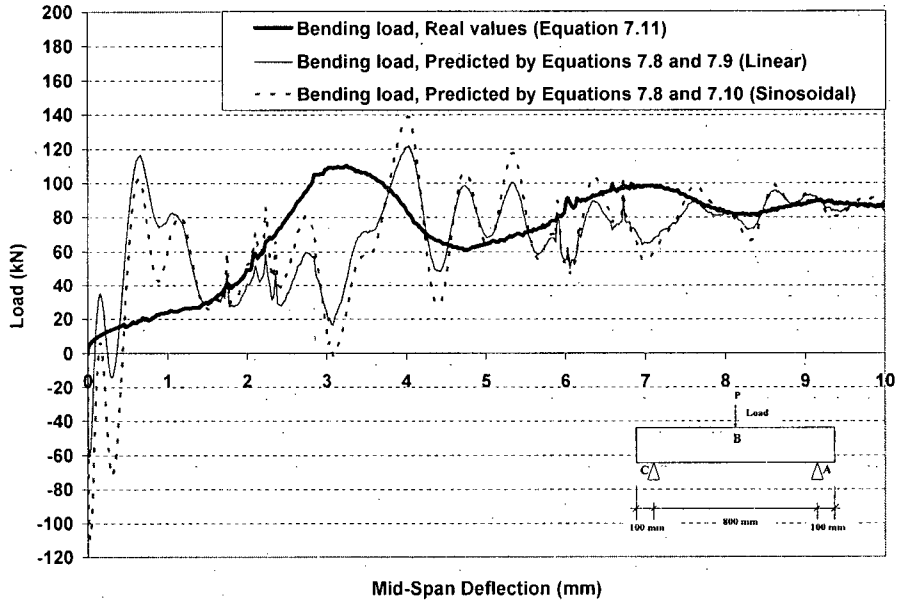

Figure 7.43 – *Bending Load for Beam BI-400*

It is seen that the prediction of inertia load using equations (7.9) and (7.10) is not accurate, but as shown earlier the deflected shape of an RC beam can be considered linear as oppose to sinusoidal and as a result, equation (7.9) predicts better than equation (7.10) as shown in Figure 7.42.

$P_i(t)$ is a generalized point load representing inertia load at the mid-span of the beam at time t, but in reality, the inertia load of the beam is a body force distributed throughout the body of the beam. This, at least to some extent, can explain why the inertia load predicted by Equations (7.9) and (7.10) is not accurate and why Equation (7.12) can predict the exact value of this load.

A large portion of the peak load measured by the instrumented tup is the inertia load. This is shown in Figure 7.44. At the peak load measured by the instrumented tup, the inertia load, to accelerate the beam from its rest position, may account for 75% to 98% of the total load.

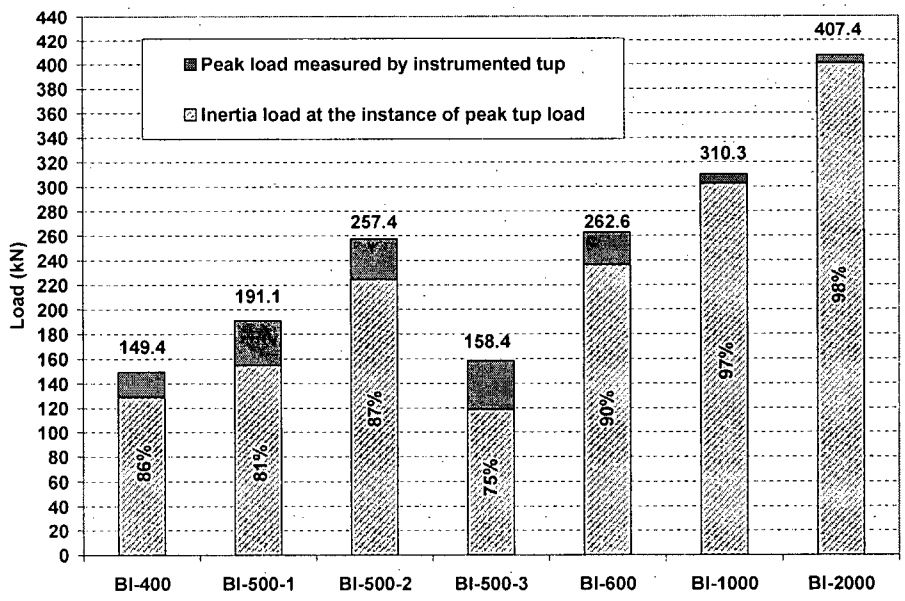

Figure 7.44 – *Inertia Load at the Peak of Tup load*

7.4 Energy Absorption

The energy expended in deflecting and fracturing the beam is calculated from the area under the true bending load vs. deflection and tup load vs. deflection and compared with energy stored in (or released by) the dropping hammer. The results are shown in Figure 7.45 (a) and (b). Energy stored in the dropping hammer is calculated as:

$$E_{hammer} = m.g.h \tag{7.13}$$

where,

E_{hammer} = Potential energy stored in dropping hammer (N.mm)

m = Mass of the dropping hammer (kg)

g = Acceleration due to gravity(= 9.81 m/s^2)

h = Height of the dropping hammer (m)

Figure 7.45 shows a good agreement between the calculated absorbed energy in RC beam using two different approaches; 1) by calculating the area under true bending load (load cell A + load cell C) vs. mid-span deflection curve and 2) by calculating the area under tup load (load cell B) vs. mid-span deflection. In perfect conditions, the values obtained by these two methods should be exactly the same. The difference which is the work done by fictitious inertia force, $P_i(t)$, should be equal to zero.

In this study, the ratio of absorbed energy to input energy (energy absorbed by RC beam to energy released by the hammer) was in the range of 76% to 89% with a mean value of 83% if area under true bending load vs. mid-span deflection is used for calculation. If area under tup load vs. mid-span deflection is used, this range is changed to 67% to 85% with a mean value of 76%. Therefore, one can conclude that about 80% of the input energy is absorbed by the RC beam.

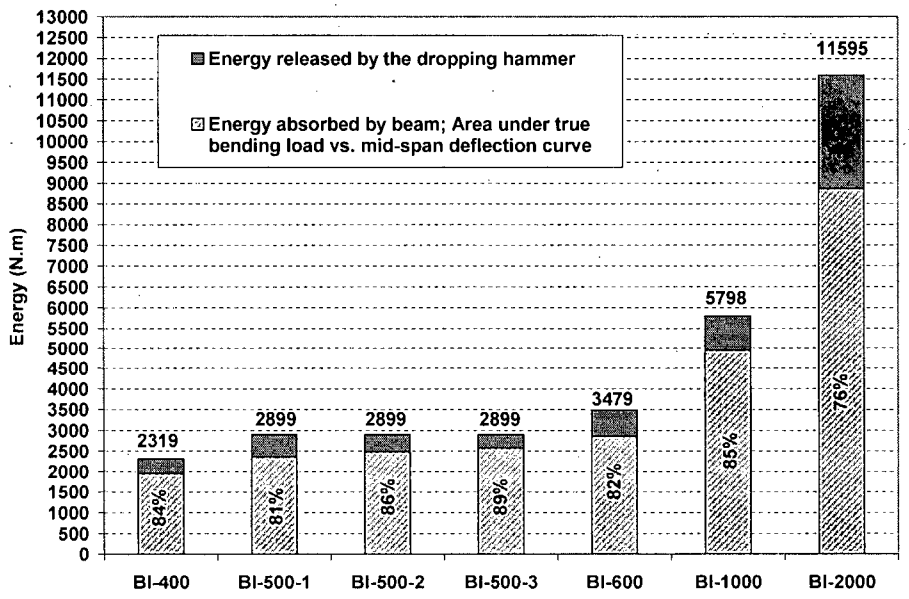

(a)

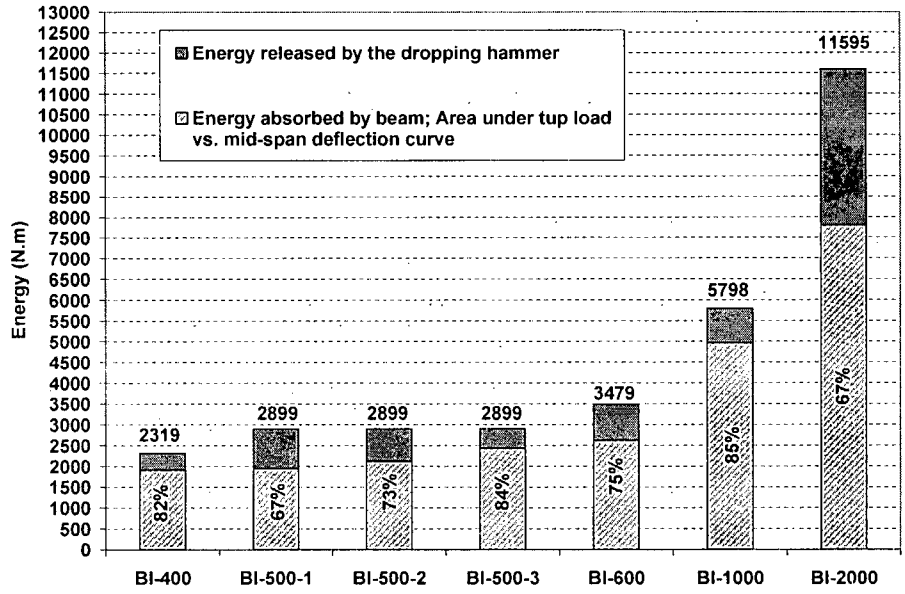

(b)

Figure 7.45 – *Energy Evaluations for Different Drop Height from (a) True Bending Load; (b) Tup Load*

7.5 RC Beams Strengthened by Fabric GFRP

The Wabo®MBrace GFRP fabric system was used to strengthen the 2 remaining RC beams for flexure and shear. One layer of GFRP fabric with a thickness of about 1.2 mm, length of 750 mm and width of 150 mm was applied longitudinally on the tension (bottom) side of the beam for flexural strengthening and an extra layer with fibers perpendicular to the fiber direction of the first layer was applied on 3 sides (i.e. 2 sides and bottom side) for shear strengthening.

One of these beams was tested under quasi-static loading, while the other one was tested under impact with a 600 mm hammer drop height (i.e. impact velocity, V_I, of 3.43 m/s). Load vs. mid-span deflection of these RC beams are shown in Figure 7.46 (a) and (b). It is important to note that while the control RC beam (i.e. when no fabric GFRP was used) failed in flexure, the strengthened RC beams failed in shear indicating that shear strengthening was not as effective as flexural strengthening and perhaps more layers of GFRP were needed to overcome the deficiency of shear strength in these beams.

In general, these tests showed that fabric GFRP can effectively increase RC beam's capacity under both, quasi-static and impact load conditions.

Load carrying capacity of these beams are compared in Table 7.5. While an 84% increase in load carrying capacity was observed in quasi-static loading, the same GFRP system was able to increase the capacity by only 38% under impact loading. It is also worth mentioning while the maximum bending load under impact loading for un-strengthened RC beam was 2.26 times its static bending capacity; the ratio of maximum impact load to static load for strengthened RC beam was 1.69. This difference can certainly be explained by the change in failure mode from bending to shear when fabric GFRP was applied to these RC beams. The area under the load-deflection curve in Figure 7.46 (b) was measured and it was found that about 86% of the input energy was absorbed by the strengthened RC beam during the impact.

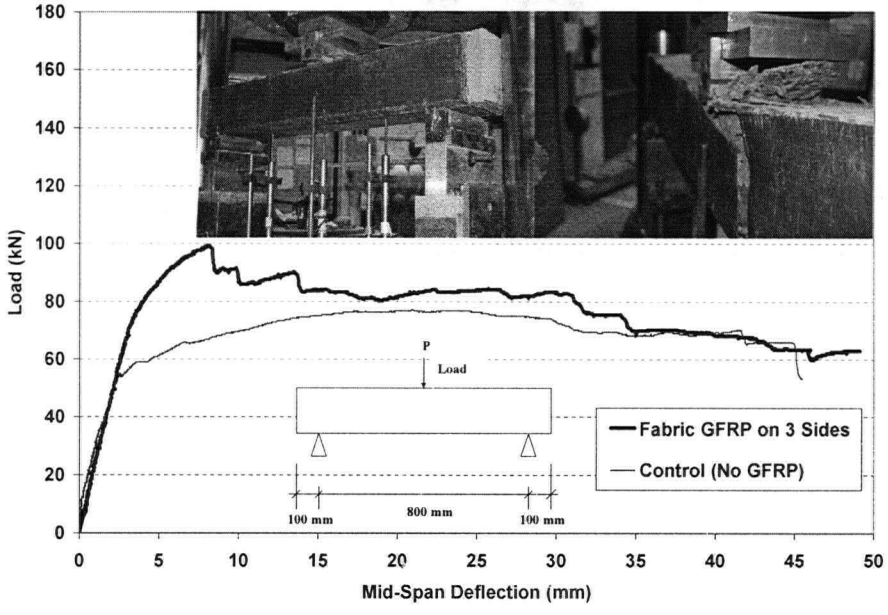

(a)

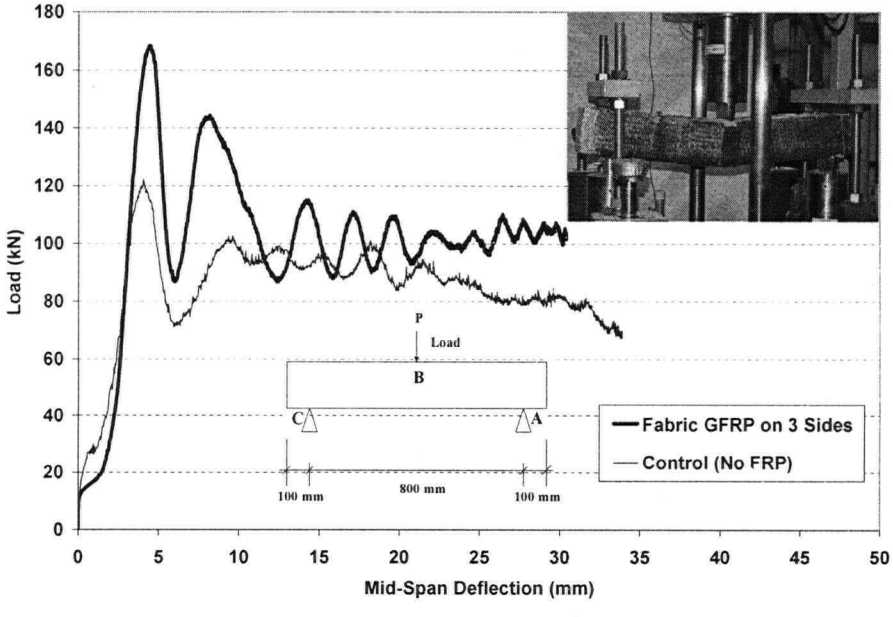

(b)

Figure 7.46 – *Load vs. Mid-Span Deflection for RC Beam Strengthened in Shear and Flexure Using Fabric GFRP;*
(a) Quasi-Static Loading, (b) Impact Loading (V_I = 3.43 m/s)

Table 7.5 –*Load Carrying Capacity of RC Beams Strengthened by Fabric GFRP*

Loading Type	Load Carrying Capacity (kN)	Increase in Load Carrying Capacity (%)
Quasi-Static	99.4 (54)*	84%
Impact	168.4 (122.2)*	38%

* Numbers in brackets are the load carrying capacity of un-strengthened RC beams

7.6 Conclusions

Based on the results and discussions reported in this chapter, the following conclusions can be drawn:

1. Load carrying capacity of RC beams under impact loading can be obtained using instrumented anvil supports.
2. The use of steel yokes at the support provides more reliable and accurate results.
3. Loads measured by the instrumented tup will result in misleading conclusions due to inertia effect.
4. There is a time lag between maximum load captured by the instrumented tup and maximum load captured by instrumented supports. This lag is really due to stress pulse travel from centre to support. This time lag shows that the inertia load effect must be taken into account.
5. Inertia load at any time instant t can be obtained by subtracting the summation of support load cells (i.e. true bending load) from the load obtained by the instrumented tup.
6. Bending load capacity of an RC beam under impact loading can be estimated as 2.3 times its static capacity for the conditions and details of tests performed here. Note that Kishi et al. [106] tested 4 different types of RC

beams (different cross-sectional areas and different reinforcement ratios) and, interestingly, found that the load carrying capacities of these beams under impact loading were always greater than 2.0 times their static capacities.

7. After a certain impact velocity, bending load capacity of RC beams remains constant and increase in stress (or strain) rate will not increase their load carrying capacity.
8. About 80% of the input energy in an impact test (i.e. energy imparted to the dropping hammer) was absorbed by the RC beam.
9. Fabric GFRP can increase the load carrying capacity of RC beams in both static and impact loading conditions.
10. The use of fabric GFRP may change the mode of failure, and as a result, the load carrying capacity of an RC beam strengthened by fabric GFRP under impact loading can be much lower than the anticipated 2.3 times its static capacity (see conclusion 6 above).

8

BEHAVIOR OF SHEAR STRENGTHENED RC BEAMS UNDER QUASI-STATIC LOADING

8.1 Introduction

RC beams with deficiency in their shear strength (i.e. expected to fail in shear) were retrofitted using Sprayed GFRP. Different thicknesses and schemes were used and their effectiveness was evaluated under quasi-static loading. The most promising ones were then tested under impact loading using a fully instrumented drop weight impact machine described in Chapter 6.

Three beams were also strengthened in shear using Wabo®MBrace fabric GFRP and tested under quasi-static loading. In this Chapter test results obtained under quasi-static loading are provided and discussed in detail.

8.2 Beam Design and Testing Procedure

A total of 48 RC beams were cast to investigate the shear strengthening using Sprayed and fabric GFRP under quasi-static and impact loading. These beams contained flexural reinforcement but none or less than the required stirrups. Total length of these beams was 1 m and they were tested over an 800 mm span. Load configuration and cross-sectional details are shown in Figure 8.1.

Parameters needed for calculating the load carrying capacity of beam shown in Figure 8.1 are tabulated in Table 8.1. Since not enough shear reinforcement was provided, the maximum strength of the beam would be governed by the shear strength of concrete as well as the shear strength provided by the steel stirrups where applicable. Calculations (see Appendix B) show that if resistance factors are not considered, the capacity of this beam under quasi-static loading is of 131 kN if enough reinforcement is provided for shear. At this point, tension reinforcement would start yielding. It is also worth noting that the beam was designed to produce a typical shear failure mode since not enough stirrups were provided and the shear strength of the concrete was far below the flexural strength of the beam. The RC beam with no stirrups and with stirrups (Φ4.75 @ 160 mm) is predicted to have a capacity of about 80 kN and 100.2 kN, respectively (see Appendix B).

Table 8.1 – *Properties of RC Beams*

Parameter	Definition	Value	Unit
b	Width of compression face of member	150	mm
h	Overall depth of beam	150	mm
d	Distance from extreme compression fiber to centroid of tension reinforcement	120	mm
d'	Distance from extreme compression fiber to centroid of compression reinforcement	20	mm
f_c'	Specified compressive strength of concrete	44	MPa
f_y	Specified yield strength of tension reinforcement	440	MPa
f_{yc}	Specified yield strength of compression reinforcement	474	MPa
f_{ys}	Specified yield strength of shear reinforcement	600	MPa
A_s	Area of tension reinforcement	600	mm^2
A_s'	Area of compression reinforcement	200	mm^2
A_v	Area of shear reinforcement	35.4	mm^2

In quasi-static loading conditions, all of the beams were tested in 3-point loading using a Baldwin 400 kips Universal Testing Machine. ASTM C78 *Flexural Strength of Concrete* specifies a rate of increase in the flexural stress of 0.86 – 1.21 MPa/min for flexural testing. As calculated and mentioned in Chapter 7, in this study the load was monitored visually throughout the testing to ensure a consistent loading within the range of 2419 – 3403 N/min with a target rate of 2900 N/min. Three LVDTs were used to capture the deflection at the mid-span as well as two more points along the beam as shown in Figure 8.1. The test setup for quasi-static loading is shown in Figure 8.2. Applied load and deflections were constantly monitored and recorded using a data acquisition system based on a PC.

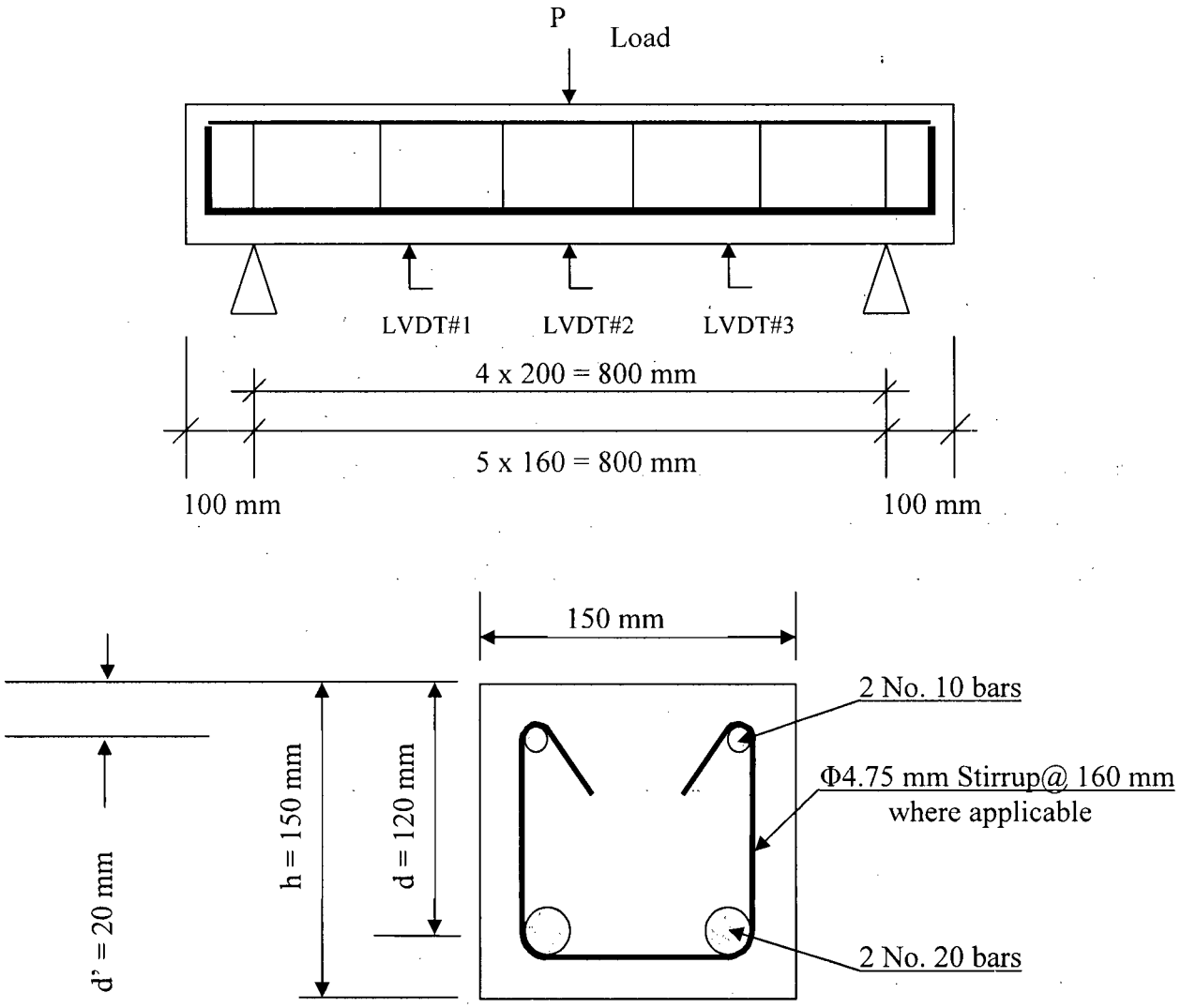

Figure 8.1 – *Load Configuration and Cross-Sectional Details of RC Beams*

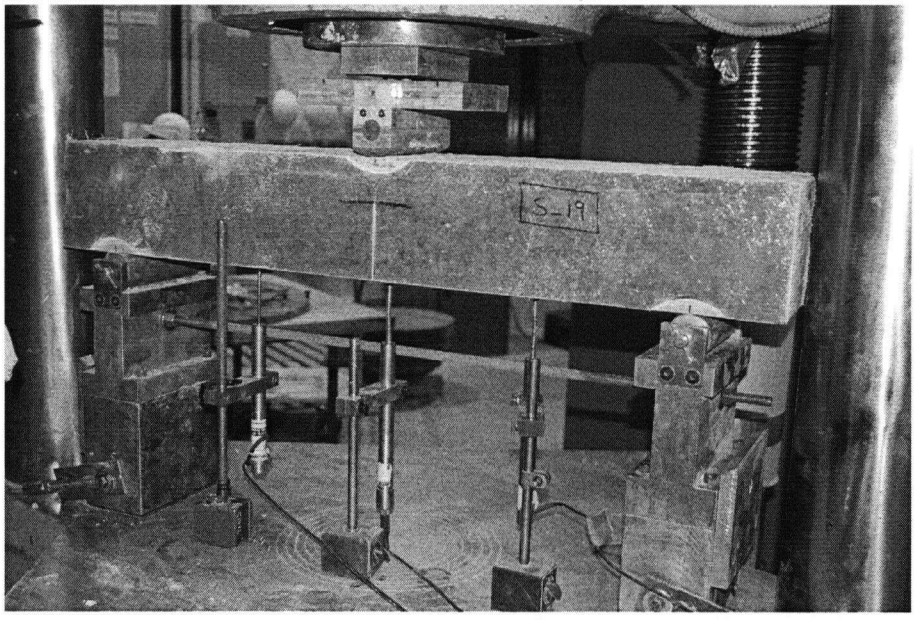

Figure 8.2 – *Beam Test Setup under Quasi-Static Loading*

In impact loading, all beams were tested using the Drop Weight Impact Machine described in Chapter 6. An impact velocity of 3.96 m/s (drop height of 800 mm) was used in all cases, except in two cases where a velocity of 3.43 m/s (drop height of 600 mm) was used.

8.3 Specimen Preparation

All specimens were identical in dimensions. Casting was done on a vibrating table to ensure proper consolidation of the concrete. Specimens were demolded after one day and immersed in lime saturated water. At the age of 28 days, the beams were removed from the curing tank and set out to dry under normal laboratory conditions. A minimum of one week of such a drying was allowed prior to any testing, surface preparation or spraying.

Surface preparation is the key for successful strengthening using externally bonded FRP. The surface must be dry, clean, and free of oil, debris and loose materials. Different techniques were used for surface treatment before applying Sprayed GFRP and they are discussed later.

8.4 Retrofit Schemes

Different configurations can be used for shear strengthening of RC beams using externally bonded GFRP. In general, the number of surfaces around the beam and the thickness of strengthening materials are of greatest interest. Throughout this investigation, different retrofit schemes with different thicknesses with and without mechanical fasteners were studied.

In FRP wrap systems, FRPs are bonded on the lateral faces of the beam with the fibers perpendicular or inclined to the longitudinal axis of the beam. The FRPs can also be placed on both lateral faces in a continuous way underneath the beam web resembling U-shaped external stirrups. The performance of the U-shaped bands can be further increased by adding additional longitudinal FRP strips over the ends of the U-shaped bands. Three beams were retrofitted using Wabo®MBrace fabric GFRP; one with a layer of fabric on both lateral faces with the fibers perpendicular to the longitudinal axis, one with U-shaped external stirrups and one with the U-shaped bands with an additional longitudinal FRP strips over the U-shaped bands. These beams were tested under quasi-static loading and the results were compared with the control beam (i.e. with no strengthening) and beams strengthened with Sprayed GFRP.

Sprayed GFRP was applied either on both lateral faces or on three faces excluding the top (i.e. compression face). Boyd [115] reported a difficulty during the retrofit process which was the inability of the fibers to stay in place when bent around sharp corners. To overcome this problem and to avoid possible failure of the FRP due to stress concentrations at the corners of the beam section, when Sprayed or fabric GFRP was applied on three sides of the beam, the corners of the beam section were rounded to a radius of 35 mm. This was also recommended by ISIS Canada [52].

Different thicknesses of Sprayed GFRP was applied and studied in this project. For surface preparation, different techniques such as sandblasting, epoxy glue and hammering the surface were investigated. Through bolts and nuts and Hilti nails using

powder actuated fastening tool were also tried with emphasis on concrete-GFRP bond strength enhancement.

8.5 Results and Discussion

A total of 33 RC beams were tested under quasi-static loading. Beam designations and details are tabulated in Table 8.2. The following notations are used for beam designations:

C: Control

NS: No Stirrups

S: Stirrups (Φ4.75 @ 160 mm)

SS: Stirrups (3Φ4.75 @ 50 mm)

B2: Sprayed GFRP on 2 lateral sides of the Beam

B3: Sprayed GFRP on 3 sides of the Beam

SB: Sand Blasted (i.e. concrete surface)

EP: Epoxy was used before spraying the GFRP (i.e. primer and putty, Wabo® MBrace system)

4B: 4 Through Bolts

6B: 6 Through Bolts

6H: 6 Through Holes

Hilti: Hilti nails using powder actuated fastening tool were used

B2F: Fabric GFRP on 2 sides of the Beam

BUF: U-shaped Fabric GFRP bands

BU2F: U-shaped Fabric GFRP bands + longitudinal GFRP strips over the bands

Table 8.2 – *RC Beams Designations and Details*

Beam Designation	Number of Stirrups			Sprayed GFRP	Wabo®MBrace fabric GFRP	Number of Sides with GFRP and GFRP Dimensions				Through Bolts and Nuts as Mechanical Fasteners		Hilti Nails as Mechanical Fasteners	Epoxy Glue (Putty) was Used to Increase Bond Strength	Concrete Surface was Sandblasted	Concrete Surface was Hammered to Increase Bond Strength
							2 Sides								
	No Stirrups	Φ4.75 mm @ 160 mm	3Φ4.75 mm @ 50 mm			No Sides (Control)	Thickness (mm)	Width (mm)	3 Sides, Thickness (mm)	4 Bolts	6 Bolts				
C-NS	✓			✓		✓									
C-S-1		✓		✓		✓									
C-S-2		✓		✓		✓									
C-SS			✓	✓		✓									
C-S-6H		✓		✓		✓									
C-NS-6B	✓			✓		✓					✓				
B2-NS-SB	✓			✓			3	100						✓	
B2-NS-EP	✓			✓			2.2	100					✓	✓	
B2-S-EP		✓		✓			6	150					✓	✓	
B2-NS	✓			✓			4	100							✓
B2-S-1		✓		✓			3.5	150							✓

Table 8.2 (Continued) – *RC Beams Designations and Details*

Beam Designation	Number of Stirrups			Sprayed GFRP	Wabo®MBrace fabric GFRP	Number of Sides with GFRP and Its Dimensions				Through Bolts and Nuts as Mechanical Fasteners		Hilti Nails as Mechanical Fasteners	Epoxy Glue (Putty) was used to Increase Bond Strength	Concrete Surface was Sandblasted	Concrete Surface was hammered to Increase Bond Strength
							2 Sides								
	No Stirrups	Φ4.75 mm @ 160 mm	3Φ4.75 mm @ 50 mm			No Sides (Control)	Thickness (mm)	Width (mm)	3 Sides, Thickness (mm)	4 Bolts	6 Bolts				
B2-S-2		✓		✓			4.5	150							✓
B2-S-3		✓		✓			5.6	150							✓
B2-S-4		✓		✓			6	150							✓
B2-S-5		✓		✓			7	150							✓
B2-NS-Hilti	✓			✓			2.2	100				✓		✓	
B2-4B-NS-1	✓			✓			1.8	100		✓				✓	
B2-4B-NS-2	✓			✓			2.5	100		✓				✓	
B2-4B-NS-3	✓			✓			4	100		✓				✓	
B2-4B-S-1		✓		✓			3.5	150		✓					✓
B2-4B-S-2		✓		✓			4.2	150		✓					✓
B2-4B-S-3		✓		✓			4.5	150		✓					✓

Table 8.2 (Continued) – *RC Beams Designations and Details*

Beam Designation	Number of Stirrups			Sprayed GFRP	Wabo®MBrace fabric GFRP	Number of Sides with GFRP and Its Dimensions				Through Bolts and Nuts as Mechanical Fasteners		Hilti Nails as Mechanical Fasteners	Epoxy Glue (Putty) was used to Increase Bond Strength	Concrete Surface was Sandblasted	Concrete Surface was hammered to Increase Bond Strength
							2 Sides								
	No Stirrups	Φ4.75 mm @ 160 mm	3Φ4.75 mm @ 50 mm			No Sides (Control)	Thickness (mm)	Width (mm)	3 Sides, Thickness (mm)	4 Bolts	6 Bolts				
B2-6B-NS-1	✓			✓			3.5	100			✓			✓	
B2-6B-NS-2	✓			✓			4	100			✓			✓	
B2-6B-NS-3	✓			✓			4.5	100			✓			✓	
B2-6B-S-1		✓		✓			4	100			✓			✓	
B3-S-1		✓		✓					3.2						✓
B3-S-2		✓		✓					4						✓
B3-S-3		✓		✓					7						✓
B3-S-4		✓		✓					8						✓
B2F-NS	✓				✓		1.2	120					✓	✓	
BUF-NS	✓				✓		1.2	U					✓	✓	
BU2F-NS	✓				✓		1.2	U					✓	✓	

8.5.1 Control Beams with No GFRP

Six beams were tested under quasi-static loading without the GFRP coating. Results are reported here and will be used later as bench marks for comparing the results.

8.5.1.1 Control Beam with No GFRP and No Stirrups

One beam (beam C-NS in Table 8.2) was tested under quasi-static loading with no stirrups and no GFRP. The result of this test is shown in Figure 8.3. A typical shear failure was observed in this beam with a crack of about 45°. This shear crack became flatter at the load point as shown in Figure 8.3. Load carrying capacity was in good agreement with the predicted value (see Appendix B).

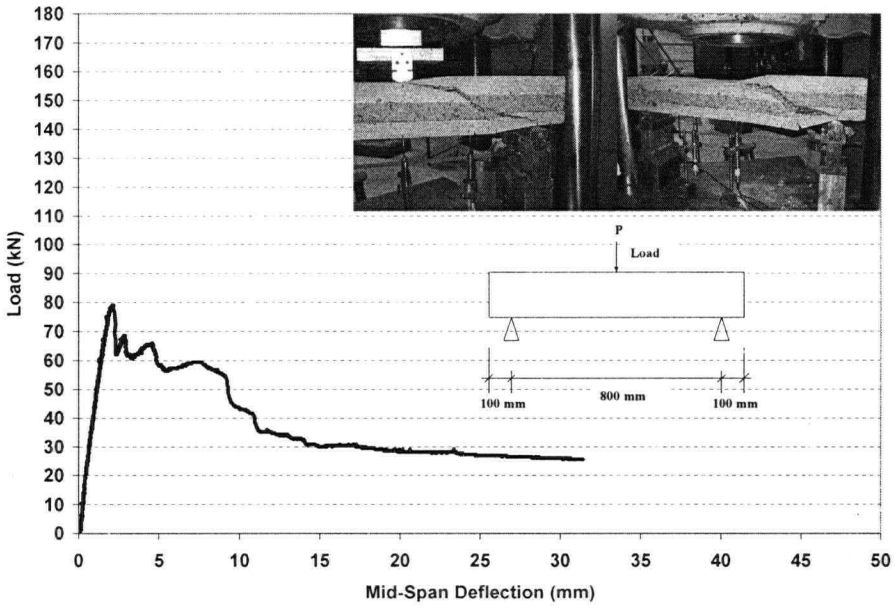

Figure 8.3 – *Load vs. Mid-Span Deflection of Control RC Beam C-NS*

8.5.1.2 Control Beams with No GFRP and Stirrups at 160 mm

Two beams (beams C-S-1 and C-S-2 in Table 8.2) were tested under quasi-static loading with no GFRP and Φ4.75 stirrups @ 160 mm. The results of these tests are shown in Figures 8.4 and 8.5. The presence of stirrups produced multiple cracks as compared to one large crack in the RC beam with no stirrups (compare Figure 8.3 with Figures 8.4 and 8.5). Load carrying capacity was about 10% less than the expected value (see Appendix B).

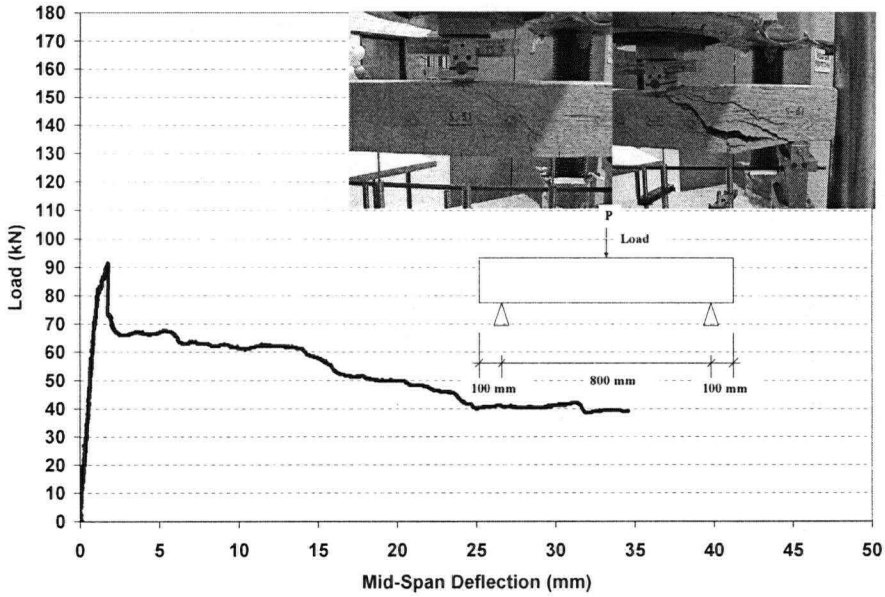

Figure 8.4 – *Load vs. Mid-Span Deflection of Control RC Beam C-S-1*

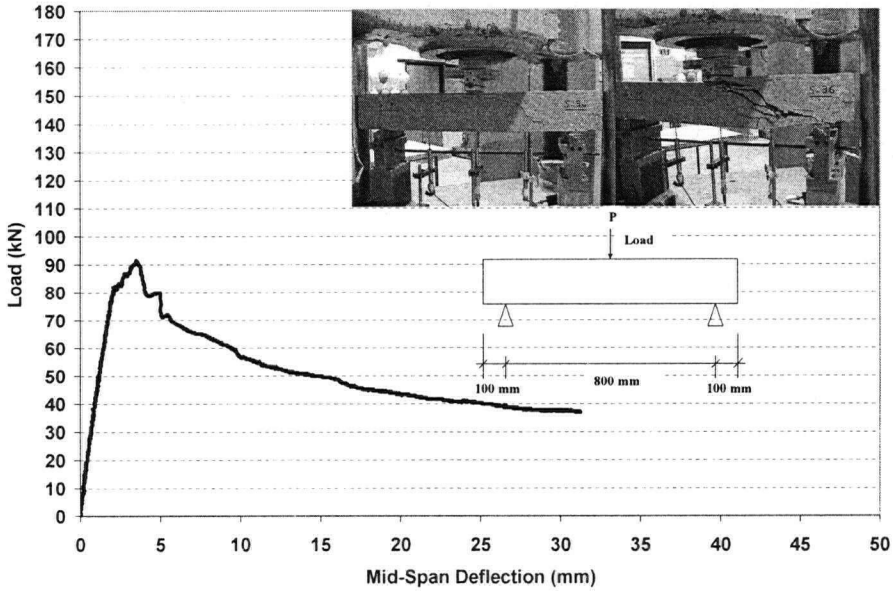

Figure 8.5 – *Load vs. Mid-Span Deflection of Control RC Beam C-S-2*

8.5.1.3 Control Beam with No GFRP and Stirrups at 50 mm

One beam (beam C-SS in Table 8.2) was tested under quasi-static loading with no GFRP and 3Φ4.75 stirrups @ 50 mm. The result of this test is shown in Figure 8.6. Flexural and shear cracks were observed during the test and the beam ultimately failed in shear after reaching its flexural capacity. Since the amount of tension reinforcement (600 mm^2) was about 2.7% of the concrete cross sectional area (150 mm × 150 mm), undeformed reinforcing bars for shear (i.e. 3Φ4.75 @ 50 mm stirrups) were not quite effective to capture shear cracks after yielding of tension reinforcement. As a result, when tension reinforcement started yielding the shear cracks propagated toward the concrete compression zone and failure took place when the shear cracks entered the concrete compression region, which also showed some crushing. This can be seen in pictures illustrated in Figure 8.6.

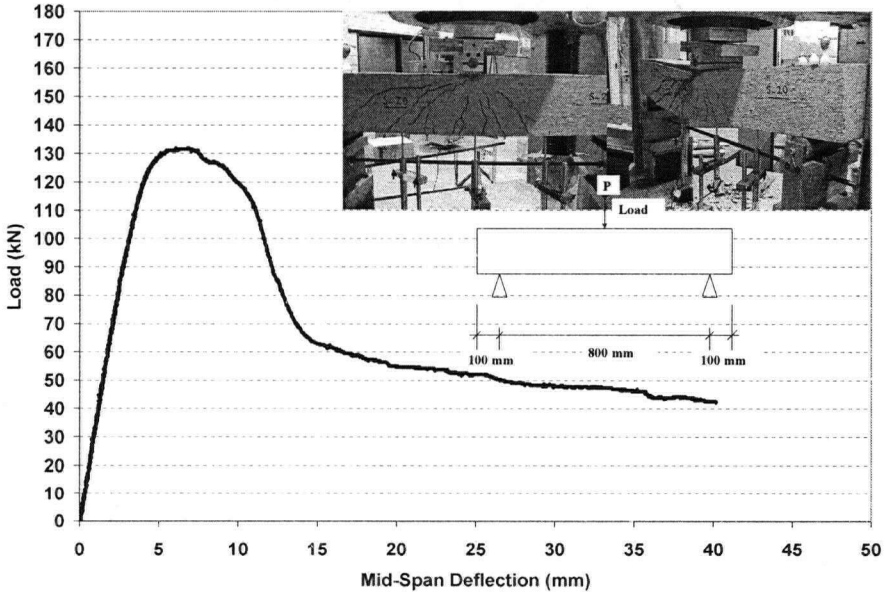

Figure 8.6 – *Load vs. Mid-Span Deflection of Control RC Beam C-SS*

8.5.1.4 Control Beam with No GFRP, Stirrups at 160 mm and 6 Through-Holes

One beam (beam C-S-6H in Table 8.2) was tested under quasi-static loading with Φ4.75 stirrups @ 160 mm, no GFRP and 6 through holes with a diameter of 12.5 mm (½

in.). The location of these holes is illustrated in Figure 8.7 and the result of this test is shown in Figure 8.8.

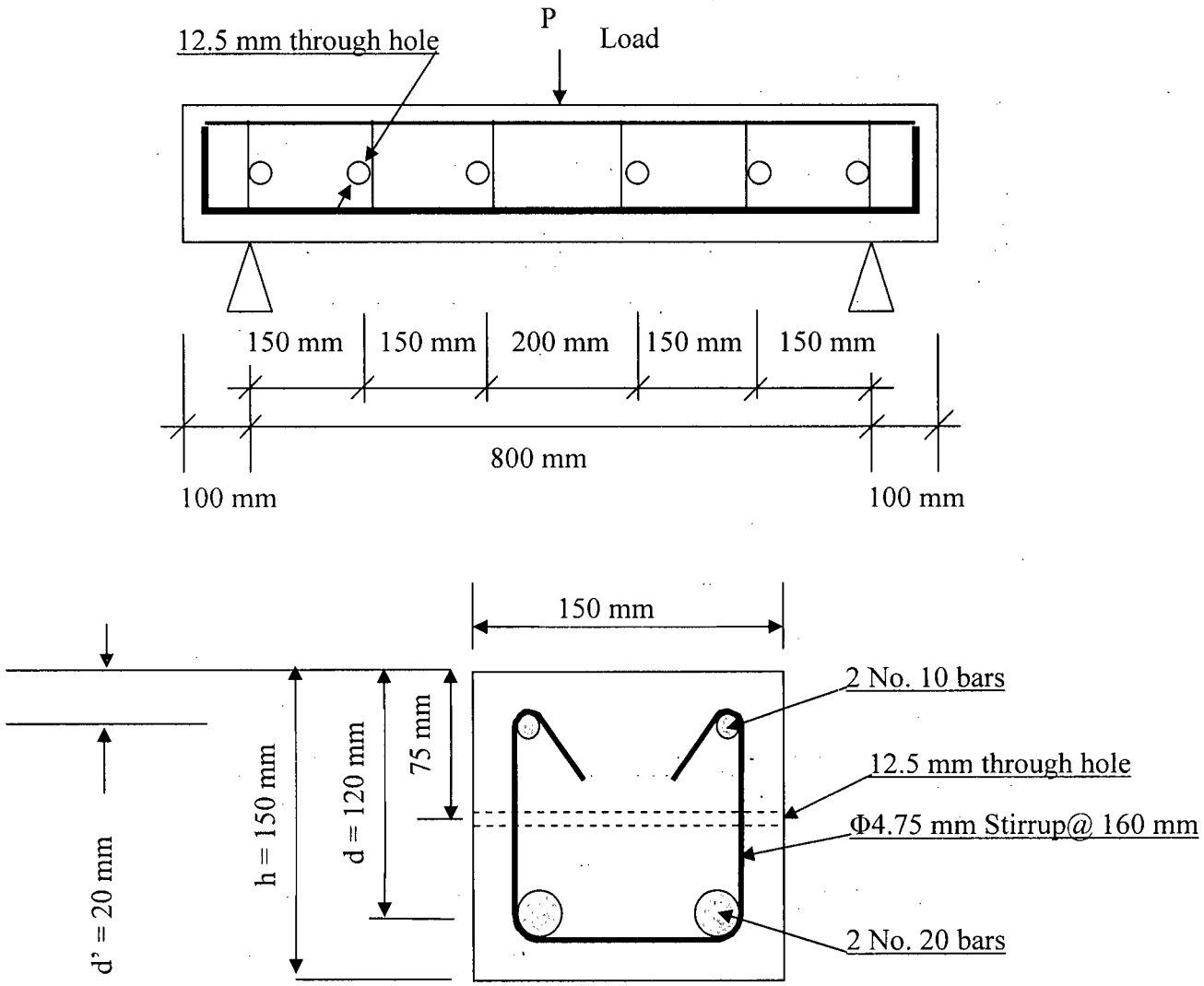

Figure 8.7 – *Cross-Sectional Details of RC Beam C-S-6H*

The purpose of this test was to find out how much decrease in load carrying capacity of this beam could take place if through-holes were created for GFRP bond enhancement. It was observed that only 4% of the load carrying capacity of this beam was lost due to the presence of the through-holes. Load carrying capacity of beam C-S-6H was 87.7 kN which was about 3.9 kN less than that of beams C-S-1 and C-S-2.

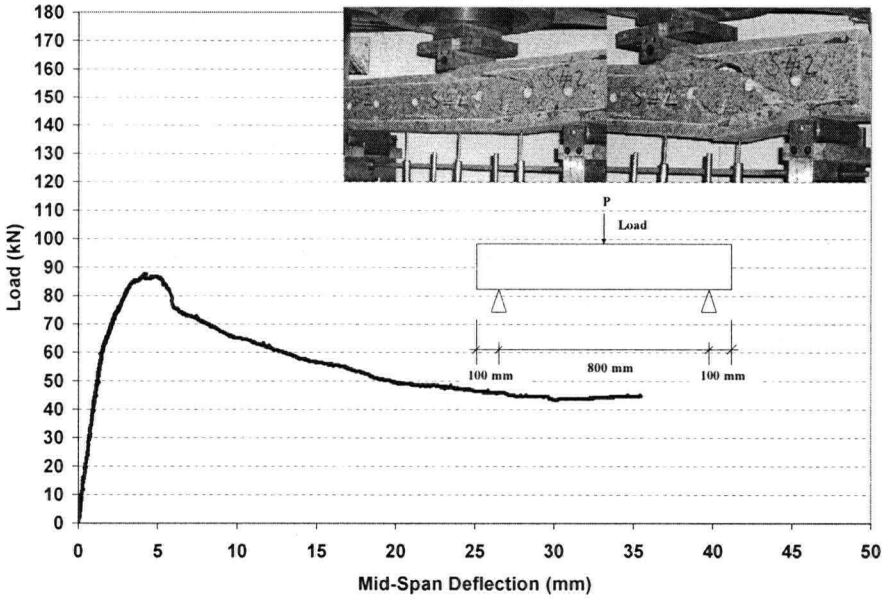

Figure 8.8 – *Load vs. Mid-Span Deflection of Control RC Beam C-S-6H*

8.5.1.5 Control Beam with No GFRP, No Stirrups and 6 through Bolts and Nuts

One beam (beam C-NS-6B in Table 8.2) was tested under quasi-static loading with no stirrups, no GFRP and 6 through bolts and nuts. The location of these bolts and their details are illustrated in Figure 8.9 and the result of this test is shown in Figure 8.10.

A torque of 67.8 N.m (50 lb.ft) was applied to tighten the nuts on both sides of the beam as shown in Figure 8.9. This torque was kept constant during the research and was applied to all beams containing through bolts and nuts.

The purpose of this test was to find out the benefits of these bolts in increasing the shear capacity of the beam, if any. As a result, it was found that the use of these bolts and nuts overcame the weakness of having through holes in RC beam and the shear capacity of RC beam was maintained to its original capacity with no through holes. It was also noticed that the applied torque provided more confinement for concrete, and as a result, more energy was used up during the beam failure compare to beam C-NS with no bolts.

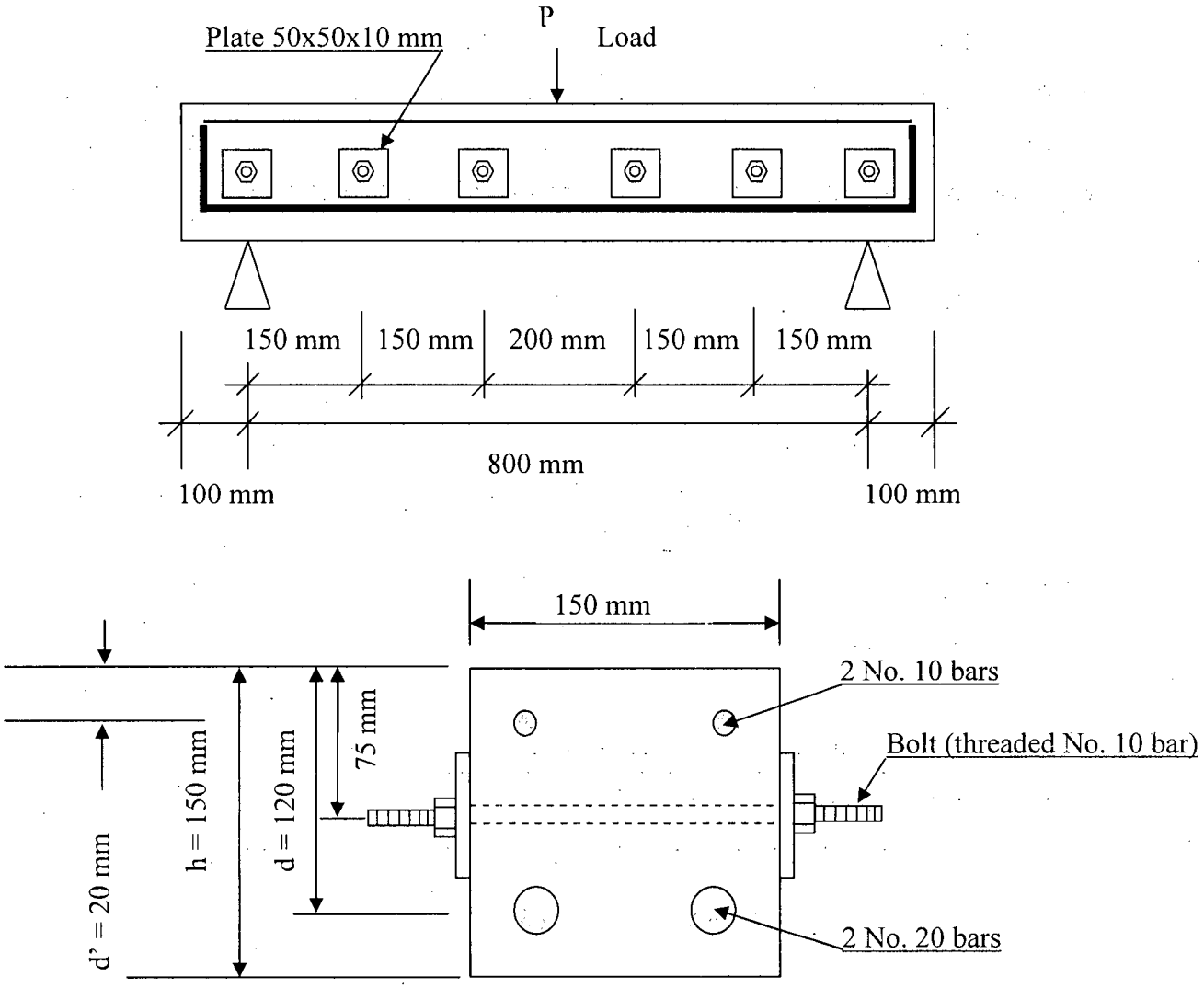

Figure 8.9 – *Cross-Sectional Details of RC Beam C-NS-6B*

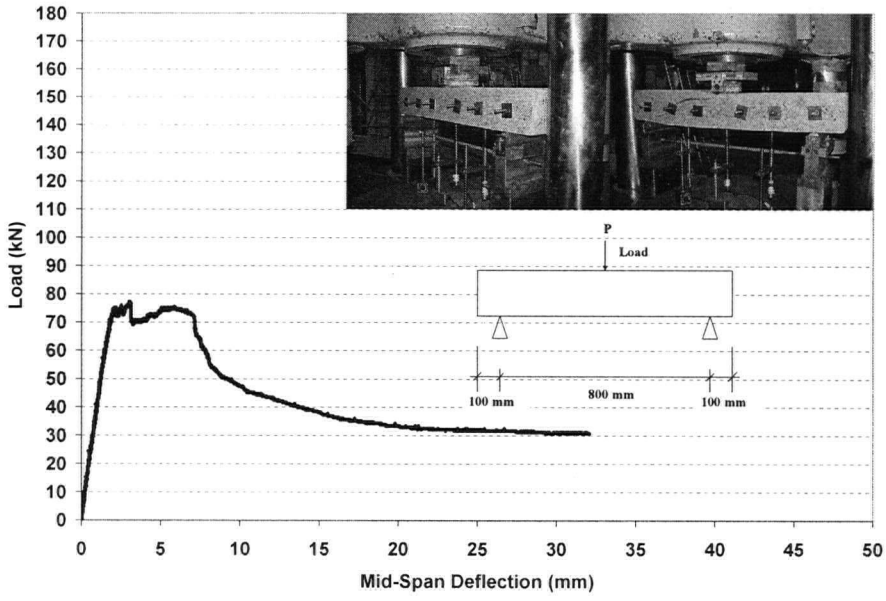

Figure 8.10 – *Load vs. Mid-Span Deflection of Control RC Beam C-NS-6B*

8.5.2 Sprayed GFRP on Two Sides

Twenty beams in total were strengthened by Sprayed GFRP on their lateral sides. Different techniques were used to evaluate the effectiveness of Sprayed GFRP in shear strengthening of RC beams. In the following sections these techniques will be discussed and the results will be compared. Each result will also be compared with its corresponding control specimen as described in Section 8.5.1.1.

8.5.2.1 Beams with No Mechanical Fasteners

Nine beams were tested with Sprayed GFRP applied to their lateral sides and no mechanical fasteners were used. The purpose of these tests was to find out the best type of concrete surface to create a stronger GFRP-concrete bond. Three different techniques were employed:

1. Concrete surface was sandblasted and then washed by a high pressure washer. Beam was left for a couple of days in the laboratory environment to make sure that the surface was completely dried before applying the Sprayed GFRP.

2. Concrete surface was roughened using a small pneumatic concrete chisel. This technique provided a rougher surface than sandblasting. Then, concrete surface was washed using a high pressure washer and dried before Sprayed GFRP application.

3. Concrete surface was sandblasted and then washed by a high pressure washer. After the surface got dried, Wabo®MBrace primer and putty as explained in Chapter 4 were applied to the concrete surface prior to Sprayed GFRP application.

Figure 8.11 shows the prepared surface before Sprayed GFRP application using pneumatic concrete chisel. This pneumatic tool weighs around 1.7 kg with a stroke speed of 2600 min^{-1}, rated air pressure of 0.59 MPa and rated air consumption of about 3 m^3/min.

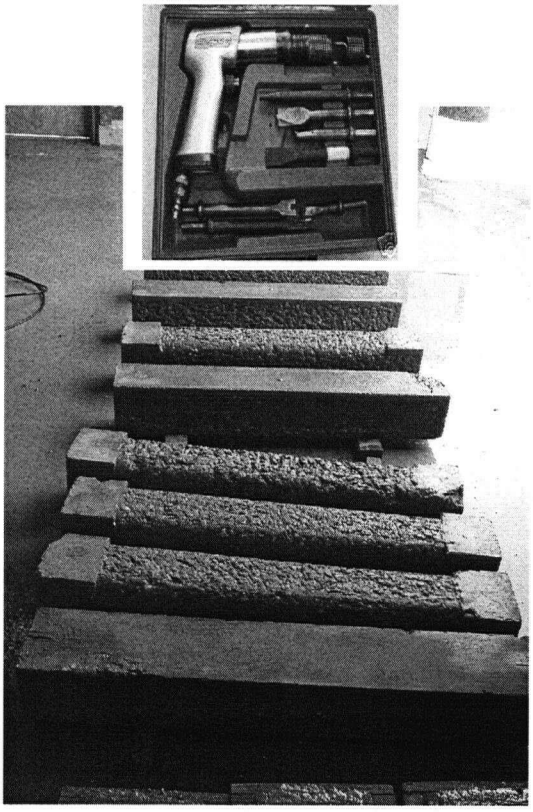

Figure 8.11 – *Surface Preparation using Pneumatic Concrete Chisel*

One beam (beam B2-NS-SB) was tested while Sprayed GFRP was applied after preparing the surface using sandblast technique. The beam contained no stirrups and its

details can be found in Table 8.2. Figure 8.12 shows the test result of this beam while the test result of its control beam (beam C-NS) is also included.

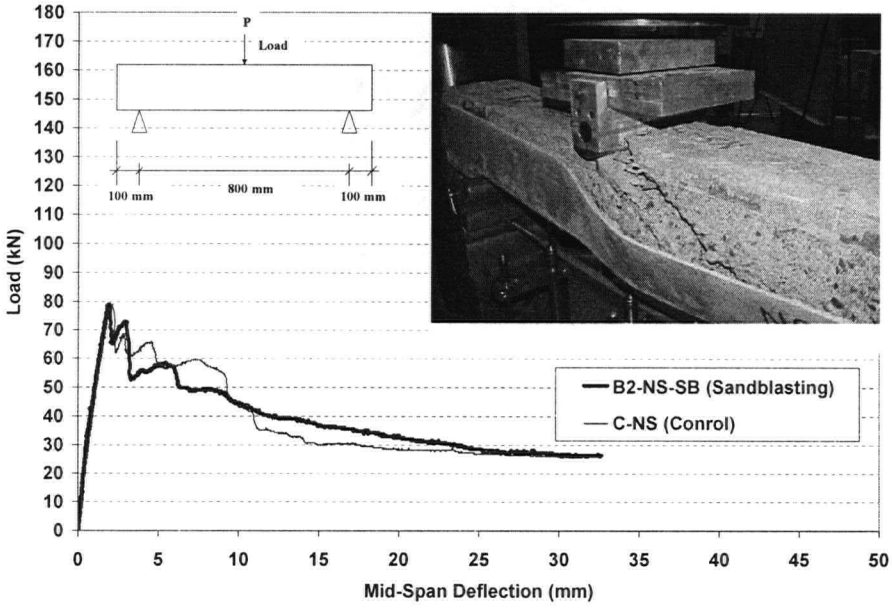

Figure 8.12 – *Load vs. Mid-Span Deflection of RC Beam B2-NS-SB*

It is clear that sandblasting technique was not an effective way to enhance the Sprayed GFRP-concrete bond. This bond failed before having any contribution to the enhancement of shear strength of this RC beam. As a result, the load carrying capacity was unchanged due to premature bond failure as shown in Figure 8.12.

Two beams (Beam B2-NS-EP and Beam B2-S-EP) were tested while Sprayed GFRP was applied over the cured Wabo®MBrace primer and putty. The purpose of these tests was to identify the effectiveness of this technique in providing a better Sprayed GFRP-concrete bond. Figure 8.13 shows the test result of beam B2-NS-EP (beam with no stirrups, details are tabulated in Table 8.2). Test result of its control beam (beam C-NS) is also included in Figure 8.13 for comparison. Test result of beam B2-S-EP (beam with Φ4.75 stirrups @ 160 mm with tabulated details in Table 8.2) is shown in Figure 8.14 while the test result of its control beam (beam C-S-2) is also included in the same Figure.

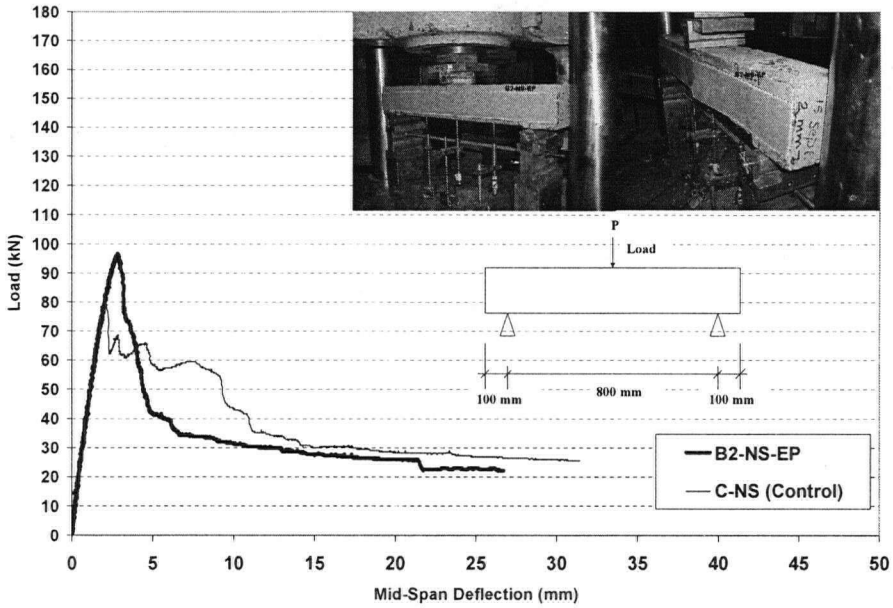

Figure 8.13 – *Load vs. Mid-Span Deflection of RC Beam B2-NS-EP*

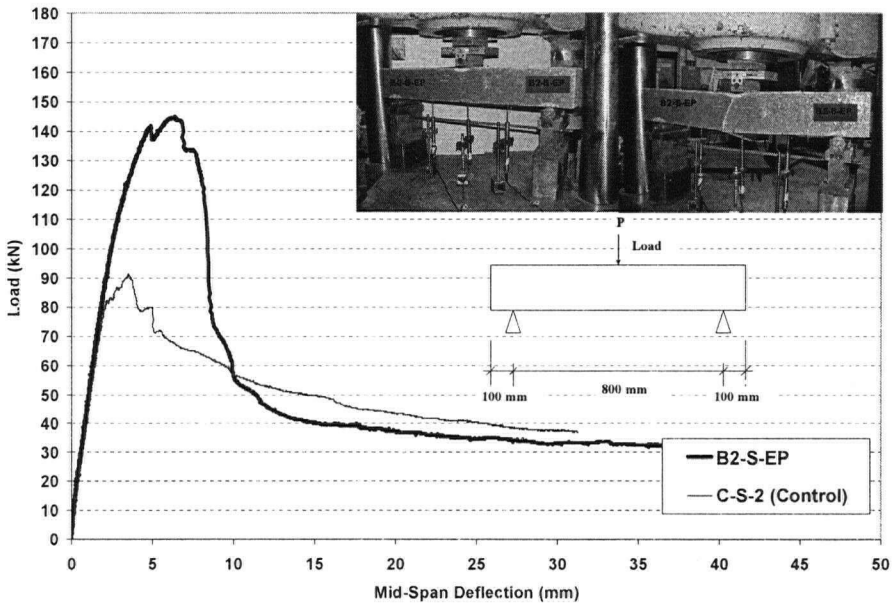

Figure 8.14 – *Load vs. Mid-Span Deflection of RC Beam B2-S-EP*

From these test results, one can conclude that the Sprayed GFRP-concrete bond showed an improvement by introducing an intermediate layer of Wabo®MBrace primer and putty compare to sandblasting technique. Load carrying capacity of these beams

increased and this increase was proportional to the cross-sectional area of the applied Sprayed GFRP on the lateral sides of the RC beam.

Six beams (beam B2-NS and beams B2-S-1, B2-S-2, B2-S-3, B2-S-4 and B2-S-5) were tested while Sprayed GFRP was applied on the lateral sides of the beam over a roughened surface using the pneumatic concrete chisel. The purpose of these tests was to identify the effectiveness of this technique in providing a better Sprayed GFRP-concrete bond. Figure 8.15 shows the test result of beam B2-NS (beam with no stirrups, details are tabulated in Table 8.2). Test result of its control beam (beam C-NS) is also included in Figure 8.15 for comparison. Test results of beams B2-S-1, B2-S-2, B2-S-3, B2-S-4 and B2-S-5 (beams with Φ4.75 stirrups @ 160 mm with tabulated details in Table 8.2) are shown in Figures 8.16 to 8.20 while the test result of their control beam (beam C-S-2) is also included in each Figure.

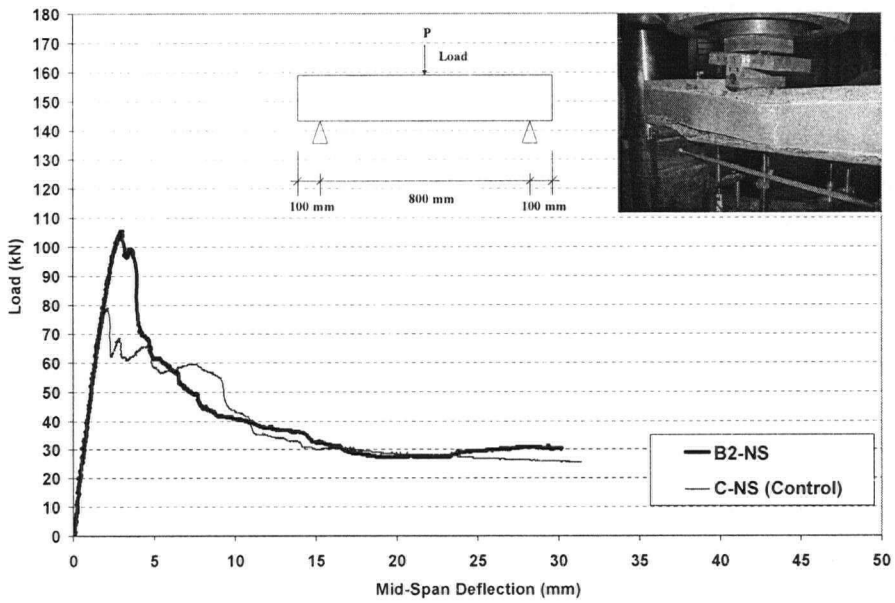

Figure 8.15 – *Load vs. Mid-Span Deflection of RC Beam B2-NS*

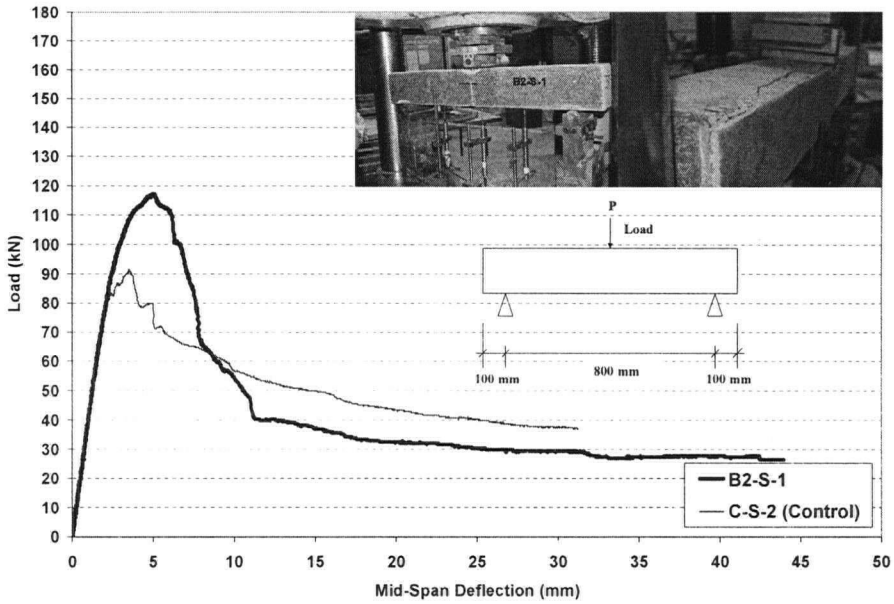

Figure 8.16 – *Load vs. Mid-Span Deflection of RC Beam B2-S-1*

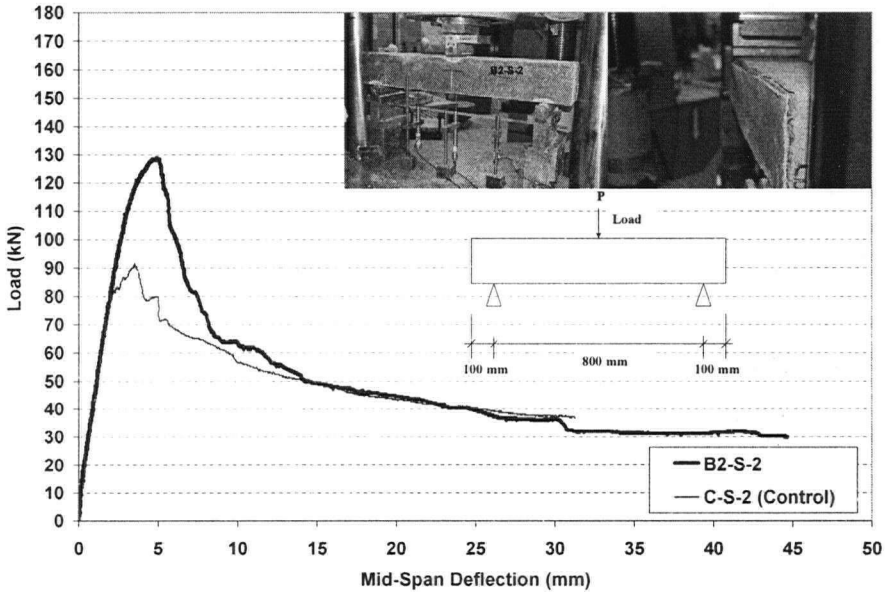

Figure 8.17 – *Load vs. Mid-Span Deflection of RC Beam B2-S-2*

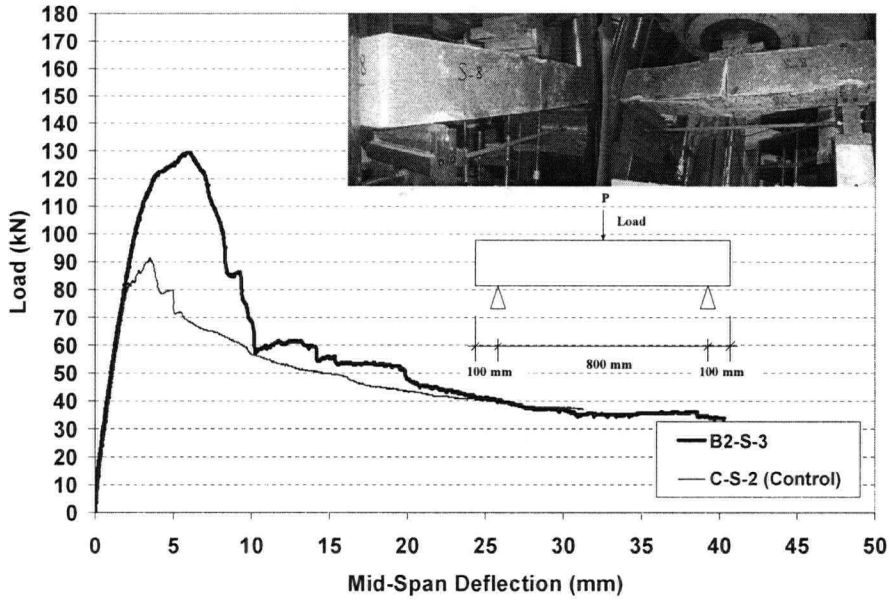

Figure 8.18 – *Load vs. Mid-Span Deflection of RC Beam B2-S-3*

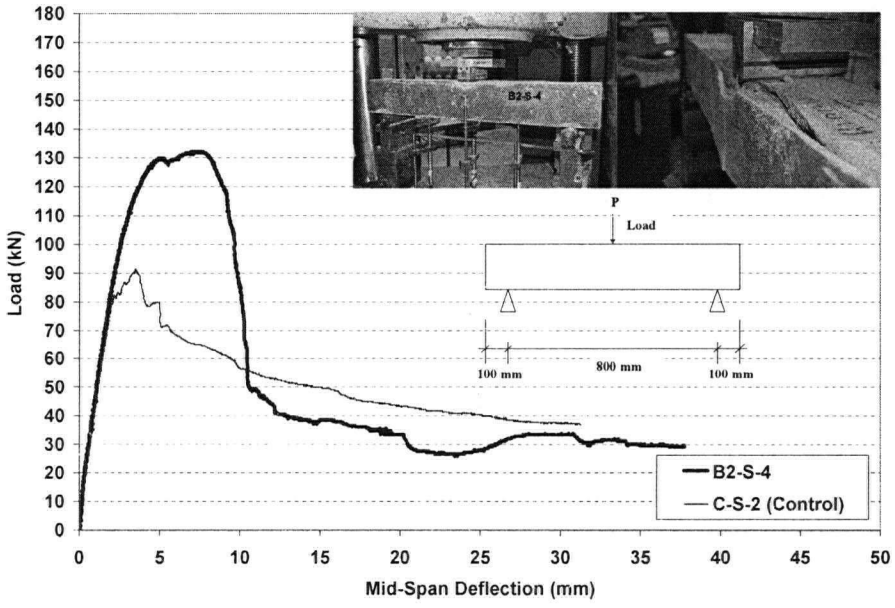

Figure 8.19 – *Load vs. Mid-Span Deflection of RC Beam B2-S-4*

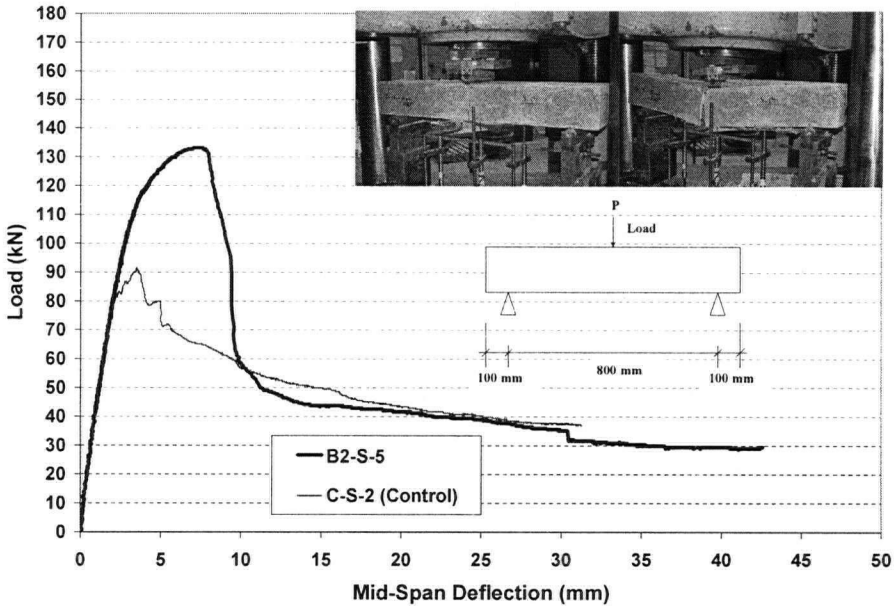

Figure 8.20 – *Load vs. Mid-Span Deflection of RC Beam B2-S-5*

Roughening the concrete surface using pneumatic chisel as shown in Figures 8.15 to 8.20 appears to be a promising technique in enhancing the bond between concrete and GFRP. It was also noticed that load carrying capacity was proportional to the cross-sectional area of GFRP material to a certain point, beyond which increasing this area did not increase the load carrying capacity. This will be addressed and discussed in detail later in this Chapter.

Figures 8.21 (a) to (e) show crack development in beam B2-S-1 under 3-point quasi-static loading and Figure 8.21 (f) shows the strong bond between GFRP and concrete which was clearly greater than tensile/shear strength of concrete and concrete-rebar bond strength. It is worth mentioning that all Sprayed GFRP plates were cut at the mid-span of the beam (both cases: Sprayed GFRP on 2 lateral sides and on 3 sides) to make sure that the GFRP contribution only in shear strengthening would be measured. It is obvious that since Sprayed GFRP consist of randomly distributed chopped fibers, unlike unidirectional FRP fabrics, any portion of this composite material underneath the neutral axis of the RC beam will increase the flexural capacity of the beam. By cutting the cured Sprayed GFRP at the mid-span and underneath the neutral axis the

contribution of this composite material toward flexural strengthening is minimized and therefore, shear strengthening benefits of Sprayed GFRP can be calculated and formulated based on its geometry and properties.

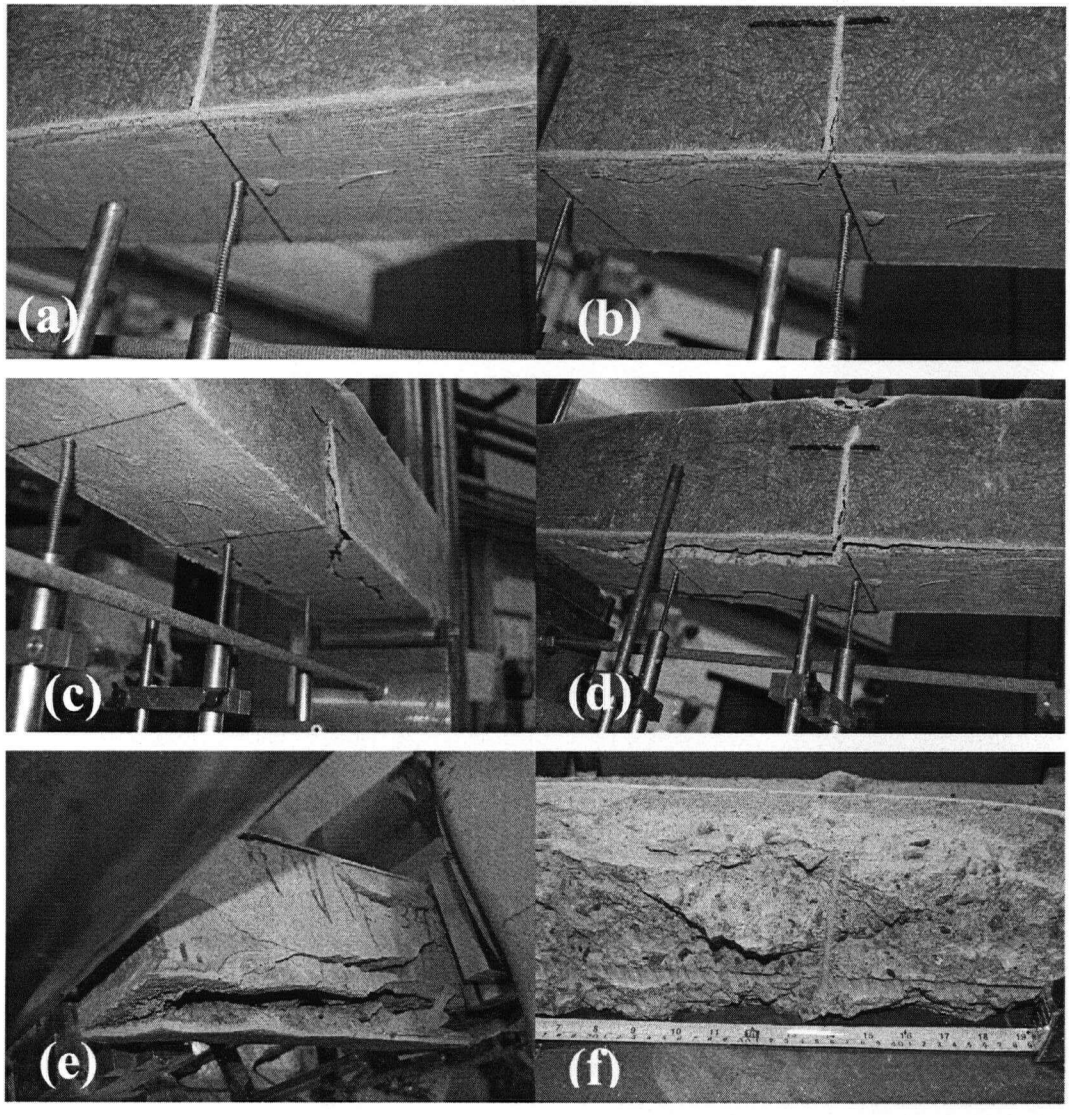

Figure 8.21 – *Beam B2-S-1: (a) to (e) Crack Development under 3-Point Loading; (f) Strong Sprayed GFRP-Concrete Bond*

8.5.2.2 Using Hilti Nails as Mechanical Fasteners

Stainless steel Hilti nails using a powder actuated fastening tool were shot on to the sides of the RC beam. There were 12 nails on each side of the beam spaced approximately 75 mm apart and inserted at the middle of the beam depth. They were Hilti X-AL-H 32P8 nails with a diameter of 4.5 mm and a length of 32 mm. The FRP was sprayed after the nails were inserted. The head of the inserted nail was covered by Sprayed FRP to make sure that a composite action between FRP and nail would be achieved. Load vs. mid-span deflection response of this beam, beam B2-NS-Hilti, is provided in Figure 8.22. For comparison test result of its control specimen, beam C-NS, is also included in this Figure. One can easily conclude, by observing Figure 8.22, that there was no benefit in this technique, at least for this beam size and the type of nails used. Fracturing the concrete surface using powder actuated fastening tool, as observed during the nail shooting, at least to some extent, can explain why this technique was not a successful one.

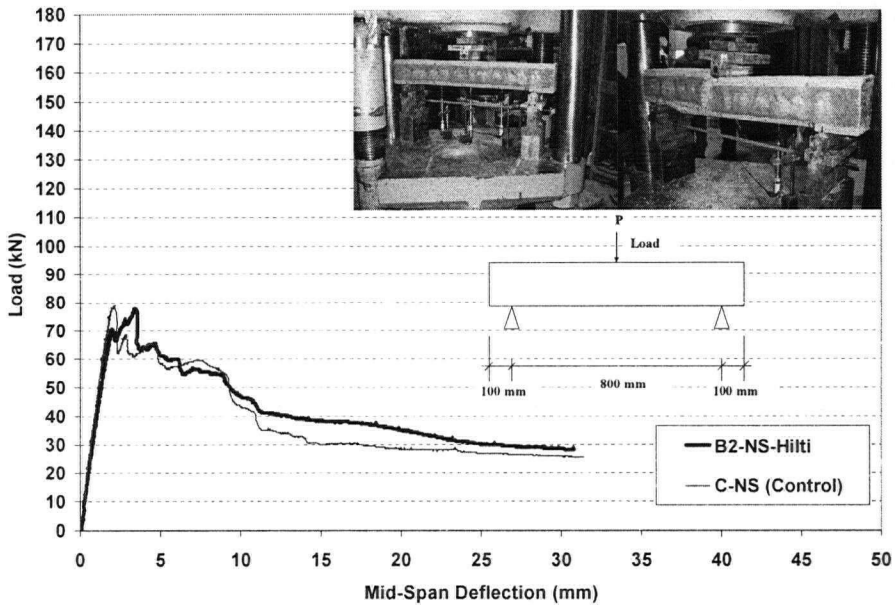

Figure 8.22 – *Load vs. Mid-Span Deflection of RC Beam B2-NS-Hilti*

8.5.2.3 Using Through-Bolts and Nuts as Mechanical Fasteners

Ten beams were tested using through bolts and nuts as mechanical fasteners to overcome the premature failure due to FRP debonding, if any, and to observe FRP rupture at the beam's failure. There were either 4 or 6 bolts as mechanical fasteners and the test results of these two groups of tests are discussed in this section.

8.5.2.3.1 Using 4 Through-Bolts as Mechanical Fasteners

Six beams were tested using 4 bolts: 3 beams with no stirrups and 100 mm width Sprayed FRP on their lateral sides and 3 beams with Φ4.75 stirrups at 160 mm and 150 mm width Sprayed FRP on their lateral sides. Cross-sectional details and bolt locations are shown in Figure 8.23.

Load vs. mid-span deflection curves of beams B2-4B-NS-1, B2-4B-NS-2 and B2-4B-NS-3 with their control specimen (Beam C-NS-6B) are reported in Figures 8.24 to 8.26. Figures 8.27 to 8.29 show load vs. mid-span deflection curves for beams B2-4B-S-1, B2-4B-S-2 and B2-4B-S-3 along while their control specimen (Beam C-S-6H).

From illustrated pictures in Figures 8.24 to 8.29, one can conclude that the presence of through bolts as mechanical fasteners can certainly prevent premature GFRP debonding failure.

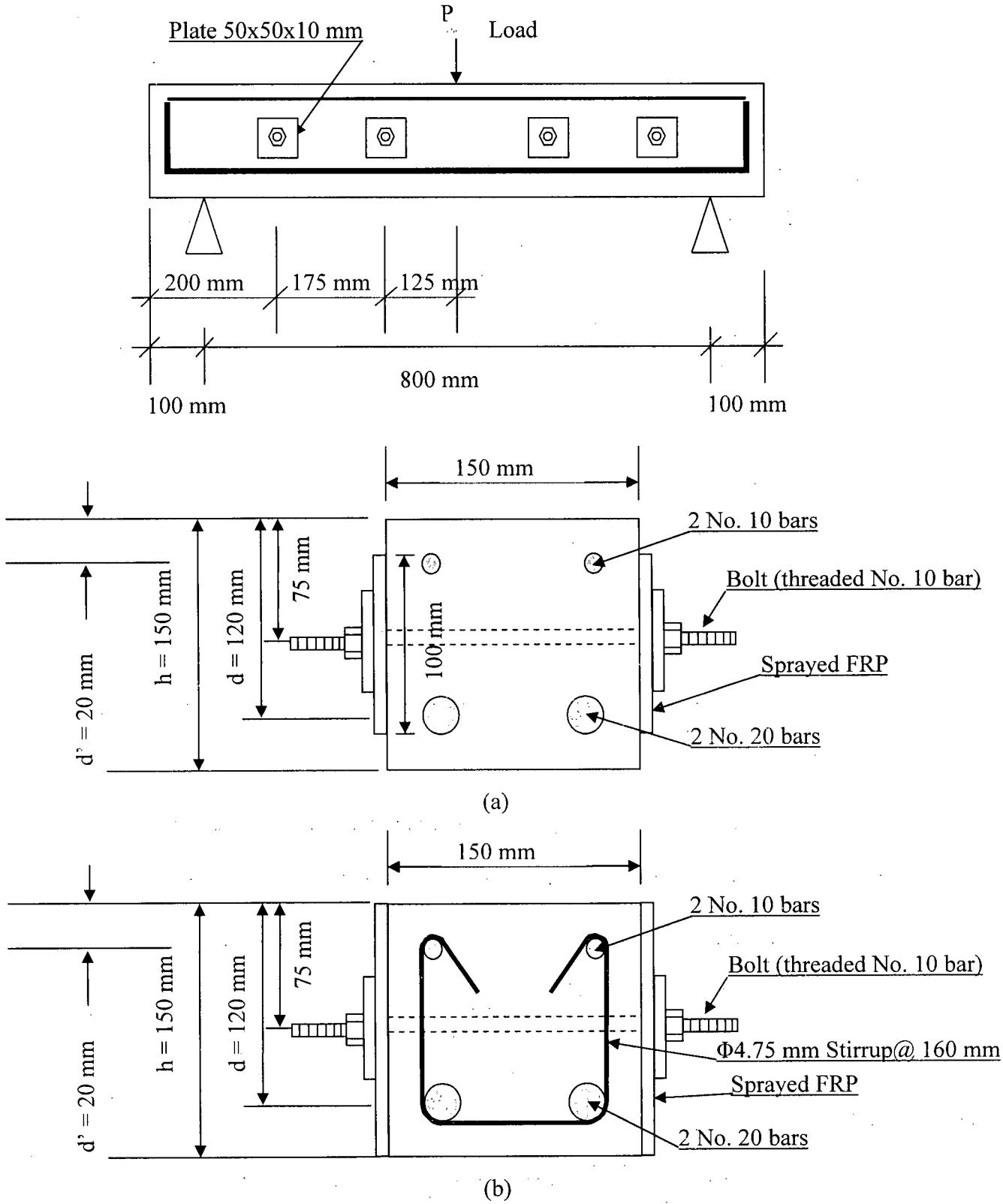

Figure 8.23 – *Cross-Sectional Details of RC Beams; (a) B2-4B-NS-1 to B2-4B-NS-3; (b) B2-4B-S-1 to B2-4B-S-3*

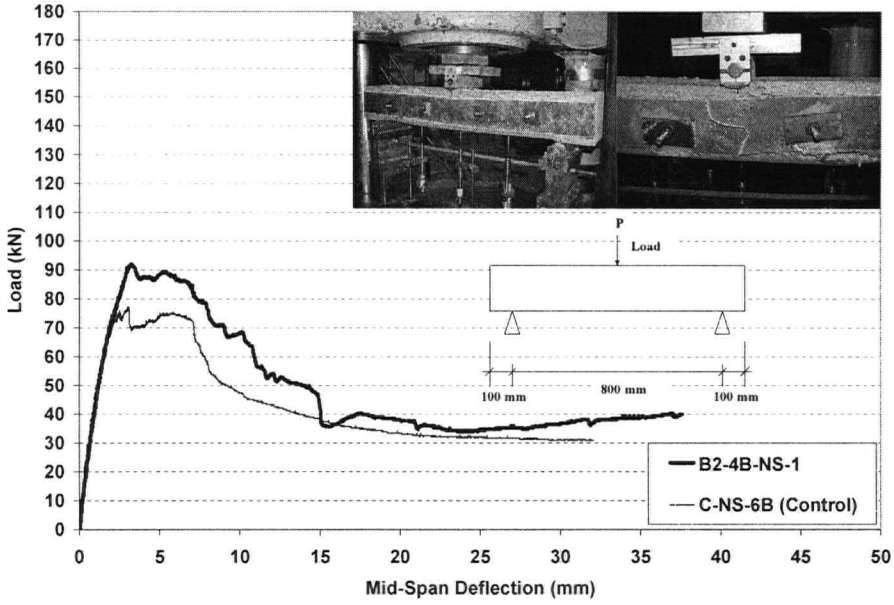

Figure 8.24 – *Load vs. Mid-Span Deflection of RC Beam B2-4B-NS-1*

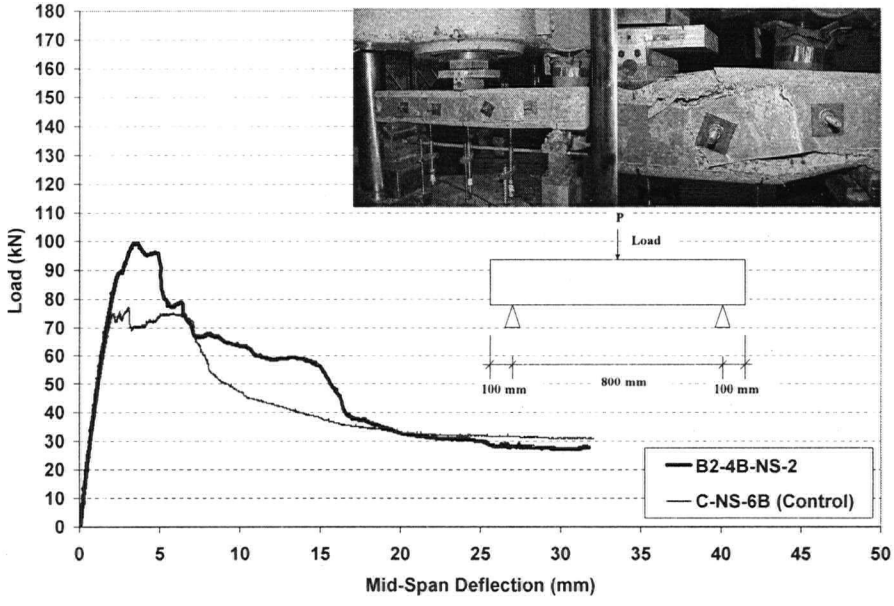

Figure 8.25 – *Load vs. Mid-Span Deflection of RC Beam B2-4B-NS-2*

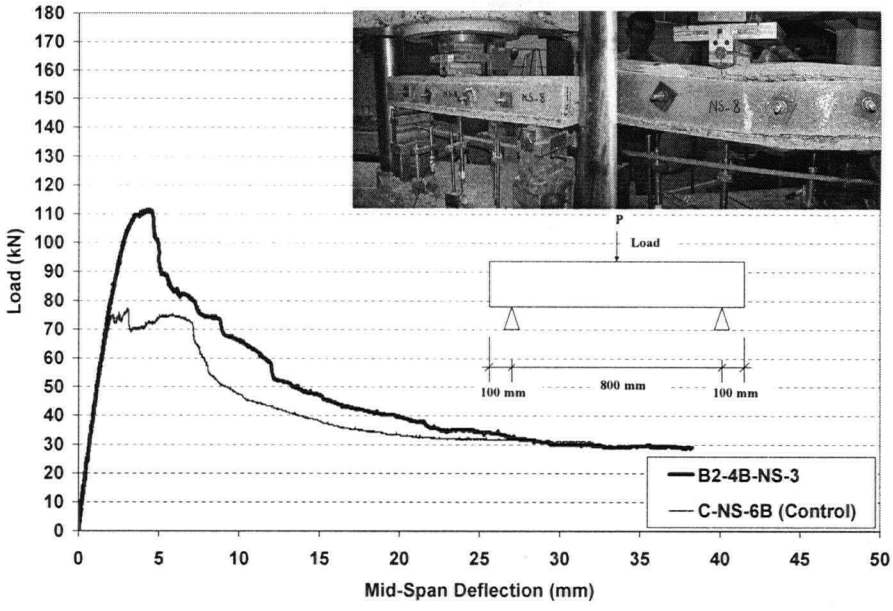

Figure 8.26 – *Load vs. Mid-Span Deflection of RC Beam B2-4B-NS-3*

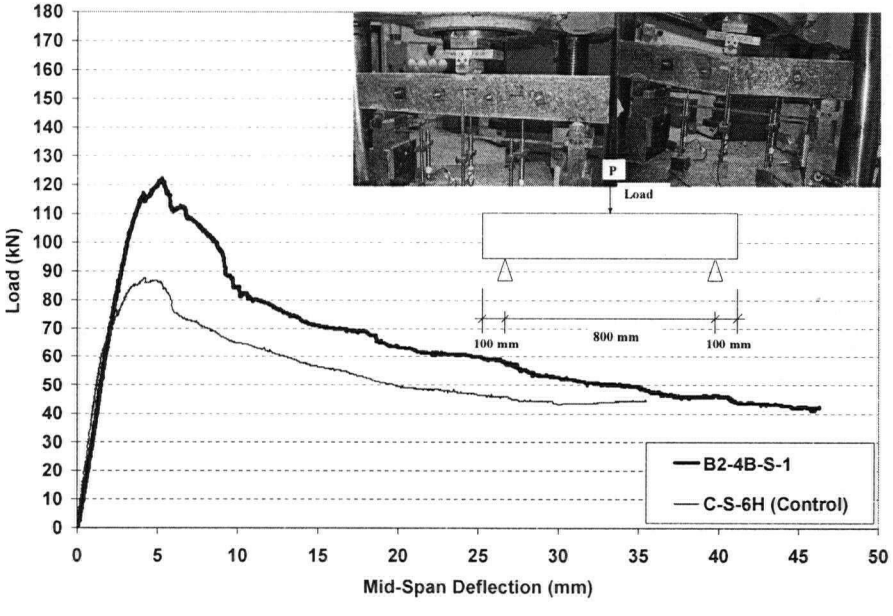

Figure 8.27 – *Load vs. Mid-Span Deflection of RC Beam B2-4B-S-1*

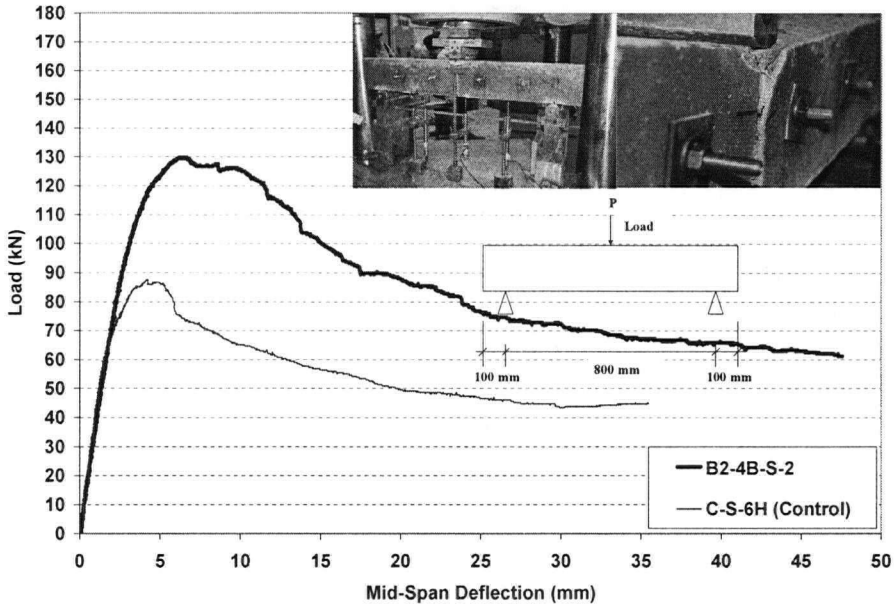

Figure 8.28 – *Load vs. Mid-Span Deflection of RC Beam B2-4B-S-2*

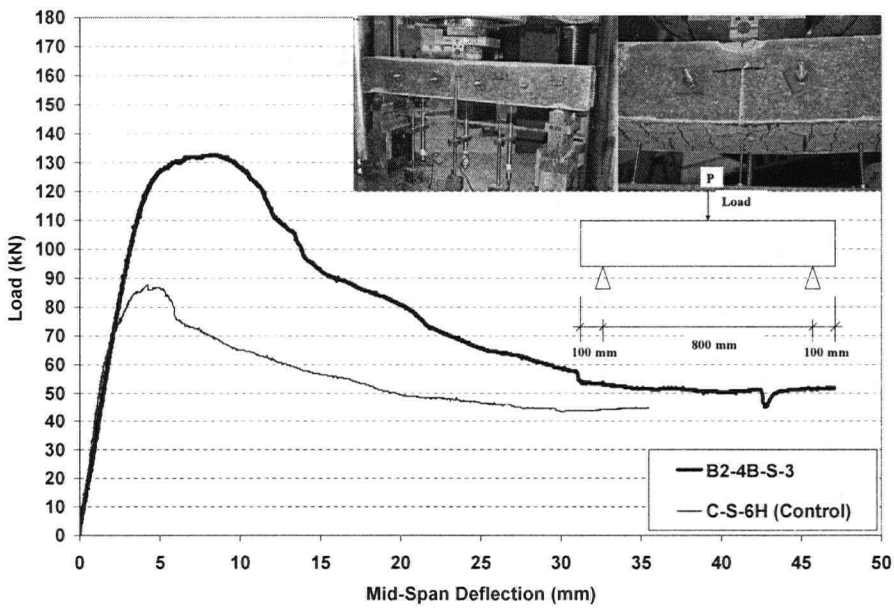

Figure 8.29 – *Load vs. Mid-Span Deflection of RC Beam B2-4B-S-3*

8.5.2.3.2 Using 6 Through-Bolts as Mechanical Fasteners

Four beams were tested using 6 bolts: 3 beams with no stirrups and 100 mm width Sprayed FRP on their lateral sides and one beam with Φ4.75 stirrups at 160 mm spacing and 100 mm width Sprayed FRP on its lateral sides. Cross-sectional details and bolt locations are shown in Figure 8.30.

Load vs. mid-span deflection curves of beams B2-6B-NS-1, B2-6B-NS-2 and B2-6B-NS-3 with their control specimen's test result (beam C-NS-6B) are reported in Figures 8.31 to 8.33. Figure 8.34 shows load vs. mid-span deflection curve for beam B2-6B-S-1while its control specimen's load-deflection response (beam C-S-6H) is also included.

Again, from the pictures in Figures 8.31 to 8.34, one can conclude that the presence of through bolts as mechanical fasteners can certainly prevent premature GFRP debonding failure. In all cases (beams with 4 and 6 bolts reported here and in section 8.5.1.2.3.1) GFRP rupture was observed. Depending on GFRP thickness this rupture can occur before (i.e. at the same time of) or after shear failure of RC beam. Contribution of GFRP in shear strengthening, which was proportional to its cross-sectional area to a certain point, will be addressed later in this Chapter.

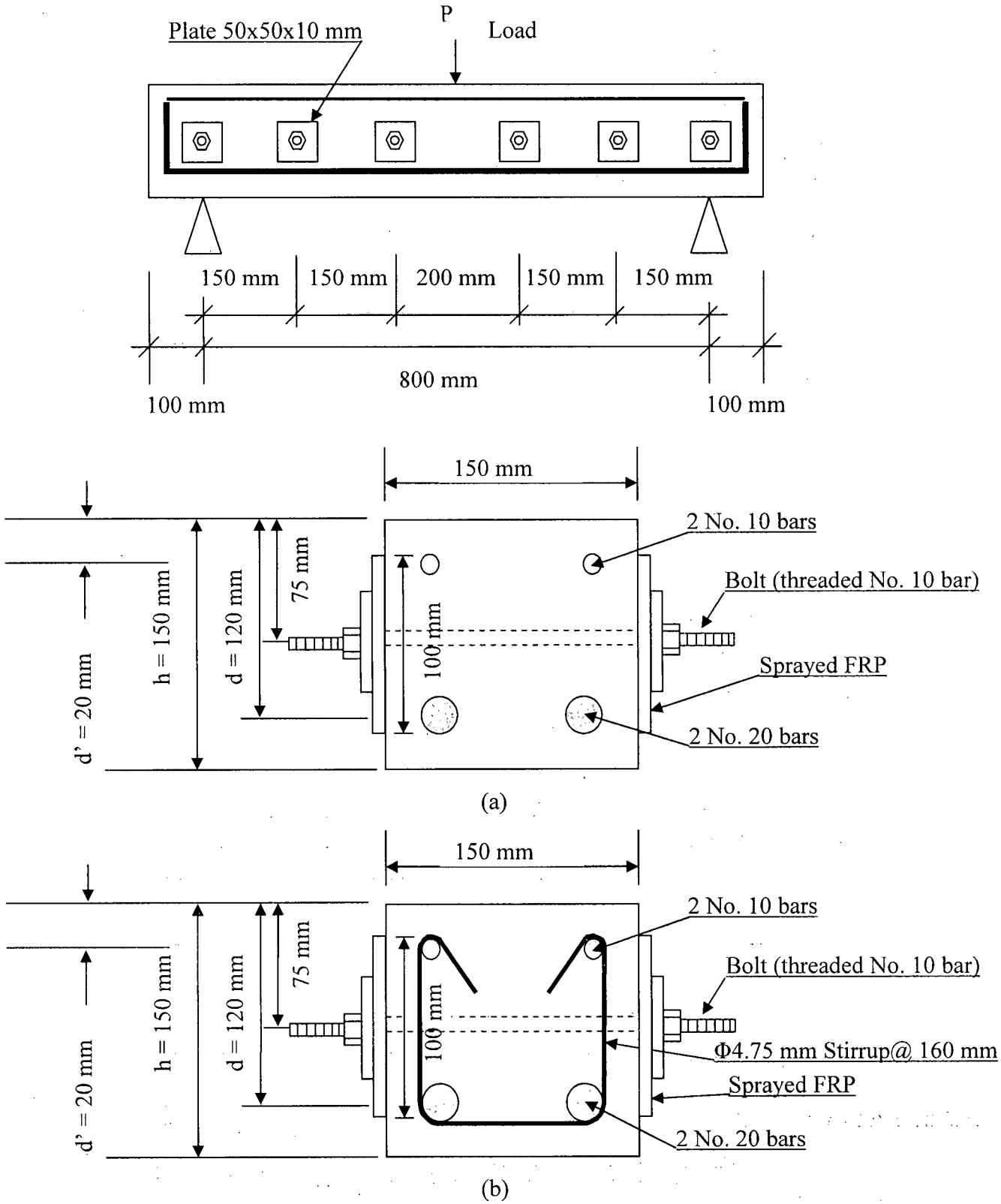

Figure 8.30 – *Cross-Sectional Details of RC Beams; (a) B2-6B-NS-1 to B2-6B-NS-3; (b) B2-6B-S-1*

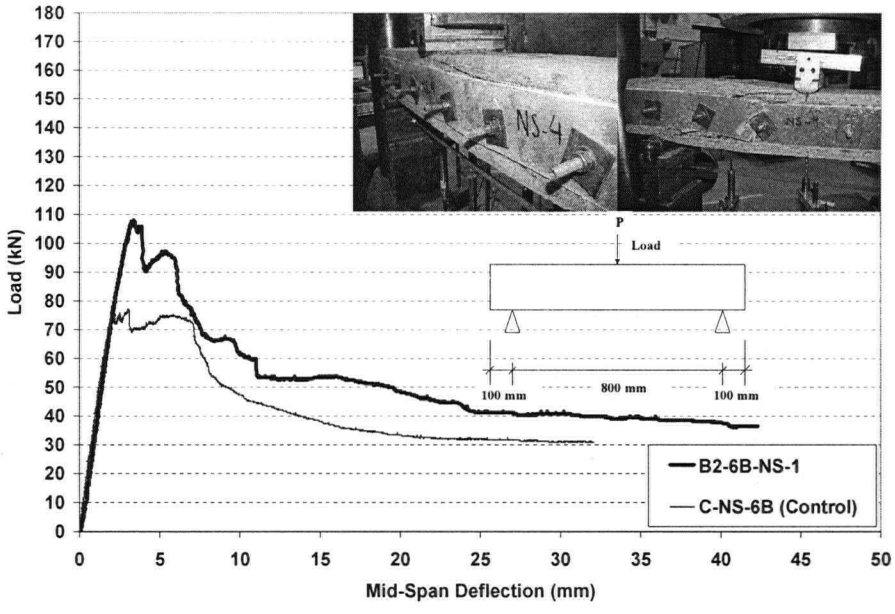

Figure 8.31 – *Load vs. Mid-Span Deflection of RC Beam B2-6B-NS-1*

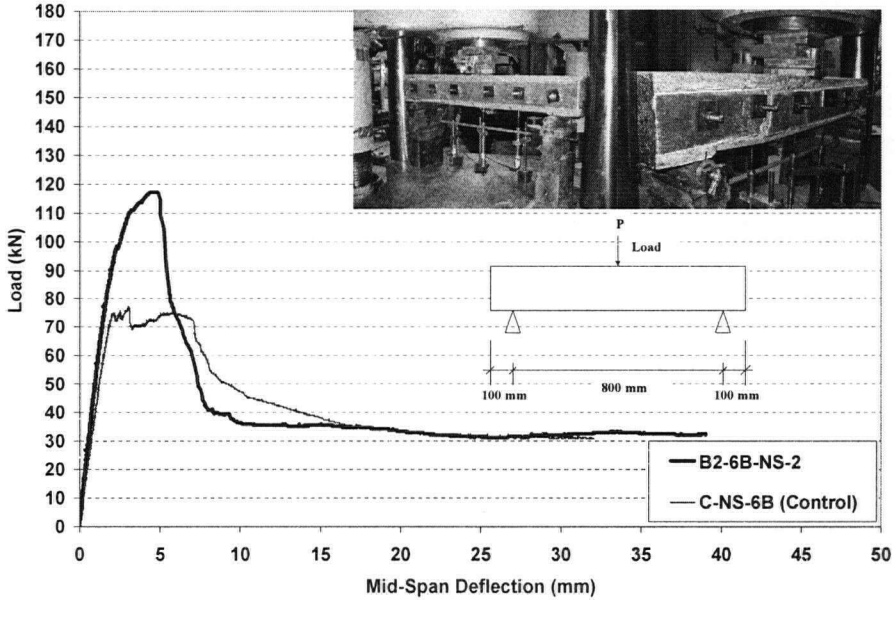

Figure 8.32 – *Load vs. Mid-Span Deflection of RC Beam B2-6B-NS-2*

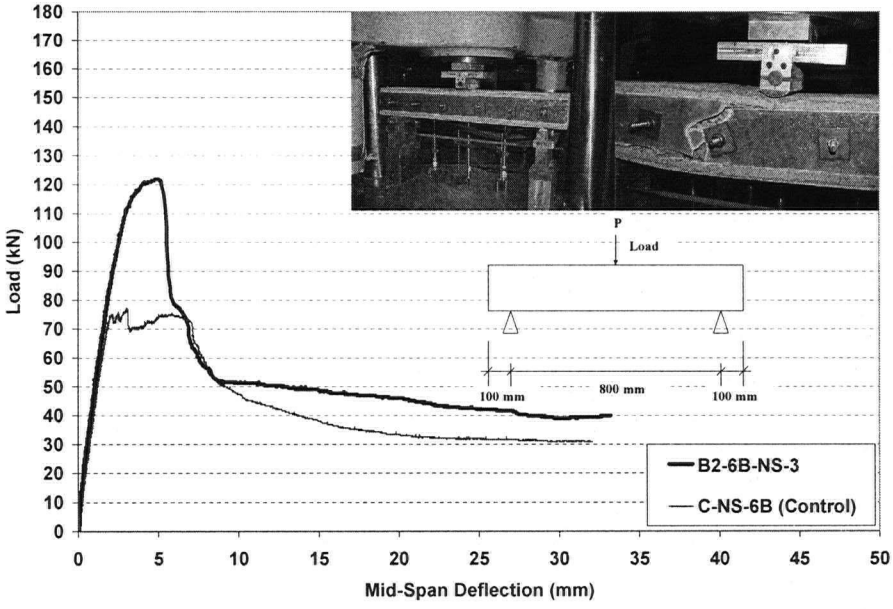

Figure 8.33 – *Load vs. Mid-Span Deflection of RC Beam B2-6B-NS-3*

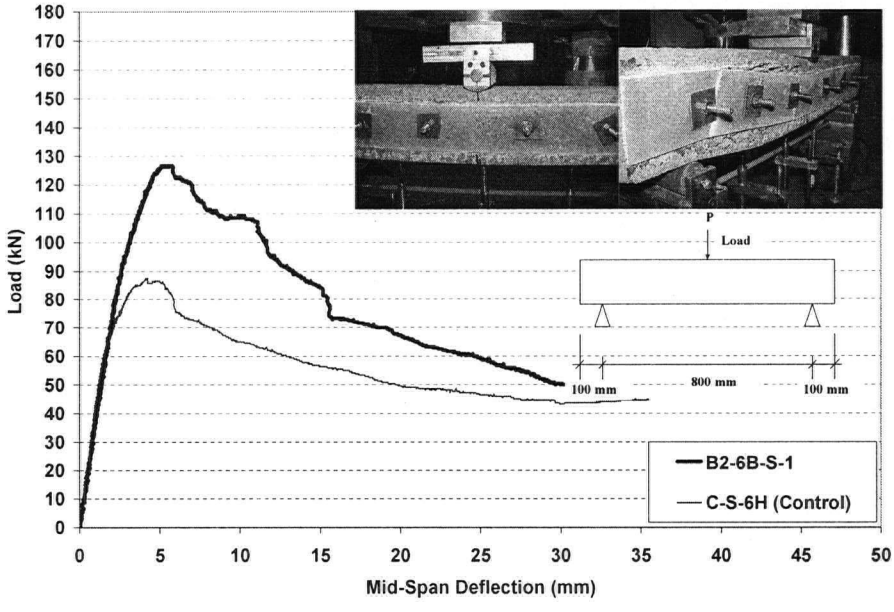

Figure 8.34 – *Load vs. Mid-Span Deflection of RC Beam B2-6B-S-1*

8.5.3 Sprayed GFRP on Three Sides

Four beams, all with Φ4.75 stirrups at 160 mm, were strengthened using Sprayed GFRP on their 3 sides (i.e. U-shaped). As mentioned earlier, since shear strengthening was the primary focus of this research, the GFRP was cut at the mid-span of the beam underneath the neutral axis of the beam's cross-section to minimize its contribution in flexural strengthening (see top right picture in Figure 8.37 for an example). In this way, contribution of GFRP to shear strength of RC beam, if any, would be explored. Load vs. mid-span deflection curves are shown in Figures 8.35 to 8.38 for beams B3-S-1 to B3-S-4, respectively. To show the benefits of this technique, test result of beam C-S-2 (control beam) is also included in each Figure. Notice that beams B3-S-3 and B3-S-4 showed significant increase in their load carrying capacity and a clear tension-steel yielding was observed in these two beams. In all 4 beams, the mode of failure was changed from shear to flexure.

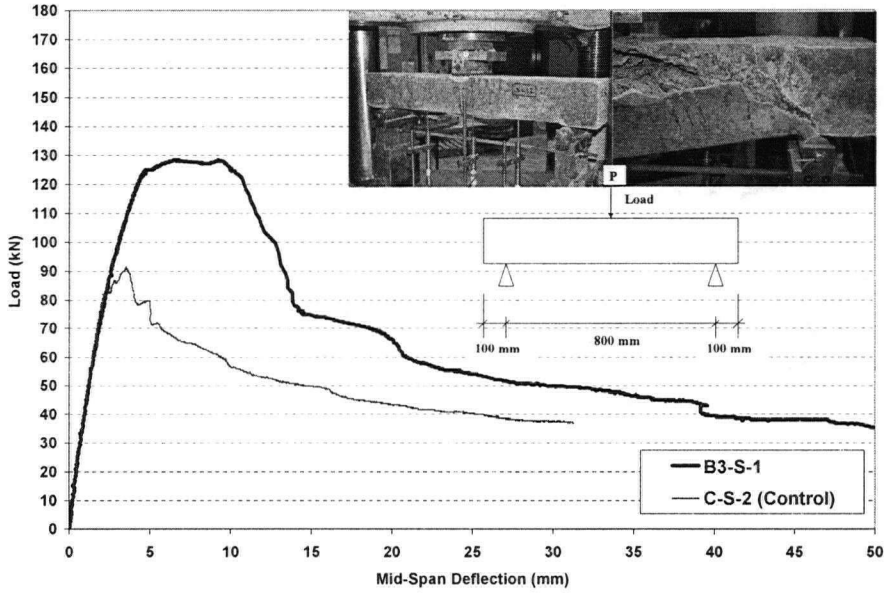

Figure 8.35 – *Load vs. Mid-Span Deflection of RC Beam B3-S-1*

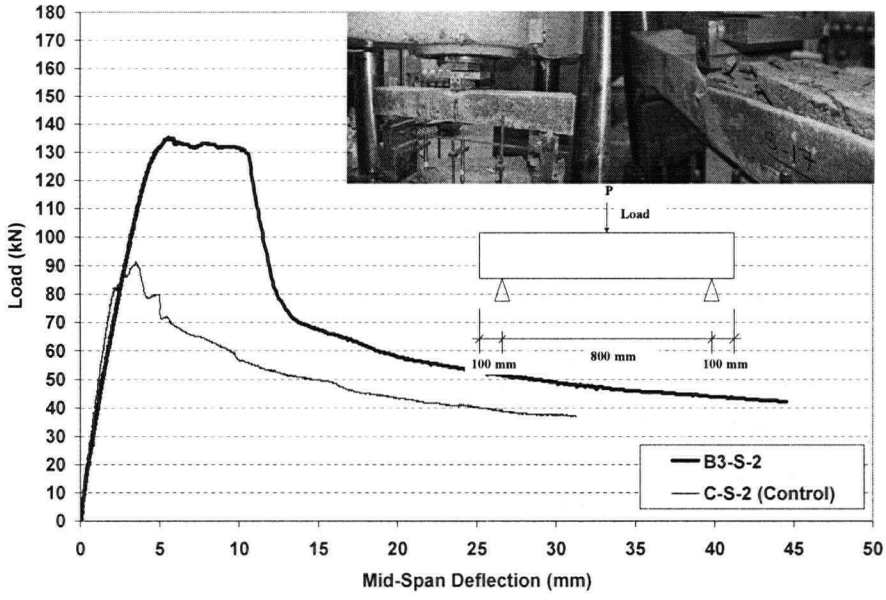

Figure 8.36 – *Load vs. Mid-Span Deflection of RC Beam B3-S-2*

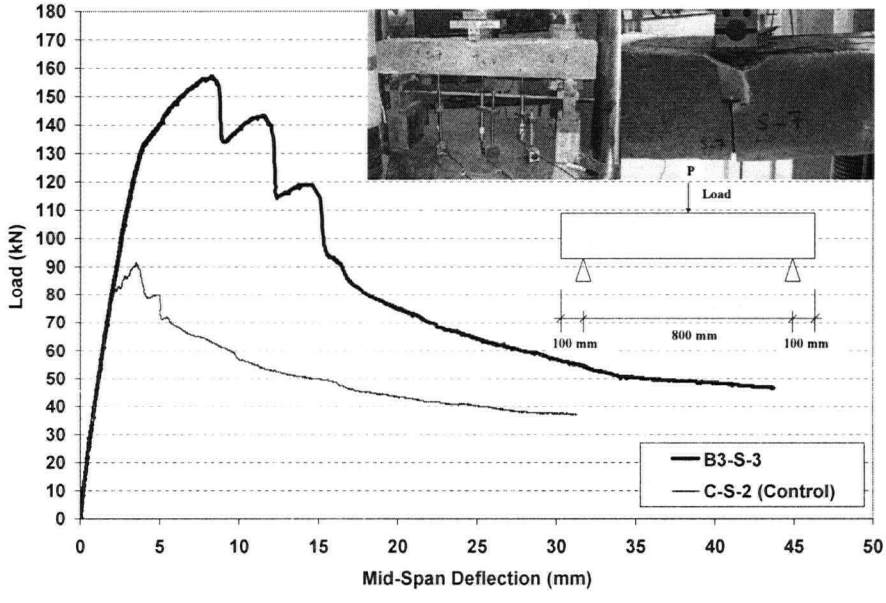

Figure 8.37 – *Load vs. Mid-Span Deflection of RC Beam B3-S-3*

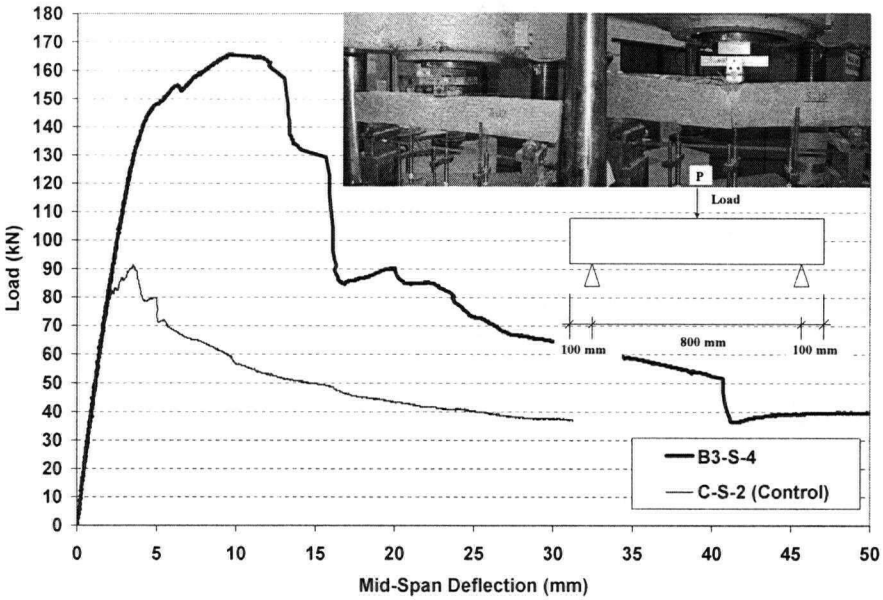

Figure 8.38 – *Load vs. Mid-Span Deflection of RC Beam B3-S-4*

8.5.4 Fabric GFRP

Three beams were strengthened for shear using the Wabo®MBrace fabric system. The thickness of each layer of GFRP fabric was approximately 1.2 mm. Details of the GFRP fabric configuration for these 3 beams are provided in Figure 8.39. Beam B2F-NS was strengthened for shear by applying one layer of fabric on its two lateral sides, beam BUF-NS by applying 50 mm width GFRP strips at every 65 mm, and finally beam BU2F-NS same as beam BUF-NS with an extra longitudinal layer of GFRP to increase the development length of U-shaped strips. Cross-sectional detail of this beam is provided in Figure 8.40.

Load vs. mid-span deflection of beam B2F-NS under quasi-static loading is shown and compared with its control specimen (beam C-NS) in Figure 8.41. Test results of beams BUF-NS and BU2F-NS are shown in Figures 8.42 and 8.43, respectively.

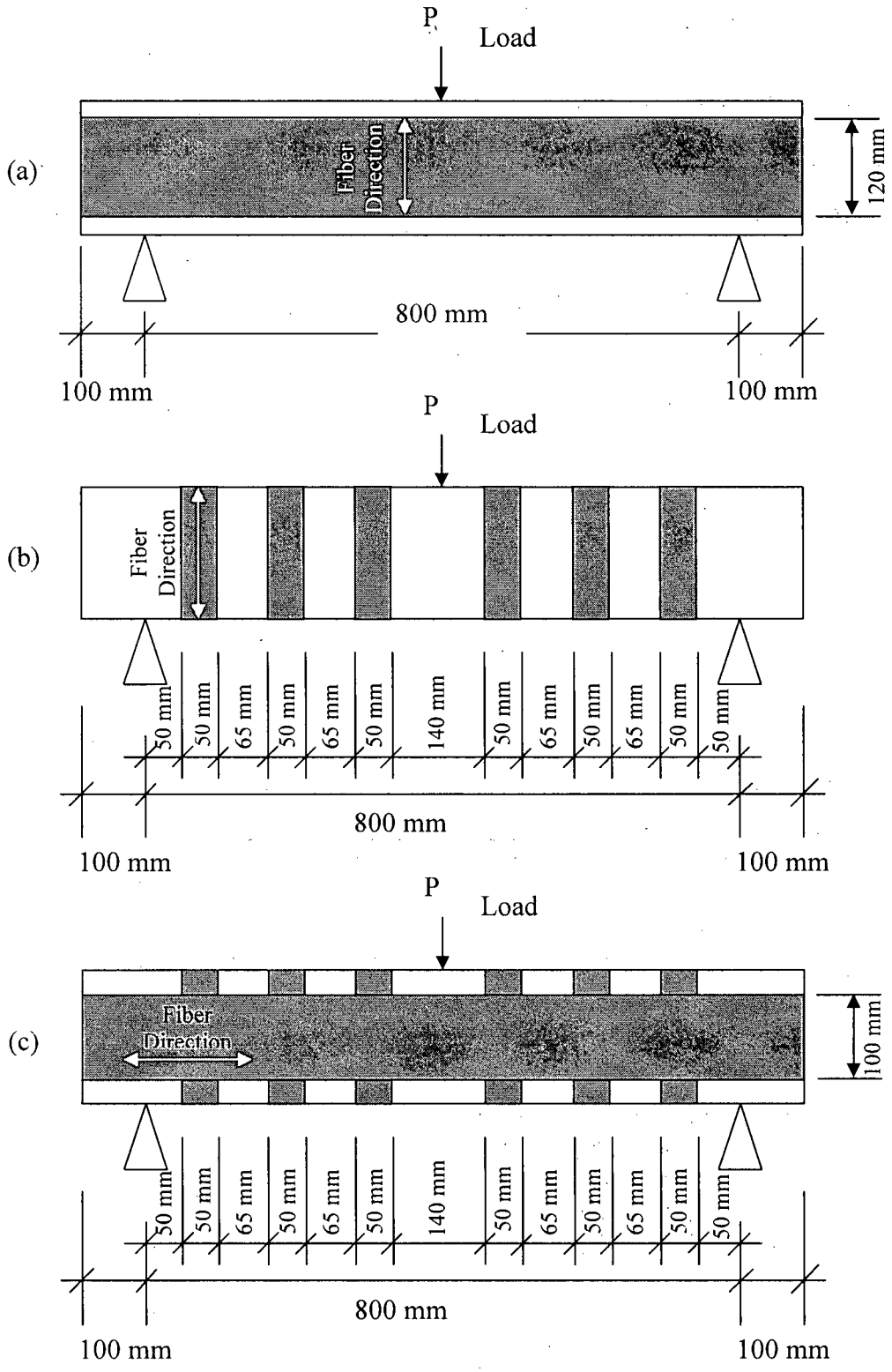

Figure 8.39 – *Configuration of Wabo®MBrace Fabric System; (a) Beam B2F-NS (Two Sides Bonded); (b) Beam BUF-NS (U-Shaped); (c) Beam BU2F-NS*

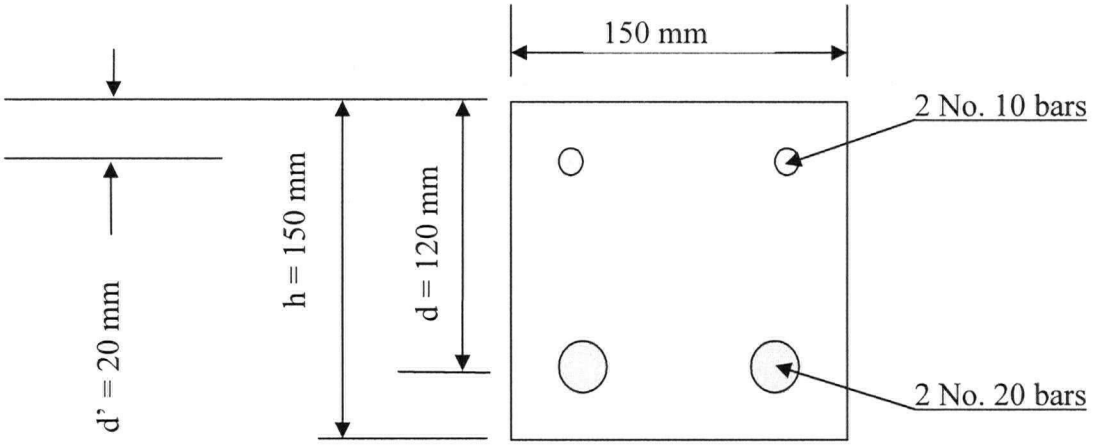

Figure 8.40 – *Cross-Sectional Details of Beams B2F-NS, BUF-NS and BU2F-NS before Strengthening*

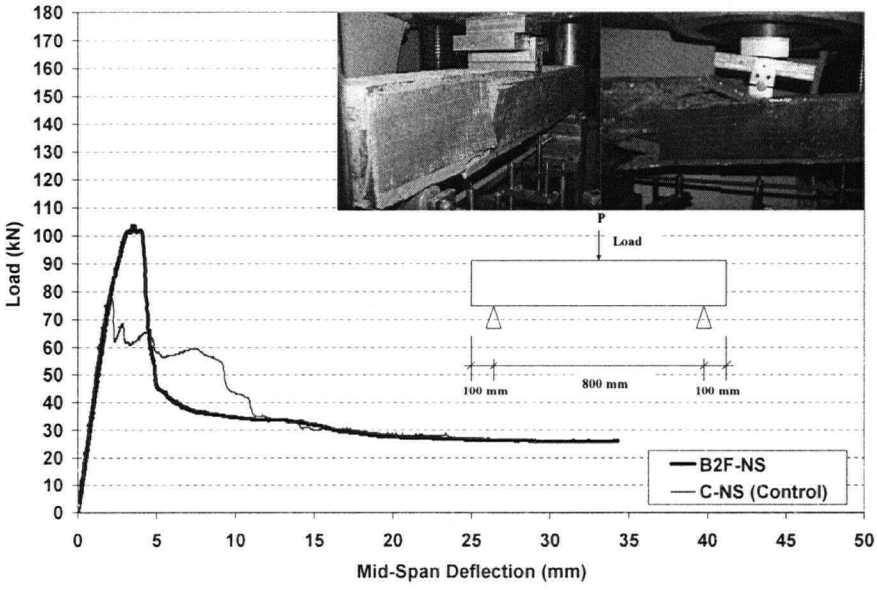

Figure 8.41 – *Load vs. Mid-Span Deflection of RC Beam B2F-NS*

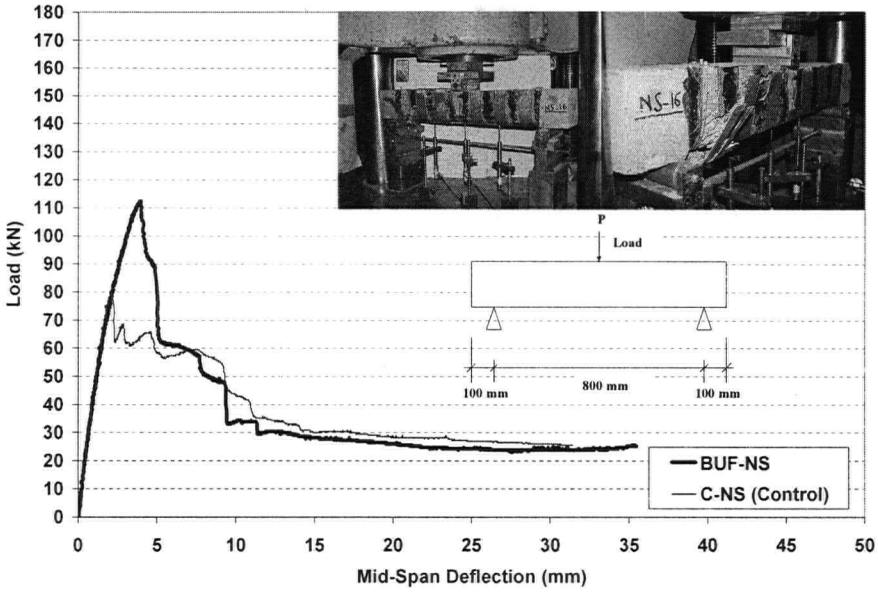

Figure 8.42 – *Load vs. Mid-Span Deflection of RC Beam BUF-NS*

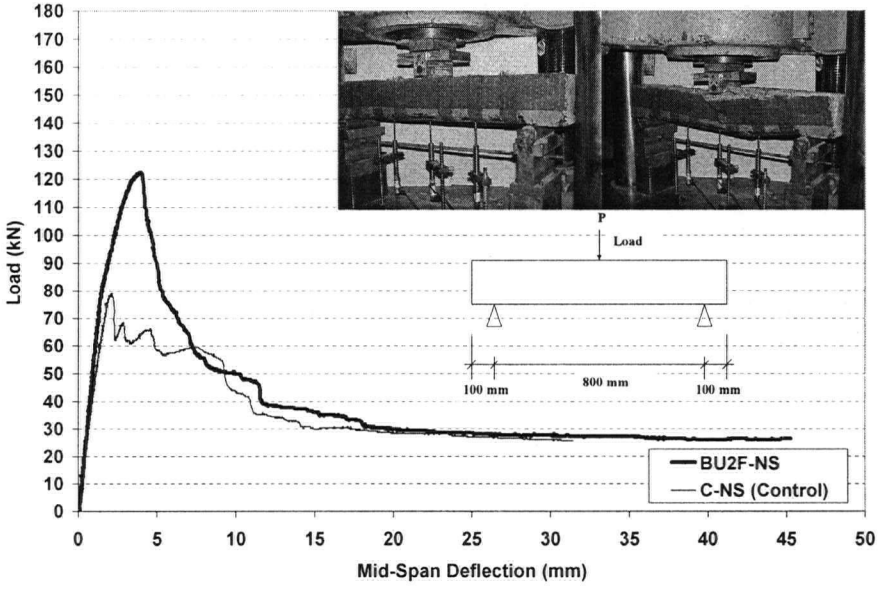

Figure 8.43 – *Load vs. Mid-Span Deflection of RC Beam BU2F-NS*

From these 3 tests, one can conclude that GFRP fabric is effective in shear strengthening of RC beams if applied properly. Shear failure of RC beams strengthened with GFRP fabric is quite catastrophic and sudden. As a result, it is important to provide enough shear FRP reinforcement to make sure that flexural failure will occur first. Since GFRP-concrete bond plays an important role in externally bonded FRPs, providing mechanical fasteners which may prevent premature debonding failure is strongly recommended.

8.6. Modeling and Proposed Equation

In all tests performed in this study, the Sprayed GFRP fracture occurred after the peak load (shear capacity) was reached. This, in turn, showed that after a certain strain in Sprayed GFRP, which was clearly less than its strain at rupture, there would be no contribution of the FRP to shear strength of RC beams.

If we consider a single shear crack in an RC beam with a 45° angle with respect to the horizontal axis, the horizontal projection of the crack can be taken as d_{frp}, which is shown in Figure 8.44.

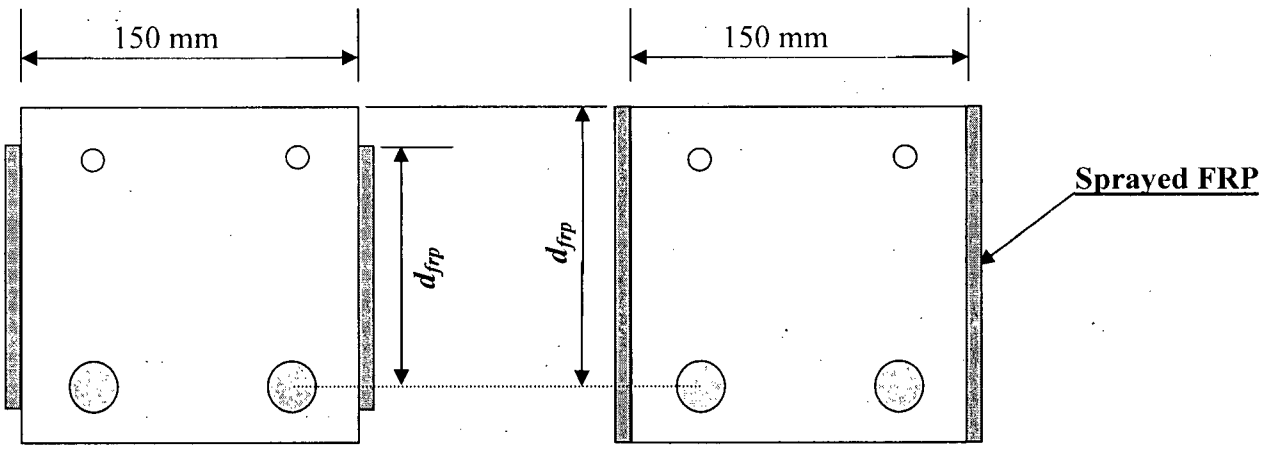

Figure 8.44 – *Depth of FRP Shear Reinforcement*

Therefore, for Sprayed GFRP applied continuously on both sides of an RC beam with a thickness of t_{frp} on each side and modulus of elasticity of E_{frp}, the product of $2 \times t_{frp} \times d_{frp} \times E_{frp} \times \varepsilon_{frp}$ will give the shear resisted by the Sprayed GFRP.

Strengthened beams can be divided into four groups:

1. Sprayed GFRP on two sides with mechanical fasteners,
2. Sprayed GFRP on two sides with epoxy interlayer,
3. Sprayed GFRP on 3 sides (U-shaped),
4. Sprayed GFRP on two sides with no mechanical fasteners or epoxy interlayer.

The shear contribution of Sprayed GFRP for different beams tested in this study as well as the product of $2 \times t_{frp} \times d_{frp} \times E_{frp}$ are tabulated in Table 8.3.

Contribution of Sprayed GFRP to shear strength (i.e. column (4) in Table 8.3) vs. $2 \times t_{frp} \times d_{frp} \times E_{frp}$ product (i.e. column (8) in Table 8.3) is drawn in Figures 8.45 and 8.46. Figure 8.45 shows the results for RC beams strengthened by Sprayed GFRP on three sides, two sides with mechanical fasteners and two sides with epoxy, while Figure 8.46 demonstrates the results for those strengthened on two sides with no mechanical fasteners and no epoxy.

From the first set of specimens shown in Figure 8.45 a value of 0.003 will be achieved for ε_{frp}, while a value of 0.002 is attained for ε_{frp} from Figure 8.46.

Table 8.3 – *Product of* $(2 \times t_{frp} \times d_{frp} \times E_{frp})$ *for Different Configurations of Sprayed GFRP*

Sprayed GFRP Configuration	Beam Name	Peak Load [kN]	Peak Load of Control Beam [kN]	Contribution of GFRP in Shear Strength [kN] ((2)-(3))	d_{frp}, FRP Width [mm]	t_{frp}, FRP Thickness [mm]	E_{frp}, Tensile Modulus of Elasticity of FRP [MPa]	$E_{frp}.2t_{frp}.d_{frp}$ (2x(6)x(7)x(5))
	(1)	(2)	(3)	(4)	(5)	(6)	(7)	(8)
Sprayed FRP on two sides with Epoxy	B2-NS-EP	96.8	79	17.8	100	2.2	14000	6160
	B2-S-EP	144.9	91.6	53.3	120	6	14000	20160
Sprayed FRP on two sides with mechanical fasteners	B2-4B-NS-1	92	77.2	14.8	100	1.8	14000	5040
	B2-4B-NS-2	99.4	77.2	22.2	100	2.5	14000	7000
	B2-4B-NS-3	111.5	77.2	34.3	100	4	14000	11200
	B2-4B-S-1	122.4	87.7	34.7	120	3.5	14000	11760
	B2-4B-S-2	129.8	87.7	42.1	120	4.2	14000	14112
	B2-4B-S-3	132.8	87.7	45.1	120	4.5	14000	15120
	B2-6B-NS-1	108.1	77.2	30.9	100	3.5	14000	9800
	B2-6B-NS-2	117.2	77.2	40	100	4	14000	11200
	B2-6B-NS-3	121.9	77.2	44.7	100	4.5	14000	12600
	B2-6B-S-1	126.7	87.7	39	100	4	14000	11200
Sprayed FRP on three sides	B3-S-1	128.5	91.6	36.9	120	3.2	14000	10752
	B3-S-2	135.4	91.6	43.8	120	4	14000	13440
	B3-S-3	157.1	91.6	65.5	120	7	14000	23520
	B3-S-4	166	91.6	74.4	120	8	14000	26880
Sprayed FRP on two sides (no epoxy, no mechanical fasteners)	B2-NS	105.5	79	26.5	100	4	14000	11200
	B2-S-1	117.2	91.6	25.6	120	3.5	14000	11760
	B2-S-2	128.9	91.6	37.3	120	4.5	14000	15120
	B2-S-3	129.3	91.6	37.7	120	5.6	14000	18816
	B2-S-4	132.1	91.6	40.5	120	6	14000	20160
	B2-S-5	133.2	91.6	41.6	120	7	14000	23520

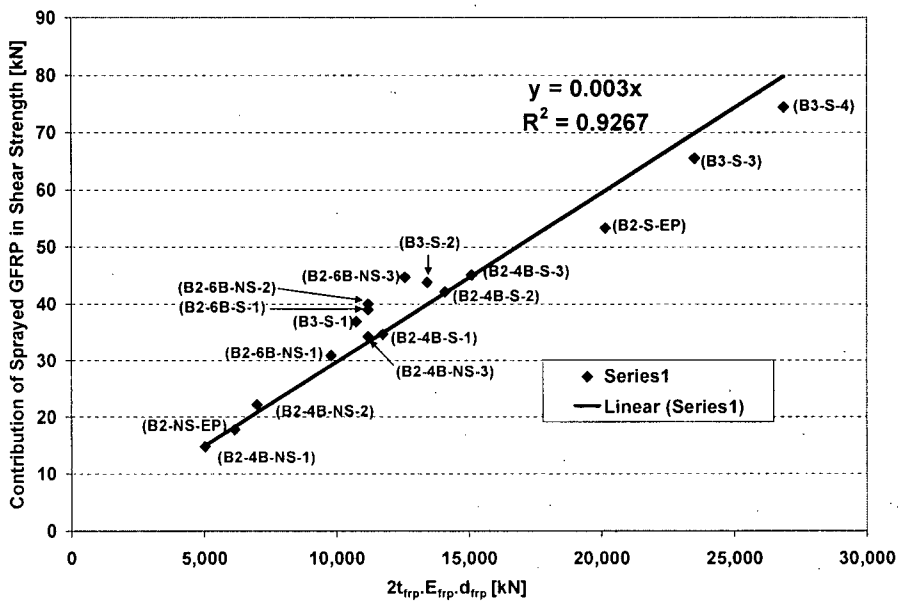

Figure 8.45 – *Contribution of Sprayed GFRP in shear strength vs. $2\times t_{frp}\times E_{frp}$ for RC beams strengthened by Sprayed GFRP on three sides, two sides with mechanical fasteners and two sides with epoxy.*

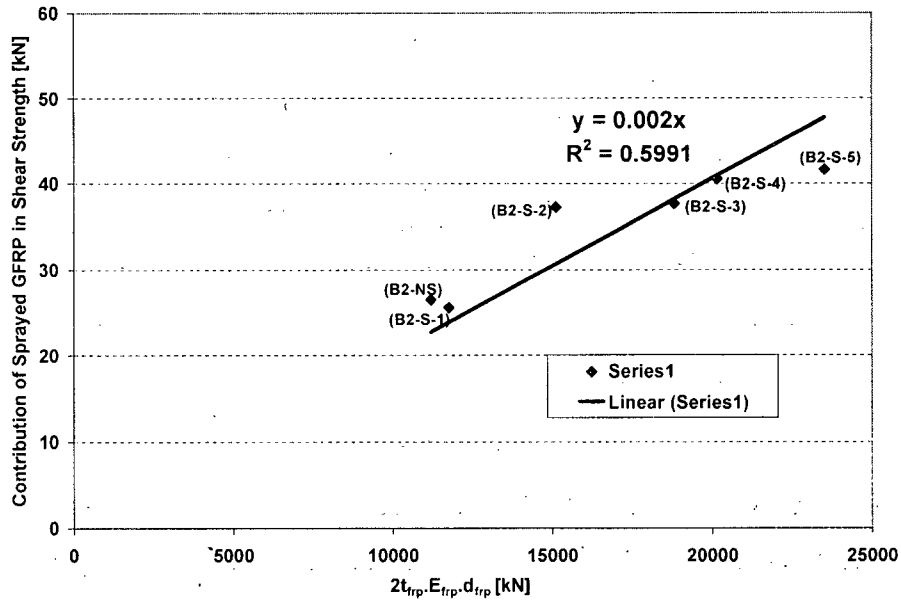

Figure 8.46 – *Contribution of Sprayed GFRP in shear strength vs. $2\times t_{frp}\times E_{frp}$ for RC beams strengthened by Sprayed GFRP on two sides with no mechanical fasteners and no epoxy.*

Based on the results reported in Figures 8.45 and 8.46, the following equation is proposed to calculate the contribution of Sprayed GFRP composites in shear strength of RC beams:

$$V_{frp} = 2t_{frp}d_{frp}E_{frp}\varepsilon_{frp} \tag{8.1}$$

where,

V_{frp} = contribution of Sprayed GFRP in shear strength of RC beam [N]

t_{frp} = average thickness of the Sprayed GFRP [mm]

d_{frp} = depth of FRP shear reinforcement as shown in Figure 8.44 [mm]

E_{frp} = modulus of elasticity of FRP composite

$$\varepsilon_{frp} = \begin{cases} 0.002 & \text{for side bonding to the web when no mechanical fasteners/epoxy are used} \\ 0.003 & \text{for side bonding to the web when mechanical fasteners are used} \\ 0.003 & \text{for side bonding to the web when an interlayer of epoxy is used} \\ 0.003 & \text{for continuous U - shaped around the bottom of the web} \end{cases}$$

Validity of this equation is shown in Table 8.4. It is clear that the calculated values for V_{frp} are very close to their experimental values. The proposed equation (Equation 8.1) is very similar to Equation 11.5 of CSA S-806-02. As a result, this proposed equation can easily be implemented in the Canadian Standard Code for shear strengthening design using Sprayed GFRP composites.

Table 8.4 – *Validity of Proposed Equation to Calculate the Contribution of Sprayed GFRP in Shear Strength of RC Beam*

Sprayed GFRP Configuration	Beam Name	Peak Load [kN]	Peak Load of Control Beam [kN]	Contribution of GFRP in Shear Strength [kN] ((2)-(3))	d_{frp}, FRP Width [mm]	t_{frp}, FRP Thickness [mm]	E_{frp}, Tensile Modulus of Elasticity of FRP [MPa]	ε_{frp}, Effective Strain of FRP	V_{frp} [kN]= $2t_{frp}.d_{frp}.E_{frp}.\varepsilon_{frp}$ (2x(6)x(5)x(7)x(8))	V_{calc}/V_{exp} (9)/(4)
	(1)	(2)	(3)	(4)	(5)	(6)	(7)	(8)	(9)	(10)
Sprayed FRP on two sides with Epoxy	B2-NS-EP	96.8	79	17.8	100	2.2	14000	0.003	18.5	1.04
	B2-S-EP	144.9	91.6	53.3	120	6	14000	0.003	60.5	1.13
Sprayed FRP on two sides with mechanical fasteners	B2-4B-NS-1	92	77.2	14.8	100	1.8	14000	0.003	15.1	1.02
	B2-4B-NS-2	99.4	77.2	22.2	100	2.5	14000	0.003	21.0	0.95
	B2-4B-NS-3	111.5	77.2	34.3	100	4	14000	0.003	33.6	0.98
	B2-4B-S-1	122.4	87.7	34.7	120	3.5	14000	0.003	35.3	1.02
	B2-4B-S-2	129.8	87.7	42.1	120	4.2	14000	0.003	42.3	1.01
	B2-4B-S-3	132.8	87.7	45.1	120	4.5	14000	0.003	45.4	1.01
	B2-6B-NS-1	108.1	77.2	30.9	100	3.5	14000	0.003	29.4	0.95
	B2-6B-NS-2	117.2	77.2	40	100	4	14000	0.003	33.6	0.84
	B2-6B-NS-3	121.9	77.2	44.7	100	4.5	14000	0.003	37.8	0.85
	B2-6B-S-1	126.7	87.7	39	100	4	14000	0.003	33.6	0.86
Sprayed FRP on three sides	B3-S-1	128.5	91.6	36.9	120	3.2	14000	0.003	32.3	0.87
	B3-S-2	135.4	91.6	43.8	120	4	14000	0.003	40.3	0.92
	B3-S-3	157.1	91.6	65.5	120	7	14000	0.003	70.6	1.08
	B3-S-4	166	91.6	74.4	120	8	14000	0.003	80.6	1.08
Sprayed FRP on two sides (no epoxy, no mechanical fasteners)	B2-NS	105.5	79	26.5	100	4	14000	0.002	22.4	0.85
	B2-S-1	117.2	91.6	25.6	120	3.5	14000	0.002	23.5	0.92
	B2-S-2	128.9	91.6	37.3	120	4.5	14000	0.002	30.2	0.81
	B2-S-3	129.3	91.6	37.7	120	5.6	14000	0.002	37.6	1.00
	B2-S-4	132.1	91.6	40.5	120	6	14000	0.002	40.3	1.00
	B2-S-5	133.2	91.6	41.6	120	7	14000	0.002	47.0	1.13

There are some important things that should be mentioned here:

1. In Sprayed GFRP application, since U-shaped wrapping will always be applied continuously in practice, in the proposed equation s_{frp} (i.e. spacing of FRP shear reinforcement) has not been used. This makes the proposed equation simple to apply.

2. CSA S-806-02 restricts the summation of shear resistance provided by steel stirrups (V_s) and FRP composite (V_{frp}) to a certain value (Clause 11.3.2.2 Equation (11.2)) as follows:

$$V_s + V_{frp} \leq 0.6\lambda\phi_c\sqrt{f_c'}b_w d \qquad (8.2)$$

where,

λ = factor to account for low-density concrete

ϕ_c = resistance factor of concrete

f_c' = specified compressive strength of concrete [MPa]

b_w = width of the web of a beam [mm]

d = distance from extreme compression fiber to centroid of tension reinforcement [mm]

It is equally important to keep this restriction in mind while designing shear strengthened RC beams using Sprayed GFRP. In other words, when Sprayed GFRP coating exceeds a certain thickness, Equation (8.2) will rightly put an upper limit for FRP contribution in shear strength of RC beam.

3. While ε_{frp} is either 0.002 or 0.004 for fabric FRP (Equation (11.5) of CSA-S806-02) and 0.002 or 0.003 for Sprayed GFRP (Equation 8.1), in shear strengthening of RC beams there is not really a major benefit in using ultra high strength fabric FRP, and Sprayed GFRP with its strain at rupture of 0.63% can be considered a more economical product compare to fabric FRP with a strain to rupture of about 2.1% (i.e. 5 to 10 times more than 0.004 and 0.002, respectively). It is worth mentioning that all these limits are actually derived from FRP-concrete bond limitations.

4. It is worth noting that ε_{frp}, effective strain of FRP in Equation (8.1), is governed by to the compressive strength of concrete. ε_{frp} can be assumed as a maximum strain of GFRP at which the integrity of concrete and secure activation of the aggregate interlock mechanism are maintained. Since in this study the compressive strength of concrete was constant, the relationship between effective strain of Sprayed GFRP and compressive strength of concrete could not be established. In general, if we consider a relationship

such as the one proposed by ISIS Canada (Equation 2.40) for wrap GFRP, the following equation (or an equation with similar format) can be used to predict the effective strain of Sprayed GFRP for an RC beam with a different concrete compressive strength:

$$\varepsilon_{frp,f_c'} = \left(\frac{f_c'}{44}\right)^{0.31} \tag{8.3}$$

where,

$\varepsilon_{frp,f_c'}$ = effective strain of Sprayed GFRP corresponding to compressive strength of concrete used in RC beam

f_c' = compressive strength of concrete in RC beam, MPa

5. Note that resistance factor of FRP composites, ϕ_{frp}, has not been introduced into the proposed Equation 8.1. In CSA S806-02 a value of 0.75 is recommended for resistance factor of FRP composites, and this value can also be applied in Equation (8.1) as a safety factor.

Implementing ϕ_{frp} into Equation (8.1), it can be written as:

$$V_{frp} = 2\phi_{frp} t_{frp} d_{frp} E_{frp} \varepsilon_{frp} \tag{8.4}$$

where, ϕ_{frp} is the resistant factor for Sprayed GFRP composite and a value of 0.75, based on CSA S806-02, is recommended.

For the GFRP wrap (i.e. beams B2F-NS, BUF-NS and BU2F-NS), the validity of Equation (11.5) of CSA-S806-02 is reported in Table 8.5. It is seen that this equation works fine for U-shaped wrap continuous around the bottom of the web (i.e. Beams BUF-NS and BU2F-NS) but predicts higher than experimental value for side bonding FRP fabric (i.e. Beam B2F-NS). Note that ϕ_F = resistance factor of FRP composites (= 0.75, Clause 7.2.7.2) is not applied in Table 8.6. and this to some extent can adjust the predicted value and bring it closer to the experimental one.

Table 8.5 – *Checking the Validity of CSA-S806-02 Equation (11.5) to Calculate the Contribution of Fabric GFRP in Shear Strength of RC Beam, For* ***(a) Side Bonding to the Web, (b) U-Shaped, and (c) U-Shaped +Side Bonding***

	Beam Name		
	B2F-NS (a)	BUF-NS (b)	BU2F-NS (c)
Peak Load [kN]	103.7	11.2	122.4
Peak Load of Control Beam [kN]	79	79	79
Contribution of GFRP in Shear Strength [kN], V_{calc}	24.7	33.4	43.4
d_{frp}, FRP Width [mm]	105	120	120
t_{frp}, FRP Thickness [mm]	1.2	1.2	1.2
E_{frp}, Tensile Modulus of Elasticity of FRP [MPa]	72400	72400	72400
ε_{frp}, Effective Strain of FRP	0.002	0.004	0.004
A_{frp}, Cross-Sectional Area of FRP [mm^2]	----	50*1.2=60	50*1.2=60
s_{frp}, Spacing of FRP Shear Reinforcement [mm]	----	65	65
V_{frp} [kN]= $E_{frp}.\varepsilon_{frp}.2t_{frp}.d_{frp}$	36.5	------	------
V_{frp} [kN]= $E_{frp}.\varepsilon_{frp}.A_{frp}.d_{frp}/s_{frp}$	------	32.1	32.1
V_{calc}/V_{exp}	1.48	0.96	0.74

8.7. Energy Evaluation

Peak loads and absorbed energy up to 10 mm, 15 mm and 20 mm mid-span deflection of the tested RC beams are provided in Table 8.6. Figures 8.47 and 8.48 compare peak load and absorbed energy up to 15 mm mid-span deflection of each strengthened beam with its control beam, respectively. The test results of beams B2-NS-SB and B2-NS-Hilti are not included in Figures 8.47 and 8.48 as no benefit was observed in sandblasting or using the Hilti nails. Based on the information provided in Table 8.6 and Figures 8.47 and 8.48, one can draw the following conclusions:

1. Although using Wabo®MBrace primer and putty as an intermediate layer between concrete and Sprayed GFRP (beams B2-NS-EP and B2-S-EP) increased the load carrying capacity, the energy absorption capacity was not increased as much as the load carrying capacity (it even decreased for beam B2-NS-EP).

2. Roughening concrete surface using a pneumatic concrete chisel was an effective way to increase the concrete-FRP bond. This, in turn, increased the energy absorption capacity of strengthened beams as well.

3. Using through-bolts and nuts effectively increased both the load carrying capacity and the energy absorption capacity in strengthened beams. Either sandblasting or roughening the concrete surface by a chisel can be employed when this type of mechanical fastener is used.

4. U-shaped Sprayed GFRP was the most promising way to gain maximum possible benefits in shear strengthening from these advanced materials. Tension steel yielding was observed in a flexural failure type in beams B3-S-3 and B3-S-4. Confinement provided by U-shaped Sprayed GFRP also effectively increased the energy absorption capacity of these strengthened beams. As a result, it should always be recommended to apply U-shaped Sprayed GFRP configuration for shear strengthening, where possible.

5. Wabo®MBrace fabric system increased the load carrying capacity of RC beams when used as shear reinforcement. As with Sprayed GFRPs, U-shaped was seen as a more effective configuration than side bonding alone. Bonding additional longitudinal FRP strips over the end of the U-shaped bands improved the performance of the U-shaped bands, and as a result, beam BU2F-NS showed a higher load carrying capacity than that of beam BUF-NS. Again (see conclusion 1 for beams B2-NS-EP and B2-S-EP), increase in energy absorption capacity of beams strengthened in shear by Wabo®MBrace fabric system was not as high as the increase in the load carrying capacity. Brittleness of the Wabo®MBrace Putty, at least to some extent, may explain this observation.

6. Presence of steel stirrups was effective in increasing the load carrying and energy absorption capacities of strengthened RC beams. This is a benefit, because, in practice, RC beams contain steel stirrups and adding Sprayed GFRP as external shear reinforcement can more effectively increase the beams performance under large loads compared to those with no stirrups.

Table 8.6 – *Peak Loads and Area under the Load vs. Mid-Span Deflection Curves of RC Beams*

Beam Name	Peak Load [kN]	Area under the Load vs. Mid-Span Deflection Curve [N.m]		
		Up to 10 mm Deflection	Up to 15 mm Deflection	Up to 20 mm Deflection
C-NS	79	559	735	883
C-NS-6B	77.2	612	825	1000
C-S-6H	87.7	690	996	1262
C-SS	131.9	1024	1465	1757
C-S-1	91.6	647	934	1168
C-S-2	91.6	659	926	1157
B2-NS-SB	79	526	728	904
B2-NS-EP	96.8	474	625	760
B2-S-EP	144.9	1033	1261	1454
B2-NS	105.5	599	786	935
B2-S-1	117.2	809	1020	1190
B2-S-2	128.9	843	1129	1363
B2-S-3	129.3	962	1265	1529
B2-S-4	132.1	1051	1285	1461
B2-S-5	133.2	1005	1246	1460
B2-NS-Hilti	77.7	558	764	952
B2-4B-NS-1	92	734	1005	1196
B2-4B-NS-2	99.4	722	1019	1223
B2-4B-NS-3	111.5	782	1056	1270
B2-4B-S-1	122.4	893	1282	1623
B2-4B-S-2	129.8	1016	1590	2053
B2-4B-S-3	132.8	1033	1591	2024
B2-6B-NS-1	108.1	733	1011	1269
B2-6B-NS-2	117.2	717	895	1069
B2-6B-NS-3	121.9	773	1025	1263
B2-6B-S-1	126.7	976	1440	1812
B3-S-1	128.5	1030	1544	1898
B3-S-2	135.4	1050	1503	1817
B3-S-3	157.1	1192	1839	2249
B3-S-4	166	1423	2121	2491
B2F-NS	103.7	699	951	1155
BUF-NS	112.4	637	792	928
BU2F-NS	122.4	739	945	1108

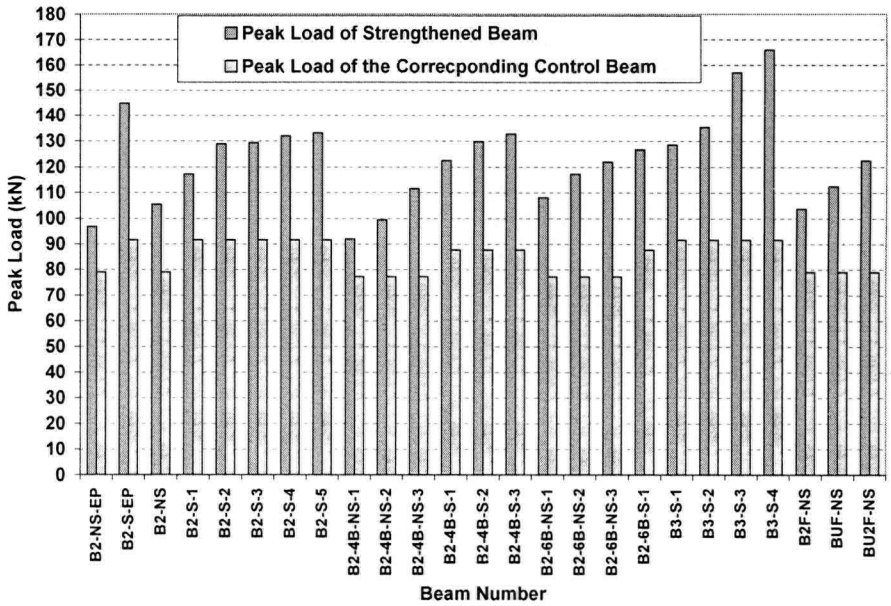

Figure 8.47 – *Comparison of Load Carrying Capacity*

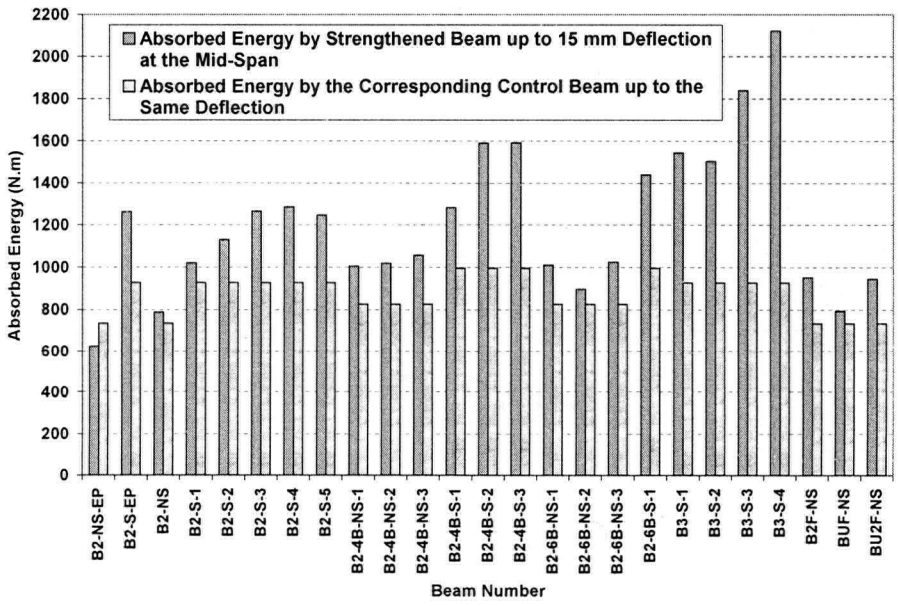

Figure 8.48 – *Comparison of Energy Absorption Capacity*

9

BEHAVIOR OF SHEAR STRENGTHENED RC BEAMS UNDER IMPACT LOADING

9.1 Introduction

RC beams with deficiency in their shear strength were retrofitted using Sprayed GFRP. Different thicknesses and schemes were used and their effectiveness was evaluated under quasi-static loading and reported in Chapter 8. The most promising ones were then tested under impact loading using a fully instrumented drop weight impact machine described in Chapter 6. Test results of these beams are provided and discussed in this Chapter.

Beam design, specimen preparation, testing procedure under quasi-static loading, and retrofit schemes were all described in Chapter 8. Testing procedure under impact loading was discussed in Chapter 7.

9.2 Test Results

A total of 15 identical RC beams (Figure 8.1) were cast to investigate their behavior under impact loading with and without Sprayed GFRP as external shear reinforcement. Three beams were tested under impact with 600 mm and 800 mm drop height (impact velocity of 3.43 m/s and 3.96 m/s, respectively). The remaining 12 beams were strengthened with Sprayed GFRP and tested under impact loading. One beam was tested

with an impact velocity of 3.43 m/s, while others were tested with 3.96 m/s impact velocity. Table 8.1 tabulates the beams designation and configuration. Results obtained in Chapter 8 showed that the Sprayed GFRP is more beneficial as external shear reinforcement if used in conjunction with steel stirrups. As a result, all beams tested under impact with their results presented in this Chapter contained Φ4.75 @ 160 mm steel stirrups.

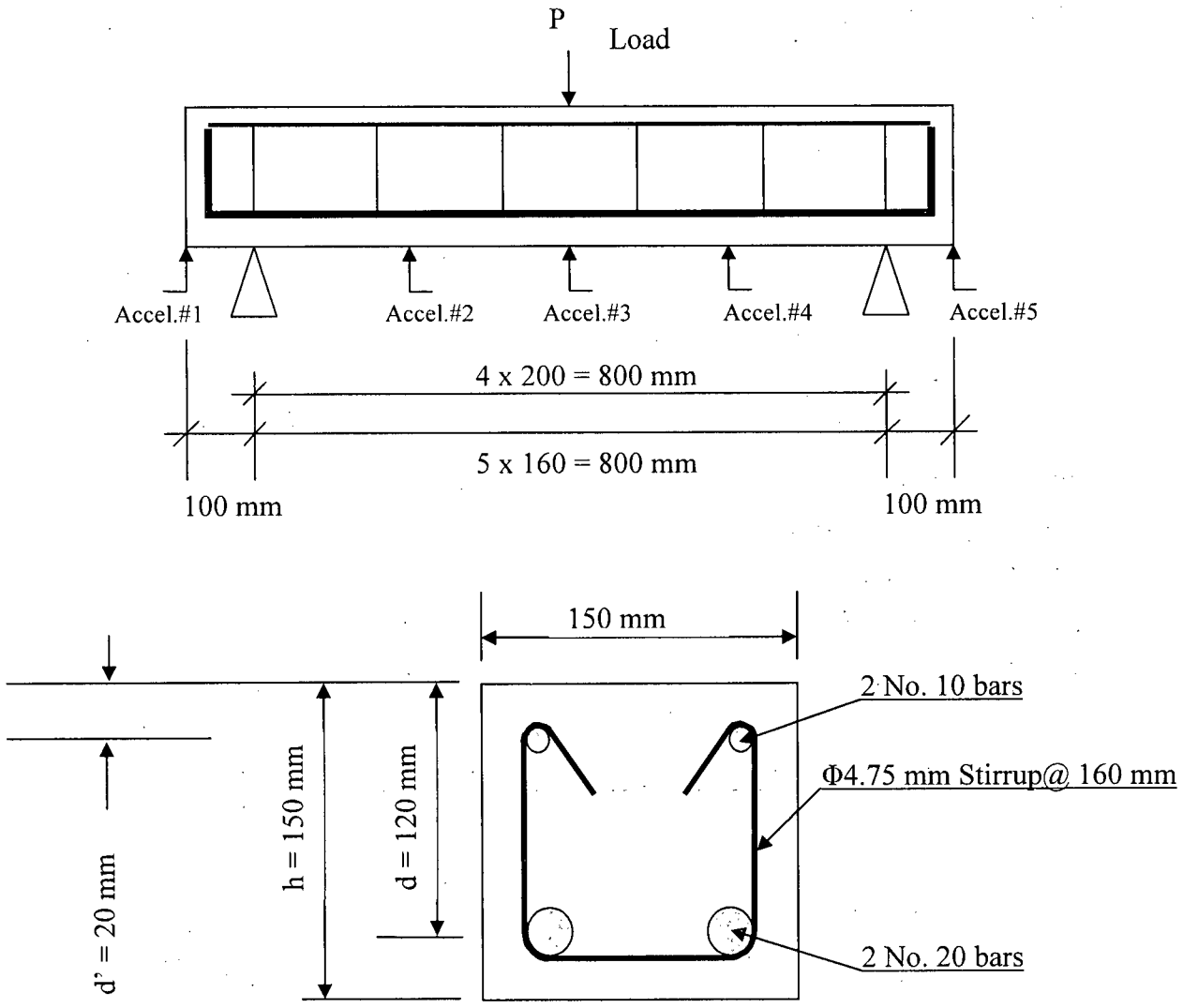

Figure 8.1 – *RC Beam Cross-Sectional Details and Location of the Accelerometers in Impact Loading*

Table 9.1 – *RC Beams Designations and Details*

Beam Designation	Drop Height (mm)	Sprayed GFRP Width (mm)	Sprayed GFRP Thickness (mm)		
			2 Sided	2 Sided + 4 Bolts	3 Sided
PI-600	600	NA	———	———	———
PI-800-1	800	NA	———	———	———
PI-800-2	800	NA	———	———	———
SI-2S-800-1	800	150	3.3	———	———
SI-2S-800-2	800	150	4.6	———	———
SI-2S-800-3	800	150	6.5	———	———
SI-2S-800-4	800	150	10.3	———	———
SI-4B-800-1	800	150	———	2.4	———
SI-4B-800-2	800	150	———	4.0	———
SI-4B-800-3	800	150	———	6.5	———
SI-3S-800-1	800	150	———	———	1.9
SI-3S-800-2	800	150	———	———	2.8
SI-3S-800-3	800	150	———	———	3.2
SI-3S-800-4	800	150	———	———	6.2
SI-3S-600	600	150	———	———	10.7

Note: **P**: **P**lain RC beam (no Sprayed GFRP was applied), **I**: Tested under **I**mpact loading, **S**: **Sprayed** GFRP was applied as external shear reinforcement, **2S**: Sprayed GFRP was applied on **2** lateral **S**ides of the beam, **4B**: **4** through **B**olts were used as mechanical fasteners, **3S**: Sprayed GFRP was applied on **3** lateral **S**ides of the beam

All beams (quasi-static and impact loading) were tested under 3-point loading. In impact loading, all beams were tested using drop weight impact machine described in Chapter 6.

Parameters needed for calculating load carrying capacity of RC beams before retrofitting by Sprayed GFRP are reported in Chapter 8 (Table 8.1). Since not enough shear reinforcement was provided, the maximum strength of the beam would be governed by the shear strength of concrete as well as the shear strength of steel stirrups. Calculations (see Appendix B) show that if resistance factors are not considered, the capacity of this beam under quasi-static loading is 131 kN if enough reinforcement is provided for shear. At this point, tension reinforcement starts yielding. It is also worth noting that the beam was designed to produce a typical shear failure mode since not enough stirrups were provided and shear strength of concrete was far below the flexural strength of the beam. RC beam with no stirrup and with stirrups (Φ4.75 @ 160 mm) is predicted to have a capacity of about 80 kN and 100.2 kN, respectively (see Appendix B).

9.2.1 Control Beams with No Sprayed GFRP (Plain RC Beams)

Three beams (PI-600, PI-800-1 and PI-800-2) were tested under impact loading while no GFRP composites were applied to them. Load vs. mid-span deflection of these beams are reported in Figures 9.2 to 9.4 and will be used later as bench marks for comparing the results.

The same beam was tested under quasi-static loading and results are shown in Chapter 8 (Figures 8.4 and 8.5 for beams C-S-1 and C-S-2, respectively). The results of impact tests for plain RC beams are compared with the quasi-static test results in Figures 9.2 to 9.4.

Under impact loading a very wide shear crack was created starting from the point of impact towards one of the supports. Shear cracks, as also observed in quasi-static load condition, were inclined at almost 10° to 15° with respect to horizon at the point of impact and at the support and at about 45° at the midpoint between these two locations (as examples, see illustrated pictures in Figures 9.2 and 9.4).

Rupture of stirrup was observed in beam PI-800-1 and is shown in illustrated picture in Figure 9.3.

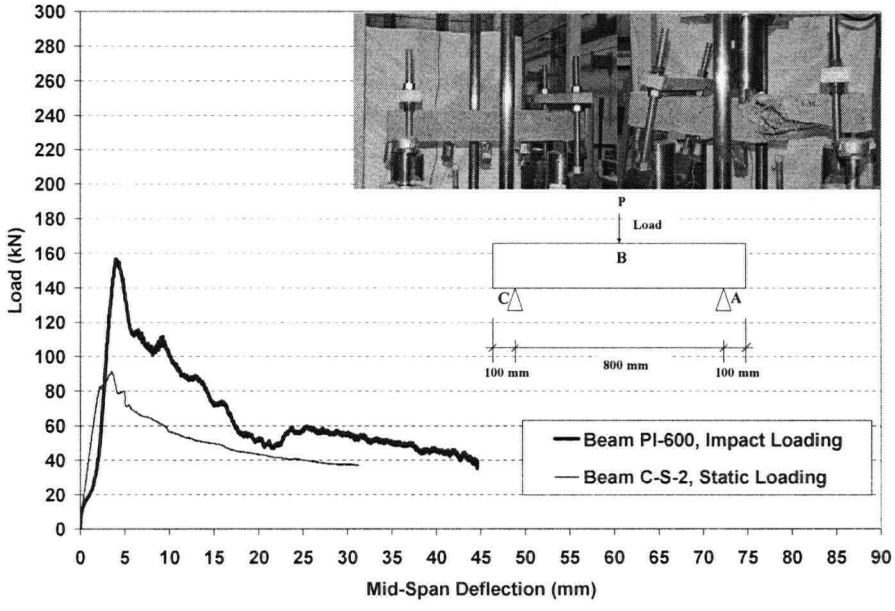

Figure 9.2 – *Load vs. Mid-Span Deflection of Control (Plain) RC Beam PI-600*

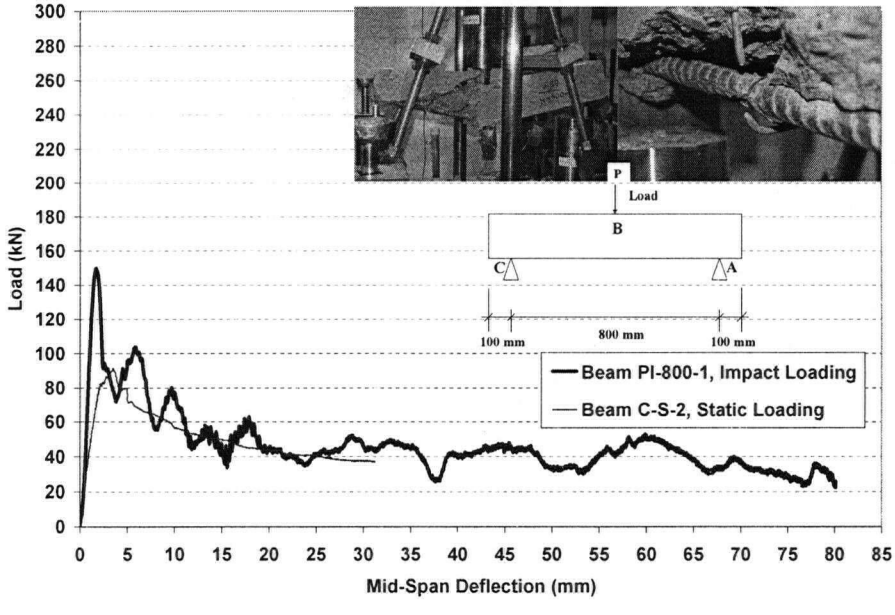

Figure 9.3 – *Load vs. Mid-Span Deflection of Control (Plain) RC Beam PI-800-1*

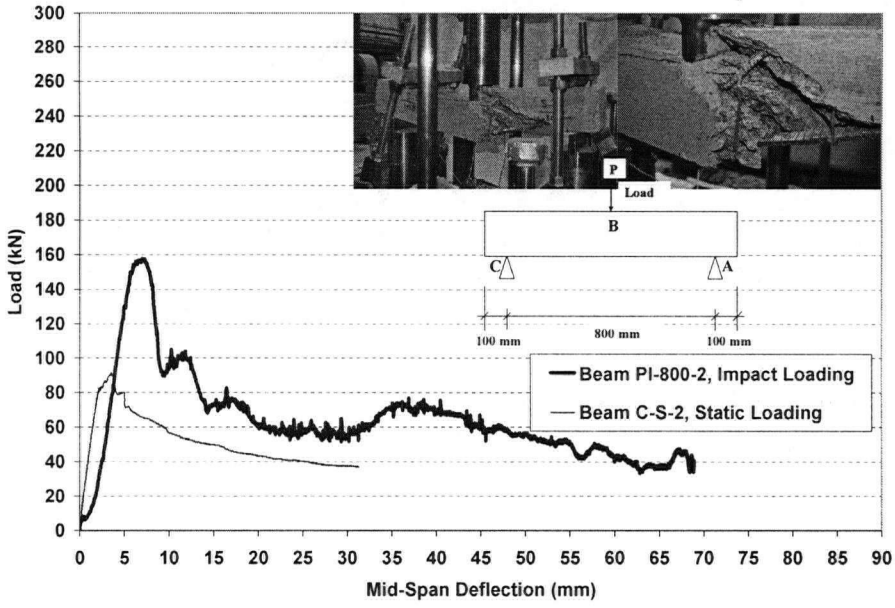

Figure 9.4 – *Load vs. Mid-Span Deflection of Control (Plain) RC Beam PI-800-2*

Figures 9.2 to 9.4 show that the load carrying capacity of the RC beam did not change when the drop height (i.e. impact velocity) was increased from 600 mm to 800 mm. This is in agreement with findings reported in Chapter 7, flexural type failure of RC beams under impact loading. In other words, when stress (or strain) rate of loading increases, load carrying capacity of shear failure type of RC beams also increases, but only to a certain point at which load carrying capacity will not be increased by increasing the impact velocity.

9.2.2 Sprayed GFRP on Two Sides

Seven beams in total were strengthened by Sprayed GFRP on their sides. Two different techniques, through bolts and roughening concrete surface using pneumatic chisel, were used to increase the FRP-concrete bond and the effectiveness of Sprayed GFRP in shear strengthening of RC beams. In the following sections the results of these 7 beams will be discussed and compared.

As mentioned in Chapter 8, all Sprayed GFRP plates were cut at the mid-span of the beam (both cases: Sprayed GFRP on 2 lateral sides and on 3 sides) to make sure that the GFRP contribution only in shear strengthening would be measured.

9.2.2.1 No Mechanical Fasteners

Four beams (beam SI-2S-800-1, SI-2S-800-2, SI-2S-800-3, and SI-2S-800-4) were tested with 150 mm width Sprayed GFRP applied to their lateral sides and no mechanical fasteners were used. The concrete surface was roughened using a small air pneumatic concrete chisel. This technique provided a rougher surface than the sandblasting technique. Then, the concrete surface was washed using a high pressure washer and dried before Sprayed GFRP application. This technique was explained in Chapter 8. All these beams were tested under an 800 mm dropping hammer height.

Test results of these beams are shown in Figures 9.5 to 9.8 while the test result of beam PI-800-1, as reference, is also included in each Figure.

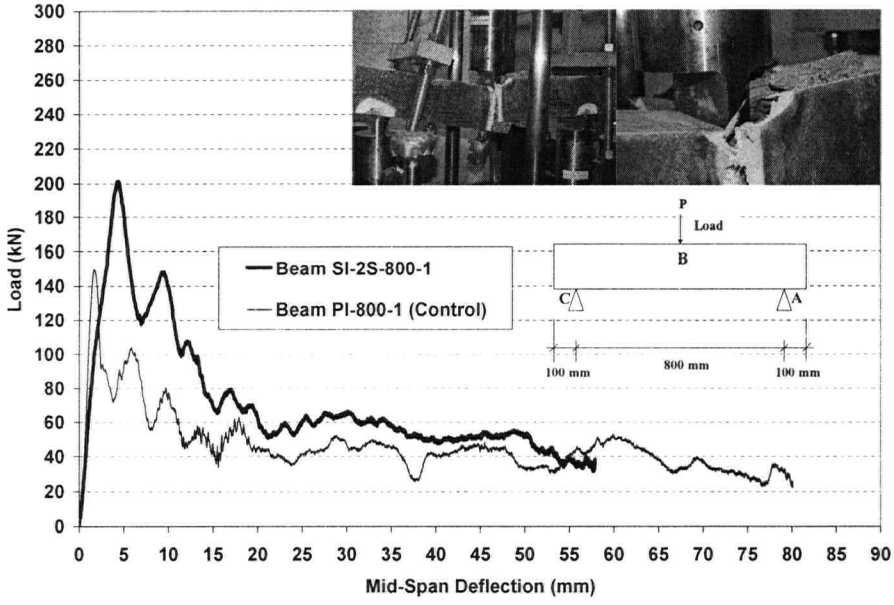

Figure 9.5 – *Load vs. Mid-Span Deflection of RC Beam SI-2S-800-1*

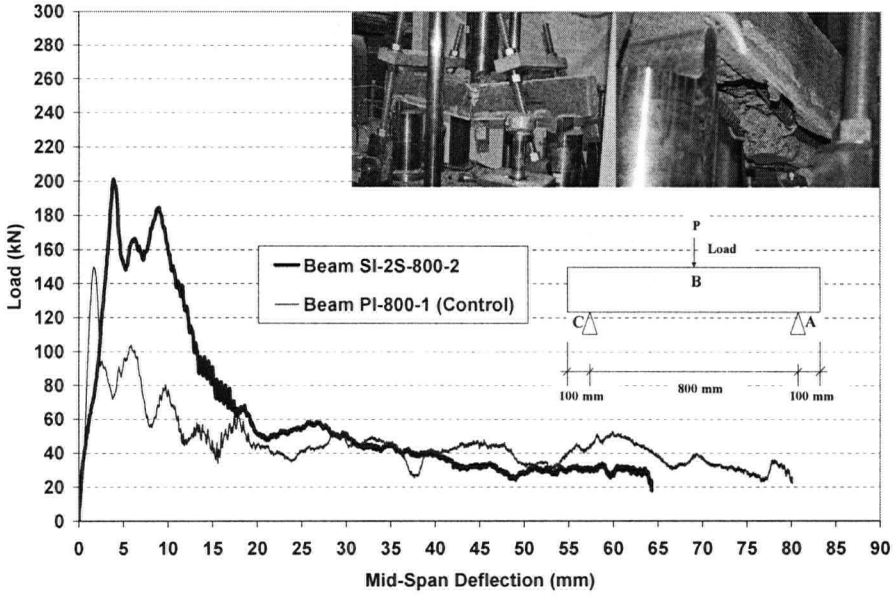

Figure 9.6 – *Load vs. Mid-Span Deflection of RC Beam SI-2S-800-2*

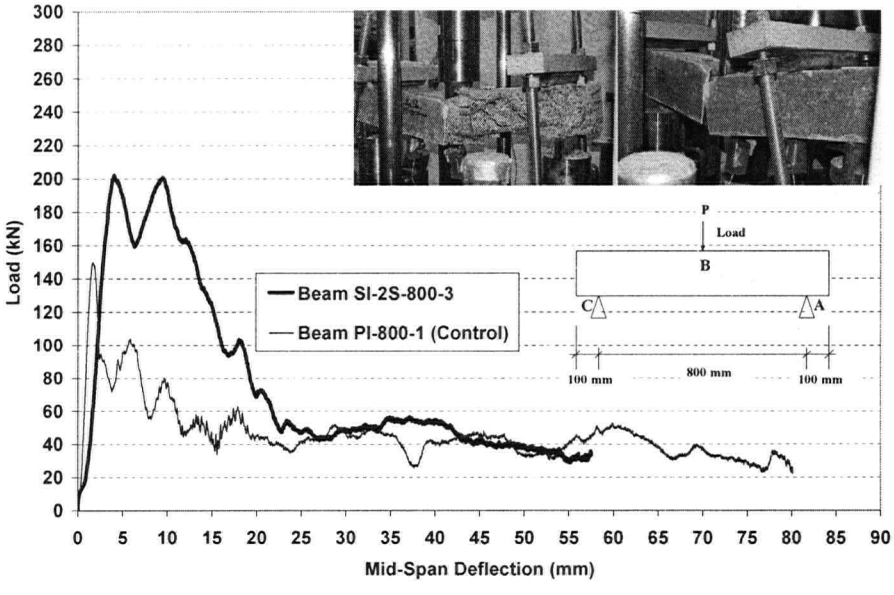

Figure 9.7 – *Load vs. Mid-Span Deflection of RC Beam SI-2S-800-3*

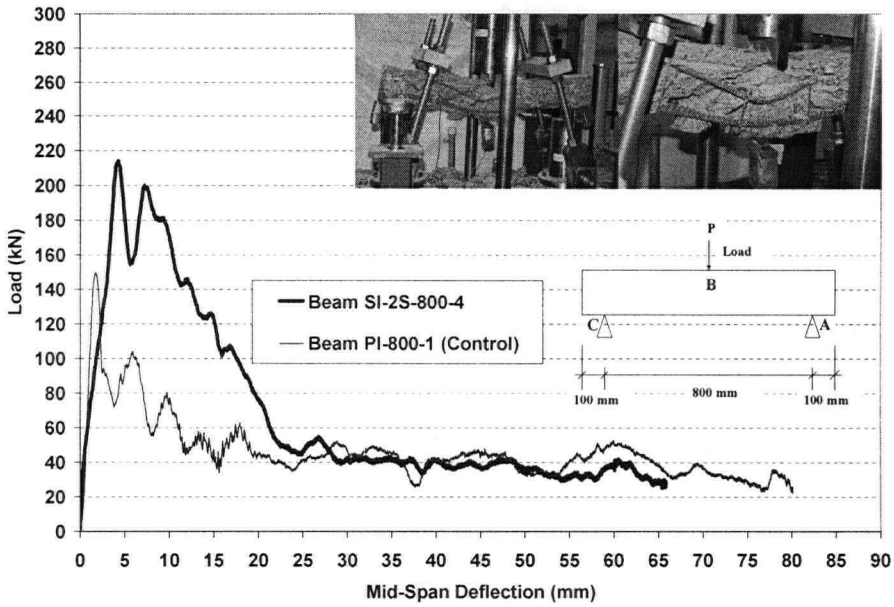

Figure 9.8 – *Load vs. Mid-Span Deflection of RC Beam SI-2S-800-4*

Increasing the Sprayed GFRP thickness did not increase the load carrying capacity of RC beams. While thinner Sprayed GFRP laminates were still attached to the lateral sides of RC beams, thicker ones were totally detached from the surface after impact. It is worth mentioning that roughening concrete surface using a pneumatic chisel was quite effective in increasing the bond between FRP and concrete. This can easily be seen in Figures 9.7 and 9.8.

9.2.2.2 Using 4 Through-Bolts as Mechanical Fasteners

Three beams were tested using 4 through bolts with Φ4.75 internal stirrups at 160 mm and 150 mm width externally-bonded Sprayed FRP on their lateral sides. Cross-sectional details and bolts' location are shown in Figure 9.9.

Load vs. mid-span deflection curves of beams SI-4B-800-1, SI-4B-800-2 and SI-4B-800-3 along with their control specimen's test result (beam PI-800-1) are reported in Figures 9.10 to 9.12.

From Figures 9.10 to 9.12, one can conclude that the presence of through bolts as mechanical fasteners will hold the Sprayed GFRP during the impact and as a result, GFRP rupture was observed in all cases. This phenomenon was not detected in impact tests on RC beams strengthened by GFRP with no mechanical fasteners (Section 9.2.2.1).

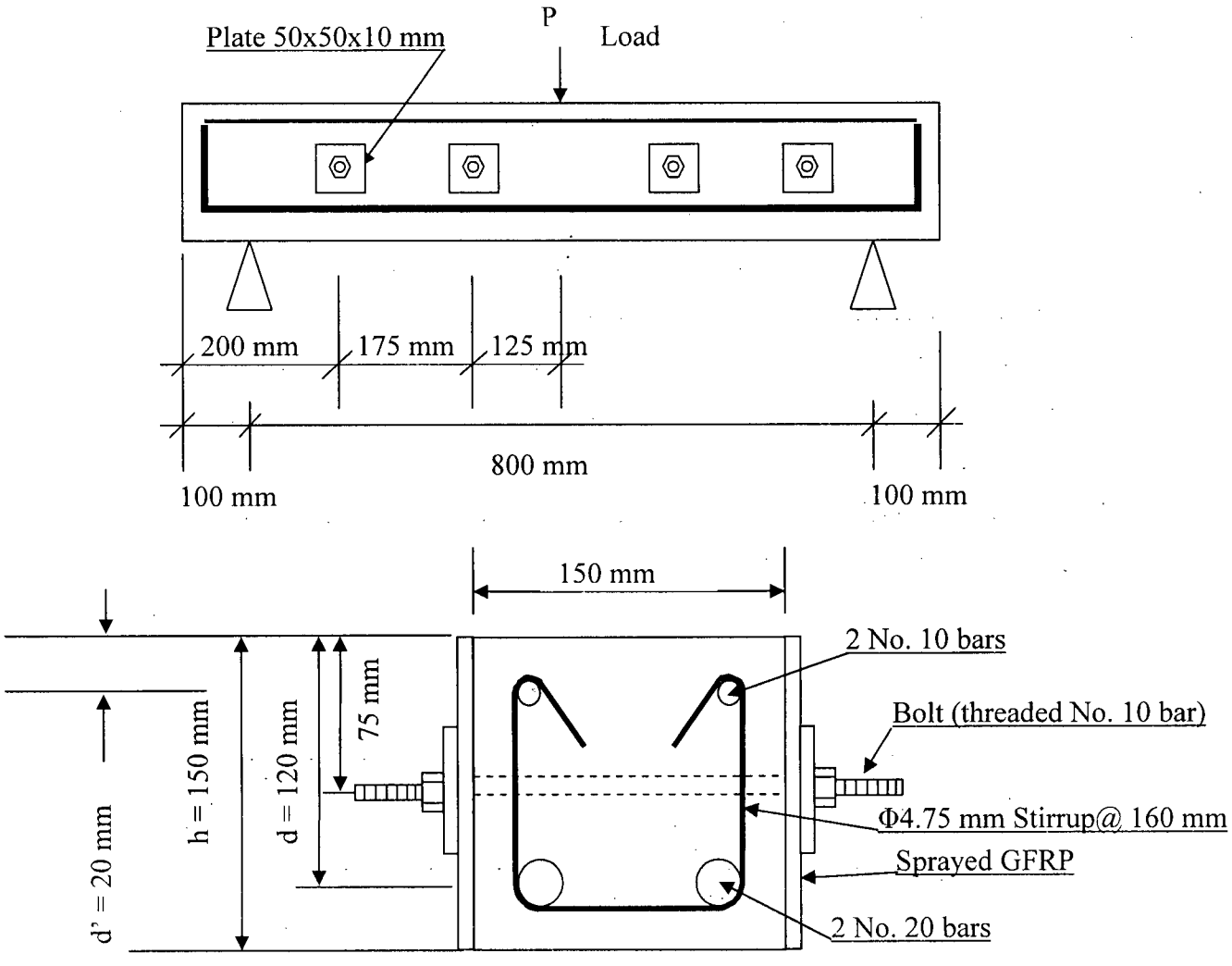

Figure 9.9 – *Cross-Sectional Details of RC Beams: SI-4B-800-1 to SI-4B-800-3*

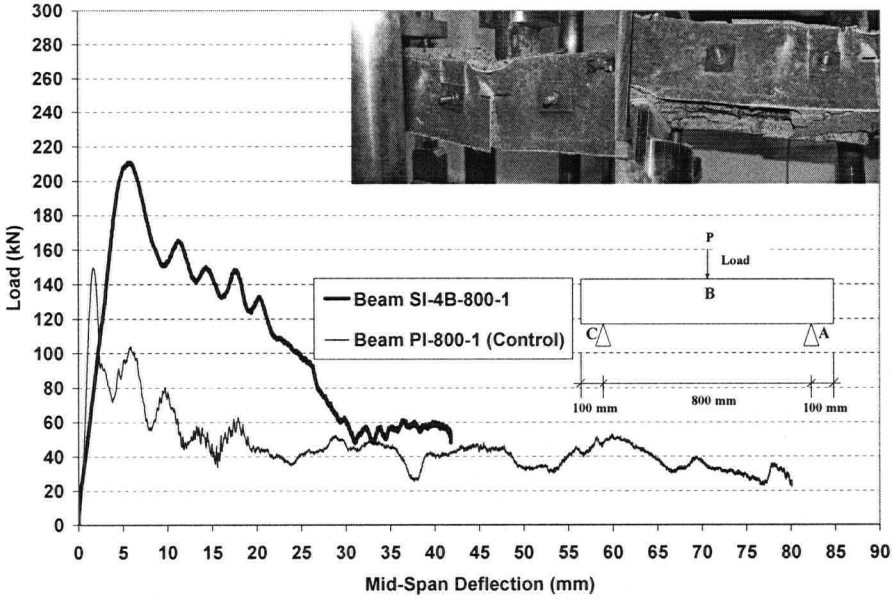

Figure 9.10 – *Load vs. Mid-Span Deflection of RC Beam SI-4B-800-1*

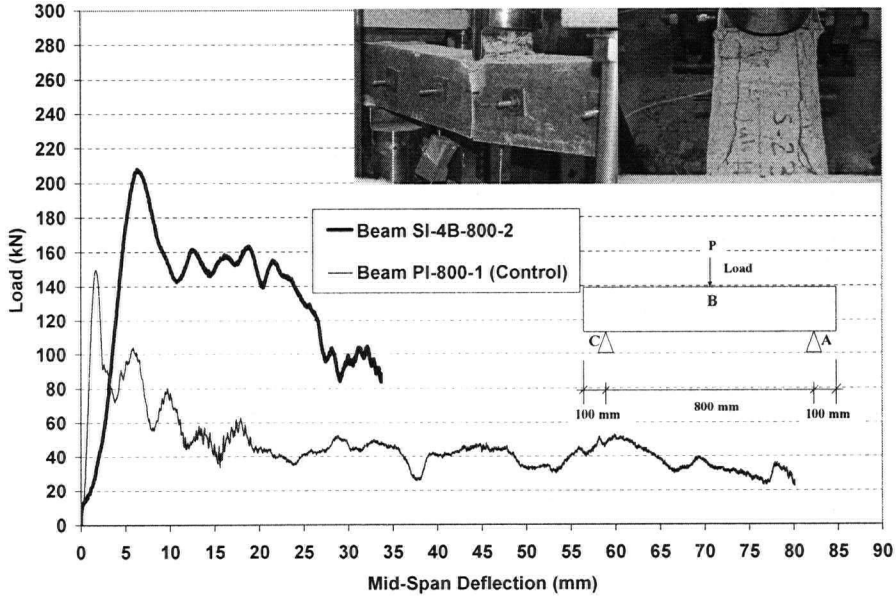

Figure 9.11 – *Load vs. Mid-Span Deflection of RC Beam SI-4B-800-2*

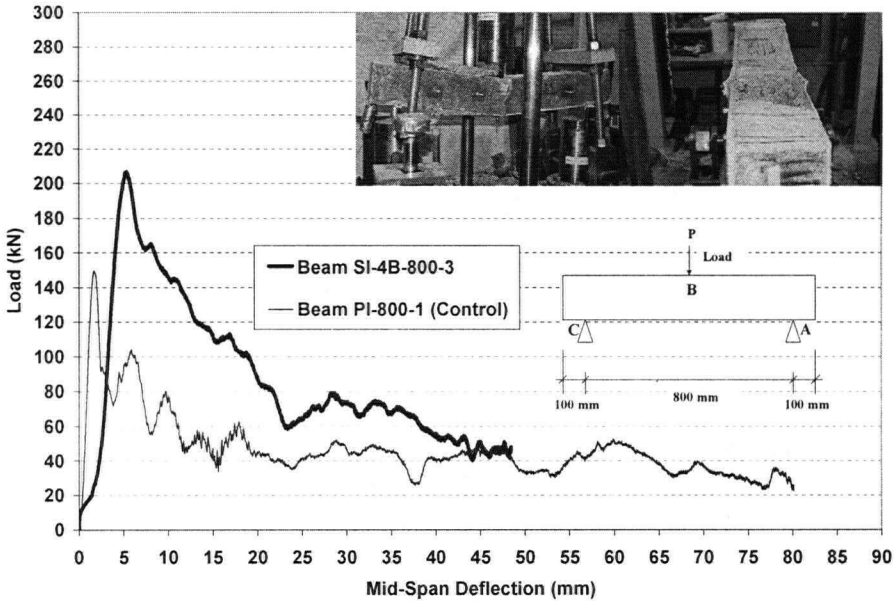

Figure 9.12 – *Load vs. Mid-Span Deflection of RC Beam SI-4B-800-3*

Although the presence of through bolts could hold the Sprayed GFRP in place during the impact, surprisingly, the load carrying capacity did not increase either by increasing the GFRP thickness or by the presence of through bolts as mechanical fasteners. Compared with RC beams strengthened by Sprayed GFRP on their lateral sides with no mechanical fasteners, the presence of through bolts had limited influence on the test results of strengthened RC beams with the same thickness.

9.2.3 Sprayed GFRP on Three Sides

Five beams, all with Φ4.75 stirrups at 160 mm, were strengthened using Sprayed GFRP on their 3 sides (i.e. complete U-shaped). As mentioned earlier, since shear strengthening was the primary focus of this research, GFRP was cut at the mid-span of the beam underneath the neutral axis of the beam's cross-section to minimize its contribution in flexural strengthening. In this way, contribution of the GFRP to the shear strength of RC beam, if any, would be explored. Load vs. mid-span deflection curves are shown in Figures 9.13 to 9.17 for beams SI-3S-800-1, SI-3S-800-2, SI-3S-800-3, SI-3S-800-4, SI-3S-600, , respectively. To show the benefits of this technique, the test result of the control beam is also included in each Figure.

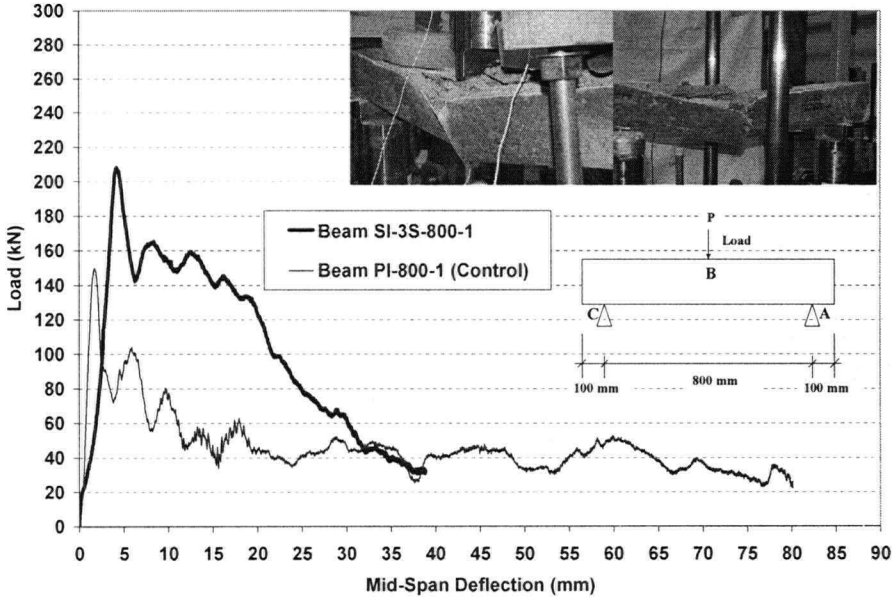

Figure 9.13 – *Load vs. Mid-Span Deflection of RC Beam SI-3S-800-1*

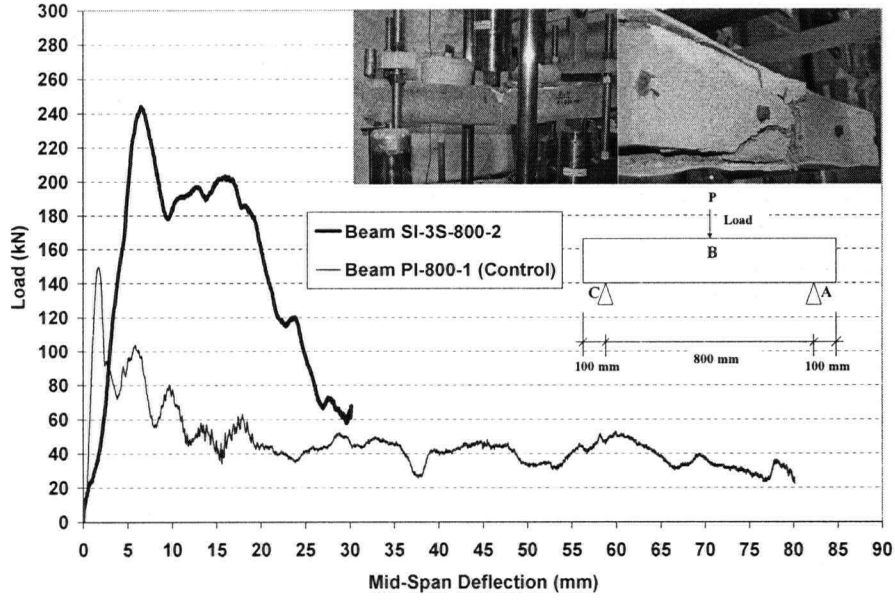

Figure 9.14 – *Load vs. Mid-Span Deflection of RC Beam SI-3S-800-2*

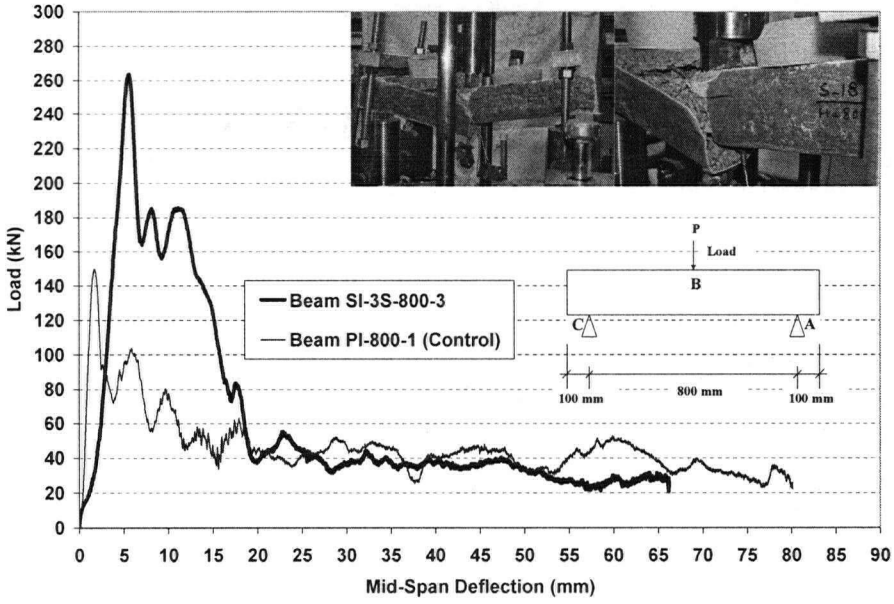

Figure 9.15 – *Load vs. Mid-Span Deflection of RC Beam SI-3S-800-3*

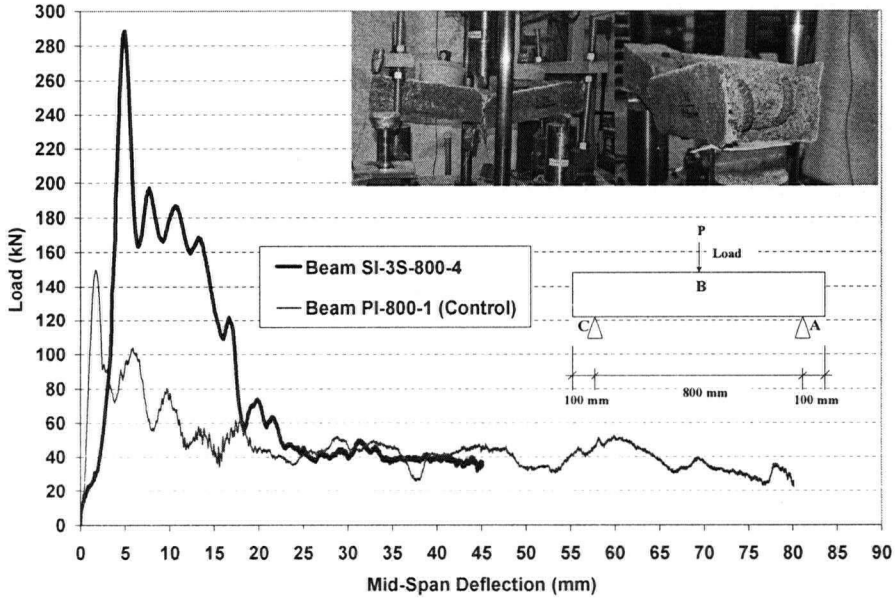

Figure 9.16 – *Load vs. Mid-Span Deflection of RC Beam SI-3S-800-4*

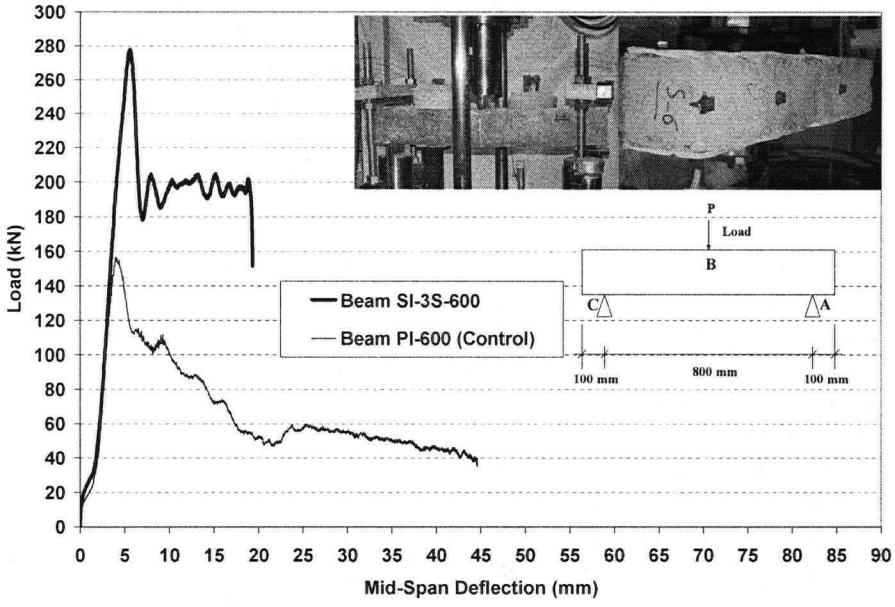

Figure 9.17 – *Load vs. Mid-Span Deflection of RC Beam SI-3S-600*

Compared to other techniques (i.e. Sprayed GFRP on 2 lateral sides with and without mechanical fasteners), Sprayed GFRP on 3 sides was quite sensitive to GFRP thickness (note the increase in load carrying capacity of strengthened RC beams from Figure 9.13 to Figure 9.16).

Figure 9.17 shows that while a plain RC beam (i.e. beam PI-600) failed fully and lost its load carrying capacity under a 600 mm drop height, strengthened RC beam under the same drop height not only showed a higher load carrying capacity, but also kept a high load carrying capacity at the end of impact, even higher than the load carrying capacity of a plain RC beam. To verify this statement, this damaged strengthened RC beam was tested again under an 800 mm drop height impact load and the test result is shown in Figure 9.18. It is clearly seen that the load carrying capacity of this damaged strengthened RC beam was greater than that of a sound, undamaged plain RC beam; even under a higher impact load (i.e. load carrying capacity of plain RC beam under a 600 mm drop height was less than that of a damaged strengthened RC beam under an 800 mm drop height impact load). Note that there was no repair done on the damaged RC beam (i.e. beam SI-3S-600) prior to the second test.

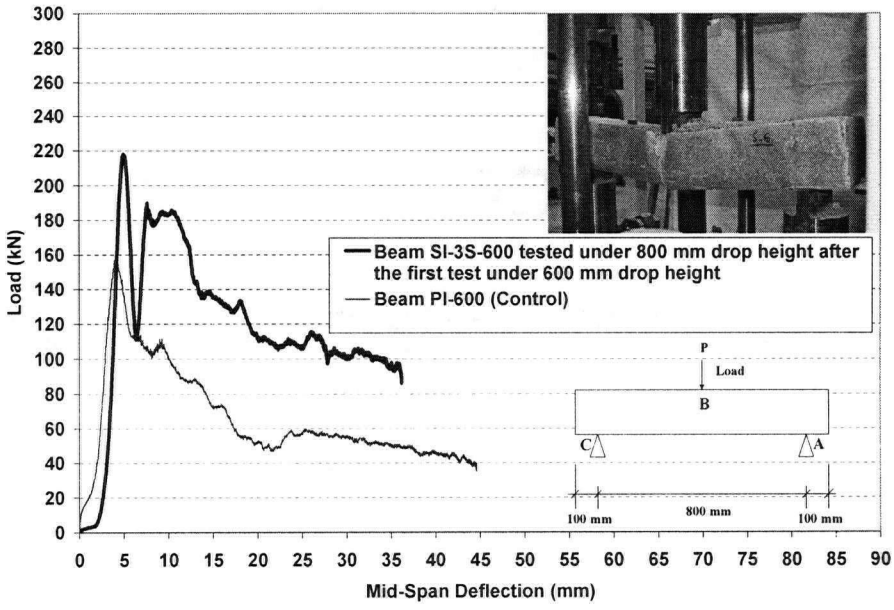

Figure 9.18 – *Load vs. Mid-Span Deflection of Damaged RC Beam SI-3S-600 under an 800 mm Drop Height (i.e. Beam was Tested under a 600 mm Drop Height before)*

9.3 Discussion

Load carrying capacity of RC beams strengthened by Sprayed GFRP was increased in both quasi-static and impact loading. Load capacity as well as the energy absorption capability of various systems were compared in Chapter 8. In this Chapter, their behavior under impact loading will be discussed and compared with quasi-static loading condition.

9.3.1 Peak Load

As discussed in Chapter 7, the peak load under impact loading can be obtained by summing the output of the support load cells. All of the impact loads reported in this Chapter were derived from the support load cells. The load recorded by the tup load cell cannot be used to obtain the load carrying capacity of an RC beam under impact because of inertia effect, as discussed previously. Therefore, in this Chapter recorded tup loads are not reported.

Load carrying capacity (i.e. maximum recorded true bending load or summation of support load cells) of all RC beams with and without retrofit and area under the load vs. mid-span deflection curve (i.e. energy absorbed by each beam) are tabulated in Table 9.2. These data are also plotted in Figure 9.19.

Table 9.2 – *Peak Loads and Energy Absorbed by RC Beams under Impact Loading*

Beam Designation	Drop Height (mm)	Peak Load (kN)	Area under Load vs. Mid-Span Deflection (N.m)
PI-600	600	156.7	2937
PI-800-1	800	149.7	3728
PI-800-2	800	157.6	4422
SI-2S-800-1	800	201.2	4142
SI-2S-800-2	800	201.3	4021
SI-2S-800-3	800	202.2	4460
SI-2S-800-4	800	213.9	4547
SI-4B-800-1	800	211.0	4430
SI-4B-800-2	800	208.0	4411
SI-4B-800-3	800	206.9	4208
SI-3S-800-1	800	208.2	3976
SI-3S-800-2	800	244.2	4381
SI-3S-800-3	800	263.6	4176
SI-3S-800-4	800	288.5	3783
SI-3S-600	600	277.9	3412

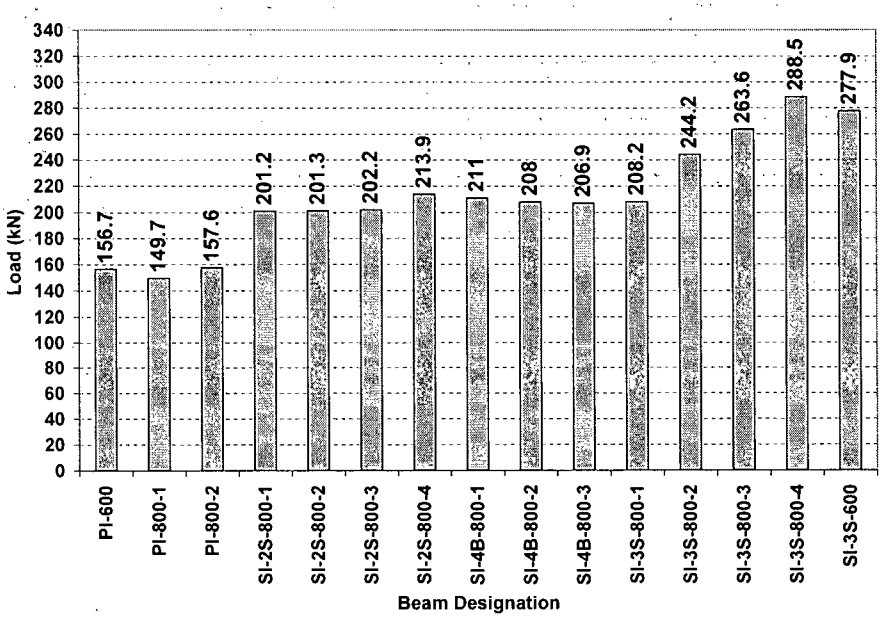

Figure 9.19 – *Load Carrying Capacity of Different Plain and Strengthened RC Beams*

9.3.2 Energy Evaluation

The energy expended in deflecting and fracturing the beam is calculated from the area under the bending load vs. deflection curve and compared with energy stored in (or released by) the dropping hammer. The results are shown in Figure 9.20. Energy stored in the drop hammer is calculated based on Equation 7.13 (Chapter 7).

In this study, the ratio of absorbed energy to input energy (energy absorbed by the beam to incident energy in the hammer) was in the range of 80% to 98% with a mean value of 91%. Therefore, one can conclude that about 91% of the input energy was absorbed by the RC beam.

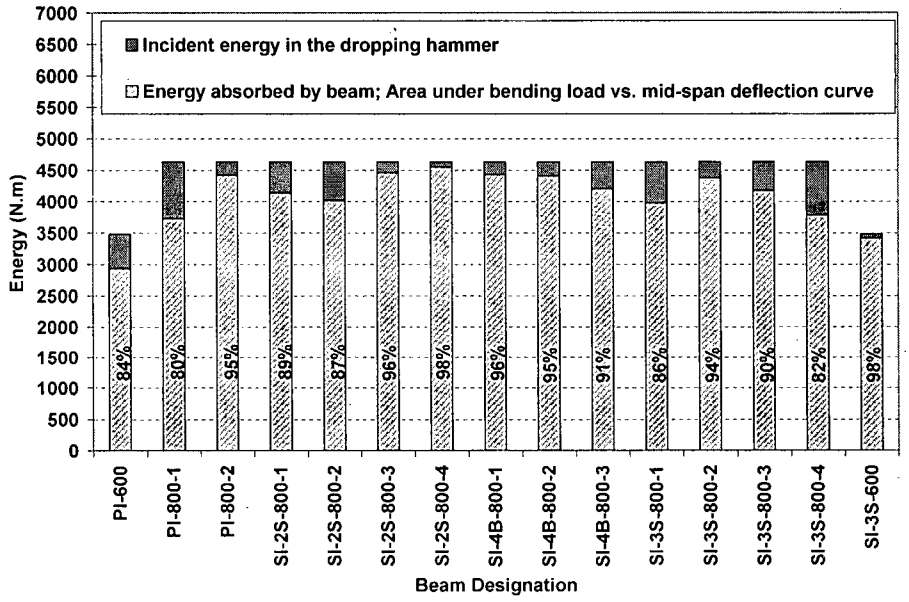

Figure 9.20 – *Energy Balance for Different Plain and Strengthened RC Beams*

9.3.3 Static vs. Impact

Average load carrying capacities of RC beams (plain and strengthened) in both static and impact loading are compared in Figure 9.21. To have a meaningful comparison, beams with the same shear and longitudinal reinforcement, Sprayed GFRP configuration and thickness are compared. Note that the average load carrying capacity of beams PI-600, PI-800-1 and PI-800-2, 154.7 kN, is used as the load carrying capacity of the control specimen (i.e. plain RC beam) under impact loading. The following beams were chosen for comparison:

1. Plain RC beams: C-S-1 with average capacity of PI-600, PI-800-1 and PI-800-2,
2. Sprayed GFRP on two sides with no mechanical fasteners: Beam B2-S-1 and Beam SI-2S-800-1 with an FRP thickness of about 3.5 mm for both,
3. Sprayed GFRP on two sides with 4 through bolts as mechanical fasteners: Beam B2-4B-S-2 and Beam SI-4B-800-2 with an FRP thickness of about 4 mm for both,
4. Sprayed GFRP on three sides: Beam B3-S-1 and Beam SI-3S-800-3 with an FRP thickness of about 3.2 mm for both,

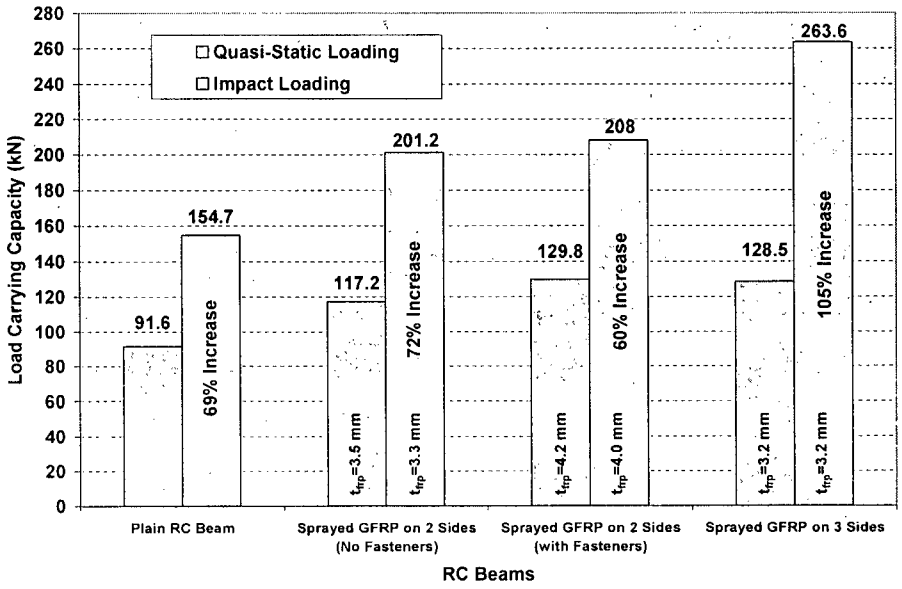

Figure 9.21 – *Load Carrying Capacity, Static vs. Impact*

As expected, the highest increase in load carrying capacity is achieved by Sprayed GFRP on 3 sides. This figure shows that Sprayed GFRP is definitely a promising technique in enhancing impact resistance of RC beams. It also proves that the composite material should be applied on 3 sides of the beam, wherever possible to gain the maximum benefits out of this material. Note that the thickness of composite material for the RC beams strengthened on their three sides, although quite similar to other beams, was the smallest among all the strengthened RC beams shown in Figure 9.21.

9.3.4 Contribution of Sprayed GFRP in Dynamic Shear Strength of RC Beams

Strengthened beams can be divided into three groups:

1. Sprayed GFRP on two sides with no mechanical fasteners,
2. Sprayed GFRP on two sides with mechanical fasteners,
3. Sprayed GFRP on 3 sides (U-shaped).

The dynamic shear contribution of Sprayed GFRP of all three groups is tabulated in Table 9.3 for strengthened RC beams tested under impact loading. The beams tested under the same drop height of 800 mm are compared in this Table.

Table 9.3 – *Dynamic Contribution of Sprayed GFRP in Shear Strength of RC Beams*

Sprayed GFRP Configuration	Beam	Peak Load [kN]	Peak Load of Control Beam [kN]	Dynamic Contribution of Sprayed GFRP in Shear Strength [kN] ((2)-(3))	d_{frp}, FRP Width [mm]	t_{frp}, FRP Thickness [mm]
	(1)	(2)	(3)	(4)	(5)	(6)
Sprayed FRP on two sides with no mechanical fasteners	SI-2S-800-1	201.2	154.7	46.5	120	3.3
	SI-2S-800-2	201.3	154.7	46.6	120	4.6
	SI-2S-800-3	202.2	154.7	47.5	120	6.5
	SI-2S-800-4	213.9	154.7	59.2	120	10.3
Sprayed FRP on two sides with mechanical fasteners	SI-4B-800-1	211	154.7	56.3	120	2.4
	SI-4B-800-2	208	154.7	53.3	120	4
	SI-4B-800-3	206.9	154.7	52.2	120	6.5
Sprayed FRP on three sides	SI-3S-800-1	208.2	154.7	53.5	120	1.9
	SI-3S-800-2	244.2	154.7	89.5	120	2.8
	SI-3S-800-3	263.6	154.7	108.9	120	3.2
	SI-3S-800-4	288.5	154.7	133.8	120	6.2

Contribution of Sprayed GFRP in shear strength of RC beams vs. the thickness of FRP under impact loading for different configurations of FRP is shown in Figure 9.22.

It is seen that while increasing the thickness of Sprayed GFRP when applied on 3 sides increased the contribution of Sprayed GFRP in shear strength of RC beams under impact loading, it was not effective in RC beams with Sprayed GFRP on 2 sides, with or without mechanical fasteners. These findings are in disagreement with the results reported in Chapter 8 where it was shown that the shear contribution of Sprayed GFRP increased by increasing its thickness under quasi-static loading.

In all tests performed in this study, the Sprayed GFRP fracture did not occur at the location of the shear cracks. This, in turn, showed that after a certain strain in Sprayed GFRP, which was clearly less than its strain at rupture, there would be no contribution of this composite to dynamic shear strength of RC beams.

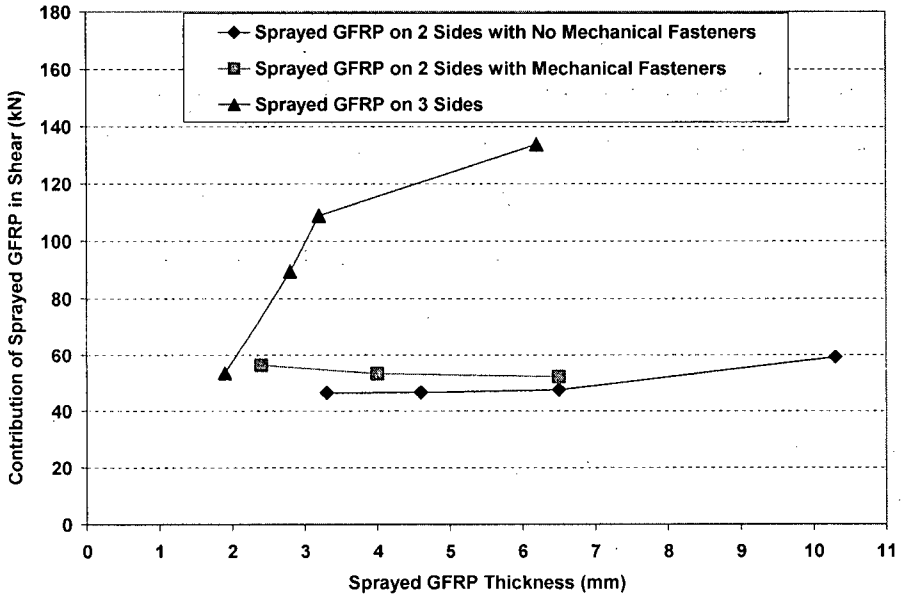

Figure 9.22 – *Contribution of Sprayed GFRP in Shear Strength of RC Beams vs. Its Thickness under Impact Loading*

As discussed in Chapter 8, if we consider a single shear crack in an RC beam with a 45° angle with respect to the horizon (as seen in plain RC beams tested in this project), the horizontal projection of the crack can be taken as d_{frp} (for d_{frp} see Figure 8.44 in Chapter 8).

Therefore, for Sprayed GFRP applied continuously on both sides of an RC beam with a thickness of t_{frp} on each side and a dynamic modulus of elasticity of E_{frp_d}, the product of $2 \times t_{frp} \times d_{frp} \times E_{frp\_d} \times \varepsilon_{frp}$ will give the shear resisted by the Sprayed GFRP under impact loading.

Dynamic contribution of Sprayed GFRP to shear strength for RC beams with FRP on 3 sides vs. $2 \times t_{frp} \times d_{frp}$ product, using Table 9.3, is shown in Figure 9.23.

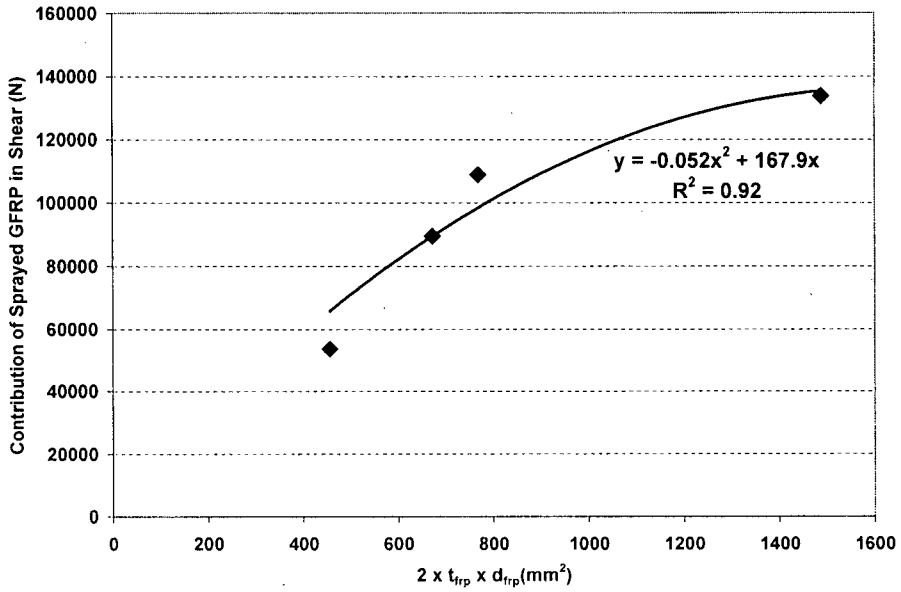

Figure 9.23 – *Contribution of Sprayed GFRP in Shear vs.* $2 \times t_{frp} \times d_{frp}$ *for RC Beams with Sprayed GFRP on 3 Sides*

Figure 9.23 shows that the contribution of Sprayed GFRP in dynamic shear strength of RC beams may stay at a constant level beyond a certain thickness of Sprayed GFRP. This, in turn, may also explain why the dynamic shear contribution did not increase by increasing the Sprayed GFRP thickness in 2-sided beams; all the thickness tested here may have been greater than the threshold thickness for 2-sided beams. In other words, in RC beams with Sprayed GFRP on their 3 sides, this threshold thickness seems to be much greater than that for the 2-sided beams.

In general, the dynamic contribution of Sprayed GFRP to the shear strength of RC beams, based on the above discussion, can be expressed by the following equation:

$$V_{frp\_d} = 2t_{frp} d_{frp} E_{frp\_d} \varepsilon_{frp} \tag{9.1}$$

where,

V_{frp_d} = dynamic contribution of Sprayed GFRP in shear strength of RC beam [N]

t_{frp} = average thickness of the Sprayed GFRP [mm]

d_{frp} = depth of FRP shear reinforcement as shown in Figure 8.44 (Chapter 8) [mm]

E_{frp_d} = dynamic modulus of elasticity of Sprayed GFRP composite [MPa]

ε_{frp} = strain of Sprayed GFRP; a maximum strain of GFRP at which the integrity of concrete and secure activation of the aggregate interlock mechanism are maintained.

Equation (9.1) can be used to calculate the values of $E_{frp\_d} \times \varepsilon_{frp}$ for beams SI-3S-800-1 to SI-3S-800-4. These values are reported in Table 9.4.

Table 9.4 – $E_{frp\_d} \times \varepsilon_{frp}$ *for RC Beams with Sprayed GFRP on their 3 Sides*

Beam Designation	Contribution of Sprayed GFRP in Shear (N)	$2 \times t_{frp} \times d_{frp}$ (mm^2)	$E_{frp\_d} \times \varepsilon_{frp}$ (MPa.mm/mm)
(1)	(2)	(3)	(4)=(2)/(3)
SI-3S-800-1	53500	456	117.3
SI-3S-800-2	89500	672	133.2
SI-3S-800-3	108900	768	141.8
SI-3S-800-4	133800	1488	89.9

If the dynamic modulus of elasticity of Sprayed GFRP considered to be the same as its static modulus of elasticity (14000 MPa), ε_{frp} can be calculated. These calculated values are reported in Table 9.5.

Table 9.5 – ε_{frp} *for RC Beams with Sprayed GFRP on their 3 Sides (Static Modulus of Elasticity Is Considered)*

Beam Designation	$E_{frp\_d} \times \varepsilon_{frp}$ (MPa.mm/mm)	Assumed Modulus of Elasticity (MPa)	ε_{frp} (mm/mm)
(1)	(2)	(3)	(4)=(2)/(3)
SI-3S-800-1	117.3	14000	0.0084
SI-3S-800-2	133.2	14000	0.0095
SI-3S-800-3	141.8	14000	0.0101
SI-3S-800-4	89.9	14000	0.0064

It is seen that the values obtained for ε_{frp} are even higher than the strain at rupture for Sprayed GFRP under static loading. Since rupture of Sprayed GFRP, under impact loading, was not observed at the vicinity of the shear cracks, one can conclude that the dynamic modulus of elasticity of Sprayed GFRP must be higher than its static value.

It can also be assumed that ε_{frp}, the maximum strain of GFRP at which the integrity of concrete and secure activation of the aggregate interlock mechanism are maintained, remains unchanged in both static and impact loading. This assumption is closer to the reality than previous one (i.e. unchanged modulus of elasticity of Sprayed GFRP). Based on this assumption, E_{frp_d}, dynamic modulus of elasticity of Sprayed GFRP composite, and DIF_{frp}, Dynamic Increase Factor for modulus of elasticity of Sprayed GFRP are calculated and results are reported in Table 9.6. DIF_{frp} is calculated as follows:

$$DIF_{frp} = \frac{E_{frp\_d}}{E_{frp}} \tag{9.2}$$

where,

DIF_{frp} = Dynamic Increase Factor for modulus of elasticity of Sprayed GFRP

E_{frp_d} = dynamic modulus of elasticity of Sprayed GFRP composite [MPa]

E_{frp} = modulus of elasticity of Sprayed GFRP composite (static loading) [MPa]

Table 9.6 – *DIF_{frp} (dynamic modulus of elasticity to static modulus of elasticity of Sprayed GFRP) for RC Beams with Sprayed GFRP on their 3 Sides*

Beam	$E_{frp\_d} \times \varepsilon_{frp}$ (MPa.mm/mm)	Assumed ε_{frp} (mm/mm)	E_{frp_d} (MPa)	E_{frp} (MPa)	DIF_{frp}
(1)	(2)	(3)	(4)=(2)/(3)	(5)	(6)=(4)/(5)
SI-3S-800-1	117.3	0.003	39100	14000	2.79
SI-3S-800-2	133.2	0.003	44400	14000	3.17
SI-3S-800-3	141.8	0.003	47267	14000	3.38
SI-3S-800-4	89.9	0.003	29967	14000	2.14

As mentioned in Chapter 7, an average stress rate of 0.017 MPa/sec (1.035 MPa/min) was applied to RC beams under quasi-static loading. Equation 7.1 (Chapter 7) was used to calculate the stress rate of RC beams retrofitted by Sprayed GFRP on their 3 sides under impact loading. As a result, the ratio of dynamic stress rate to static stress rate for these beams is tabulated in Table 9.7. Figure 9.24 shows the relationship between this ratio and DIF_{frp}. Based on this relationship the following equation is proposed to calculate the DIF_{frp}:

$$DIF_{frp} = -4\times10^{-16}\left(\frac{\dot{\sigma}_{dynamic}}{\dot{\sigma}_{static}}\right)^2 + 7\times10^{-8}\left(\frac{\dot{\sigma}_{dynamic}}{\dot{\sigma}_{static}}\right) + 1.0 \qquad (9.3)$$

where,

DIF_{frp} = Dynamic Increase Factor for modulus of elasticity of Sprayed GFRP

$\dot{\sigma}_{dynamic}$ = stress rate under dynamic loading [MPa/sec]

$\dot{\sigma}_{static}$ = stress rate under quasi-static loading [MPa/sec]

Combining Equations 9.1 to 9.3, the following equation is proposed to calculate the dynamic contribution of Sprayed GFRP in shear strength of RC beam:

$$V_{frp\_d} = 2t_{frp}d_{frp}DIF_{frp}E_{frp}\varepsilon_{frp} \qquad (9.4)$$

where,

V_{frp_d} = dynamic contribution of Sprayed GFRP in shear strength of RC beam [N]

t_{frp} = average thickness of the Sprayed GFRP [mm]

d_{frp} = depth of FRP shear reinforcement as shown in Figure 8.44 (Chapter 8) [mm]

DIF_{frp} = Dynamic Increase Factor for modulus of elasticity of Sprayed GFRP (Equation 9.3)

E_{frp} = modulus of elasticity of Sprayed GFRP composite [MPa]

ε_{frp} = 0.003 (effective strain of Sprayed GFRP for continuous U-shaped around the bottom of the web)

It should be noted that V_{frp_d} in Equation 9.4 was derived assuming that under impact loading, the effective strain of Sprayed GFRP, ε_{frp} was the same as that one under static loading. Since this strain is the maximum strain of Sprayed GFRP at which the integrity of concrete and secure activation of the aggregate interlock mechanism are maintained, the above assumption seems to be a reasonable one.

Table 9.7 – *The Ratio of Dynamic Stress Rate to Static Stress Rate for RC Beams with Sprayed GFRP on their 3 Sides*

Beam	Peak Load [kN]	Peak Stress [MPa]	Time to Peak Load [sec]	Stress Rate [MPa/sec]	Static Stress Rate [MPa/sec]	(Dynamic-Stress-Rate)/ (Static-Stress-Rate)	DIF_{frp}
SI-3S-800-1	208.2	740.3	0.0016	462667	0.017	27215686	2.79
SI-3S-800-2	244.2	868.3	0.00153	567495	0.017	33382033	3.17
SI-3S-800-3	263.6	937.2	0.00121	774582	0.017	45563658	3.38
SI-3S-800-4	288.5	1025.8	0.00267	384186	0.017	22599202	2.14

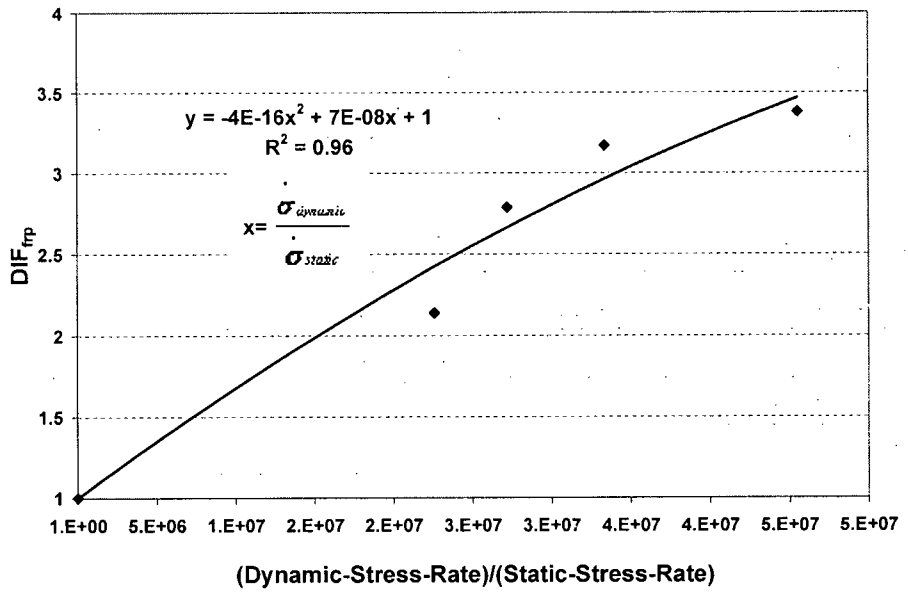

Figure 9.24 – *Dynamic Increase Factor for Modulus of Elasticity of FRP (DIF_{frp}) vs. the Ratio of Dynamic Stress Rate to Static Stress Rate* $(\frac{\dot{\sigma}_{dynamic}}{\dot{\sigma}_{static}})$

It is worth mentioning that DIF_{frp}, which was considered to be an increase factor for modulus of elasticity of FRP under dynamic loading can also be assumed an increase factor for effective stress of FRP (i.e. $E_{frp}\varepsilon_{frp}$) under dynamic loading and, as discussed, it is a function of dynamic-stress-rate to static-stress-rate ratio. Further investigations are required to determine the actual value of DIF_{frp} for different types of Sprayed GFRP.

9.4 Conclusions

Based on the results and discussions reported here, the following conclusions can be drawn:

1. Sprayed GFRP was an effective material to increase shear capacity of RC beams under impact loading.

2. Shear load capacity of plain RC beam without retrofit under impact loading was about 1.7 times of its static capacity for the conditions and details of tests performed here.

3. When RC beams were strengthened by Sprayed GFRP on their lateral sides (2-sided retrofit), increase in FRP thickness did not increase the load carrying capacity under impact loading and this was true for both cases: with and without mechanical fasteners. Shear load capacity of above mentioned strengthened RC beams under impact loading were about 1.7 times and 1.6 times of their static capacity for beams without and with mechanical fasteners, respectively, for the conditions and details of tests performed here.

4. When RC beams were strengthened by Sprayed GFRP on their three sides (U-shaped), increase in FRP thickness increased the load carrying capacity under impact loading. Shear load capacity of above mentioned strengthened

RC beam under impact loading was about 2.1 times its static capacity for the conditions and details of tests performed here.

5. Sprayed GFRP under impact loading possessed a higher modulus of elasticity or at least a higher effective stress (i.e. $E_{frp}\varepsilon_{frp}$) compared with that under static loading. An equation was proposed to calculate the dynamic contribution of Sprayed GFRP in shear strength of RC beam based on the dynamic stress rate. Further investigations are required to determine the dynamic increase factor for different types of Sprayed GFRP.

10

CONCLUSIONS AND RECOMMENDATIONS

10.1 Conclusions

This research project can be divided into 3 major parts; behavior of reinforced concrete beams under impact loading (discussed in Chapter 7), behavior of shear strengthened RC beams under quasi-static loading (discussed in Chapter 8), and behavior of shear strengthened RC beams under impact loading (discussed in Chapter 9). In this Chapter the most important findings are reported.

10.1.1 RC Beams under Impact Loading

Behavior of reinforced concrete beams under impact loading was investigated using a unique setup designed and developed at the University of British Columbia. The following conclusions were drawn from this investigation:

1. Load carrying capacity of RC beams under impact loading can be obtained using instrumented supports. The summation of the loads recorded by these supports will provide the true bending load applied on the RC beam during the impact. It was also noted that the use of steel yokes at the support provided more reliable and accurate results.

2. Loads measured by the instrumented tup will result in misleading conclusions due to inertia effects. There is a time lag between maximum load captured by the instrumented tup and maximum load captured by

instrumented supports. This time lag, which is really due to stress pulse travel from centre to support, shows that the inertia load effect must be taken into account.

3. Inertia load at any time instant t can be obtained by subtracting the summation of support load cells (i.e. true bending load) from the load obtained by the instrumented tup. This method was compared with another method which was used previously by other researchers. It was shown that the inertia load calculated by the proposed method was more accurate.

4. Bending load capacity of the RC beam investigated in this study under impact loading was about 2.3 times its static capacity. It was also noted that after a certain impact velocity, bending load capacity of RC beams remained constant and increase in stress (or strain) rate did not increase their load carrying capacity.

5. About 80% of the input energy in an impact test was absorbed by RC beam.

10.1.2 Response of Retrofitted RC Beams under Static Loading

RC beams with deficiency in their shear strength were retrofitted using Sprayed GFRP and Wabo®MBrace fabric GFRP. Sprayed GFRP material used throughout this research project exhibited a maximum composite tensile strength of 69 MPa, an elastic modulus of 14 GPa at a fiber volume fraction of 24.7% and an elongation to break of 0.63%. Wabo®MBrace EG 900 (unidirectional E-glass fiber fabric) with a maximum composite tensile strength of 1517 MPa, an elastic modulus of 72.4 GPa, and an elongation to break of 2.1% was also used for shear strengthening of RC beams for comparison.

The following conclusions were drawn:

1. Using Wabo®MBrace primer and putty as intermediate layer between concrete and Sprayed GFRP although increased the load carrying capacity, the energy absorption capacity was not increased as much as the load carrying capacity.

2. Roughening concrete surface using a pneumatic concrete chisel was an effective way to increase the concrete-FRP bond. This, in turn, increased the energy absorption capacity of strengthened beams as well.

3. Using through-bolts and nuts effectively increased both load carrying capacity and the energy absorption capacity in strengthened beams. Either sandblasting or roughening the concrete surface by a chisel can be employed when this type of mechanical fasteners are used.

4. U-shaped Sprayed GFRP was the most promising way to gain maximum possible benefits in shear strengthening from these advanced materials. Confinement provided by U-shaped Sprayed GFRP also effectively increased the energy absorption capacity of the strengthened beams. As a result, it should always be recommended to apply U-shaped Sprayed GFRP configuration for shear strengthening, where possible.

5. Wabo®MBrace fabric system was effective in increasing the load carrying capacity of RC beams when used as shear reinforcement. As with Sprayed GFRPs, U-shaped was seen as more effective than side bonding alone. Bonding additional longitudinal FRP strips over the end of the U-shaped bands improved the performance of the U-shaped bands. Increase in energy absorption capacity of beams strengthened in shear by Wabo®MBrace fabric system was not as high as the increase in the load carrying capacity. Brittleness of Wabo®MBrace Putty, at least to some extent, may explain this observation.

6. The presence of steel stirrups was effective in increasing the load carrying and energy absorption capacities of strengthened RC beams. This is a benefit, because, in practice, RC beams contain steel stirrups and adding Sprayed GFRP as external shear reinforcement can more effectively increase beams' performance under large loads compared to those with no stirrups.

The following equation was proposed to calculate the contribution of sprayed GFRP composites to the shear strength of RC beams:

$$V_{frp} = 2t_{frp}d_{frp}E_{frp}\varepsilon_{frp} \tag{8.1}$$

where,

V_{frp} = contribution of Sprayed GFRP in shear strength of RC beam [N]

t_{frp} = average thickness of the Sprayed GFRP [mm]

d_{frp} = depth of FRP shear reinforcement as shown in Figure 8.44 [mm]

E_{frp} = modulus of elasticity of FRP composite

$$\varepsilon_{frp} = \begin{cases} 0.002 & \text{for side bonding to the web when no mechanical fasteners/epoxy are used} \\ 0.003 & \text{for side bonding to the web when mechanical fasteners are used} \\ 0.003 & \text{for side bonding to the web when an interlayer of epoxy is used} \\ 0.003 & \text{for continuous U - shaped around the bottom of the web} \end{cases}$$

The validity of this equation was checked and a perfect prediction vs. experimental values was observed.

10.1.3 Response of Retrofitted RC Beams under Impact Loading

RC beams with deficiency in their shear strength were retrofitted using Sprayed GFRP. The following conclusions were drawn:

1. Sprayed GFRP was found to be an effective material to increase shear capacity of RC beams under impact loading.

2. When RC beams were strengthened by Sprayed GFRP on their lateral sides (2-sided retrofit), increase in FRP thickness did not increase the load carrying capacity under impact loading and this was true for both cases: with and without mechanical fasteners.

3. When RC beams were strengthened by Sprayed GFRP on their three sides (U-shaped), increase in FRP thickness increased the load carrying capacity under impact loading.

4. Sprayed GFRP under impact loading possessed a higher modulus of elasticity or at least a higher effective stress (i.e. $E_{frp}\varepsilon_{frp}$) compared with that under static loading. The following equations were proposed to calculate the contribution of U-shaped Sprayed GFRP in shear strength of RC beam under impact loading:

$$V_{frp\_d} = 2t_{frp}d_{frp}DIF_{frp}E_{frp}\varepsilon_{frp} \tag{9.4}$$

where,

V_{frp_d} = dynamic contribution of Sprayed GFRP in shear strength of RC beam [N]

t_{frp} = average thickness of the Sprayed GFRP [mm]

d_{frp} = depth of FRP shear reinforcement as shown in Figure 8.44 (Chapter 8) [mm]

E_{frp} = modulus of elasticity of Sprayed GFRP composite [MPa]

ε_{frp} = 0.003 (effective strain of Sprayed GFRP for continuous U-shaped around the bottom of the web)

and,

$$DIF_{frp} = -4\times10^{-16}\left(\frac{\dot{\sigma}_{dynamic}}{\dot{\sigma}_{static}}\right)^2 + 7\times10^{-8}\left(\frac{\dot{\sigma}_{dynamic}}{\dot{\sigma}_{static}}\right) + 1.0 \tag{9.3}$$

where,

DIF_{frp} = Dynamic Increase Factor for modulus of elasticity of Sprayed GFRP

$\dot{\sigma}_{dynamic}$ = stress rate under dynamic loading [MPa/sec]

$\dot{\sigma}_{static}$ = stress rate under quasi-static loading [MPa/sec]

10.2 Recommendations for Future Research

One of the most important suggestions for future research is to investigate the feasibility of implementing this technique in the field. Although this technique was used recently for shear strengthening of the girders of an existing bridge, its long term performance in different climates must be studied.

The spraying of overhead surfaces is very difficult and was one of the main reasons why shear strengthening was chosen in this study. Modification of the apparatus used in this research for spraying GFRP onto the concrete surface to overcome the above mentioned problem is also very important.

In this study only one type of fiber (i.e. glass) was used. Other candidates for this technique are carbon and aramid fibers. Other types of resins can also be used. Determining the best fiber and resin types for both structural and durability performance are quite important.

Investigation of the concrete-FRP bond and a better understanding of the debonding process is one of the most important needs for research in this field. In this research different techniques such as roughening the concrete surface using a pneumatic chisel, sandblasting the concrete surface, shooting steel nails onto the concrete surface, applying epoxy glue onto the concrete surface and through bolts and nuts were tried to increase the bond strength between Sprayed GFRP and concrete. Other techniques to increase the bond mechanically or chemically can also be investigated.

It is found in this research that in shear strengthening of RC beams there is not really a major benefit in using ultra high strength fabric FRP, and Sprayed GFRP with its strain at rupture of 0.63% can be considered a more economical product compare to fabric FRP with a strain to rupture of about 2.1% (see conclusions in Chapter 8). On the other hand, the fabric FRP will be more effective in flexural strengthening of RC beams, especially by keeping in mind that the spraying of overhead surfaces is very difficult. Therefore, a hybrid system using fabric FRP as flexural strengthening materials and Sprayed GFRP as shear strengthening material would be a feasible system. The feasibility of this hybrid system should be investigated in the future.

Long term durability of this Sprayed FRP and FRP-concrete interface must also be fully investigated. Other topics for future research include low temperature effects on Sprayed FRP and FRP-concrete bond performance (especially in cold regions of Canada), feasibility of using other types of polymers in Sprayed FRP composites, comprehensive study on rebound of Sprayed FRP and how to reduce it, optimizing the stress-strain response of the Sprayed FRP itself to get maximum strength/toughness, and application of fire-retardants on Sprayed FRP to make it more fire resistance. There are no Code equations available for strengthening of RC structures with Sprayed FRP and therefore, a design manual is needed for practicing engineers.

REFERENCES

[1] Grace, Nabil F. *Strengthening of negative moment region of reinforced concrete beams using carbon fiber-reinforced polymer strips.* **ACI Structural Journal**, Vol. 98, No. 3, 2001, pp 347-358.

[2] Deniaud, Christophe, and Cheng, J.J. Roger. *Shear behavior of reinforced concrete T-beams with externally bonded fiber-reinforced sheets.* **ACI Structural Journal**, Vol. 98, No. 3, 2001, pp 386-394.

[3] Arduini, Marco; Nanni, Antonio; and Romagnolo, Mariano. *Performance of decommissioned reinforced concrete girders strengthened with fiber-reinforced polymer laminates.* **ACI Structural Journal**, Vol. 99, No. 5, 2002, pp 652-659.

[4] Tureyen, A. Koray, and Frosch, Robert J. *Shear tests of FRP-reinforced concrete beams without stirrups.* **ACI Structural Journa**l, Vol. 99, No. 4, 2002, pp 427-434.

[5] Sheikh, Shamim A.; DeRose, David; and Mardukhi, Jamil. *Retrofitting of concrete structures for shear and flexure with fiber-reinforced polymers.* **ACI Structural Journal**, Vol. 99, No. 4, 2002, pp 451-459.

[6] Chaallal, Omar; Shahawy, Mohsen; and Munzer, Hassan. *Prformance of reinforced concrete T-girders strengthened in shear with carbon fiber-reinforced polymer fabric.* **ACI Structural Journal**, Vol. 99, No. 3, 2002, pp 335-343.

[7] Adhikary, Bimal Babu; Mutsuyoshi, Hiroshi; and Ashraf, Muhammad. *Shear strengthening of reinforced concrete beams using fiber-reinforced polymer sheets with bonded anchorage.* **ACI Structural Journal**, Vol. 101, No. 5, 2004, pp 660-668.

[8] Deniaud, Christophe, and Cheng, J.J. Roger. *Simplified shear design method for concrete beams strengthened with fiber reinforced polymer sheets.* **Journal of Composites for Construction**, Vol. 8, No. 5, 2004, pp 425-433.

[9] Deniaud, Christophe, and Cheng, J.J. Roger. *Reinforced concrete T-beams strengthened in shear with fiber reinforced polymer sheets.* **Journal of Composites for Construction**, Vol. 7, No. 4, 2003, pp 302-310.

[10] Zhang, Zhichao; Hsu, Cheng-tzu Thomas; and Moren, Jon. *Shear strengthening of reinforced concrete deep beams using carbon fiber reinforced polymer laminates.* **Journal of Composites for Construction**, Vol. 8, No. 5, 2004, pp 403-414.

[11] Zhang, Zhichao, and Hsu, Cheng-tzu Thomas. *Shear strengthening of reinforced concrete beams using carbon-fiber-reinforced polymer laminates.* **Journal of Composites for Construction**, Vol. 9, No. 2, 2005, pp 158-169.

[12] Adhikary, Bimal Babu, and Mutsuyoshi, Hiroshi. *Behavior of concrete beams strengthened in shear with carbon-fiber sheets.* **Journal of Composites for Construction**, Vol. 8, No. 3, 2004, pp 258-264.

[13] Pellegrino, Carlo, and Modena, Claudio. *Fiber reinforced polymer shear strengthening of reinforced concrete beams with transverse steel reinforcement.* **Journal of Composites for Construction**, Vol. 6, No. 2, 2002, pp 104-111.

[14] Breña, Sergio F., and Marci, Beth M. *Effect of carbon-fiber-reinforced polymer laminate configuration on the behavior of strengthened reinforced concrete beams.* **Journal of Composites for Construction**, Vol. 8, No. 3, 2004, pp 229-240.

[15] Deniaud, Christophe, and Cheng, J.J. Roger. *Shear rehabilitation of G-girder bridges in Alberta using fibre reinforced polymer sheets.* **Canadian Journal of Civil Engineering**, Vol. 27, No. 4, 2000, pp 960-971.

[16] Deniaud, Christophe, and Cheng, J.J. Roger. *Review of shear design methods for reinforced concrete beams strengthened with fibre reinforced polymer sheets.* **Canadian Journal of Civil Engineering**, Vol. 28, No. 2, 2001, pp 271-281.

[17] Wang, Y.C., and Chen, C.H. *Analytical study on reinforced concrete beams strengthened for flexure and shear with composite plates.* **Composite Structures**, Vol. 59, 2003, pp 137-148.

[18] Kachlakev, D., and McCurry, D.D. *Behavior of full-scale reinforced concrete beams retrofitted for shear and flexural with FRP laminates.* **Composites, Part B: engineering**, Part B Vol. 31, 2000, pp 445-452.

[19] Aprile, Alessandro, and Benedetti, Andrea. *Coupled flexural-shear design of R/C beams strengthened with FRP.* **Composites, Part B: engineering**, Part B Vol. 35, 2004, pp 1-25.

[20] Täljsten, Björn. *Strengthening concrete beams for shear with CFRP sheets.* **Construction and Building Materials**, Vol. 17, 2003, pp 15-26.

[21] Islam, M.R.; Mansur, M.A.; and Maalej, M. *Shear strengthening of RC deep beams using externally bonded FRP systems.* **Cement & Concrete Composites**, Vol. 27, 2005, pp 413-420.

[22] Chen, J.F., and Teng, J.G. *Shear capacity of fiber-reinforced polymer-strengthened reinforced concrete beams: fiber reinforced polymer rupture.* **Journal of Structural Engineering**, Vol. 129, No. 5, 2003, pp 615-625.

[23] Reed, Calvin E., and Peterman, Robert J. *Evaluation of prestressed concrete girders strengthened with carbon fiber reinforced polymer sheets.* **Journal of Bridge Engineering**, Vol. 9, No. 2, 2004, pp 185-192.

[24] Issa, Camille A., and AbouJouadeh, Abdo. *Carbon fiber reinforced polymer strengthening of reinforced concrete beams: Experimental study.* **Journal of Architectural Engineering**, Forum, 2004, pp 121-125.

[25] Triantafillou Thanasis C., and Antonopoulos, Costas P. *Design of concrete flexural members strengthened in shear with FRP.* **Journal of Composites for Construction**, Vol. 4, No. 4, 2000, pp 198-205.

[26] Ross, Sherrill; Boyd, Andrew; Johnson, Martin; Sexsmith, Robert; and Banthia, Nemy. *Potential Retrofit Methods for Concrete Channel Beam Bridges Using Glass Fiber Reinforced Polymer.* **Journal of Bridge Engineering**, Vol. 9, No. 1, 2004, pp 66-74.

[27] Banthia, N., and Boyd, A. J. *Sprayed fiber reinforced polymers: From laboratory to a real bridge.* **ACI Conc. Int.**, Vol. 24, No.11, 2002, pp 47-52.

[28] Banthia, N., Yan, C., and Nandakumar, N. *Sprayed fiber reinforced plastics (FRPs) for repair of concrete structures.* **Advanced Composite Materials in Bridges and Structures**, 2nd Int. Conf., Montreal, Canadian Society of Civil Engineers, 1996.

[29] Boyd, A. J., and Banthia, N. *Shear strengthening of reinforced concrete beams with sprayed GFRP.* Proc., **Structural Faults and Repair**, 8th Int. Conf., London, England, July 1999.

[30] De Lorenzis, Laura, and Nanni, Antonio. *Shear strengthening of reinforced concrete beams with near-surface mounted fiber-reinforced polymer rods.* **ACI Structural Journal**, Vol. 98, No. 1, 2001, pp 60-68.

[31] Barton, B., Wobbe, E., Dharani, L.R., Silva, P., Birman, V., Nanni, A., Alkhrdaji, T., Thomasd, J., Tunis, G. *Characterization of reinforced concrete beams*

strengthened by steel reinforced polymer and grout (SRP and SRG) composites. **Materials Science and Engineering A**, Vol. 412, 2005, pp 129-136.

[32] Swamy, R.N.; Jones, R., and Bloxham, J.W. *Structural behavior of reinforced concrete beams strengthened by epoxy-bonded steel plates.* **Structural Engineering**, Vol. 65A, No. 2, 1987, pp 59-68.

[33] Jones, R.; Swamy, R.N., and Charif, A. *Plate separation and anchorage of reinforced concrete beams strengthened by epoxy bonded steel plates.* **Structural Engineering**, Vol. 66, No. 5, 1988, pp 85-94.

[34] Germert, D.V. *Special design aspects of adhesive bonding plates.* **Repair and strengthening of concrete members with adhesive bonded plates-SP-165 ACI**, 1996, pp 25-41.

[35] Roberts, T.M. and Haji-Kazemi, H. *Theoretical study of the behavior of reinforced concrete beams strengthened by externally bonded steel plates.* Proc., **International Civil Engineering Part 2**, 1989, pp 39-55.

[36] Oehlers, D.J. *Reinforced concrete beams with plates glued to their soffits.* **Journal of Structural Engineering**, ASCE, Vol. 118, No. 8, 1992, pp 2023-2037.

[37] Mohamed, A.M.S.; Oehlers, D.J., and Bradford, M. *Design rules for gluing steel plates to the tension faces of reinforced concrete beams and slabs.* Proc., **Sixth East Asia–Pacific Conf on Structural Engineering & Construction**, Taipei, 1998, pp 2069-2074.

[38] Oehlers, D.J.; Mohamed, A.M.S., and Luo, W. *Upgrading continuous reinforced concrete beams by gluing steel plates to their tension faces.* **Journal of Structural Engineering**, ASCE, Vol. 124, No. 3, 1998, pp 224-232.

[39] Hamoush, S.A., and Ahmad, S.H. *Debonding of steel plate strengthened concrete beams*. **Journal of Structural Engineering**, ASCE, Vol. 116, No. 2, 1990, pp 256-371.

[40] Hussain, M.; Sharif, A.; Basunbul, I.A.; Baluch, M.H., and Al-Sulaimani, G.J. *Flexural behavior of pre-cracked reinforced concrete beams strengthened externally by steel plates*. **ACI Structural Journal**, Vol. 92, No. 1, 1995, pp 14-22.

[41] Baluch, M.H.; Ziraba, Y.N., and Basunbul, I.A. *Shear strength of plated RC beams*. **Magazine of Concrete Research**, Vol. 47, No. 173, 1995, pp 369-374.

[42] Ziraba, Y.N.; Baluch, M.H.; Basunbul, I.A.; Sharif, A.M.; Azad, A.K., and Al-Sulaimani, G.J. *Guidelines toward the design of reinforced concrete beams with external plates*. **ACI Structural Journal**, Vol. 91, No. 6, 1994, pp 639-646.

[43] Ziraba, Y.N. and Baluch, M.H. *Computational model for reinforced concrete beams strengthened by epoxy bonded steel plates*. **Finite Element Analysis and Design**, Vol. 20, 1995, pp 253-271.

[44] Swamy R.N.; Jones R., and Charif A. *Contribution of externally bonded steel plate reinforcement to the shear resistance of reinforced concrete beams*. **Repair and strengthening of concrete members with adhesive bonded plates-SP-165 ACI**, 1996, pp 1-24.

[45] Sharif, A.; Al-Sulaimani, G.J., and Hussain, M. *Strengthening of shear damaged RC beams by external plate bonding of steel plates*. **Magazine of Concrete Research**, Vol. 47, No. 173, No.1995, pp. 329-334.

[46] Adhikary, Bimal Babu; Mutsuyoshi, Hiroshi; and Sano, Masashi. *Shear strengthening of reinforced concrete beams using steel plates bonded on beam web:*

experiments and analysis. **Construction and Building Materials**, Vol. 14, 2000, pp 237-244.

[47] Moore, P.W. *An overview of composite construction in the United States.* **Proceedings of an Engineering Foundation Conference**, ASCE, New Hampshire, 1987, pp 1-17.

[48] Newmark, N.M.; Siess, C.P.; and Viest, I.M. *Tests and analysis of composite beams with incomplete interaction.* **Proceedings of the Society of Experimental Stress analysis**, Vol. 9, No. 1, 1952, pp 75-92.

[49] Szilard, R. *Design of prestressed composite steel structures.* **Journal of the Structural Division**, ASCE, 85, 1959, pp 97-123.

[50] ACI Committee 440, 2002, *Guide for the Design and Construction of Externally Bonded FRP Systems for Strengthening Concrete Structures (ACI 440.2R-02).* **American Concrete Institute**, Farmington Hills, Mich., 45 pp.

[51] CSA-S806-02, 2002, *Design and Construction of Building Components with Fibre-Reinforced Polymer.* **Canadian Standards Association**, Rexdale, Ontario, 177 pp.

[52] *Strengthening Reinforced Concrete Structures with Externally-Bonded Fiber Reinforced Polymers.* **ISIS Canada Design Manual**, No. 4. September 2001.

[53] fib-TG9.3, *Design and Use of Externally Bonded Fiber Polymer Reinforcement (FRP EBR) for Reinforced Concrete Structures.* **Bulletin 14**, July 2001, 138 pp.

[54] Meier, U. Strengthening of structures using carbon fibre/epoxy composites. **Construction and Building Materials**, Vol. 9, No. 6, 1995, pp 341-351.

[55] Li, W.; Albrecht, P., and Saadatmanesh, H. *Strengthening of composite steel-concrete bridges*. **Journal of Structural Engineering**, Vol. 121, 1995, pp 1842-1849.

[56] Tang, Taiping, and Saadatmanesh, Hamid. *Analytical and experimental studies of fiber-reinforced polymer-strengthened concrete beams under impact loading*. **ACI Structural Journal**, Vol. 102, No. 1, 2005, pp 139-149.

[57] Tang, Taiping, and Saadatmanesh, Hamid. *Behavior of concrete beams strengthened with fiber-reinforced polymer laminates under impact loading*. **Journal of Composites for Construction**, Vol. 7, No. 3, 2003, pp 209-218.

[58] Erki, M.A., and Meire, U. *Impact loading of concrete beams externally strengthened with GFRP laminates*. **Journal of Composites for Construction**, Vol. 3, No. 3, 1999, pp 117-124.

[59] White, Timothy W.; Soudki, Khaled A., and Erki, Marie-Anne. *Response of RC beams strengthened with CFRP laminates and subjected to a high rate of loading*. **Journal of Composites for Construction**, Vol. 5. No. 3, 2001, pp 153-162.

[60] Hamed, E. and Rabinovitch, O. *Dynamic Behavior of Reinforced Concrete Beams Strengthened with Composite Materials*. **Journal of Composites for Construction**, Vol. 9, No. 5, 2005, pp 429-440.

[61] Berset, J.-D. *Strengthening of reinforced concrete beams for shear using FRP composites*. **MSc Thesis**. Department of Civil and Environmental Engineering, Massachusetts Institute of Technology, Jan. 1992.

[62] Uji, K. *Improving shear capacity of existing reinforced concrete members by applying carbon fiber sheets*. **Transactions of the Japan Concrete Institute**, Vol. 14, 2005, pp 253-266.

[63] Dolan, C.W.; Rider, W.; Chajes, M.J.; and DeAscanis, M. *Pre-stressed concrete beams using non-metallic tendons and external shear reinforcement.* **Fiber-Reinforced Plastic Reinforcement for Concrete Structures-SP-138-ACI,** American Concrete Institute, Detroit, 1992, pp 475-495.

[64] Al-Sulaimani, G.J.; Sharif, A.; Basunbul, I.A.; Maluch, M.H.; and Ghaleb, B.N. *Shear repair for reinforced concrete by fiberglass plate bonding.* **ACI Structural Journal**, Vol. 91, No. 3, 1994, pp 458-464.

[65] Ohuchi, H.; Ohno, S.; Katsumata, H.; Kobatake, Y.; Meta, T.; Yamagata, K.; Inokuma, Y.; and Ogata, N. *Seismic Strengthening Design Technique for existing bridge columns with CFRP.* Proc., **Seismic Design and Retrofitting of Reinforced Concrete Bridge**s, Edited by R. Park, 1994, pp 495-514.

[66] Chajes, M.J.; Januska, T.F.; Mertz, D.R.; Thomson, T.A.; and Finch, W.W. *Shear strengthening of reinforced concrete beams using externally applied composite fabrics.* **ACI Structural Journal**, Vol. 92, No. 3, 1995, pp 295-303.

[67] Malvar, L.J.; Warren, G.E., and Inaba, C. *Rehabilitation of Navy pier beams with composite sheets.* **Non-Metallic (FRP) Reinforcement for Concrete Structures**, E & FN Spon, London, 1995, pp 534-540.

[68] Vielhaber, J. and Limberger, E. *Upgrading of concrete beams with a local lack of shear reinforcement.* **Federal Institute for Materials Research and Testing (BAM)**, Unpublished Report, Berlin, Germany, 1995.

[69] Sato, Y.; Ueda, T.; Kakuta, Y., and Tanaka, T. *Shear reinforcing effect of carbon fiber sheet attached to side of reinforced concrete beams.* Proc., **Advanced Composite Materials in Bridges and Structures**, edited by M.M. El-Badry, 1996, pp 621-627.

[70] Triantafillou, T.C. *Shear strengthening of reinforced concrete beams using epoxy-bonded FRP composites*. **ACI Structural Journal**, Vol. 95, No. 2, 1998, pp. 107-115.

[71] Triantafillou Thanasis C. and Fardis, M.N. *Strengthening of historic masonry structures with composite materials*. **Materials and Structures**, Vol. 30, pp 486-496.

[72] Priestley, M.J.N. and Seible, F. *Design of seismic retrofit measures for concrete and masonry structures*. **Construction and Building Materials**, Vol. 9, No. 6, 1995, pp 365-377.

[73] Khalifa, A.; Gold, W.J.; Nanni, A., and Aziz, A.M.I. *Contribution of externally bonded FRP to shear capacity of RC flexural members*. **Journal of Composites for Construction**, Vol. 2, No. 4, 1998, pp 195-202.

[74] Japan Concrete Institute (JCI). *Technical Report on Cementitious Fiber Reinforced Concrete*, Tokyo, 1998.

[75] Bousselham, Abdelhak, and Chaallal, Omar. *Shear strengthening reinforced concrete beams with fiber-reinforced polymer: assessment of influencing parameters and required research*. **ACI Structural Journal**, Vol. 101, No. 2, 2004, pp 219-227.

[76] Matthys, S., and Triantafillou, T. *Shear and tosion strengthening with externally bonded FRP reinforcement*. **Proceedings of the International Workshop on Composites in Construction: A reality**. Edited by: Cosensa, E.; Manfredi, G.; and Nanni, A. Capri, Italy, pp. 203-210.

[77] Joint ACI-ASCE Committee 445. *Recent approaches to shear design of structural concrete*. **Journal of Structural Engineering**, Vol. 124, No. 12, 1998, pp 1375-1417.

[78] Chaallal, O.; Nollet, M.-J., and Perraton, D. *Strengthening of reinforced concrete beams with externally bonded fiber-reinforced-plastic plates: design guidelines for shear and flexure*. **Canadian Journal of Civil Engineering**, Vol. 25, 1998, pp 692-704.

[79] *Design and construction of building components with fiber reinforced polymers*. Draft, **CSA Standarad S806**, Canadian Standard Association, Rexdale, Ontario, Canada, 2000.

[80] Malek, A.M., and Saadatmanesh, H. *Analytical study of reinforced concrete beams strengthened with web-bonded fiber reinforced plastic plates or fabrics*. **ACI Structural Journal**, Vol. 95, No. 2, 1998, pp 134-352.

[81] Concrete Society. *Design guidance for strengthening concrete structures using fibre composite materials*. **Concrete Society Technical Report No. 55**, Berkshire, UK, 2000.

[82] Cao, S. Y.; Chen, J. F.; Teng, J. G.; Hao, Z. , and Chen, J. *Debonding in RC Beams Shear Strengthened with Complete FRP Wraps*. **Journal of Composites for Construction**, Vol. 9, No. 5, 2005, pp 417-428.

[83] Wong, Rita S.Y., and Vecchio, Frank J. *Towards modeling of reinforced concrete members with externally bonded fiber-reinforced polymer composites*. **ACI Structural Journal**, Vol. 100, No. 1, 2003, pp 47-55.

[84] Tumialan, G.; Nakano, K.; Fukuyama, H., and Nanni, A. *Japanese and North American guidelines for strengthening concrete structures with FRP: a comparative review of shear provisions*. **Non-Metallic (FRP) Reinforcement for Concrete Structures**, FRPRCS-5, Cambridge, UK, 2001.

[85] Hag-Elsafi, Osman; Alampalli, Sreenivas, and Kunin, Jonathan. *In-service evaluation of a reinforced concrete T-beam bridge FRP strengthening system.* **Composite Structures**, Vol. 64, 2004, pp 179-188.

[86] Vougioukas, Emmanuel; Zeris, Christos A.; and Kotsovos, Michael D. *Toward safe and efficient use of fiber-reinforced polymer for repair and strengthening of reinforced concrete structures.* **ACI Structural Journal**, Vol. 102, No. 4, 2005, pp 525-534.

[87] Abrams, D.A. T*he effect of rate of application of load on the compressive strength of concrete.* **Proceedings ASTM**, 17, 1917, pp 364-365.

[88] Atchley, B.L. and Furr, H.L. *Strength and energy absorption capabilities of plain concrete under dynamic and static loadings.* **ACI Journal**, Vol. 64, 1967, pp 745-756.

[89] Scott, B.D.; Park, R., and Priestley, M.J.N. *Stress strain behaviour of concrete confined by overlapping hoops at low and high strain rates.* **ACI Journal**, Vol. 79, No. 1, pp 13-27.

[90] Dilger, W.; Kand, R., and Kowalczyk, R. *Ductility of plain and confined concrete under different strain rates.* **ACI Journal**, 1984, pp 73-81.

[91] Malkar, P.F.; Vitaya-Udom, K.P., and Cole, R.A. *Dynamic tensile-compressive behaviour of concrete.* **ACI Journal**, Vol. 82, No. 4, pp 484-491.

[92] Soroushian, P.; Choi, K-B., and Alhamad, A. *Dynamic constitutive behaviour of concrete.* **ACI Journal**, 1986, pp 251-259.

[93] Watstein, D. *Effect of straining rate on the compressive strength and elastic properties of concrete*. **ACI Journal**, Vol. 49, No. 8, 1953, pp 729-744.

[94] Malvar, L.J. and Ross, C.A. *Review of strain rate effects for concrete in tension*. **ACI Material Journal**, Vol. 95, No. 6, 1998, pp 735-739.

[95] Sparks, P.R.; and Menzies, J.B. *The effect of rate of loading upon the static and fatigue strengths of plain concrete in compression*. **Magazine of Concrete Research**, Vol. 25, No. 83, 1973, pp 73-80.

[96] Spooner, D.C. *Stress-strain-time relationships for concrete*. **Magazine of Concrete Research**, Vol. 23, No. 75/76, 1971, pp 127-131.

[97] US Department of the Army Technical Manual. *Design of structures to resist the effects of accidental explosions*. **TM 5-1300**, 1990.

[98] Norris, G.H.; Hansen, R.J.; Holly, M.J.; Biggs, J.M.; Namyet, S., and Minami, J.K. *Structural design for dynamic loads*. McGraw-Hill Book Company Inc., New York, USA, 1959.

[99] Wakabayashi, M.; Nakamura, T.; Yoshida, N.; Iwai, S., and Watanabe, Y. *Dynamic loading effects on the structural performance of concrete and steel materials and beams*. **Proceedings of the 7th world conference on earthquake engineering**, Istanbul, Turkey, Vol. 6, 1980, pp 271-278.

[100] Fu, H.C.; Erik, M.A., and Seckin, M. *Review of effects of loading rate on reinforced concrete*. **Journal of Structural Engineering**, Vol. 117, No. 12, 1991, pp 3660-3679.

[101] Malvar, L.J. *Review of static and dynamic properties of steel reinforcing bars*. **ACI Material Journal**, Vol. 95, No. 5, 1998, pp 609-616.

[102] Bertero, V.V.; Rea, D.; Mahin, S., and Atalay, M.B. *Rate of loading effects on uncracked and repaired reinforced concrete members*. **Proceedings of 5th world conference on earthquake engineering**, Rome, Vol. 1, 1973, pp 1461-1470.

[103] Takeda, J. and Tachikawa, H. *Deformation and fracture of concrete subjected to dynamic load*. **Proceedings of the International conference on mechanical behaviour of materials**, Kyoto, Japan, 1971, pp 267-277.

[104] Banthia, N.P. *Impact resistance of concrete*. **PhD Thesis**, The University of British Columbia, Vancouver, BC, 1987.

[105] Bentur, A.; Mindess, S. and Banthia, N. *The Behaviour of Concrete under Impact Loading: Experimental Procedures and Method of Analysis*. **Materials and Constructions**, Vol. 19, No. 113, pp 371-378.

[106] Kishi, N.; Nakano, O.; Matsuoka, K.G., and Ando, T. *Experimental study on ultimate strength of flexural-failure-type RC beams under impact loading*. **Proceedings of the International Conference on Structural Mechanics in Reactor Technology**, 2001, Washington, DC, Paper # 1525, 7 pages.

[107] Ando, T.; Kishi, N.; Mikami, H., and Matsuoka, K.G. *Weight falling impact tests on shear-failure type RC beams without stirrups*. **6th International Conference on Structures under Shock and Impact**, editors: N. Jones and C.A. Brebbia. Cambridge, England, UK, 2000, pp 579-587.

[108] Kishi, N.; Mikami, H., and Ando, T. *Impact-resistance behavior of shear-failure-type RC beams under falling-weight impact loading*. **7th International Conference on Structures under Shock and Impact**, editors: A.M. Rajendran, N.

Jones, and C.A. Brebbia. Montreal Quebec, Canad, 2002, pp 499-508.

[109] Kishi, N.; Mikami, H.; Matsuoka, K.G.; and Ando, T. *Impact behavior of shear-failure-type RC beams without shear rebar.* **International Journal of Impact Engineering**, Vol. 27, 2002, pp 955-968.

[110] Abbas, H.; Gupta, N.K.; and Alam, M. *Nonlinear response of concrete beams and plates under impact loading.* **International Journal of Impact Engineering**, Vol. 30, 2004, pp 1039-1053.

[111] Jerome, D.M. and Ross, C.A. *Simulation of the dynamic response of concrete beams externally reinforced with carbon-fiber reinforced plastic.* **Computers & Structures**, Vol. 64, No. 5/6, 1997, pp 1129-1153.

[112] ASTM C 127-88. *Standard Test Method for Specific Gravity and Absorption of Coarse Aggregate*, **ASTM International**, 5 pages.

[113] http://wbaweb.buffnet.net/main_pages/mbrace_eg900.htm

[114] ASTM D 3039. *Standard Test Method for Tensile Properties of Polymer Matrix Composite Materials.* **ASTM International**, 10-Apr-2000, 13 pages.

[115] Boyd, A.J. *Rehabilitation of reinforced concrete beams with sprayed glass fiber reinforced polymers.* **Ph.D. Thesis**, The University of British Columbia, Vancouver, BC, 2000.

[116] ASTM D 2584-68 (Reapproved 1985). *Standard Test Method for Ignition Loss of Cured Reinforced Resins.* **ASTM International**, 2 pages.

[117] Banthia, N.; Mindess, A.; Bentur, A. and Pigeon, M. *Impact Testing of Concrete Using a Drop-weight Impact Machine*. **Experimental Mechanics**, 1989, pp 63-69.

APPENDIX A

Flexural capacity of RC beam used in Chapter 7 under 3-point loading (based on CSA A23.3-94):

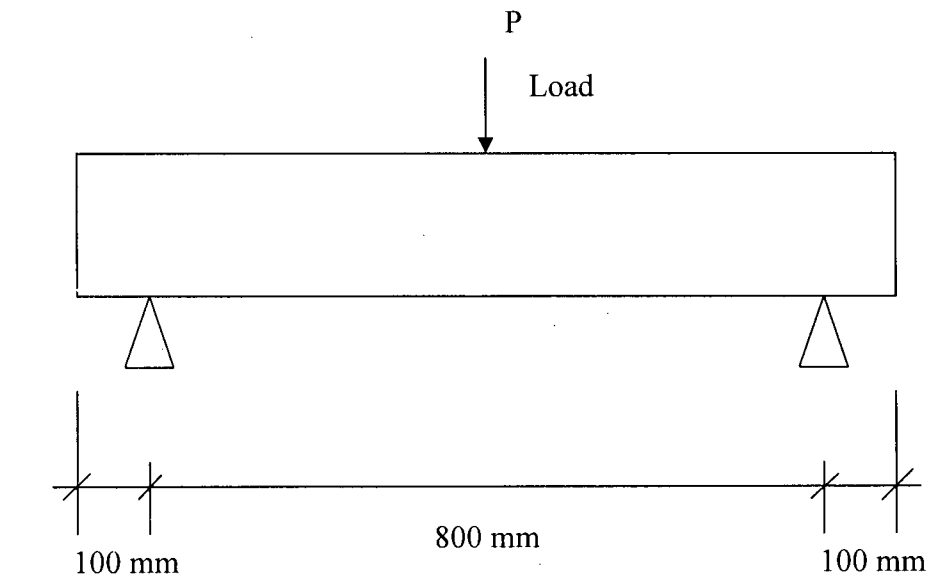

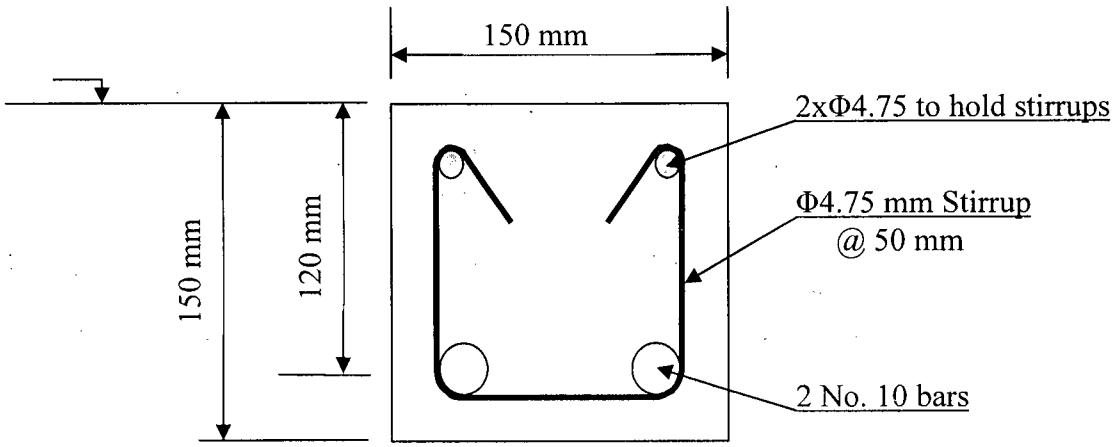

Data:

$f'_c = 44$ MPa
$b = 150$ mm
$h = 150$ mm
$d = 120$ mm
$f_y = 474$ MPa
$A_s = 2 \times 100 = 200$ mm^2

$$\alpha_1 = 0.85 - .0015 f_c' \geq 0.67 \longrightarrow \alpha_1 = 0.784$$

$$\beta_1 = 0.97 - .0025 f_c' \geq 0.67 \longrightarrow \beta_1 = 0.86$$

1. Compute *a*.

$$a = \frac{\phi_s (A_s) f_y}{\phi_c \alpha_1 f_c' b}, \; a = \frac{0.85(200)474}{0.6 \times 0.784 \times 44 \times 150} = 26mm$$

2. Check that reinforcement exceeds minimum requirements.

$$A_{s,\min} = \frac{0.2\sqrt{f_c'}}{f_y} b_t h = \frac{0.2\sqrt{44}}{400} \times 150 \times 150 = 75mm^2$$

The 200 mm^2 provided exceeds $A_{s,min}$.

3. Compute M_r.

Beam : $M_r = \phi_s (A_s) f_y (d - \frac{a}{2}), \; M_r = 8.622kN.m$

$$M_r = \frac{P[kN]}{2} \times 0.4[m], \; P = 43.1kN$$

If ϕ_s is not considered then:

$$P = 51kN$$

Appendix B

Flexural and shear capacity of RC beam used in Chapters 8 and 9 under 3-point loading (based on CSA A23.3-94):

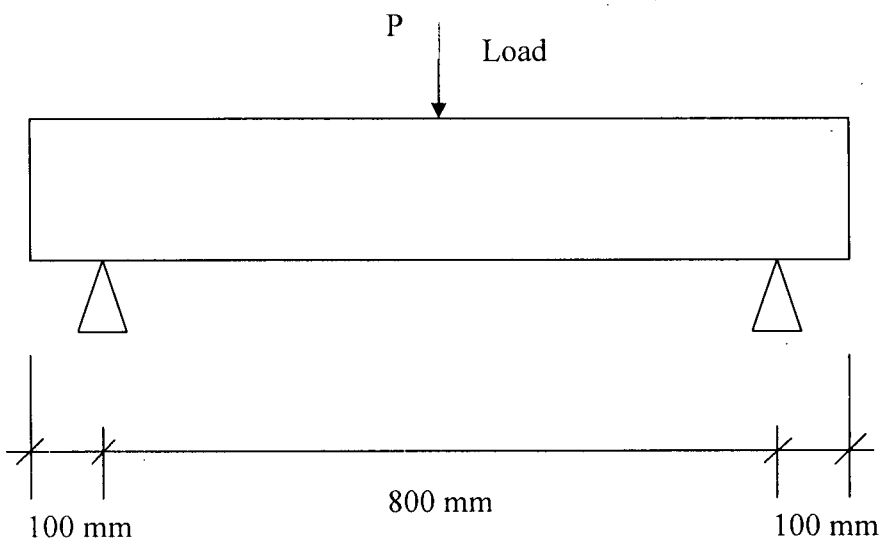

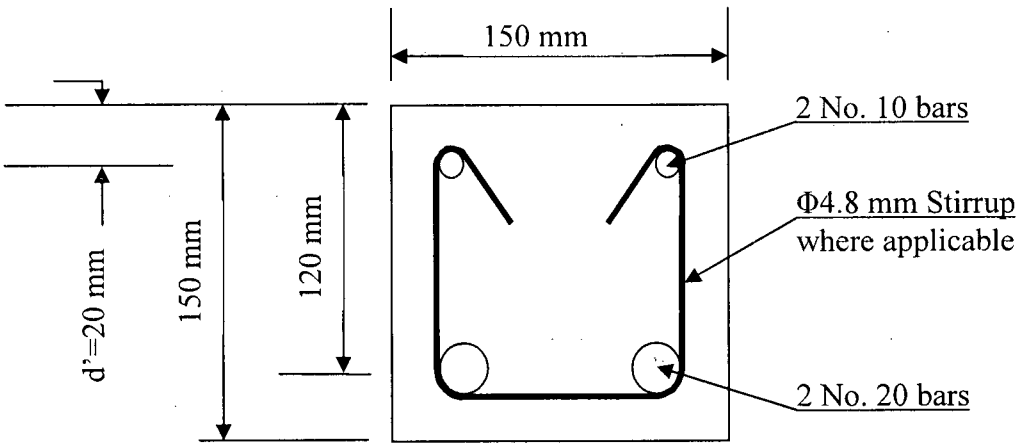

Data:

$f'_c = 44$ MPa
b = 150 mm
h = 150 mm
d = 120 mm
d' = 20 mm
$f_y = 440$ MPa
$A_s = 2 \times 300 = 600$ mm^2
$A'_s = 2 \times 100 = 200$ mm^2

$$\alpha_1 = 0.85 - .0015 f_c' \geq 0.67 \longrightarrow \alpha_1 = 0.784$$

$$\beta_1 = 0.97 - .0025 f_c' \geq 0.67 \longrightarrow \beta_1 = 0.86$$

1. Assume that $f_s' = f_y$ and $f_s = f_y$. Divide the beam into two components; Beam 1 has 2 No. 10 bars as compression reinforcement and an area of tension reinforcement, A_{s1}, equal to 2 No. 10 bars located at *d* below the top of the beam. Beam 2 has no compression steel and has

$$A_{s2} = A_s - A_{s1} = 600 - 200 = 400 \text{ mm}^2$$

2. Compute *a* for Beam 2.

$$a = \frac{\phi_s (A_s - A_s') f_y}{\phi_c \alpha_1 f_c' b}, \quad a = \frac{0.85(600 - 200)440}{0.6 \times 0.784 \times 44 \times 150} = 48mm$$

3. $f_s' = f_y$ only if $\frac{d'}{a} \leq \left(\frac{d'}{a}\right)_{\lim it}$.

$$\left(\frac{d'}{a}\right)_{\lim it} = \frac{1}{\beta_1}\left(1 - \frac{f_y}{700}\right) = 0.43, \quad \frac{d'}{a} = \frac{20}{48} = 0.42 \therefore \frac{d'}{a} \leq \left(\frac{d'}{a}\right)_{\lim it} \therefore f_s' = f_y$$

4. Check if the tension steel has yielded, $f_s = f_y$. $a_b = 0.5$

$\frac{a}{d} = \frac{48}{120} = 0.4 < 0.5$, *a* is less than a_b, therefore $f_s = f_y$ at ultimate.

5. Check that reinforcement exceeds minimum requirements.

$$A_{s,\min} = \frac{0.2\sqrt{f_c'}}{f_y} b_t h = \frac{0.2\sqrt{44}}{440} \times 150 \times 150 = 68mm^2$$

The 600 mm^2 provided exceeds $A_{s,\min}$.

6. Compute M_r.

(a) Beam 1: $M_{r1} = \phi_s A_s' f_y (d - d')$, $M_{r1} = 7.48kN.m$

(b) Beam 2: $M_{r2} = \phi_s (A_s - A_s') f_y (d - \frac{a}{2})$, $M_{r2} = 14.3 kN.m$

$$M_r = M_{r1} + M_{r2} = 21.84kN.m$$

$$M_r = \frac{P[kN]}{2} \times 0.4[m],\ P = 109.2kN$$

If ϕ_s is not considered then:

$$P = 131kN$$

Resistance of RC beam with no stirrups:

Reference: Recent Approaches to Shear Design of Structural Concrete, by ASCE-ACI Committee 445 on shear and torsion, Journal of Structural Engineering, December 1998, pp. 1375-1417. Equation (62) on page 1401 (incorporating the percentage of longitudinal tension reinforcement in shear strength of RC beam):

$$V_c = (0.8 + 100\rho)\frac{\sqrt{f_c'}}{12} b_w d,\ \rho = 0.033,\ \text{therefore } V_c = 0.34\sqrt{f_c'}\, b_w d$$

$f_c' = 43$ MPa for Beam CN-S then $V_c = 40$ kN , therefore, P= 80 kN

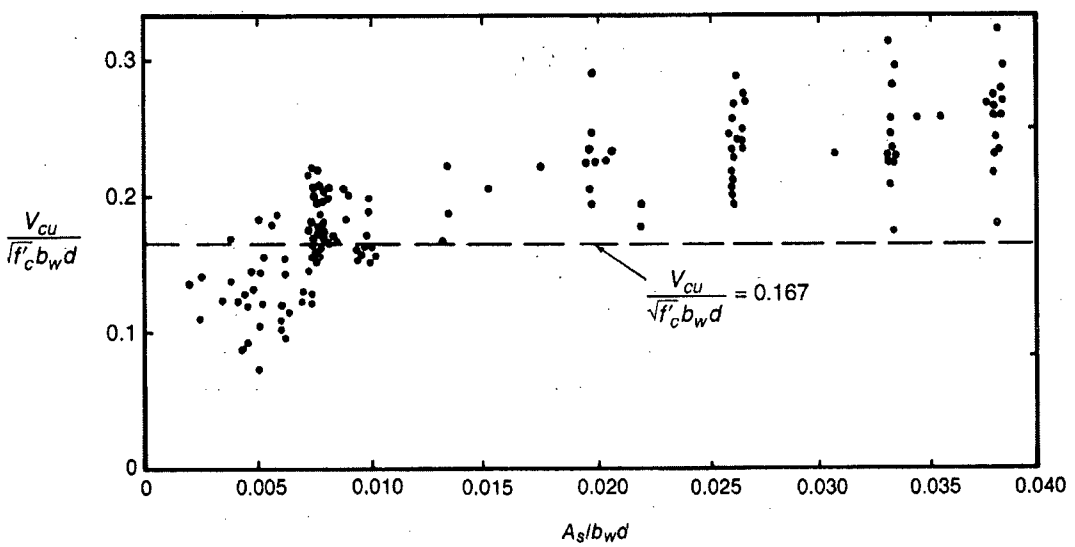

Figure - Effect of reinforcement ratio, ρ_w, on the shear capacity, V_{cu}, of beams without stirrups. [Reference: Reinforced Concrete, Mechanics and Design. James G. MacGregor, F. Michael Bartlett. First Canadian Edition, Prentice Hall Canada Inc., 2000, Page 187]

Resistance of RC beam with stirrups (Φ4.75 @ 160 mm):

ACI 318 Model Code (**ACI Committee 318, "Building Code Requirements for Structural Concrete (ACI 318-99) and Commentary (318R-99)," American Concrete Institute, Farmington Hills, Mich., 1999, 391 pp.**) the force resisted by shear reinforcement:

$$V_s = \left(\frac{A_v}{s_v} \frac{1 + 2a/d}{12} \right) f_y d$$

$A_v = 2*17.7=35.4$ mm^2
$s_v = 160$ mm
a = 400 mm
d = 120 mm
$f_y = 600$ MPa
Then, $V_s = 2*10.2 = 20.4$ kN

Therefore predicted resistance load for RC beam with stirrups (Φ4.75 @ 160 mm):
= 20.4 + 80 = 100.4 kN